STUDY OF SOLID-STATE INTEGRATED MICROWAVE CIRCUITS

Scientific Report No. 4

U26-811500-26

30 June 1967

GPO PRICE $ _____

CSFTI PRICE(S) $ _____

Hard copy (HC) _____

Microfiche (MF) _____

ff 653 July 65

FACILITY FORM 602

N68-33329 (ACCESSION NUMBER) (THRU) 1

190 (PAGES) (CODE)

CR-96449 (NASA CR OR TMX OR AD NUMBER) 09 (CATEGORY)

JUL 1968

RECEIVED

NASA STI FACILITY

INPUT BRANCH

TEXAS INSTRUMENTS
INCORPORATED

N68-25140

STUDY OF SOLID-STATE INTEGRATED MICROWAVE CIRCUITS

Scientific Report No. 4

U26-811500-26

30 June 1967

Prepared for

NATIONAL AERONAUTICS AND SPACE ADMINISTRATION
Electronics Research Center
Cambridge, Massachusetts

Work Performed Under
Contract No. NAS 12-75
Control No. ERC/R&D 65-45

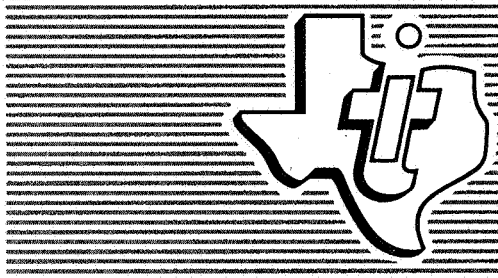

TEXAS INSTRUMENTS
INCORPORATED

PRECEDING PAGE BLANK NOT FILMED.

ABSTRACT

Microwave components, devices, and integrated techniques applicable to a low-noise, solid-state receiver in the 1- to 6-GHz frequency range are presented in this report. Data is also given on devices such as the field-effect transistor and linear integrated circuits with frequency responses extending to the VHF region.

This report relates the microwave properties of ferrites, dielectrics, thin-film, and microstrip as used in filters, isolators, and circulators. The characteristics of Schottky-barrier, varactor, avalanche and tunnel diodes are discussed as well as the power application and low-noise behavior of different transistor geometries. A summary of the characteristics of these components and devices is given in Section II.

PREFACE

This report covers work performed during the period from 13 March 1967 through 16 June 1967 under Contract No. NAS 12-75, Part II, Paragraph B, item 9, for the Electronic Research Center of the National Aeronautics and Space Adminstration.

The relative merits of microwave components, devices, and techniques regarding their utilization in receiver applications are given in this report as well as reviews on recent developments in integrated microwave circuits and devices, therefore, bringing to-date earlier work performed under item 1. Although, much of the information presented is recent and subject to continued research, it will be used in subsequent efforts to design and build an S-band telemetry receiver. Later developments and newer technologies will also be utilized where appropriate.

TABLE OF CONTENTS

TABLE OF CONTENTS (Continued)

LIST OF ILLUSTRATIONS

LIST OF ILLUSTRATIONS (Continued)

LIST OF ILLUSTRATIONS (Continued)

LIST OF ILLUSTRATIONS (Continued)

LIST OF TABLES

SECTION I

INTRODUCTION

In recent years, the capability of solid state components and techniques has been expanded well into the region of microwave frequencies. Although the basic principles of transmitting and receiving a microwave signal remain essentially the same today, many of these functions are performed by solid-state microwave devices. These advances in microwave semiconductor technology were discussed in Scientific Report No. 1 along with the recent technological advances in the use of dielectrics, thin-films, and ferrites at microwave frequencies. In this report current state-of-the-art microwave components, devices, and techniques are reviewed with special consideration given to receiver applications.

The crowded frequency spectrum necessitated moving portions of the military and space agencies telemetry bands to UHF frequencies. At these frequencies, low atmospheric noise requires the use of low noise receivers. Today's transistor can comply with this requirement and provide reasonable gain, thus competing with tunnel-diode and TWT devices.

Similarly, the rapid advancement in semiconductor devices out-dates the innovations from early days of radar and line-of-sight communication networks. For example, the mechanical tuning of cavities may be eliminated by magnetically-tuned microwave filters, and the extremely high noise figures of mixers using crystal diodes have been drastically reduced by the use of Gallium Arsenide diodes. In similar fashion, the frequency multiplication of a lower oscillator frequency to obtain a microwave frequency for injection into the first mixer stage may now be replaced by a single transistor oscillator. In addition, linear, low level functions previously performed to 200 MHz with discrete components in a receiver, are now obtainable in linear integrated circuits.

Thus, it is clear that many receiver functions at microwave frequencies may be performed by solid state electronics and integrated techniques without any degradation in performance. In this report, current devices and techniques are discussed and limitations which exist today are presented. In keeping pace with the ever expanding semiconductor technology, it may be expected that current restraints and limitations will be overcome.

SECTION II

SUMMARY

A. TRANSISTORS

Inherent noise properties is an important consideration which must be given to transistors when they are used to amplify low level signals. This is especially true of microwave transistors since their noise level asymptotically increases to a 6-dB per octave slope as the operating frequency approaches the alpha cut-off frequency of the device. The noise property of microwave transistors is the result of thermal and shot noise mechanisms in the base-emitter junction and in the collector regions. Analytical considerations given to these noise generating sources permit deriving a high frequency noise model of the microwave transistor as well as an expression for the noise figure of the device. This same analytical approach may be extended to derive the noise figure of a field-effect transistor.

Other than noise considerations, ultimate physical limitations place an upper boundary on the frequency response of a microwave transistors and this is of concern because such a limitation places constraints upon the frequency response. This limitation is base width as the charge-carrier transit time is dependent upon the distance which base carriers must travel.

Power generation at microwave frequencies create thermal problems as heat dissipation is confined to a small area. In order to dissipate more power, the device areas involved should be enlarged. Scaling-up must be accomplished while keeping the high frequency parameters intact, i.e., the $r_b c_c$ product should stay the same.

One approach to power generation is the use of overlay geometry. Present state-of-the-art overlay geometries, such as the 2N4012 device, delivers three watts at L-band when used as a fundamental amplifier. One watt at 2-GHz is obtained when the device is used as a quadrupler.

Germanium and silicon remains the major semiconductor material used in microwave transistors. The advances in diffusion technology have led to the development of new geometries such as the L187 epitaxial planar silicon structure which has a measured power gain of 7 dB at 4.0 GHz, and NPN double diffused planar Germanium devices which have a measured noise figure of 5.0 dB and a power gain of 6.5 dB at 3 GHz. The cut-off frequencies of these devices range to 7 or 8.5 GHz. The L158 geometry developed for the MERA program has a pulsed 2-watt output power at S-band. This 85-stripe device also has excellent CW performance as a class A or class C power amplifier.

The field effect transistor is now developed so that designers may utilize the low noise, vacuum tube characteristics of these devices at L-band frequencies. These devices perform well as RF amplifiers or mixers in the VHF region in stripline configurations, and microstrip techniques are certainly feasible.

B. SEMICONDUCTOR DEVICES

Varactor diodes have found wide application as frequency multipliers, divider circuits, and as capacitors in tuned networks. The capacitance of the junction may be made to vary as much as 11 to 1 by applying a reverse dc voltage bias.

Two types of varactors are in use; the abrupt junction (Schottky barrier) and the diffused junction varactor. The junction capacitance of either varactor is made to vary by variation of an applied reverse biasing voltage. In the case of the abrupt junction diode, the junction capacitance varies approximately inversely to the square root of the reverse bias voltage, whereas, the junction capacitance of a diffused junction diode varies inversely to the 1/3 power of the reverse bias voltage.

Therefore, theoretically, an octave could be tuned with as little as an 11-Vdc reverse bias with an abrupt junction varactor and 38 Vdc with a diffused junction varactor. If any circuit capacitance (either series or parallel) is present it diminishes the effect of junction capacitance change. Yet it is possible to overcome the effects of the external capacitance and achieve one-octave tuning with a conventional 28-Vdc supply voltage.

The Schottky barrier technique has also been very successfully applied to the construction of mixer diodes. In fact, all mixer diodes being constructed by Texas Instruments are of the Schottky barrier type. Research at Texas Instruments indicates that in the very near future the noise figure will be as low as five decibels at S-band and six decibels at X-band.

Two factors were responsible for the recent breakthrough to the long life Gunn effect device. The first was development of a high purity epitaxial GaAs chip. The thickness and doping levels were optimized for Gunn effect performance. The second critical factor is heat dissipation. Gunn effect devices are very inefficient (0.5 to 0.3% efficiency typical); therefore, great amounts of heat must be removed from the chip. Improved mounting techniques have resulted in proven long term CW operation at powers up to ten milliwatts. Continuous long-term output up to 50 mW or more will not be an unrealistic goal in the very near future.

In the 2—3-GHz range, the chip thickness becomes relatively large and resonant cavities become cumbersome. These facts plus low efficiency and poor frequency stability make it undesirable to use Gunn effect devices at 2.5-GHz at this time, especially in view of the fact that microwave transistors will operate reliably at this frequency.

The tunnel diode is a unique device which exhibits a region of negative resistance, i.e., the current decreases with increasing applied voltage. By definition, a positive resistance dissipates energy, so conversely, a negative resistance should be capable of supplying energy, and such is the case.

The tunnel diode is a two terminal device consisting of a single PN junction, but the conductivity of the P and N materials is 1000 times as high as that used in conventional diodes. As a result, the width of the junction (the depletion layer) is very small, of the order of 10^{-6} inch. The very small junction thickness makes it possible for valence electrons under the influence of a small forward or reverse dc bias to "tunnel" the junction without overcoming the potential barrier at the junction. As the forward dc bias is increased the flow of valence electrons across the junction decreases giving

rise to the negative resistance effect. Then as the bias is further increased, holes and electrons gain the energy to overcome the potential barrier at the junction and behavior corresponding to that of a conventional diode results. The theoretical frequency limit for this phenomenon is 10^7 MHz. The practical limit is a function of the packaging and connecting techniques. In microwave packaging, frequencies over 10 GHz are possible.

The tunnel diode amplifier operates by virtue of the fact that when the source and load conductance are made very nearly equal in magnitude to the negative conductance of the tunnel diode at the chosen bias point, the total conductance of the circuit is near zero (resistance very high). Therefore, a small varying signal introduced into the circuit (e.g. the source) results in much larger signal variations at the individual components of the circuit (e.g., the output). When the tunnel diode is connected in parallel with the source and the load, the voltage gain is unity and the current gain may be up to 30 dB. If the connection is series, the current gain is unity and the voltage gain may be up to 30 dB.

The primary advantages of the tunnel diode amplifier are high frequency capability, low power consumption, low noise, and circuit simplicity. The disadvantages are relatively low power output, a large dependence on all conductances (source, diode, and load) remaining constant over the entire operating environment, and the resulting necessity for temperature compensation.

The main application of the tunnel diode amplifiers is the first RF amplifier in microwave receivers.

The tunnel diode oscillator differs from the amplifier only in the value of the total series resistance of the circuit. It has the same advantages and disadvantages as the amplifier except that impedance matching over the environmental range is not as critical. The circuit must be designed to oscillate at the most critical environment and temperature compensation is determined by the frequency stability requirements. If these requirements are severe, crystal control may be used.

Two types of oscillations are possible. Sinusoidal oscillations utilize only the relatively linear portion of the negative conductance region. Harmonic content is held to a minimum, but as a consequence, the output power is quite low. Greater power output at the expense of considerable harmonic content can be achieved with relaxation oscillations which traverse large portions of the static VI characteristics of the diode.

The tunnel diode circuit may operate as a mixer-converter by simultaneously performing oscillation at the LO frequency, amplification at the RF frequency, mixing due to non-linearity, and amplification at the IF frequency.

Another two-terminal active device is the avalanche diode. With these diodes, microwave oscillation or amplification is obtained by biasing into the avalanche (Zener) breakdown region. The efficiency and power output are superior to Gunn devices, but a very high noise figure and frequency instability overshadow the advantages. Presently several researchers are categorizing the noise cause and effects. In one case, avalanche diodes show promise as a source for standard noise generators.

C. LINEAR INTEGRATED CIRCUITS

Current linear integrated circuits are fabricated using monolithic silicon epitaxial construction and will perform well in the frequency spectrum from dc to 200 MHz. Within this frequency range, the monolithic linear integrated circuit satisfies many functions required in receiver design. A standard operational amplifier or balanced differential configuration will perform such functions as amplification, limiting and mixing. Performance may be varied by changing external biasing or feedback configurations; therefore, a degree of circuit standardization is offered the circuit designer. The use of integrated configurations also offers the designer an increase in reliability as the number of interconnections to the active element is reduced by the monolithic diffusion process.

Operation at higher frequencies normally requires the use of thin-film hybrid processes. Although, monolithic microwave structures are feasible in theory this technology is not sufficiently developed. Presently, the semi-conductor substrate employed in monolithic fabrication presents a lossy structure at higher frequencies. As microwave frequencies are approached, the conventional passive networks require transmission line construction which present matching and isolation properties. These problems are overcome by use of thin-film processes which have provided circuits that have been successful in microwave applications.

D. THIN FILMS

As a specialized area of thin film technology, microstrip construction offers many advantages to circuit design. Even though no exact theoretical analysis of the parameters of microstrip exists, they have been determined experimentally with a sufficient degree of accuracy to ensure reliable design. The primary advantage of the microstrip is that it is deposited in a single plane and, therefore, can make direct connection to other deposited components. In similar fashion, external connections such as those from a chip device may be made easily and with the shortest possible leads.

The characteristic impedance of a microstrip is determined by the width of the line, the width of the substrate, and the dielectric constant of the substrate. This constant may range from 20 to 100 ohms with substrate materials such as silicon and ceramic. For a given substrate, the characteristic impedance is directly proportional to the $\frac{W}{h}$ ratio, where W is the width of the conductor and h is distance from the conductor to the ground plane, i.e., the substrate thickness.

The ratio of a wavelength in free space to a wavelength in the microstrip is for all practical purposes, constant in the 1—10 GHz range for a given characteristic impedance and dielectric substrate. The ratio decreases as the characteristic impedance increases and/or the dielectric constant decreases.

Another important consideration is the loss per unit length of microstrip. Loss is a function of resistivity and substrate temperature and it decreases as the resistivity increases. This loss is relatively constant from 0—100°C but increases beyond this range.

In applications where extremely small size is important, it is possible to use very high dielectric material. By increasing the dielectric constant from 10 to 100 the guide wavelength of a 50-ohm microstrip line can be reduced by a factor of 0.35. However, in many cases, the disadvantages will outweigh the advantage of decreased size.

The thermal conductivity of all the present high-dielectric materials is very poor. High characteristic impedances cannot be obtained because the width of the conductor must be very small or else the substrate thickness must be relatively large. A thick substrate is not desirable from the standpoint of heat dissipation.

In some cases it is desirable, from the standpoint of size or performance, to use lumped element components. These components are small enough so that distributed effects play no part in their operation. In the microwave region inductors may be fabricated by a small thin-film spiral with a diameter on the order of 0.060 inches or smaller. Capacitors and resistors may also be deposited onto the same substrate making an entire circuit to which the active elements may be chip mounted.

E. FERRITES

Ferrite materials exhibit ferromagnetic properties which are particularly applicable in the design of such microwave components as circulators and isolators.

The electrical behavior of a ferrite substance is specified by its complex permeability which is different for opposing circular polarization. Thus, a right circular polarized wave has different transmission constants through a ferrite sample than a negatively circular polarized wave. This nonreciprocal electrical property principle is employed to construct circulators and isolators. In the case of an isolator, this property allows transmitting a microwave signal with a minimal amount of transmission loss and prevents reflections from the load from interacting with the generating source. For circulators, this property accounts for the circulation of the applied signal to the respective ports.

For high frequency operation, ferrite dimensions on the order of 0.5cm are required. This size is compatible with integrated circuitry. The dc magnetic bias requirements are not excessive due to present high remanent ferrite materials and X-band integrated circulators are easily feasible. Integrated X-band isolators have not been reported in the literature, but such devices are also feasible.

Preparation of fine grain ferrite materials have resulted in an order of magnitude increase in the power absorption threshold, P_{cric} of ferrite materials. Thus, ferrites devices may now be devised which are capable of higher peak power handling capabilities. Previously, the small external fields required to achieve resonance would not saturate the ferrite sample and operation in the VHF range was impractical. Synthesized hexagonal ferrite of polycrystalline compounds have high values of magnetic anisotropy. Thus, smaller external magnetic fields are required for saturation and operation at lower frequency ranges are more easily obtainable.

F. FILTERS

Conventional design of microstrip ceramic parallel coupled filters at lower microwave frequencies results in physical configurations that may lead to cracking and mechanical instability. Attempts to circumvent this problem and to reduce the total length led to "folded" and vertical folded configurations having the same performance characteristics as the conventional design. Development work on two such folded 3-pole filters, indicates that the performance characteristics of the conventional design can be maintained.

Bandpass filters exhibiting extremely steep rejection skirts can be realized by means of a composite bandpass, bandstop filter. Employing a pair of band rejection filters in the composite structure, reduces the number of resonators required to achieve a given response, and permits lower midband insertion loss, and lower Q resonators.

In recent years, magnetically tunable filters constructed with such ferromagnetic materials as yttruim iron garnet (YIG) and galluim substituted YIG (GAYIG) have attracted attention. These devices have unloaded Q's greater than 1500 in a 600-MHz to 12-GHz frequency range, resulting in narrow bandwidths and low insertion loss. These filters are capable of being electronically tuned by an external magnetic field.

G. MIXERS

Microwave receivers generally require a mixing operation in order to translate the RF signal to a lower frequency where gain may be readily achieved. The mixing of the RF signal with a signal produced by a local oscillator produces a different frequency which effectively converts the incoming signal to a lower frequency. At microwave frequencies, the mixing process is conventionally accomplished by utilizing the nonlinearities of Schottky barrier mixer diodes. The nonlinearity of these diodes produce undesired spurious responses which, to some extent, may be reduced by proper filtering. In the case where two diodes are employed in the mixer configuration, an improvement is spurious reduction is achieved by applying different biasing voltages to the individual diodes. This technique reduces the higher ordered terms appearing in the power expansion expression for diode non-linearity.

The inherent intrinsic properties of the diode contribute a conversion loss to the mixing process which degrades its noise performance. In receivers where RF gain precedes the mixer stage, the noise figure performance of the mixer is not significant, but when RF gain is lacking the noise figure of the mixer causes concern. The conversion loss of modern planar junction Schottky barrier diodes is much lower as compared to older crystal point contact diodes. The major contribution to conversion loss is the series resistance of the diode. In modern diodes made of silicon and galluim arsenide, the series resistance is typically much less than 10 ohms as compared to the 50 to 100 ohms for crystal point contact diodes.

Another consideration in mixers is the proper termination of the image frequency. The broadband mixer will respond equally well to an image frequency which increases conversion losses and degrades noise performance.

A balanced mixer using a hybrid-ring configuration in which the image frequency was terminated into an open circuit and in which the RF losses were carefully controlled, the measured noise figure was 2.0 dB. Balanced S-band mixers built by Texas Instruments as a complete integrated structure on a ceramic substrate, in the developmental stage, had measured noise figures of 6.8 to 7.0 dB.

At frequencies within the VHF range, the Field-Effect-Transistor, FET, may be used as a mixer to provide conversion gain, low noise figures, and a minimum of cross-modulation. The nearly ideal square law transfer function for the FET reduces the spurious intermodulation products for this type of mixer (as compared to the diode or bipolar transistor stage).

SECTION III

TRANSISTORS

A. GENERAL

In Scientific Report No. 1, the basic principles of transistor construction which characterizes high frequency performance were considered. This section extends the discussion to the noise mechanisms inherent to high frequency devices. Recent developments in interdigital structures which permit power generation at microwave frequencies and low noise silicon and germanium devices developed since the earlier study are also discussed.

The performance of an S-band power amplifier and the noise characteristics of a low noise S-band preamplifier given in the section demonstrates the higher frequency performance obtained with active devices since the reporting of the integrated 500 MHz IF amplifier in the first report.

Research at Texas Instruments directed toward extending the frequency response and power handling capabilities of microwave transistors has resulted in diffusion processes and geometries that permit developmental silicon devices to have 7-dB power gains at 4.0 GHz[1,2] and germanium devices to have 5.4 dB noise figures at 4.0 GHz[3]. The advances in semiconductor technologies are reviewed in the following paragraphs.

1. Germanium

Advances in the alloy diffused planar process allows the same order of dimensions, tolerance control, and geometry in germanium that previously existed in the production of silicon transistors. Although germanium is the best material for achieving the highest maximum frequency of oscillation, f_{max}, in semiconductors, these transistors were limited by base and emitter stripes large enough to allow bonding to wires. Now, advances in the planarization technique allow bonding to expanded contacts, thus, freeing stripe size from the limitation[3].

Commercially available PNP planar germanium transistors such as the TIXM105 which offers low noise and high gain up to 2.25 GHz, and experimental NPN double diffused planar devices with noise figures of 5±0.5 dB and gains greater than 6.5 dB, have been achieved consistently at 3 GHz[4]. These latter devices have exhibited cutoff frequencies in the range of 7-8.5 GHz[5].

2. Silicon

Silicon remains the major semiconductor material used for power generation at high frequencies. In the past, low noise microwave transistors made of silicon could not compete with the low noise performance of germanium, but late developments in new geometries, have brought the noise figure of silicon devices to within 0.25 dB of that offered by planar germanium devices.

3. Gallium Arsenide

Gallium arsenide transistors were briefly discussed in the first scientific report and it was mentioned that these transistors are characterized by high noise figures. The development of these transistors as power devices has not been fully realized and the low noise requirement makes these transistors unsuited for receiver applications.

4. Field Effect Transistors

The low noise and low cross-modulation distortion properties of insulated gate and junction FET's are very useful in many receiver applications; however, the state-of-the-art of these devices does not extend to microwave frequencies. The present useful frequency region extends to L-Band. In this frequency range, the FET performs well as an RF amplifier or mixer for UHF systems and in high frequency IF stages of microwave receivers. A practical application of these devices is in stages requiring gain control because these devices afford ease of control in various AGC modes of operation.

B. BASIC CONSIDERATIONS

The question whether an ultimate physical limitation exists which places an upper bound on the frequency and power capabilities of microwave transistors should be examined. Such a theoretical limit has been shown to exist[6] and it is related to material parameters which are independent of device design. The relationship is given in Equation (1).

$$V_m f_T = K \tag{1}$$

where K equals 2×10^{11} volts/sec for silicon or 1×10^{11} volts/sec for germanium. V_m is the maximum allowable applied emitter-collector voltage. The parameter f_T is the charge-carrier transit-time cutoff frequency, more commonly called the gain-bandwidth frequency, and is defined:

$$f_T = \frac{1}{2\pi\tau} \tag{2}$$

where τ is the transit time for a charge carrier to transverse the emitter-collector distance while moving at an average velocity. This relationship defines the upper cut-off frequency since the minimum value of V_m must have some value, say one volt, that is sufficiently greater than thermal noise voltage to ensure normal transistor action of the base collector junction. Thus, for silicon devices, a theoretical upper limit of 200 GHz is determined, and for germanium, the highest obtainable frequency would be 100 GHz. In a practical sense, these frequencies would be less than that indicated because of such assumptions regarding uniform electric field stresses and carriers velocities are made in deriving Equation (1).

For maximum power gain at high frequencies, the magnitude of rb'Cc becomes important. This is demonstrated in the familiar expression for the maximum available power of a common emitter stage given in Equation (3).

$$PG = \frac{f_T}{8\pi f^2 r_b' C_c} \tag{3}$$

where f = frequency of operation
f_T = gain bandwidth frequency in MHz
r_b' = base spreading resistance in ohms
C_c = intrinsic collector capacitance in pfd.

The f^2 term implies a 6-dB per-octave roll-off of power gain as stated previously[7].

This equation may be solved for a particular frequency at which the stage power gain is equal to unity. The result is a frequency denoted as f_{max}. Thus,

$$f_{max} = \sqrt{\frac{f_T}{8\pi r_b' C_c}} \tag{4}$$

Since the power gain is unity at this frequency, f_{max} represents the maximum frequency of oscillation of the transistor.

It is evident that extending f_{max} requires extending f_T, which is related to base width because the charge-carrier transit time is dependent upon the distance that the base vicinity carriers must travel. Thus, one of the most important frequency limitations is base width. Presently this base width is controlled in the diffusion process where base widths as low as 0.25 micron have been realized[5]. Thinning the base increases r_b'. In experimental NPN germanium devices, the base resistances are 100-200 ohms[8] and means to reduce these values while maintaining f_T constant are being examined. In addition, the emitter junction area should be as small as possible to achieve the smallest emitter junction capacitance consistent with the allowable current rating.

Geometries used in microwave power transistor create thermal problems since the heat which must be dissipated is confined in a very small area. To overcome the problem of heat dissipation, power devices were evolved from scaling up the small area (7 mil^2) of the low power transistor. Scaling to a larger area must be done without sacrificing the high frequency parameters; i.e., f_T and the $r_b' C_c$ product must remain constant[8]. However, the collector capacity will increase roughly in the ratio of device areas.

A successful approach to scaled is to make a larger number of interdigitated fingers in one structure. This has been accomplished, keeping the emitter and base stripe width and spacing to 0.2 mils. Electrically it is more efficient than using a number of small active areas spaced apart but connected electrically by a metalization pattern over S_iO_2. Thermal resistance problems arising from the former technique can be minimized by choosing a suitable length-to-width ratio for the geometry.

C. POWER GENERATION WITH MICROWAVE TRANSISTORS

Recent advances in diffusion processes have extended the state-of-the-art of silicon devices in the field of power generation and amplification at microwave frequencies. From such advances and from the continuing research at Texas Instruments, the L187 silicon epitaxial geometry evolved making possible 7 dB power gain at 4.0 GHz without resorting to harmonic generation. These new developments in more complex diffusion techniques and base contacting systems[5] resulted from research under several programs currently conducted at Texas Instruments and are reported in the following sub-paragraphs.

1. L158 Geometry

The L158 family of silicon planar-epitaxial transistors consists of an 85-stripe device (L158 A), a 59-stripe device (L158 B) and a 17-stripe device (L158 C). Figures 1 and 2 show the configuration of L158-B and L158-C. The power output of a typical L158 device is shown, plotted as a function of frequency, in Figure 3. Extrapolating the power characteristics shown in Figure 3 at a theoretical 6-dB per octave roll off, it is seen the device provides useful power amplification between three and four gigahertz.

These devices have been used successfully on the MERA program in the fabrication of an S-band power amplifier. The performance of these devices as intermediate power devices in pulsed operation is shown in Table I. These power gains were obtained from a four-stage amplifier where the devices were cascaded to form a power amplifier operating at an S-band frequency of 2.25 GHz. The common base power gain versus frequency characteristic of each device is shown in Figure 4[9].

The L158A and L158C geometries have been successfully employed in a breadboard power amplifier configuration producing CW power outputs. The breadboard power amplifier utilized the L-158A device as a class A driver and as a class C power amplifier to produce a 1-watt power level at 2.25 GHz. The L158C device was also used as a class C amplifier shown in Figure 5. The power output of the L158A devices was limited to 540 mW to ensure safe heat dissipation of the device. The performance of the L158 devices is summarized in table II.

2. L187 Geometry

A silicon planar NPN epitaxial device, the L187 has resulted from changing the base contact system of the L146B geometry which was discussed in the first scientific report. The L187 was designed initially for use in a C-Band (5.0 GHz) oscillator. Typical common base electrical characteristics for a device housed in a TI-line* package are given in Table III.

The power gain performance of the L187 is given as a function of frequency in Figure 6. The oscillator performance of the L158 and L187 devices are compared in Figure 7. It may be seen that 1.0 watt of power output available at 2.0 GHz is generated by an oscillator employing the L158 device.

3. Other Microwave Power Devices

One approach to power generation at microwave frequencies is to use an overlay transistor[10]. The overlay construction is illustrated in Figure 8 and permits suitable scaling to large area geometry by increasing the emitter edge proportionally

*Trademark of Texas Instruments Incorporated

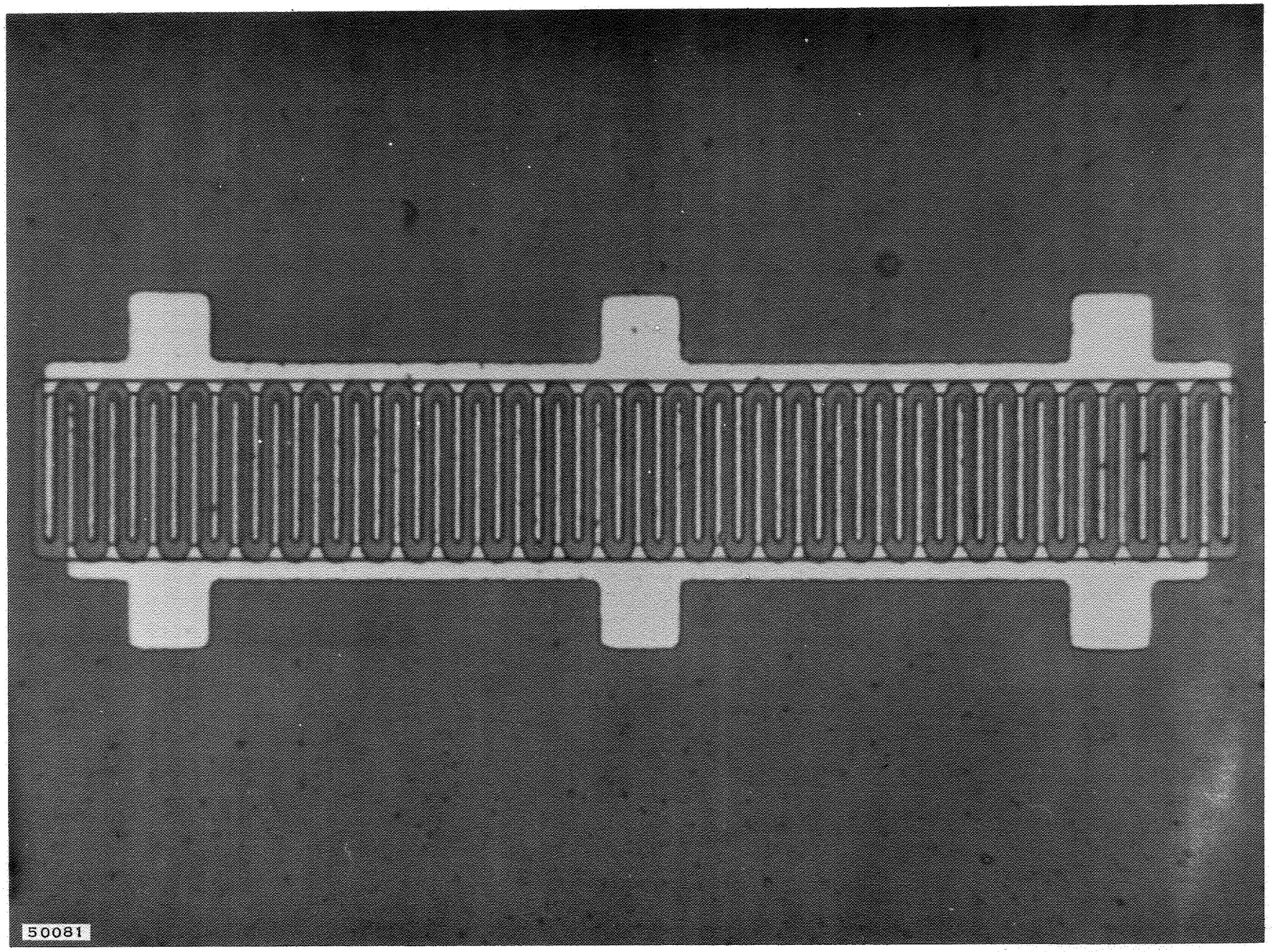

Figure 1. Photograph Showing L158B Geometry

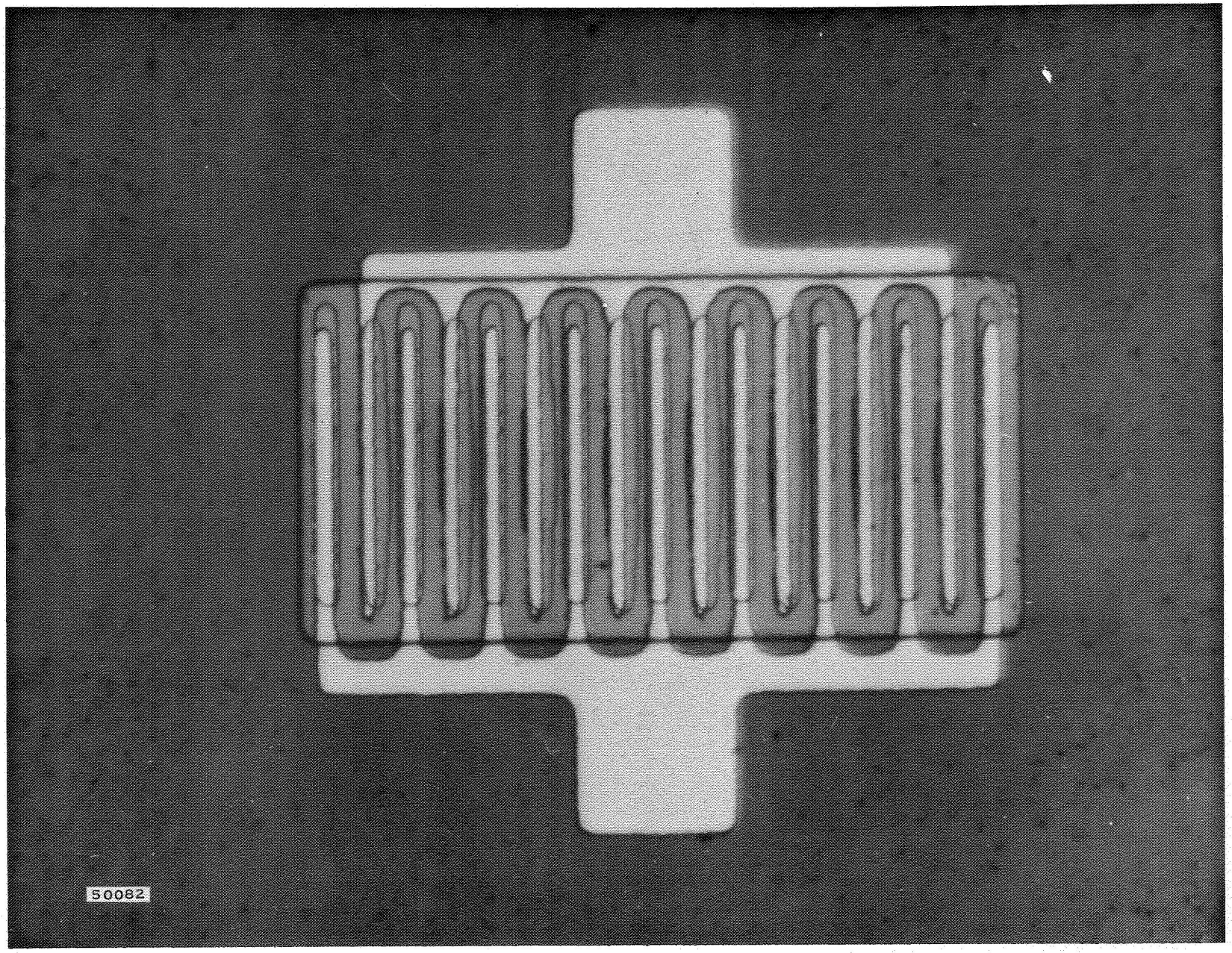

Figure 2. Photograph Showing L158C Geometry

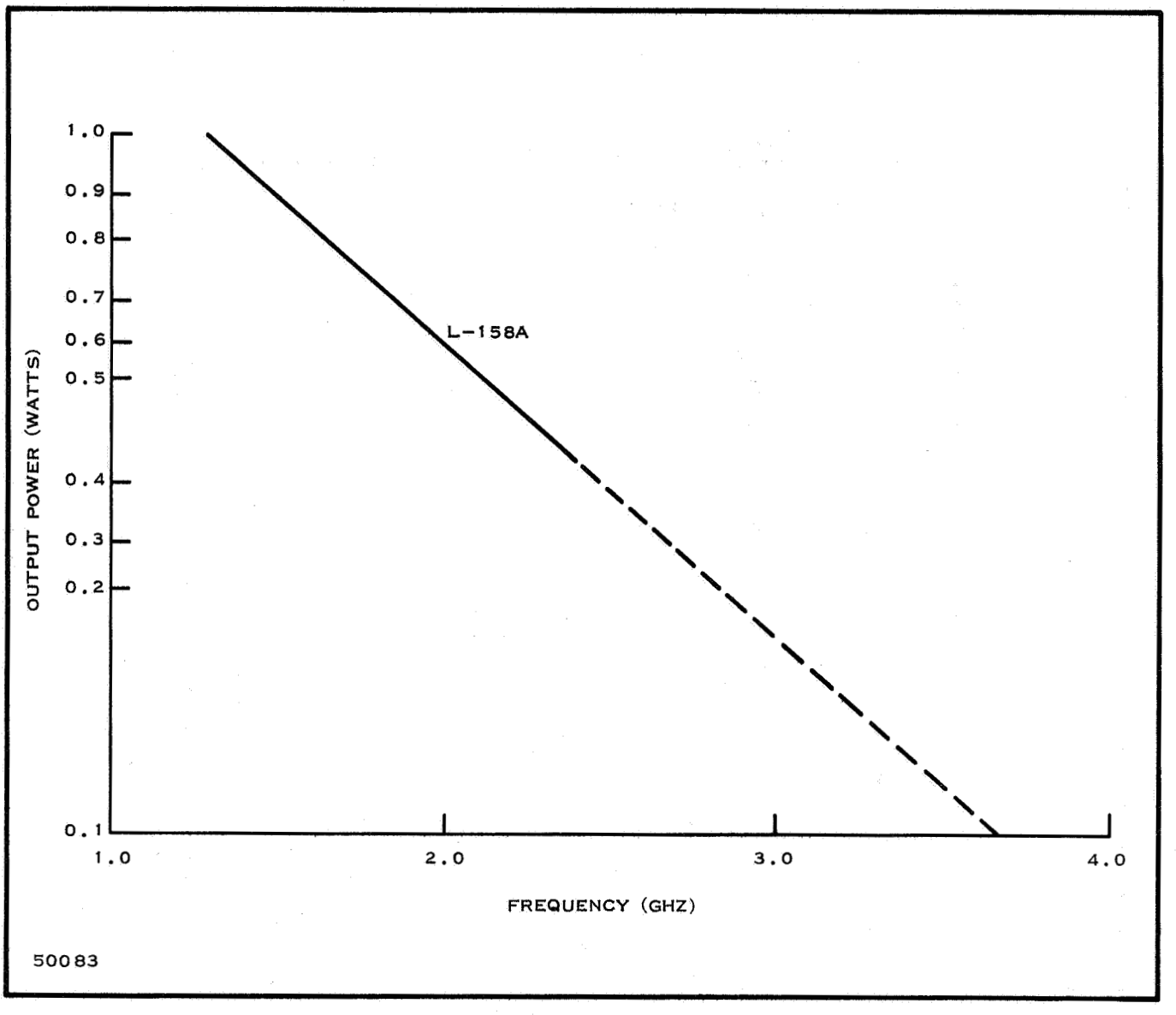

Figure 3. Typical L158 Transistor Output Power

Table I. Power Efficiency - L158 Family

Device	P out (Pulsed)	P in (Pulsed)
L158 A (85-stripe)	2000 mW	940 mW
L158 B (59-stripe)	1000 mW	360 mW
L158 C (17-stripe)	350 mW	57 mW

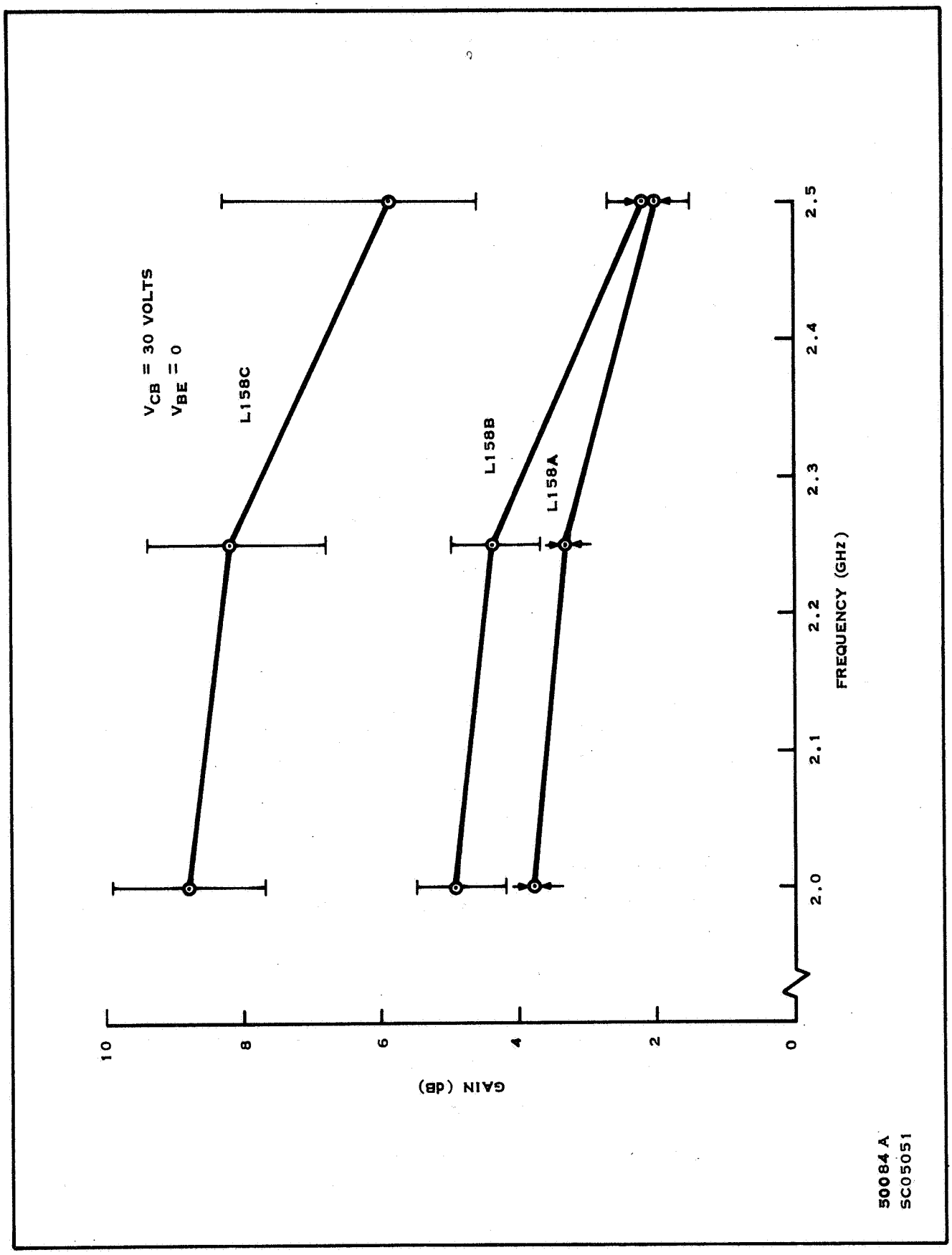

Figure 4. Power Gain of L158 Family

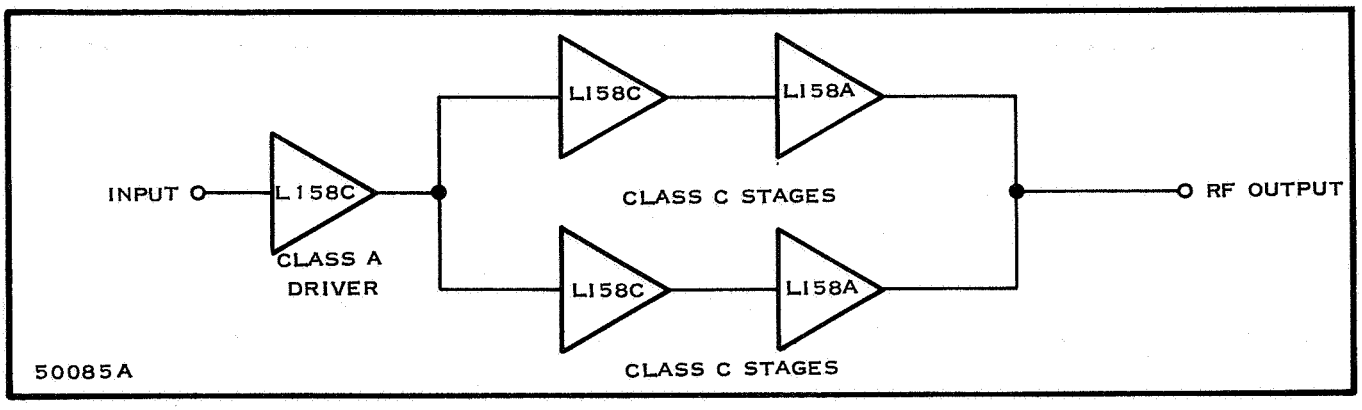

Figure 5. Class C Amplifier Using L158C Devices

Table II. Performance of L158 Devices

Frequency, 2.25 GHz, V_{cc} = +24 Vdc Device	P_{in} mW	P_{out} mW	I_c mA
L158 C, class A driver	30	255	23
L158 C, class C amplifier	59	270	30
L158 A, class C amplifier	257	540	96

Table III. Parameters of the L187

Parameter	Conditions	Minimum	Typical
BV_{CBO}	I_c = 10 mA, I_E = 0	30V	
h_{FE}	V_{CE} = 10V, I_C = 15 mA	10	
Po	V_{CC} = 15V, I_C = 30 mA f = 4.0 GHz	30 mW	40 mW

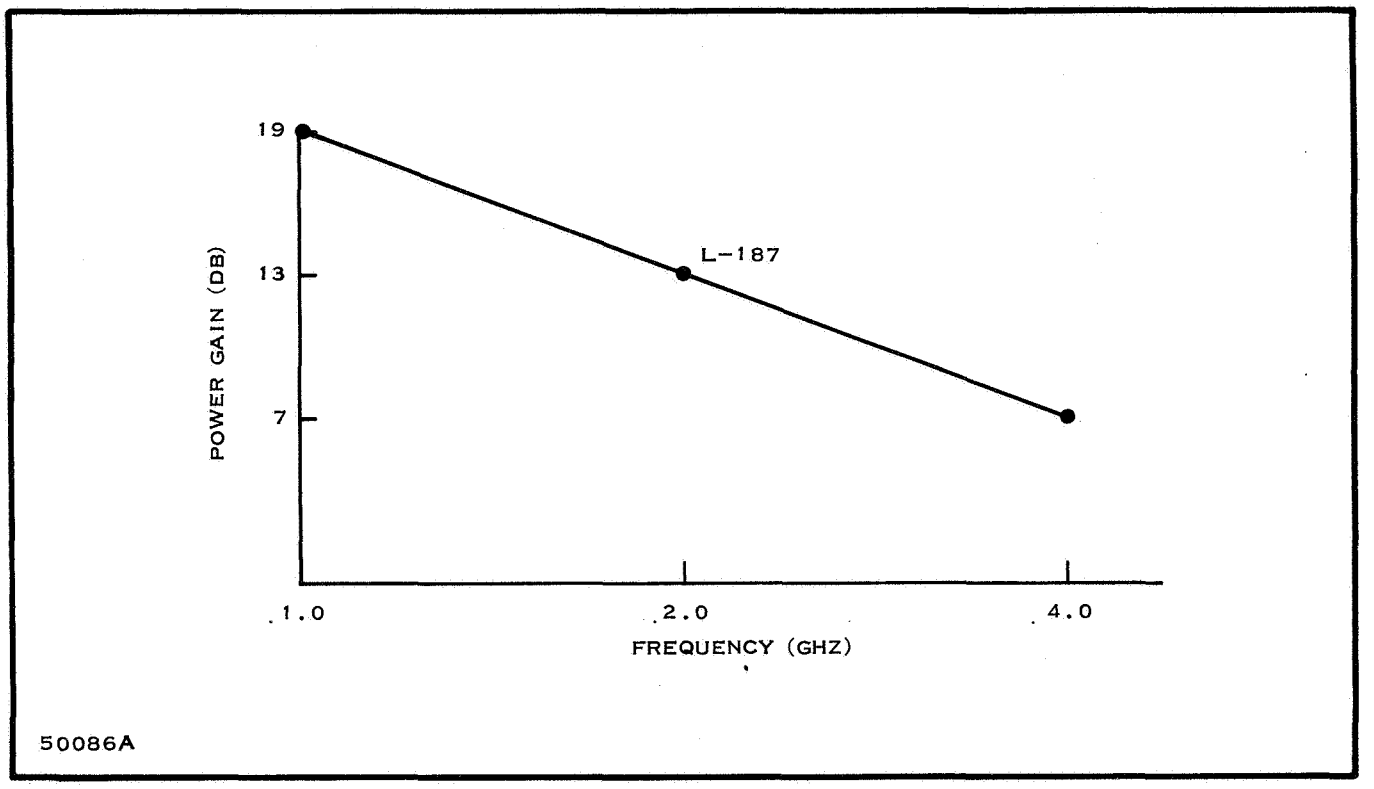

Figure 6. L-187 Performance

as the emitter area is increased. The high currents required of a transistor operating at high power outputs are handled easily by the increased ratio of emitter periphery to emitter area.

The new emitter electrode overlay was first used in the 2N3375 transistor, and is now used in a new unit, the 2N4012 transistor[11]. Both transistors are NPN planar epitaxial with a collector area of 400 square mils, emitter area of 40 square mils, and an emitter edge of 300 mils. The 2N3375 generates three watts at 500 MHz, and the 2N4012 can provide more than 2.5 watts at a frequency of one gigahertz with an efficiency of 25 percent or higher when used as a tripler. The power performance of the two devices are plotted versus frequency in Figures 9 and 10. From Figure 10, the 2N4012 used in the common emitter configuration delivers three watts of output power at 800 MHz when used as a doubler[12]. It supplies 2.7 watts at 1-GHz when used as a tripler and delivers 1.7 watts at 1.2-GHz when used as a quadrupler. State-of-the-art power output capabilities achieved in an overlay transistor operated at 28 volts are shown in Figure 11. Continuous power outputs of 20 watts at 400-MHz, 18 watts at 500-MHz, 7 watts at 1-GHz, and 1 watt at 2-GHz have been obtained with developmental units.

D. HIGH FREQUENCY FIELD EFFECT TRANSISTORS

The metal-oxide semiconductor field effect transistor (MOS-FET) and junction FET's high frequency performance has been extended to L-Band as a result of the technology advances in the fabrication of silicon microwave transistors[14]. The FET is particularly well suited in many VHF and UHF receiver stages requiring high input impedance, low cross-modulation distortion and low noise. The devices are

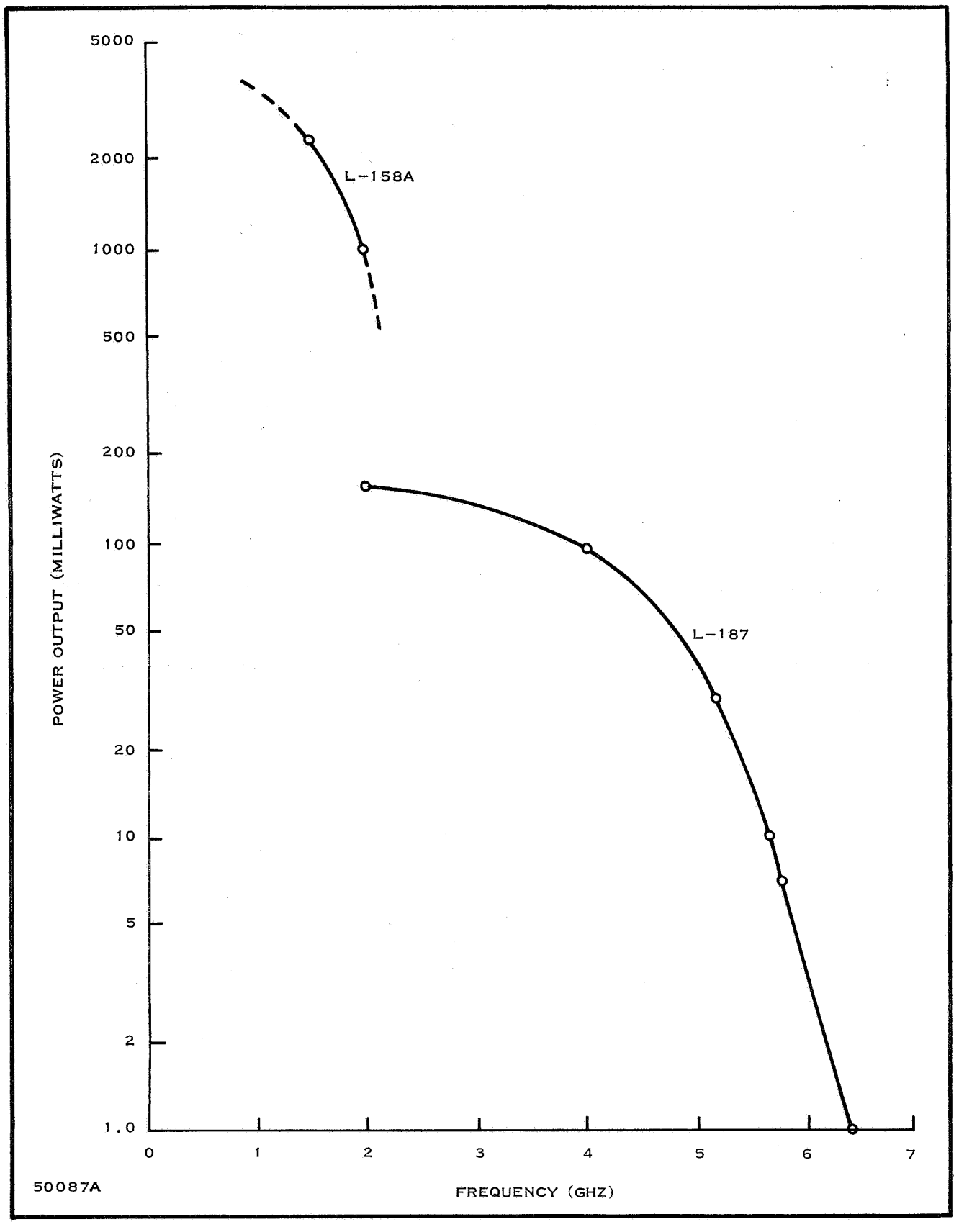

Figure 7. Oscillator Performance of the L187 and L158 Devices

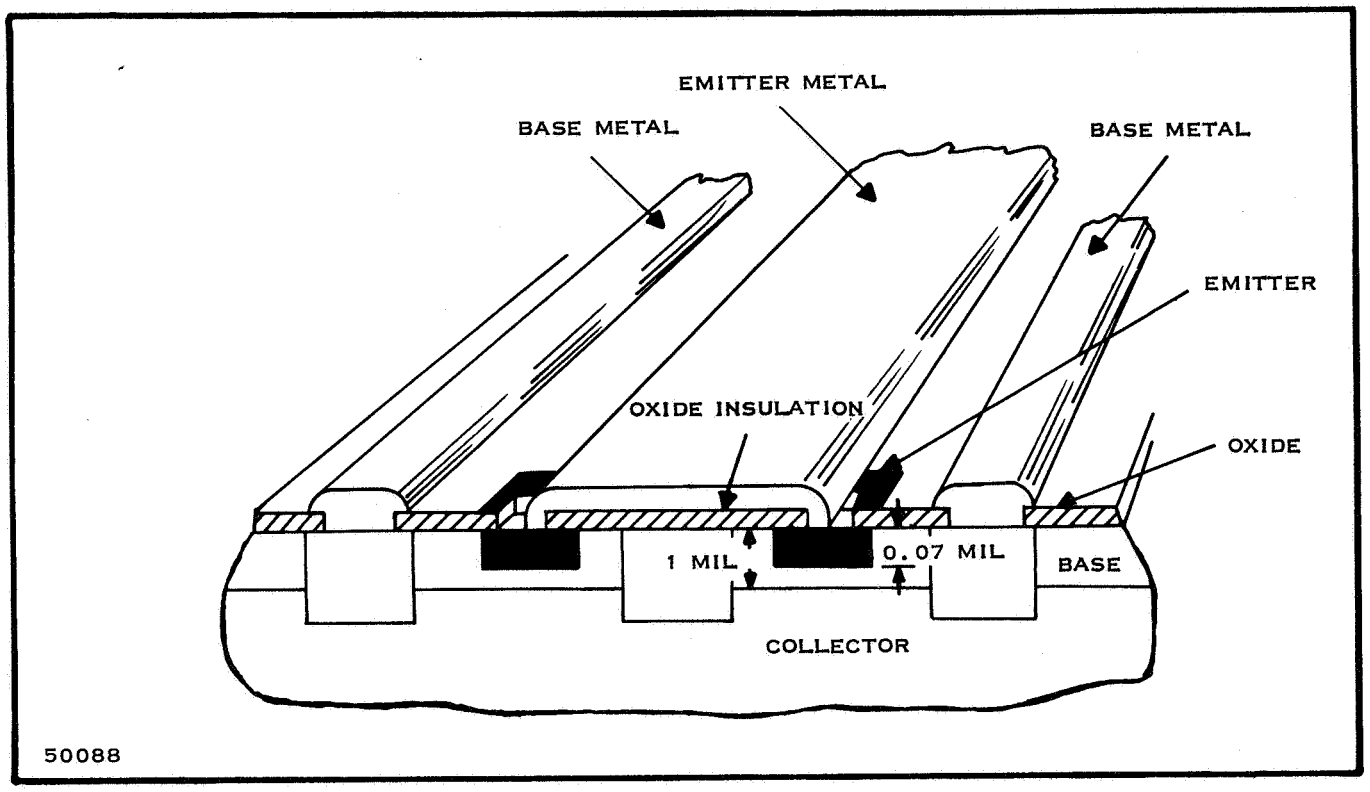

Figure 8. Cross-Section of Silicon Overlay Power Transistor

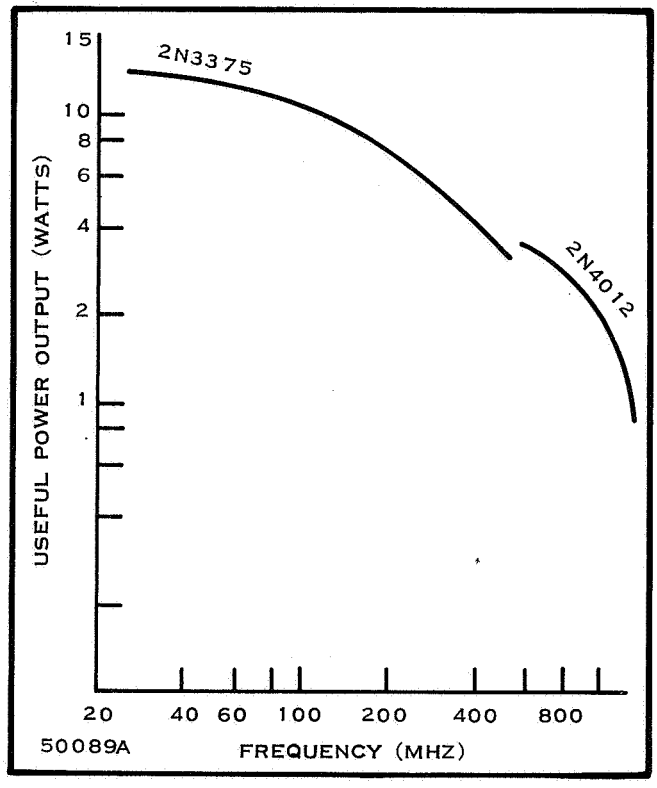

Figure 9. Power Performance for Overlay Transistors

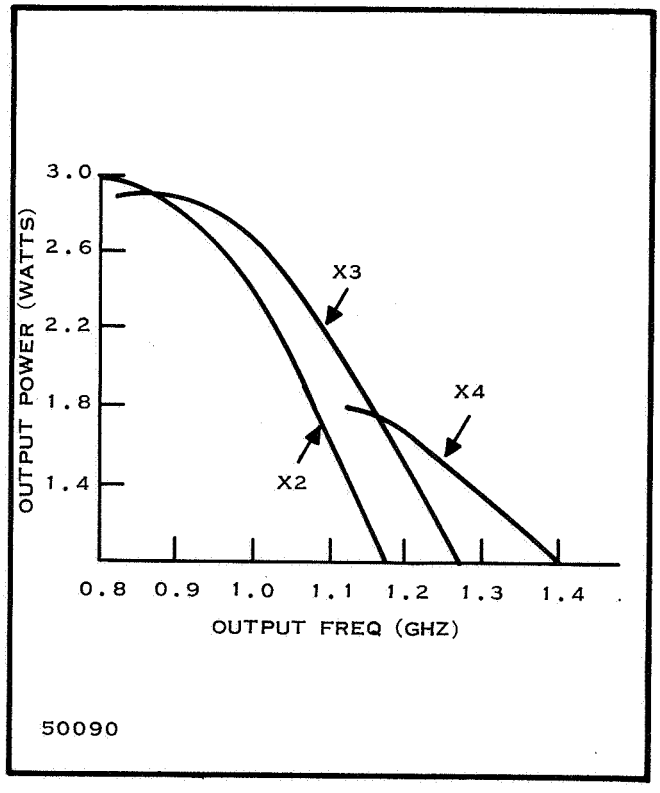

Figure 10. Power Performance of 2N4012 Harmonic Amplifier

especially well suited as IF and audio amplifiers and can be controlled in either forward or reverse AGC modes. Present commercially available FET's have gain bandwidth products of 75 to 100 MHz so that low noise, low distortion amplifiers and mixers in the VHF region are practical. Developmental FET's have been reported with larger gain bandwidth products that work satisfactorily at 1 GHz as amplifiers and oscillators and the commercially available 2N3823 has been used for a 900 MHz common-gate amplifier [15].

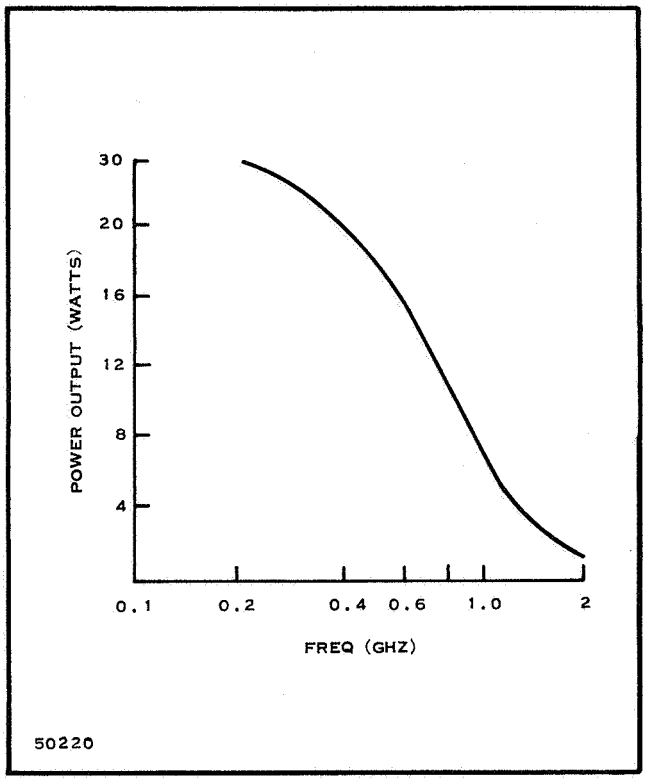

Figure 11. State-of-the-Art Performance of Overlay Transistor

A field effect transistor (FET) is essentially a semiconductor current path whose conductance is controlled by applying an electric field perpendicular to the current. A typical diffused field-effect transistor is shown in Figure 12a and its electrical equivalent diagram is shown in Figure 12b.

The devices consist of a single P or N type semiconductor bar with a contact at each end. N-type impurities are introduced into opposite sides of a P type bar as shown in Figure 12a. Contacts to the N type impurities provide the "gate" input. The contacts at each end of the bar are the drain and source connections. Comparing the FET to a vacuum tube, the "source" is analogous to the cathode, the "gate" corresponds to the grid, and the "drain" can be compared to the anode or plate. The field effect also has electrical properties similar to a vacuum tube, and as in vacuum tubes, the gain factor is expressed in transconductance, (gm). Amplification is achieved by the action of the majority of carriers within the device. For this reason, the FET is an unipolar device as compared to the bipolar junction transistor.

The construction of a high frequency FET is similar to that of the interdigitated bipolar transistor, and it is constructed in much the same fashion, except in the location of the junction relative to the terminals. To produce an n-channel device, a p-type silicon wafer with a resistivity of 3 to 10 ohm/cm is used as a starting material. A number of heavily doped n-type stripes are diffused into the surface. The ends of alternate strips are connected together and form the drain and source contacts. An insulating layer of silicon dioxide or silicon nitride is placed over the areas between the diffused n stripes. The thickness of this insulating layer is typically one to two thousand angstroms. A metalized layer is then deposited on top of the dielectric insulating layer to form the gate electrode. A cross section of this structure is shown in Figure 13. The electrical characteristics of a 2N4417 n-channel expitaxial planar silicon device is presented in Table IV. Operation of a FET can be better understood by considering a semiconductor bar having the dimensions as shown in Figure 14. The conductances through the length of the bar depends on the dimensions of the bar and the

conductivity of the semiconductor. The conductance of the bar is proportional to the total number of current carriers present. The latter being a function of large concentration of impurity atoms contributed by doping. If this concentration is uniform in every part of the bar, the conductance of the bar is

$$G_{10} = \frac{q \mu \ pWT}{L} \tag{5}$$

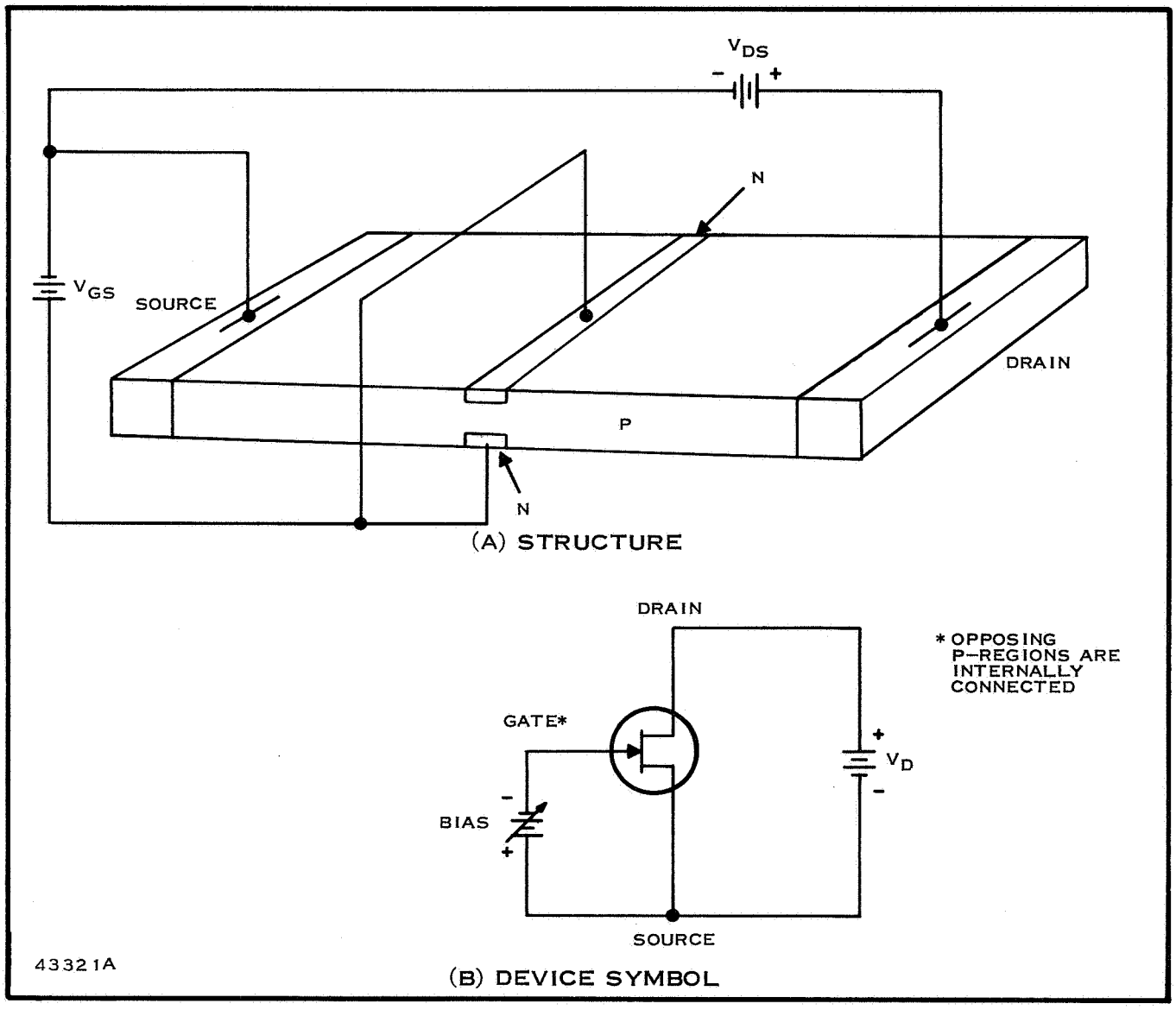

Figure 12. (a) Diffused FET Transistor, (b) Electrical Circuit

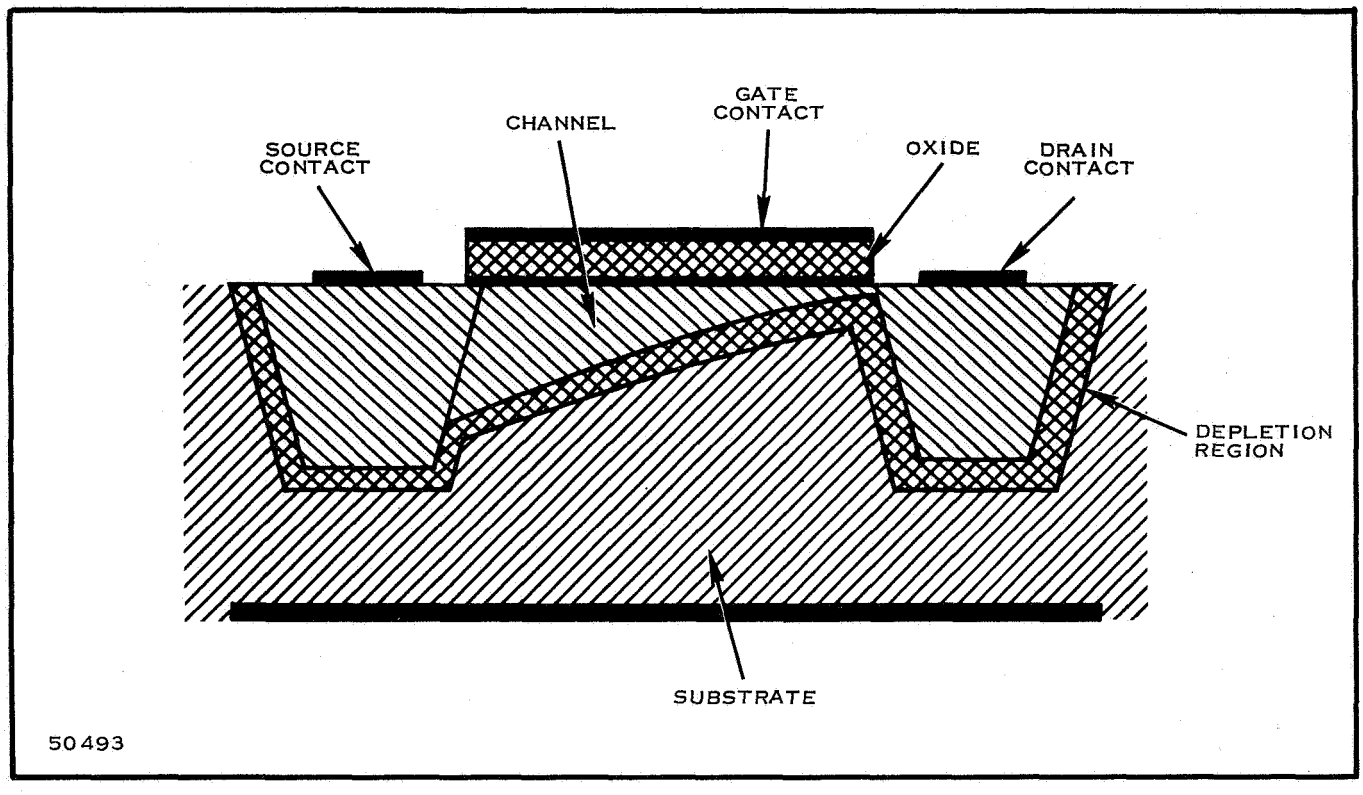

Figure 13. Cross-Section of Junction FET Device

where q = electronic charge, 1.6019×10^{-19} coulombs

μ = carrier drift mobility cm^2/volt-sec

p = impurity density, atoms/cm^3

As shown in Figure 12a, the diffused regions between the pn junction form the source and the drain terminals. The gate is a metallic layer evaporated on oxide surface which isolates the gate electrode from the semiconductor material, normally silicon. The region beneath the oxide layer forms a channel between the two diffused regions. Modulating this channel causes it to widen and extend into the high resistivity area formed by the p-doped semiconductor. The modulation of this channel width is used to realize transconductance in that the voltage applied to the gate terminal will vary the conductance (resistance) of the material in accordance with Equation (5). The FET described is known as the insulated gate or MOS (Metal Oxide Semiconductor) FET. It is a surface field-effect transistor, as compared to an unipolar or junction field-effect transistor.

The 2N3823 is a typical VHF/UHF junction FET usable to 500 MHz which may be used as a RF amplifier or mixer although recently application at 900 MHz has been reported[15]. At high frequencies, performance is governed by series resistance within the chip. The equivalent circuit and exact equations for such an FET are given below with some practical approximations[16].

Table IV. Electrical Characteristics
@25°C (UNLESS OTHERWISE NOTED)

	SYM.	2N4416 min.	2N4416 max.	2N4417 min.	2N4417 max.	UNITS	CONDITIONS
Gate Breakdown Voltage	$V_{(RR)\ GSS}$	-30		-30		V	$I_G = -1\mu A$, $V_{DS} = 0$
Total Gate Leakage Current	I_{GSS}		-100		-100	pA	$V_{GS} = -20$ V, $V_{DS} = 0$
Total Gate Leakage Current (150°C)	I_{GSS}		-100		-100	nA	$V_{GS} = -20$ V, $V_{DS} = 0$ $T_A = +150°C$
Drain Saturation Current*	I_{DSS}	5.0	15	5.0	15	mA	$V_{DS} = 15$ V, $V_{GS} = 0$
Pinchoff Voltage	$V_{GS\ (off)}$		-6.0		-6.0	V	$V_{DS} = 15$ V, $I_D = 1.0$ nA
Forward Transadmittance*	$\lvert Y_{fs} \rvert$	4500	7500	4500	7500	μmhos	$V_{DS} = 15$ V, $V_{GS} = 0$, f = 1 kHz
Output Admittance	$\lvert Y_{os} \rvert$		50		50	μmhos	$V_{DS} = 15$ V, $V_{GS} = 0$, f = 1 kHz
Small-Signal, Common-Source, Short-Circuit, Reverse Transfer Capacitance	C_{rss}		0.8		0.8	pF	$V_{DS} = 15$ V, $V_{GS} = 0$, f = 1 MHz
Small-Signal, Common-Source, Short-Circuit Input Capacitance	C_{iss}		4.0		3.5	pF	$V_{DS} = 15$ V, $V_{GS} = 0$, f = 1 MHz

* Pulsed Measurement Required. PW≈300 μsec, Duty Cycle≤1.0%.

Table IV. Electrical Characteristics (Cont)
@25°C (UNLESS OTHERWISE NOTED)

	SYM.	2N4416 min.	2N4416 max.	2N4417 min.	2N4417 max.	UNITS	CONDITIONS
Small-Signal, Common-Source, Short-Circuit Output Capacitance	C_{oss}		2.0		1.3	pF	V_{DS} = 15 V, V_{GS} = 0, f = 1 MHz
Small-Signal, Common-Source, Short-Circuit Input Conductance	RE (y_{is})		1000		1000	μmhos	V_{DS} - 15 V, V_{GS} = 0, f = 400 MHz
Small-Signal, Common-Source, Short-Circuit Input Susceptance	IM (y_{is})		10,000		10,000	μmhos	V_{DS} = 15 V, V_{GS} = 0, f = 400 MHz
Small-Signal, Common-Source, Short-Circuit Input Conductance	RE (y_{is})		100		100	μmhos	V_{DS} = 15 V, V_{GS} = 0, f = 100 MHz
Small-Signal, Common-Source, Short-Circuit Input Susceptance	IM (y_{is})		2500		2500	μmhos	V_{DS} = 15 V, V_{GS} = 0, f = 100 MHz
Small-Signal, Common-Source, Short-Circuit Output Conductance	RE (y_{os})		100		100	μmhos	V_{DS} = 15 V, V_{GS} = 0, f = 400 MHz

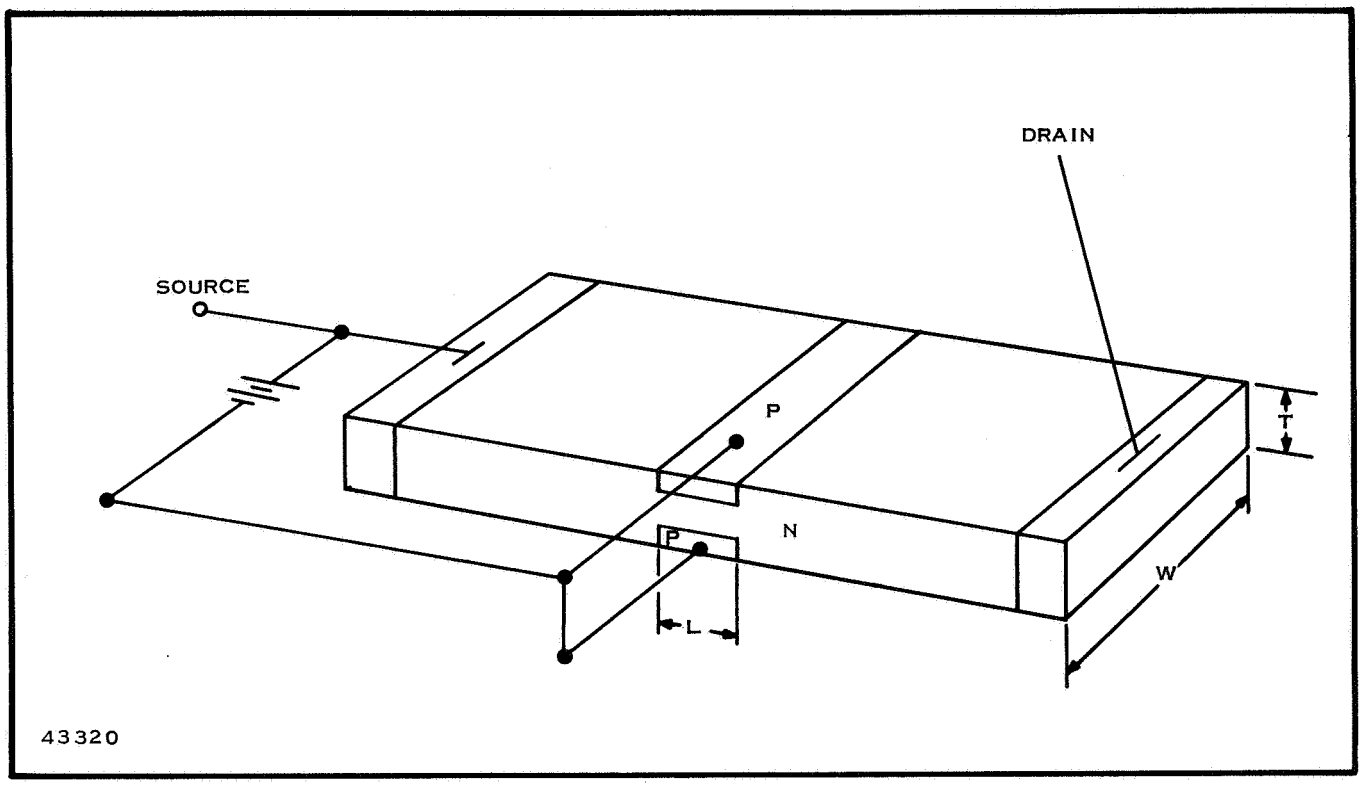

Figure 14. Semiconductor Bar

The equations for the common source VHF complex admittance parameters are approximated:

$$y_{11} = \omega^2 (Cgs+Cgd)^2 \; Rg + j\omega (Cgs+Cgd) \quad (6)$$

$$y_{12} = -\omega^2 \; Cgd^2 (Rg+Rd) - j\omega \; Cgd \quad (7)$$

$$y_{21} = gfs - j\omega \; Cgd \quad (8)$$

$$y_{22} = gos + \omega^2 \; Cgd^2 \; Cgd^2 (Rg+Rd) + j\omega \; Cgd \quad (9)$$

The input and output admittance transfer characteristics clearly show that the admittances increase as the square of the frequency (Figure 15). The power gain of a FET device may be defined as

$$P\,G_1 = 1/2\left[1 + \left(\frac{gm}{\omega C_3}\right)^2\right] \quad (10)$$

where gm is the transconductance and C_3 is the combined external gate to drain capacitance and channel to gate capacitance. As seen in Equation (10), increasing the ratio of gm/C_3 will increase the power gain. The high input impedance is the result of the gate source path and involves a reverse biased junction. As this junction is large in area, it presents a large input capacitance, thus, limiting the high frequency response. The gm term is high frequency dependent and can be expressed as

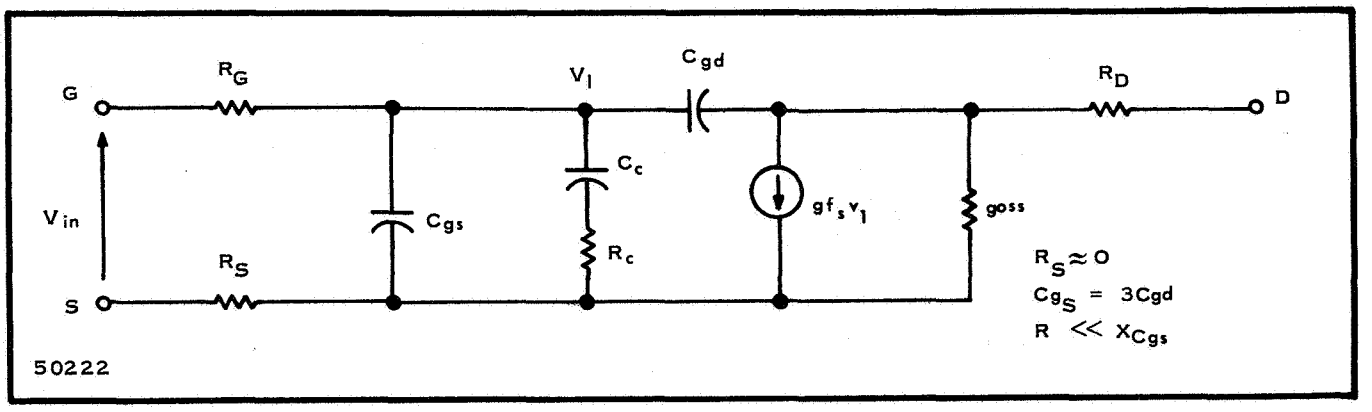

Figure 15. Junction FET Equivalent Circuit

$$gm\ (\omega) = \frac{gm_o}{1 + j\omega\, RC_G} \tag{11}$$

where gm_o = low frequency value of transconductance

R = series resistance of chip

C_G = gate to drain capacitance.

Two factors to consider in achieving a high gm is the requirement for large junction widening and a high gate area. The latter requirement necessitates a thin and narrow gate geometry. The gm cutoff frequency for the latest high frequency MOS-FET is in the order of one GHz and higher[17].

E. NOISE SOURCES IN MICROWAVE TRANSISTORS

1. General

The amount of noise inherent microwave semiconductor devices is an important consideration if the device is intended for receiver applications. This is especially true for microwave transistors as the noise contributed by the device adds significantly to the signal the transistor is amplifying. The noise figure, NF, expressed in decibels sets a figure of merit upon the noise performance of an active device. It is defined as follows:

$$NF = \frac{\text{total available noise power at output of device}}{\text{available noise power at output contributed by the generator source}} \tag{12}$$

which is the ratio of a noisy network to that of a noise-free or ideal network. At high frequencies, two commonly occurring noise mechanisms contribute to making the microwave transistor noisy; thermal noise and shot noise. Within a junction transistor, three noise sources are formulated from these noise mechanisms; shot noise in the base emitter junction, thermal noise resulting from the base resistance and shot noise in the collector-base junction.

Thermal noise phenomena, called "white noise" because of its similarity to the frequency spectrum of white light, is the result of spontaneous random

fluctuations of free electrons in a conductor. These random fluctuations are present even in the absence of an electric field and are solely a function of temperature. The random behavior of electron agitation gives rise to an instantaneous value of current; however, over a long period of time the average value of this current is zero. The mean-squared value of this current may be expressed in terms of the conductance associated with the conductor and is given in Equation (13).

$$\overline{i_{th}^2} = 4KT\, G_{th}\, \Delta f \tag{13}$$

where K is Boltzman's constant
T is temperature in degrees Kelvin
G is conductance in mhos
f is bandwidth in cycles following the conductor

For circuit applications, use can be made of Norton's constant current theorem and Equation (13) may be expressed as a mean-squared noise current generator paralleled by a noise-free conductance. This is shown in Figure 16. Since $i_{th} = V_{th}/R$ Equation (13) may be expressed in terms of mean-squared voltage[8].

$$\overline{V_{th}^2} = 4KTR\Delta f \tag{14}$$

This is the general expression for thermal noise voltage across the terminals of a device. Shot noise phenomena results from the random arrival of charges or carriers caused by diffusion when a current flow. The shot-noise energy associated with the stream of carriers is completely random with an uniform spectrum, and is proportional to the charge of an electron, the dc current and bandwidth. It may be expressed as

$$\overline{i_{SH}^2} = 2\, q\, Idc\, \Delta f \tag{15}$$

where q = charge (1.6×10^{-19} coulombs)

Idc = dc current in amperes

Δf = bandwidth in Hertz

Equation (15) is the same as the shot-noise due to the random emission of electrons from a heated surface such as the cathode of a vacuum tube.

The circuit representation of Equation (15) is the same as that for thermal noise where the mean-squared value of shot-noise current can be represented by a constant current generator paralleled by a noise-free conductance, G_{SH}, as shown in Figure 17[18].

G_{SH} is the incremental conductance of a PN junction and is representative of the dynamic resistance of a diode, r_d. This relationship is demonstrated in Equation (16)

$$r_d = \frac{1}{G_{SH}} = \frac{KT}{q\, I_{dc}} = \frac{25}{I_{dc\ (ma)}} \text{ ohms} \tag{16}$$

Since the shot-noise voltage, e_{SH}, is related to shot-noise current by the incremental conductance:

$$\overline{e_{SH}} = \frac{i_{SH}}{G_{SH}} \tag{17}$$

the equation for shot-noise mean-squared voltage may be derived from Equation (15) to be

$$\overline{e_{SH}^2} = 2\, K\, T\, rd\, \Delta f \tag{18}$$

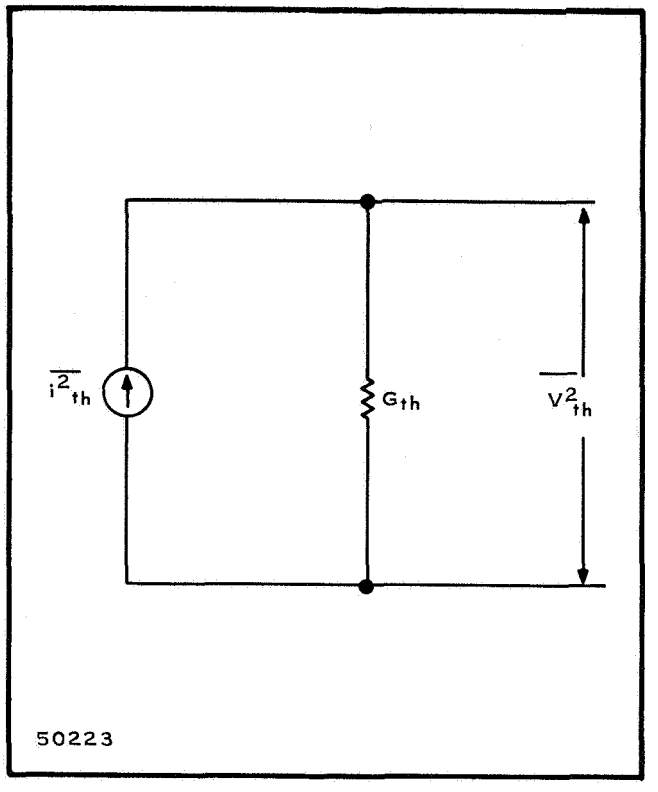

Figure 16. Circuit Presentation of Thermal Noise Current

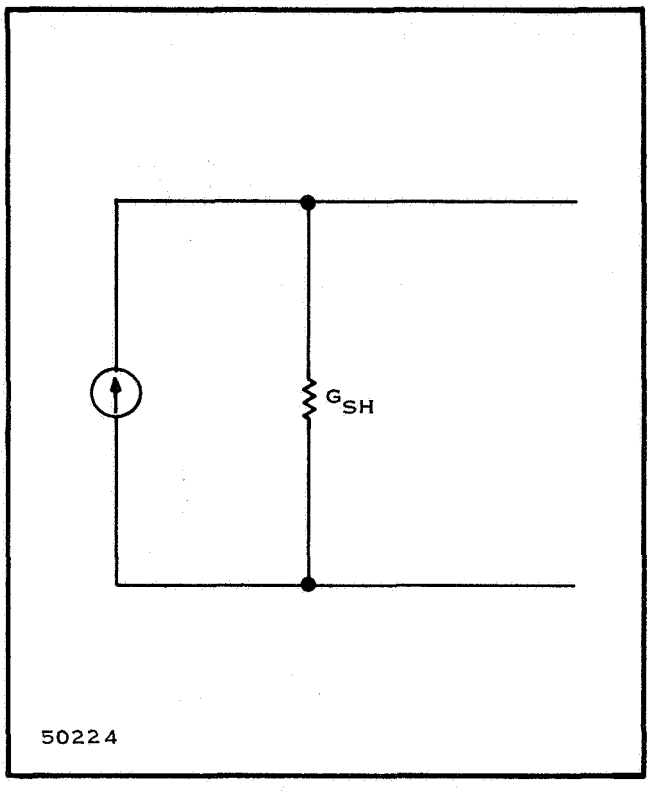

Figure 17. Circuit Presentation of Shot Noise Current

where the same constants which appear for thermal noise are present.

Equations (13) and (15) may be incorporated into a noise model for a junction transistor in a common-base configuration such as shown in Figure 18. In the noise model shown in Figure 18:

$\overline{i_p^2}$ = collector shot-noise current generator (includes noise from I_{CO})

$\overline{i_e^2}$ = emitter shot-noise current generator

r_e = emitter resistance, $25/I_E$ ohms

r_b' = base spreading resistance

r_c = collector resistance

$\overline{e_b^2}$ = base thermal noise equivalent voltage generator

α = common-base current gain

R_g = source resistance

I_{CO} = dc collector cutoff current.

The model is valid above 1 kHz and has been shown to be valid for the common emitter and common base configurations. The noise figure, NF, of a high frequency transistor has been derived from this noise model and given in the first scientific report. It is repeated in Equation (19).

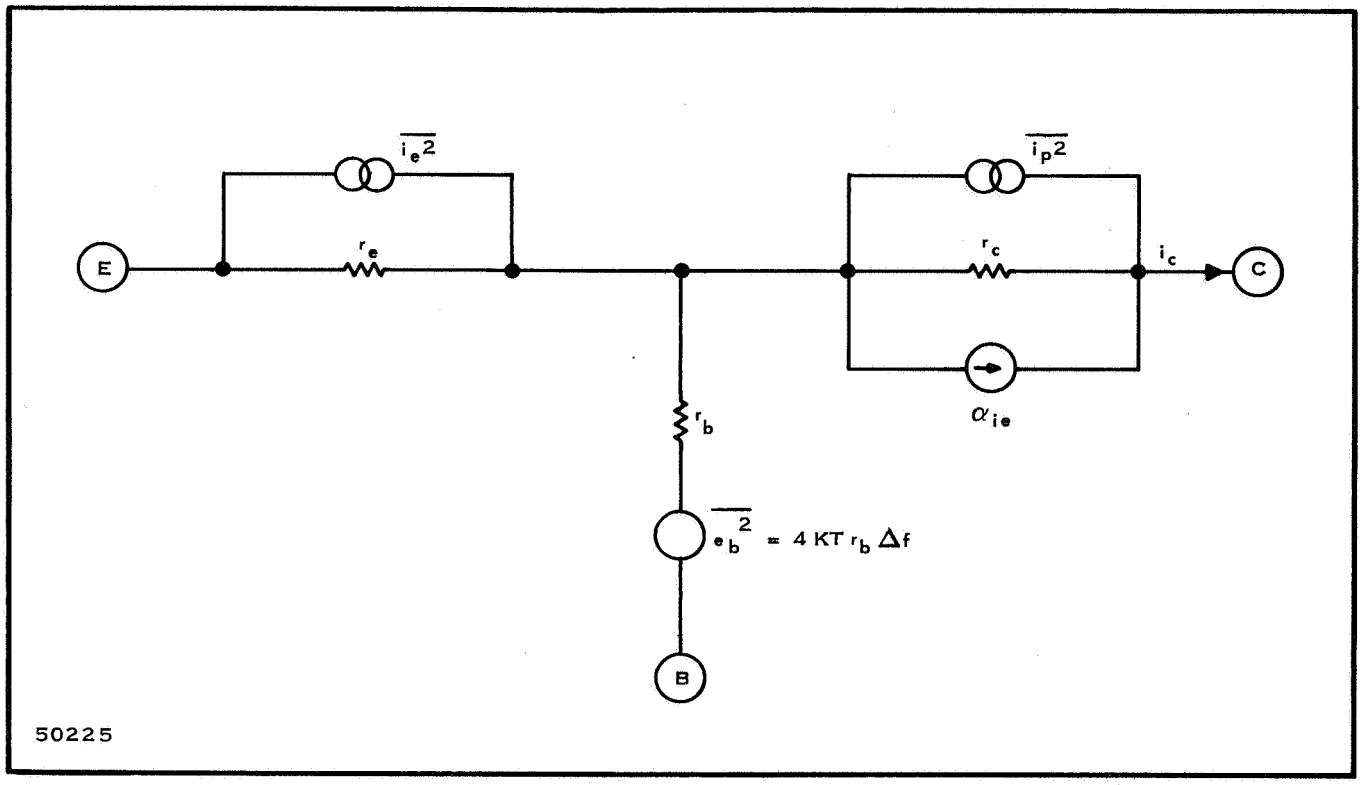

Figure 18. Noise Model for Junction Transistor

$$NF = 1 + \frac{r_b'}{R_g} + \frac{r_e}{2R_g} + \frac{(r_b' + r_e + R_g)^2}{2\alpha_o R_g r_e}\left[\frac{1}{h_{FE}} + \left(\frac{f}{f_\alpha}\right)^2 + \frac{I_{co}}{I_E}\right] \tag{19}$$

The f_α term expresses the alpha cutoff frequency where α the forward current gain, is reduced to 0.707 of its low frequency value, α_o. At this frequency, the $(\frac{f}{f_\alpha})^2$ term becomes predominant and results in the noise figure asymptotically approaching a 6-dB per octave slope. This may be accounted for in the noise model by allowing α, the forward current gain, to vary with frequency by replacing it with $\frac{\alpha_o}{1 + j\, f/f_c}$. Where f_c is the break or corner frequency.

At higher frequencies where the transit time of carriers becomes appreciable, a new conductance is introduced in the expression for shot-noise. This conductance parallels the existing conductance corresponding to dynamic resistance of the diode and is the result of carriers that cross the base-emitter junction towards the base, but return and recombine in the emitter region where they originated. The added conductance, G, is shown in Equation (20).

$$\overline{i_{SH}^2}\ (HF) = 2\,q\,I_{dc}\Delta f + 4\,KT\,(G - G_{SH})\Delta f \qquad (20)$$

2. Field Effect Transistor

The field-effect transistor (FET) is subject to the same types of noise found in conventional transistors. The noise mechanisms in the FET are quite similar to those in the diffusion transistor except for the part which capacitance plays. The noise model for the FET shown in Figure 19 accounts for the division of channel resistance[18].

In the noise model shown in Figure 19,

R_{CH} = channel resistance
r_d = dynamic drain resistance
r_s = incremental source resistance
C_{gd} = gate to drain capacitance
C_{gs} = gate to source capacitance
e_{th} = equivalent noise voltage generator
i_p = gate to source noise current generator

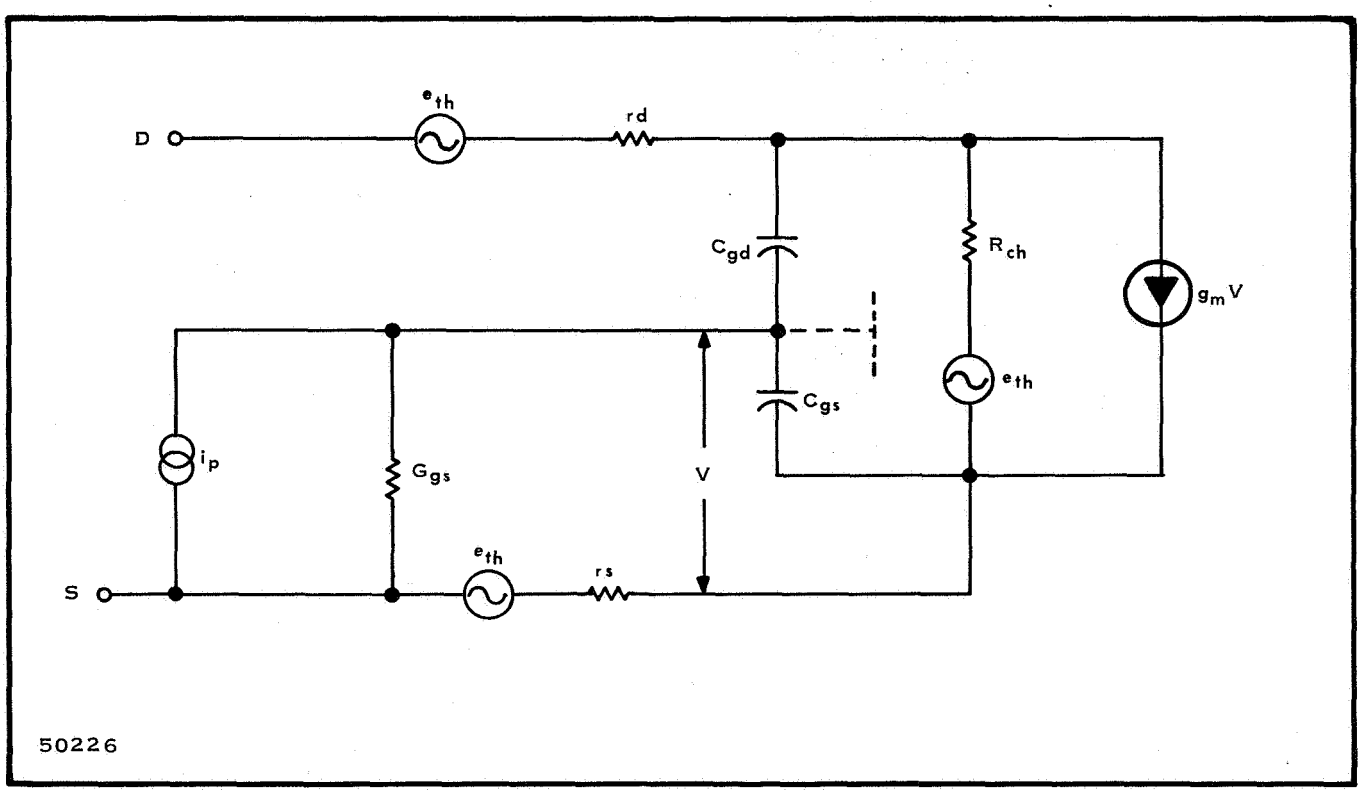

Figure 19. Noise Model for the FET

The noise generating mechanism operative in an FET are caused by the following physical phenomena:

a. The gate leakage current, which generates full shot-noise

b. A thermal noise voltage generated in the conducting channel which modulates the space-charge layer height

c. Generation - recombination noise in the space-charge layer.

The generation-recombination noise in the space-charge layer modifies the thermal noise voltage in the conducting channel and gives it a 1/f or flicker noise dependence. However, the 1/f noise does not become significant unless the FET is operating at very low frequencies. For surface or insulated gate FET's, the effect of shot noise created by the gate leakage current may be neglected as this current is small enough to be negligible.

For all frequencies above the region where the 1/f flicker noise is effective, the noise figure of the FET derived from the above noise model may be written as:

$$F = 1 + \frac{2\lambda\omega}{gm}(C_{gs} + C_{gd}) + \frac{\lambda}{gm}\left[\frac{G_S - \omega (C_{gs} + C_{gd})^2}{G_S}\right] \qquad (21)$$

where G_S = source conductance

$gm \cong \omega_C C_{gd}$

$\lambda \cong$ a constant that defines the division of channel resistance

F. ADVANCES IN LOW NOISE MICROWAVE TRANSISTORS

Present planar double-diffused germanium transistors in which bases are diffused to a depth of 0.5 and 0.8 μm are exhibiting base resistances as low as 18 ohms and base-collector time constants as low as 1 psec. These technology advances are being applied to development of NPN germanium transistors for low-noise amplification at S- and C-band. The noise performance of these transistors have noise figures of 5+0.5 dB at 3 GHz with measured gains of 6.5 to 6.8 dB. The application of double diffusion technology to NPN silicon semiconductors has resulted in the L-83 device that has a noise figure within 0.25 dB of planarized germanium devices while yielding higher gains[1].

1. L-148 Geometry

The L-148 alloy emitter, diffused base planar germanium geometry has produced the TIXM103, 104, 105 and 106 alloy emitters, diffused base planar germanium transistor. The TIXM105 and the TIXM103 offer the lowest noise figure. The noise figures of these devices are 4-5 dB at 3 GHz.

In a practical microwave receiver, the TIXM103 would serve as a low-noise input stage followed by the TIXM104 as a subsequent high-gain amplifier. A typical TIXM104 device in a second stage provides 6.5-dB gain and 6.5-dB noise at 1.5 GHz[3]. At 1.5 GHz, the TIXM103 is rated for typical 8.5 dB gains and a 5-dB noise figure when used in a high gain circuit.

The electrical features of a typical TIXM103 transistor housed in a common emitter stripline package are given in Table V.

Table V. Parameters of a Typical TIXM103 Transistor

Parameter	Minimum	Maximum	Unit
B V_{cbo}	-12		Volt
h_{fe} (V_{CE} = -9V, I_c = 7mA f = 400 MHz)	4.5		—
C_{cb} (V_{CB} = -9V, I_E = 0 f = 1 MHz)	0.2	1	pfd
NF (f = 3 GHz)		7	dB
Gain bandwidth product	1.8		GHz
Power Gain @ 3 GHz	3		dB

The noise figure and insertion gain of the TIXM103 are plotted versus frequency in Figure 20. The gain performance has been extended at higher frequencies by the newer TIXM105 and TIXM106 transistors. These transistors are identical in construction with the TIXM103; the difference being in the types of packages. The TIXM105 is mounted in TI stripline and the TIXM106 is packaged for thin-film mounting to ceramic. The TIXM105 has been directly bonded to ceramic in the laboratory and passivated. This technique eliminates package capacitances and parasitics. The electrical characteristics of the TIXM105 and TIXM106 are given in Table VI.

2. L-146B Geometry

The L-146B has low noise and a small signal geometry and is currently being used in a S-band preamplifier on the MERA programs with satisfactory results. The device was discussed in the first scientific report and is shown in the photograph of Figure 21.

The approximate internal parameters values for the L-146B are[19]

$$r_b' \approx 15\,\Omega$$
$$r_b' C_c \approx 2 \text{ psec}$$
$$f_T \approx 3.5 \text{ GHz}$$

The forward power gain is shown in Figure 22 for the device in the common emitter configuration.

The L-146A version of this geometry is currently being investigated for use as a 500-MHz IF preamplifier for the MERA program, and a secondary effort is underway to fabricate this transistor in a beam lead configuration in order to make the device

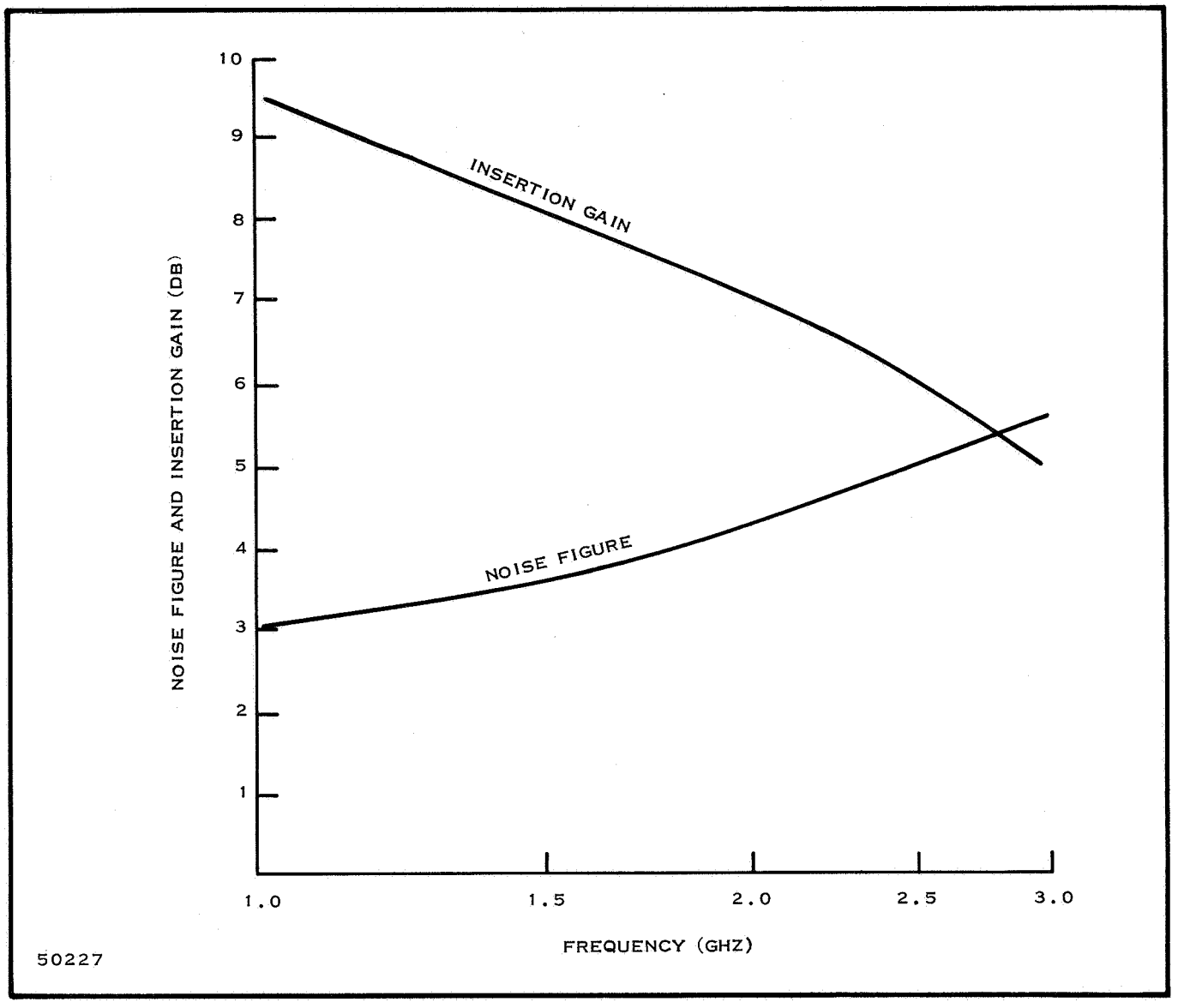

Figure 20. Noise Figure and Insertion Gain of TIXM103

compatible with thin-film circuitry. Characterization data for epitaxially construction of the L-146A transistor is shown in the Table VII. The excessive NF at 500 MHz is due to a low f_t. At the present time, transistor fabrication is being modified to improve the parameters.

3. Other Small Signal Geometries

The L-83 is a silicon device which has a 2.5 micron emitter compared to the 7.5 micron emitter of the TIXM103 germanium planar transistor. The power gain of these two devices as a function of frequency is shown in Figure 23 where the superior power capability of silicon is evident. The L-83 can deliver 10 mW at 4 GHz. The advantage of the smaller dimensions is that it helps to extend the frequency response of the device.

Table VI. Parameters of a Typical TIXM105 and TIXM106 Transistor

Electrical Characteristics at 25°C Lead Temperature

Parameter		Test Conditions	Min	Max	Unit
$V_{(BR)CBO}$	Collector-Base Breakdown Voltage	I_c = -100 A, I_E = 0	-12		V
$V_{(BR)CEO}$	Collector-Emitter Breakdown Voltage	I_c = -2 mA, I_B = 0	-10		V
$V_{(BR)EBO}$	Emitter-Base Breakdown Voltage	I_E = -100 A, I_c = 0	-0.3		V
I_{CBO}	Collector Cutoff Current	V_{CB} = -9V, I_E = 0		-6	A
h_{FE}	Static Forward Current Transfer Ratio	V_{CE} = -9V, I_c = -2 mA	10	250	
h_{fe}	Small-Signal Common-Emitter Forward Current Transfer Ratio	V_{CE} = -9V, I_c = -2 mA, f = 400 MHz	5.5		
C_{cb}	Collector-Base Capacitance	V_{CB} = -9V, I_E = 0, f = 1 MHz,	0.2	1	pF

Operating Characteristics at 25°C Lead Temperature

Parameter		Test Conditions	Min	Max	Unit
NF	Common-Emitter Spot Noise Figure	V_{CB} = -9V, I_E = 2 mA, R_G = 50 , f = 2.25 GHz,	1	4.5	dB

Guaranteed Noise Figure 4.5 dB Maximum at 2.25 GHz

Guaranteed f_T 2.2 GHz Minimum

Packaged for stripline and thin-film applications

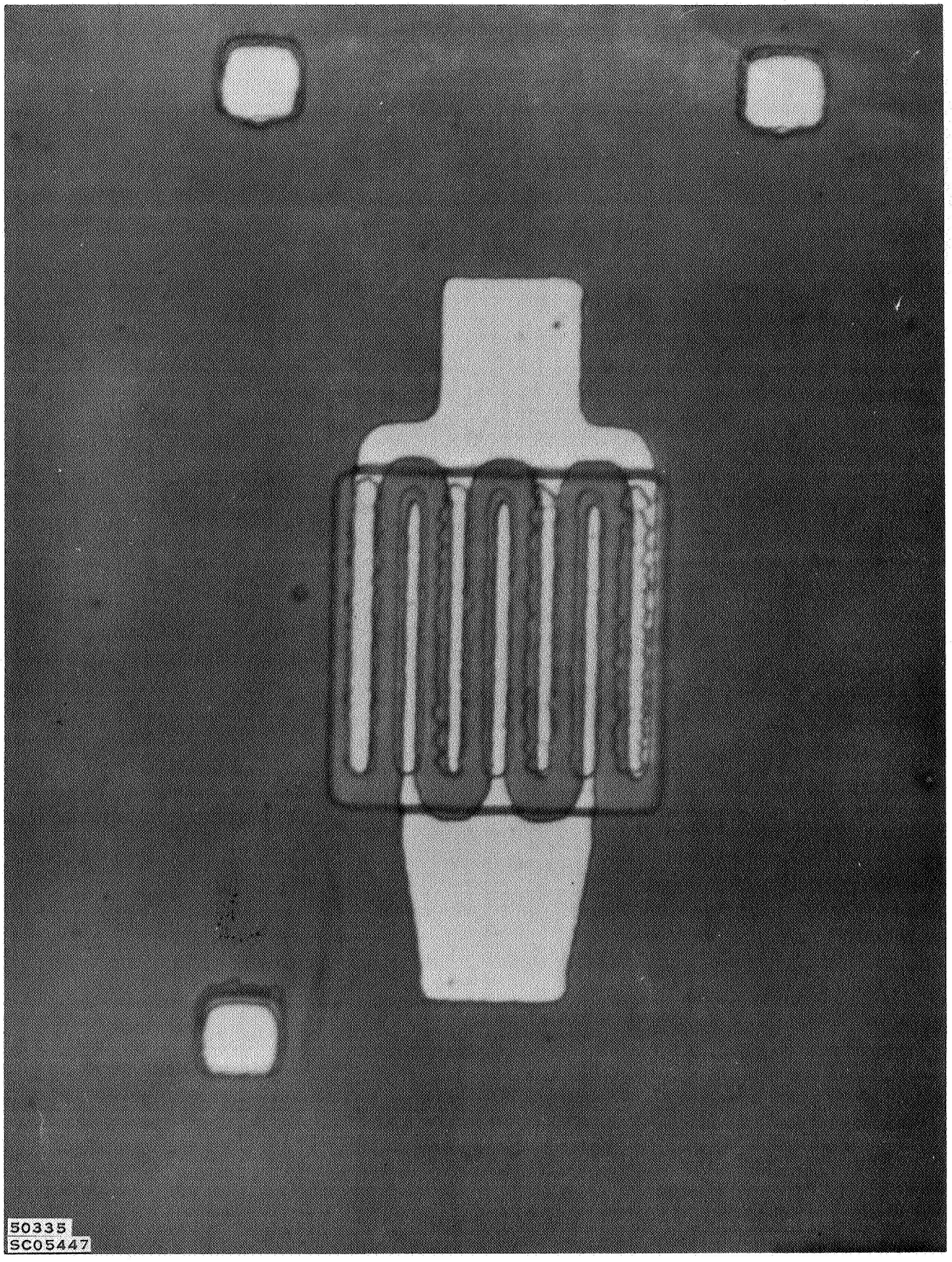

Figure 21. Geometry of the L146B

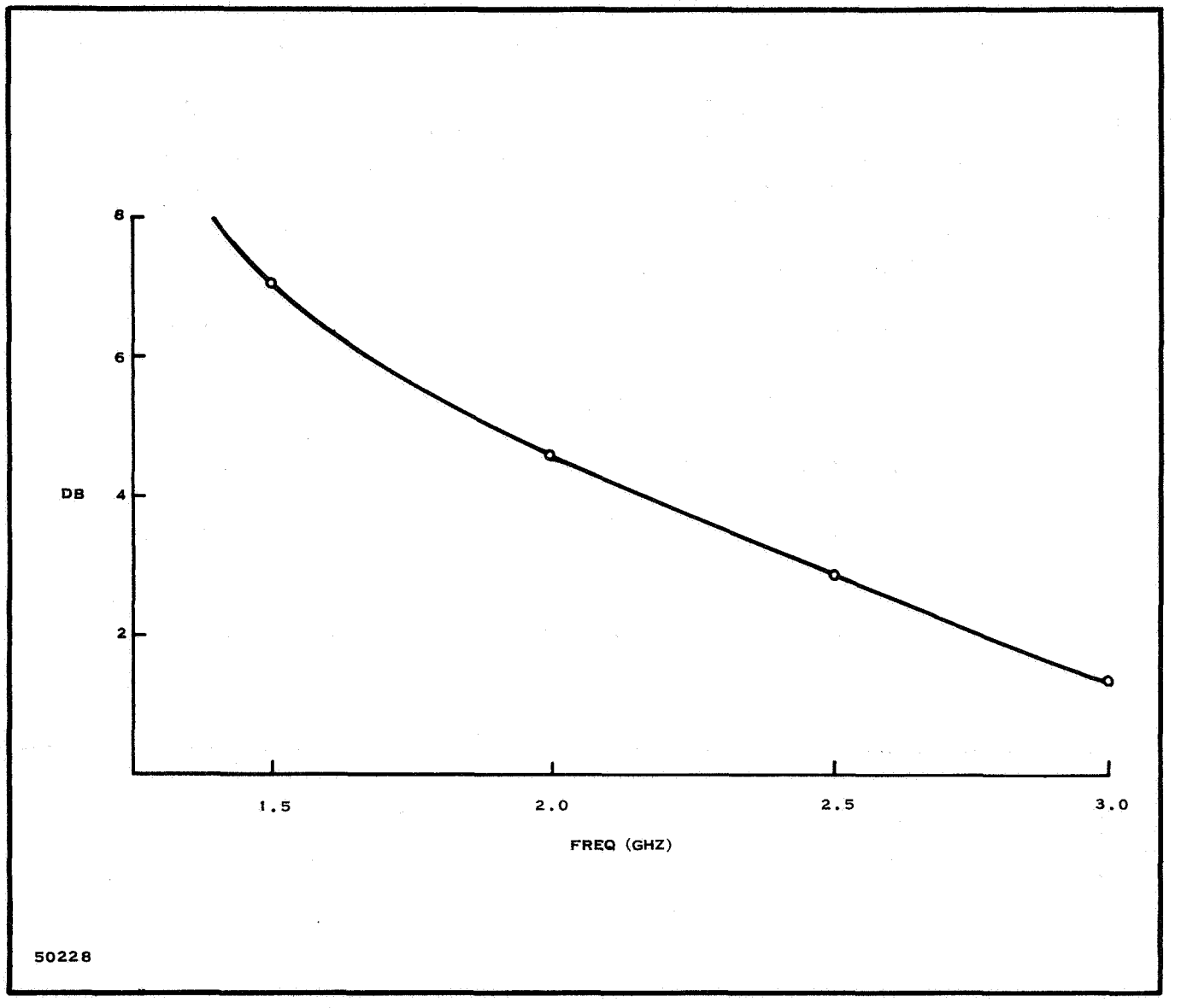

Figure 22. Forward Power Gain of L-146B Device

The improvement in photomasking technology is the main factor behind the increase in extending the upper frequency limit of transistors. Five-micron lines are routine, 2.5-micron lines have been incorporated to some extent and it has been reported that 1-micron lines are being investigated[20]. Better control of diffusion process have allowed base widths of 1000 angstroms to be achieved.

Such development in the manufacturer of microwave transistors as the factors mentioned above gave rise to the L-186 transistor. This is a double-diffused NPN silicon device built from the L-83 device with noise figure performance approximately that of planar germanium devices. The noise figure of the L-186 device is shown in Figure 24.

Table VII. Characterization Data for the L-146A

PARAMETER	VALUES
BV_{CBO} @ 10 μA	30.0V
h_{FE} @ 6V, 2 mA	35
400 MHz f_t @ 6V, 20 mA	1325 MHz
79.8 MHz $rb'C_c$ @ 6V, 10 mA	3.0 ps
79.8 MHz rb' @ 6V, 2 mA	10
79.8 MHz C_{CB} @ 6V, 1 MHz	0.586 pf
500 MHz NF @ 6V, 2 mA	4.5 dB

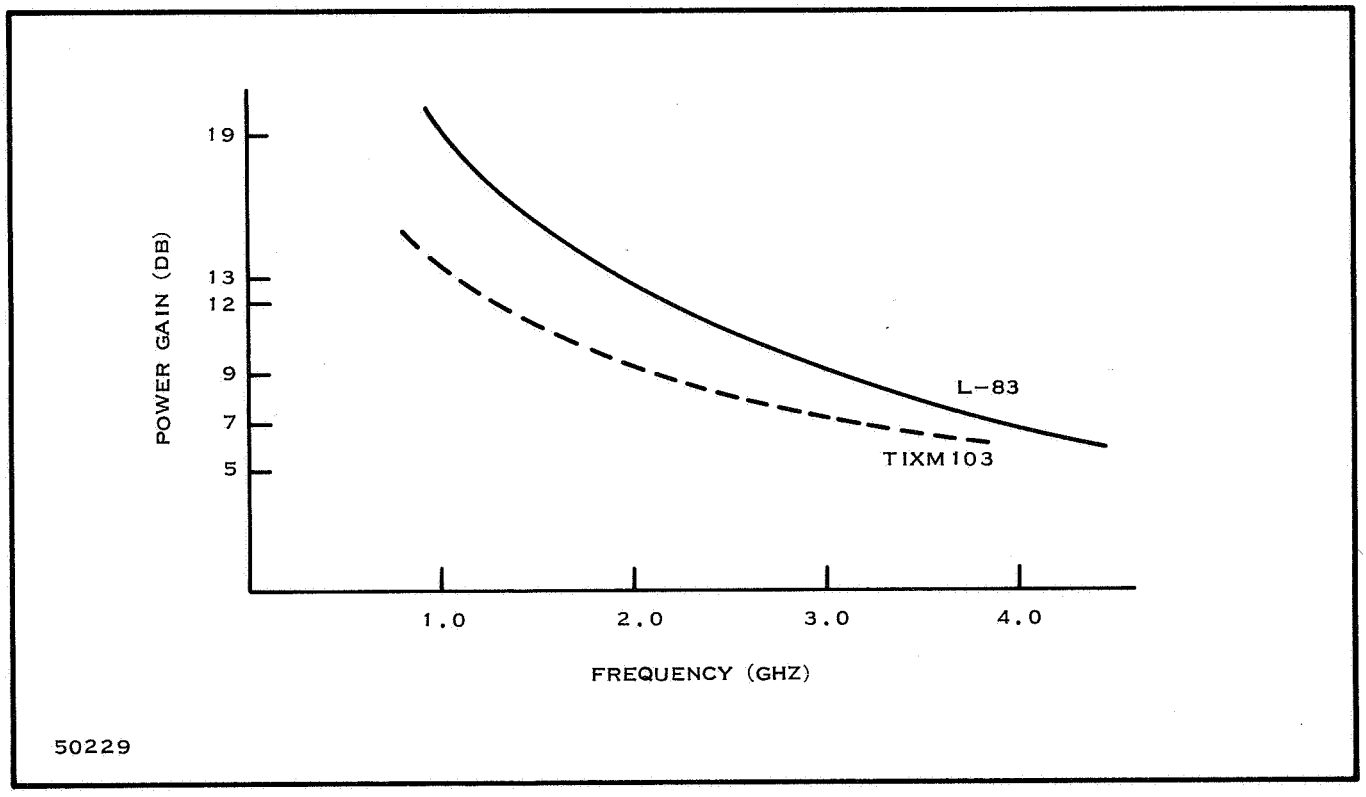

Figure 23. Power Gain of L-83 and TIXM103

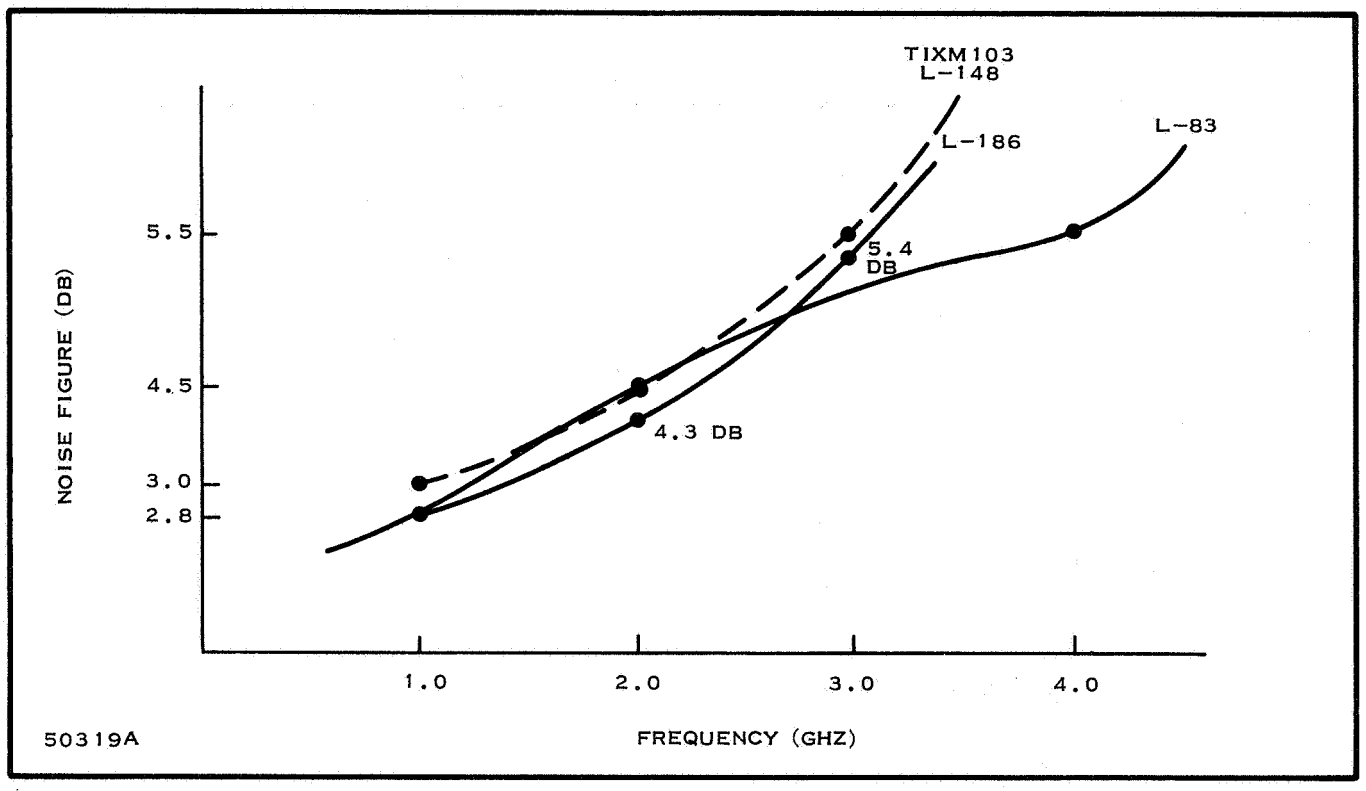

Figure 24. Noise Figure of Si NPN Double Diffused Transistor

The noise figure of the new silicon unit is approaching that of the TIXM105 (L-148) planar germanium transistors and it may be seen that the noise figure of both units closely match the noise performance of traveling wave tubes and Ga Sb tunnel diodes in Figure 25.

The power gain of the TIXM105 (L-148) transistor and the L-83 silicon device is compared in Figure 26 to a NPN germanium double diffused device, the L-153B. The latter device is currently being developed at Texas Instruments to meet the specifications given in Table VIII.

The double diffused germanium device L153B has much better gain than the alloy L-148 geometry and is expected for exceed the performance of the L-148 at higher frequencies[21]. New double diffused silicon devices are currently being pursued in the laboratory which exhibit a maximum available gain (MAG) of 14-dB at 2 GHz with a noise figure of 5.5 dB. It is expected that these devices will have a MAG in excess of 15 dB and a noise figure of three decibels in the near future.

G. MICROWAVE AMPLIFIERS

1. S-Band Amplifier (1.7 - 2.4 GHz)

A low noise, three stage microwave amplifier consisting of double-bonded TIXM103(L148) transistors biased at nine volts and two milliamperes has been constructed in Texas Instruments laboratories. The breadboard amplifier response is given in Figure 27 and indicates a measured power gain of 14 dB at band center. The

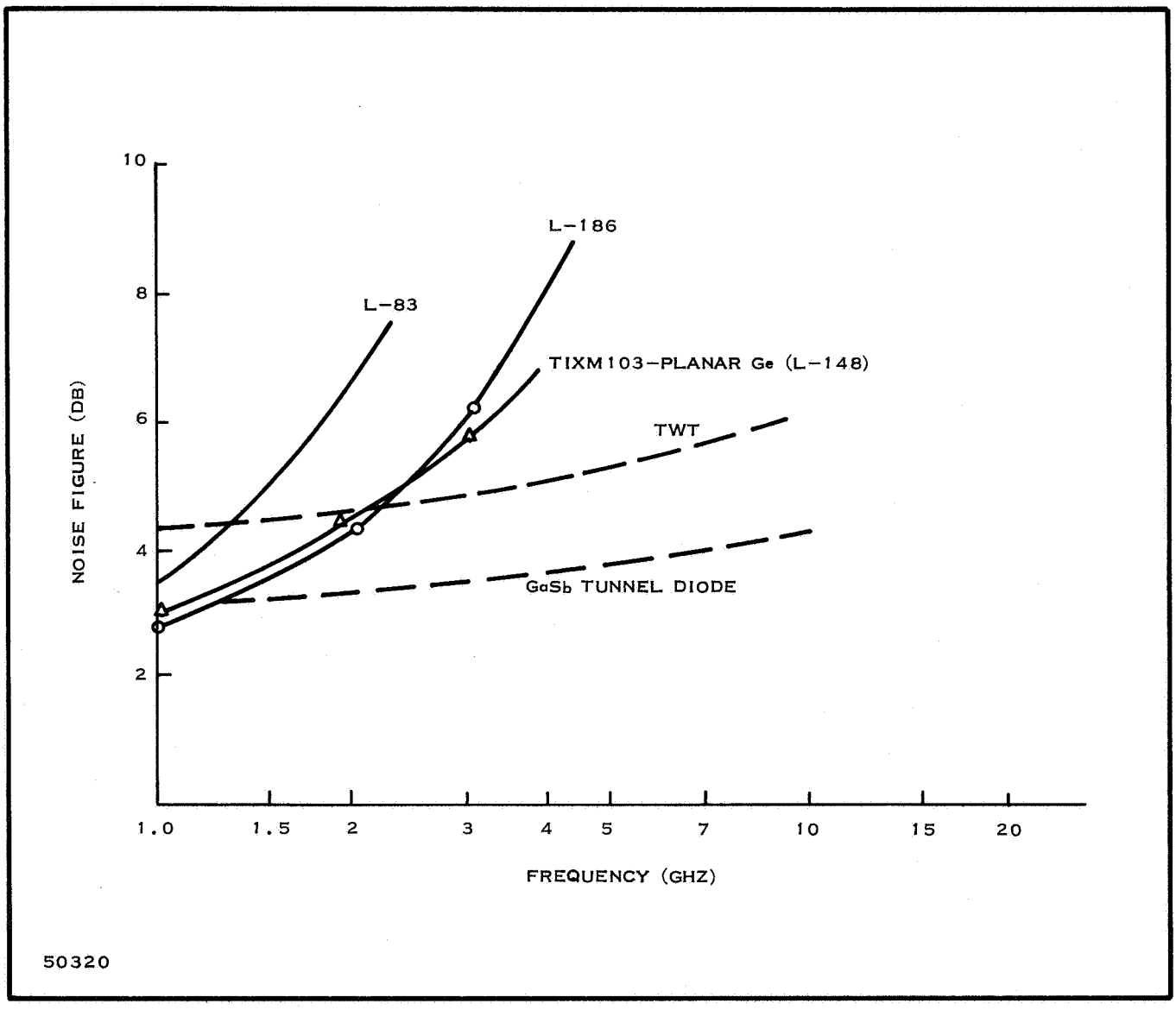

Figure 25. Noise Performance of Ge and Si Devices

high frequency end of the response is somewhat lower than desired, and it was found that this was due to a stub-length error. A plot of the noise figure is included in Figure 27. The amplifier's source admittance as well as bias conditions were optimized with respect to overall gain, and not to the overall NF. It is, therefore, possible to improve the overall NF of this amplifier.

2. S-Band Power Amplifier (2.25 GHz)

The L158 family of transistors were used as intermediate power devices in the construction of a 5-stage power amplifier to deliver two watts pulsed at 2.25 GHz. Figure 28 shows the performance of the amplifier plotted as a function of frequency. Figure 29 shows a photograph of the 5-stage breadboard. A biased class A amplifier

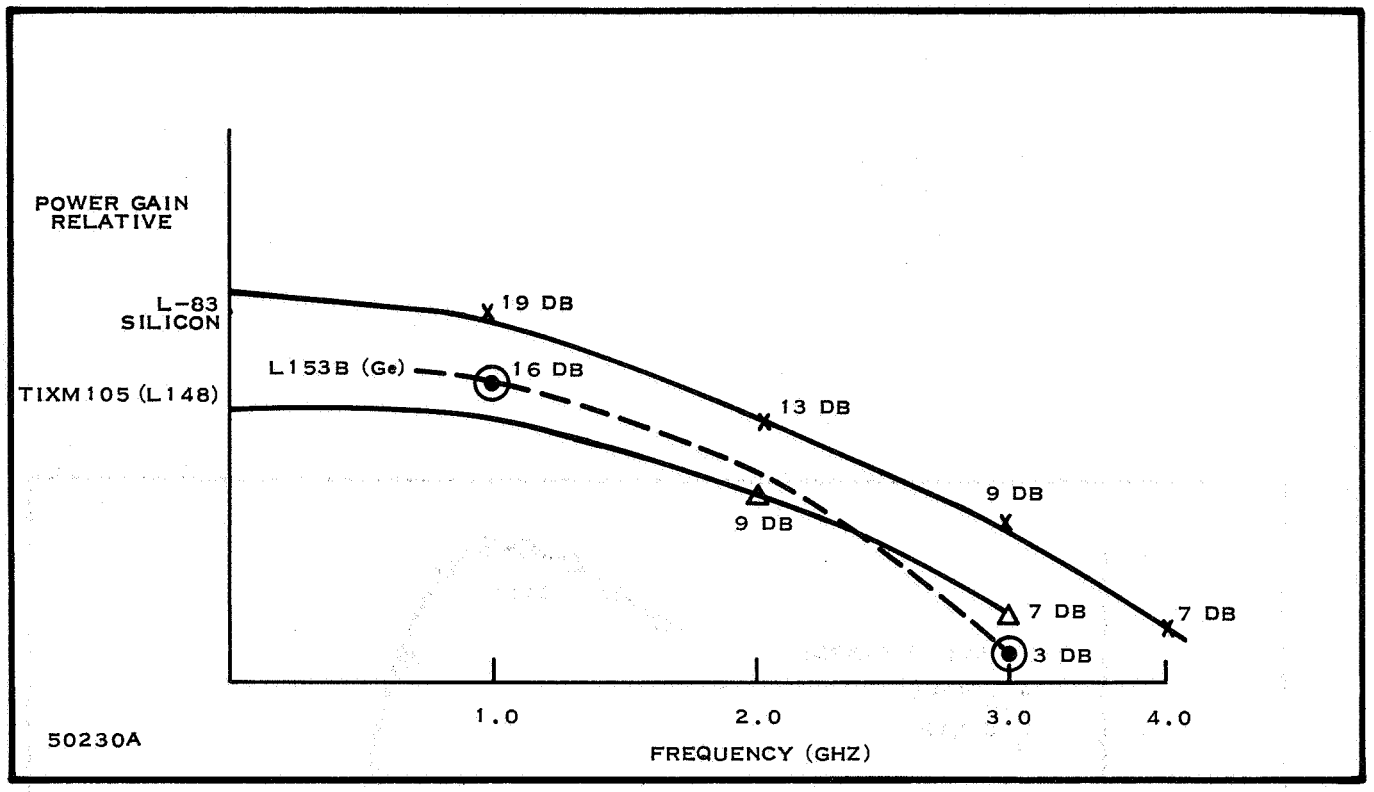

Figure 26. Power Gain of TIXM105, L-83, and L153B vs Frequency

Table VIII. Design Objectives for the L153-B Transistor

Maximum Operating Frequency	6 GHz
Noise Figure	<8 dB
Power Gain	10 dB

using the L-49 transistor was supplied to 10-mW input signal to drive the complete assembly. The power gains of the individual L158 transistor are shown in Table I.

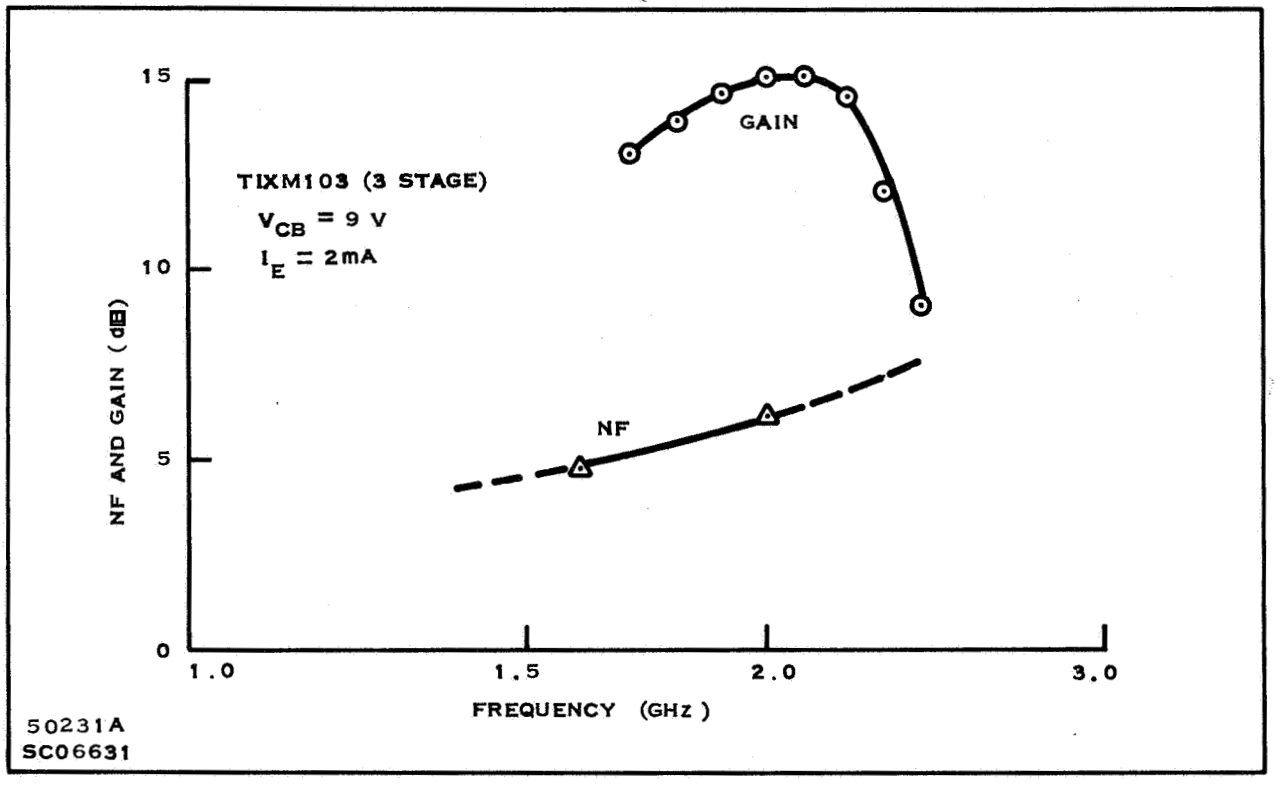

Figure 27. Transducer Gain and Noise Figure vs Frequency for TIXM103 3-Stage Teflon Microstrip Amplifier

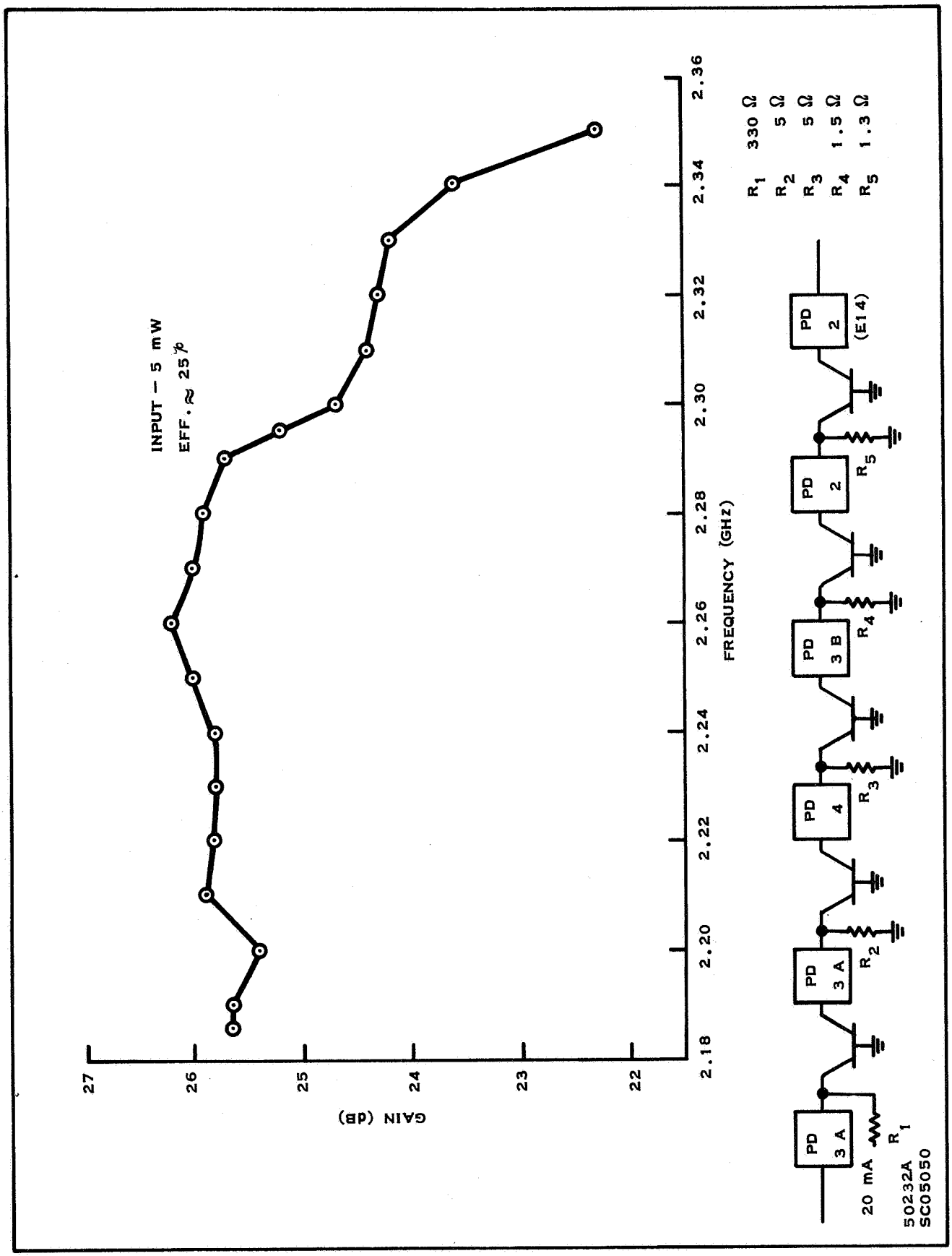

Figure 28. Graph Breadboard S-Band Amplifier Frequency Response

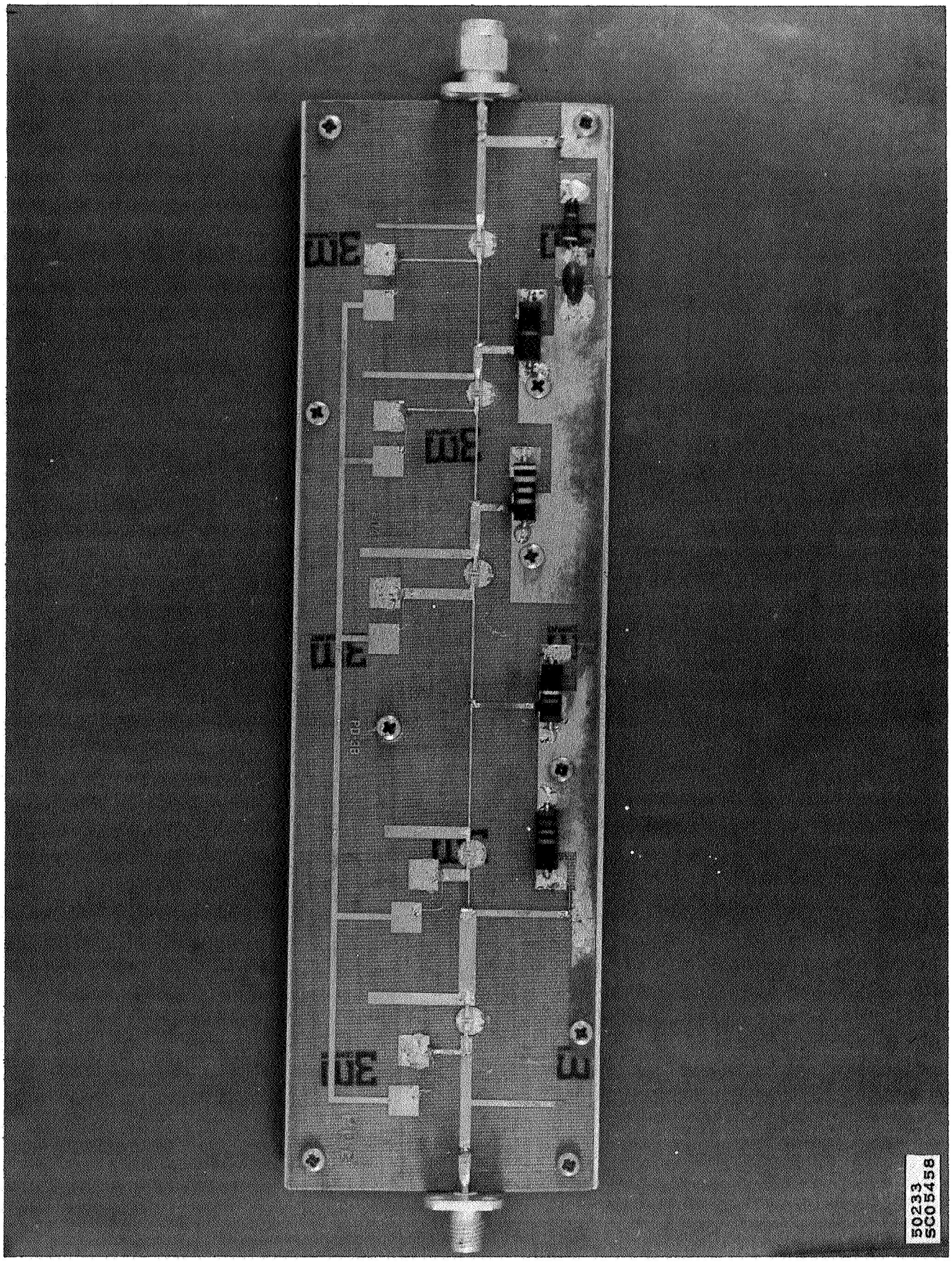

Figure 29. Photograph of a 5-Stage S-Band Amplifier Breadboard

SECTION IV

SEMICONDUCTOR DEVICES

A. GENERAL

The first and third Scientific Reports discuss in detail the characteristics of varactors, Schottky barrier diodes, PIN diodes, Step recovery diodes and to some extent the Gunn device. This report updates and expands these subjects where applicable and introduces tunnel diodes and avalanche diodes.

B. VARACTORS

In the first report the discussion of varactors is confined to their use in frequency multiplication and division circuits along with their application to integrated circuits. This report adds to those applications by examining the varactor as a variable capacitance for use in circuit tuning. In this capacity, the diffused junction varactor is compared to the abrupt junction (Schottky barrier) varactor.

The total capacitance at the terminals of a varactor may be varied by adjusting the reverse bias from 0 Vdc to its zener breakdown voltage. The exact relationship is shown in Equation (22).

$$C = C_p + C_j = C_p + \frac{C_{jo}}{\left(1 + \frac{V_b}{\phi}\right)^n} \tag{22}$$

Where C_p = Capacitance of the package

C_{jo} = Capacitance of the junction when V_b is zero

V_b = Reverse bias in Vdc

C_j = Capacitance of the junction at any value of V_b.

n = Exponent determined by junction characteristics. Equal to approximately 1/3 for diffused junctions and 1/2 for abrupt junction.

ϕ = Contact potential equal to 0.7 for silicon devices.

If the junction capacitance is much larger than the package capacitance, Equation (22) becomes

$$C \approx C_j = \frac{C_{jo}}{\left(1 + \frac{V_b}{\phi}\right)^n} \tag{23}$$

This equation is shown in Figure 30 for different values of n representing a typical abrupt junction and a diffused junction varactor diode. This figure illustrates that for positive values of reverse bias, a voltage of 65 Vdc is required to cause the

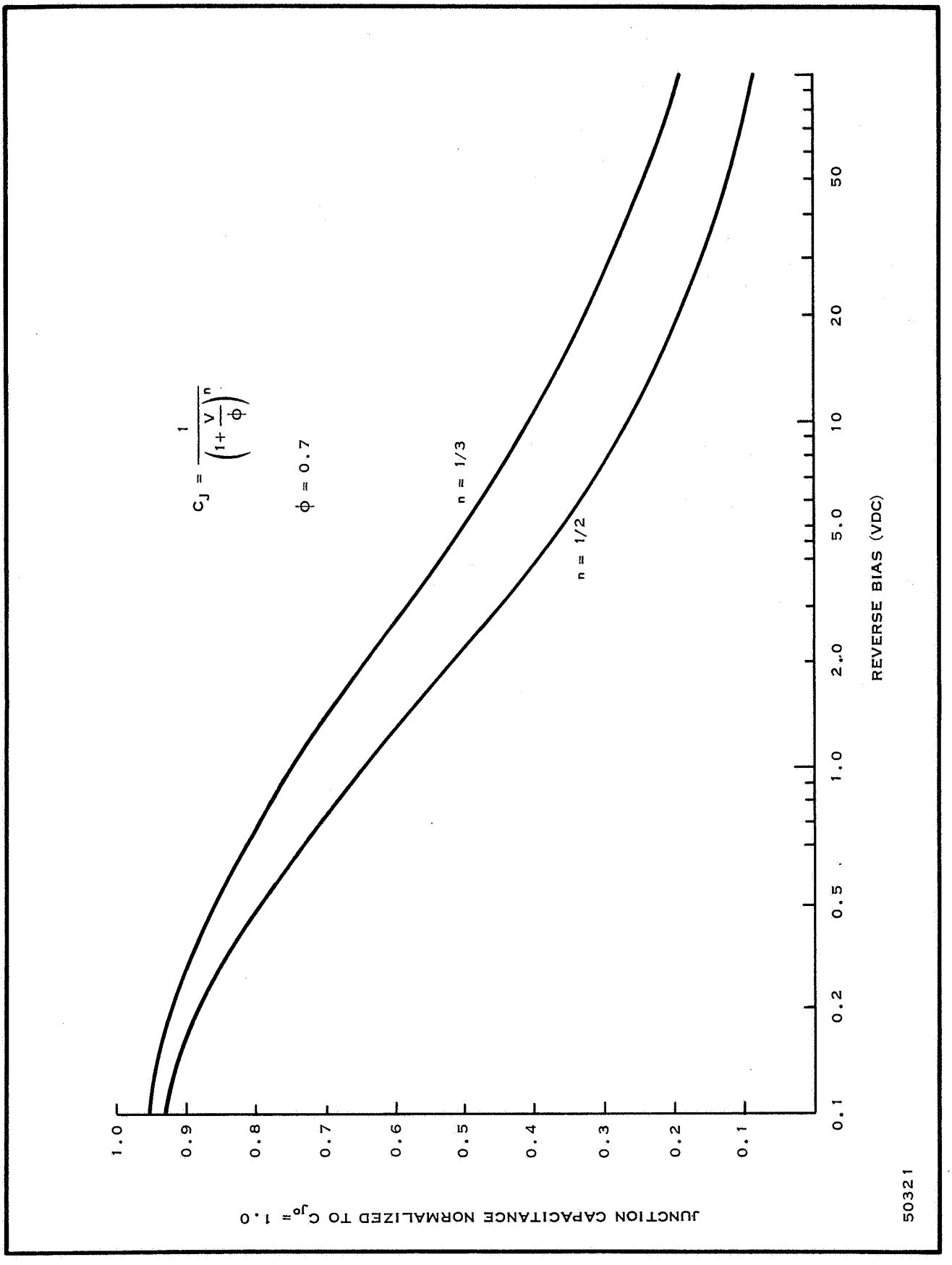

Figure 30. Junction Capacitance vs Reverse Bias

capacitance of the abrupt junction varactor to become one tenth of its value at zero bias. A voltage of 80 Vdc is required to cause the diffused junction varactor to become one fifth its value at zero bias. Any capacitance in parallel or series with the junction capacitance decreases the capacitance change ratio. Unfortunately, at microwave frequencies shunt capacitances may become appreciable. The package capacitance can be reduced to 25% or less by careful design. In cases where other parallel capacitances becomes too large, the varactor may be placed in series with an inductance large enough so that the junction capacitance change is regarded by the circuit as an inductive change.

A varactor may be used for tuning so long as the following requirements are met.

1. The effect of circuit capacitance is overcome either by the method outlined above or by keeping it substantially lower than the junction capacitance C_j.

2. The Q of the circuit need not be extremely high. It should be noted that Q diminishes with increasing frequency, as shown by:

$$Q = \frac{fco}{f} \tag{24}$$

where

f = frequency of operation

$$fco = \text{cutoff frequency} = \frac{1}{2\pi R_s C_j} \tag{25}$$

where

R_s = series resistance

3. The ac signal swing must be small compared to the reverse bias otherwise it will cause the varactor capacitance to change enough to significantly detune the circuit. If the ac peak-to-peak voltage is more than 2 volts, the minimum reverse bias should be about 10 vdc. Of course, these factors are relative to the total circuit Q and to whether the circuit being tuned is an oscillator, filter, or amplifier.

4. A dc voltage source capable of supplying adequate magnitudes of voltage must be available. A typical 28-volt supply for example, will give only about a 6.2- to -1 or 3.5- to -1 capacitance ratio, depending on the type of junction, and less when constant capacitances must be considered.

5. Total capacitance variation must be enough to accomplish the desired tuning. Assuming the resonating inductance to be constant, the frequency-capacitance relationship is

$$fo = \frac{K}{\sqrt{C}} \tag{26}$$

where

$$K = \frac{1}{2\pi\sqrt{L}}$$

This results in a frequency versus varactor bias voltage of

$$f = m\left(\frac{V_b + \phi}{\phi}\right)^{n/2} \qquad (27)$$

As can be seen from Figure 31, it takes a large reverse bias change to accomplish a relatively small frequency change even assuming that no external capacitance is affecting the varactor. Figure 32 shows the voltage bias versus frequency of a typical oscillator.

The basic varactor theory has been explained in detail in Scientific Report No. 1 and a detailed analysis of a varactor tuned tank was presented in Scientific Report No. 3. There have been no significant advances made in varactor theory since the release of these reports.

C. SCHOTTKY BARRIER DIODES

There have been no significant changes in the design of or uses for the Schottky barrier diode since the release of Scientific Report No. 1. The effort in the interim has been devoted to improvements and refinements of the previously reported techniques. The Schottky barrier techniques have been so successful at UHF and microwave frequencies that all mixer diodes presently being produced and developed at Texas Instruments are of this type. Noise figures as low as 5.3 dB at S-band and 6.5 dB at X-band have been realized and it is expected that in the near future these figures will be reduced to 5.0 dB and 6.0 dB respectively. The design of objectives of a development program at Texas Instruments are given in Table IX[22].

The IF impedance objectives may be incompatible with the minimum noise figure and high burnout capability. Current Schottky barrier diodes have an average IF impedance of about 170 ohms as compared to the 1N21 and 1N23 point contact diodes whose average IF impedance is 400 ohms. The effect of the mismatch occurring when the Schottky barrier diode is used in a system designed for point contact diodes may be determined by calculating the resulting power reflection loss. This reflection power loss decreases sharply as the IF impedance is increased; thus, it is possible that a compromise may be reached by increasing the Schottky barrier IF impedance from 170 ohms to about 250 ohms and reducing the noise figure to the level of the objective.

D. THE GUNN EFFECT DEVICES

Since the publication of Scientific Report No. 1 great strides have been made in the field of Gunn Effect Oscillators. Units now available (see Table X) will provide up to 10 mW CW output for thousand of hours. Outputs of hundreds of watts[23] are common when the device is operated in very short duty cycle pulses. The very low efficiency of the device (typically 0.5 - 3.0%) make it necessary to dissipate a lot of heat from a very small area. It is expected that as methods of heat transfer are improved CW power outputs in the order of 75 mW will be possible.

Many of the problems formerly associated with Gunn devices were solved by development of a highly pure epitaxial GaAs chip. The chip thickness is closely controlled by the epitaxial method of construction. Also with a very good GaAs chip, the doping levels are controlled precisely for optimum Gunn effect performance.

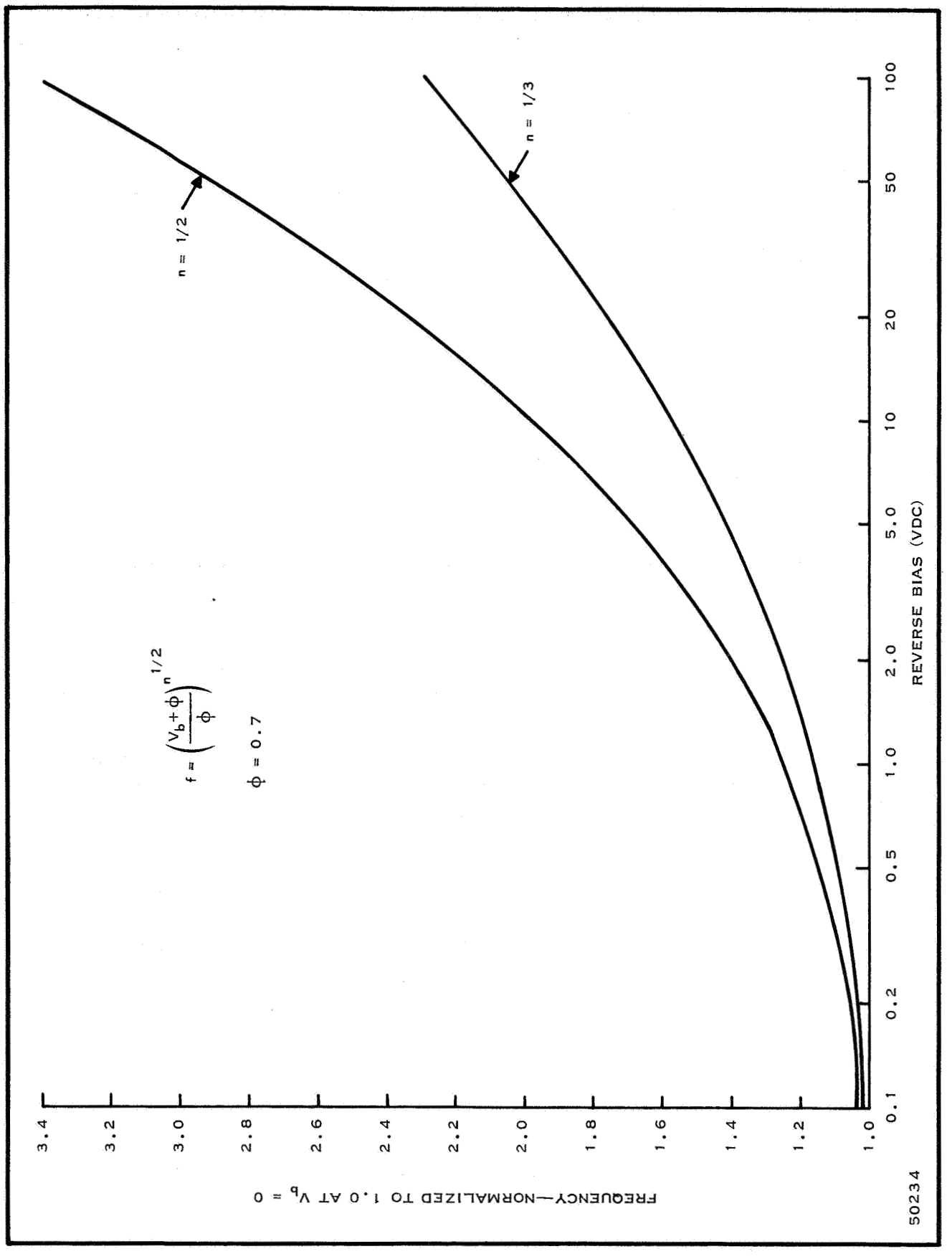

Figure 31. Reverse Bias vs Frequency

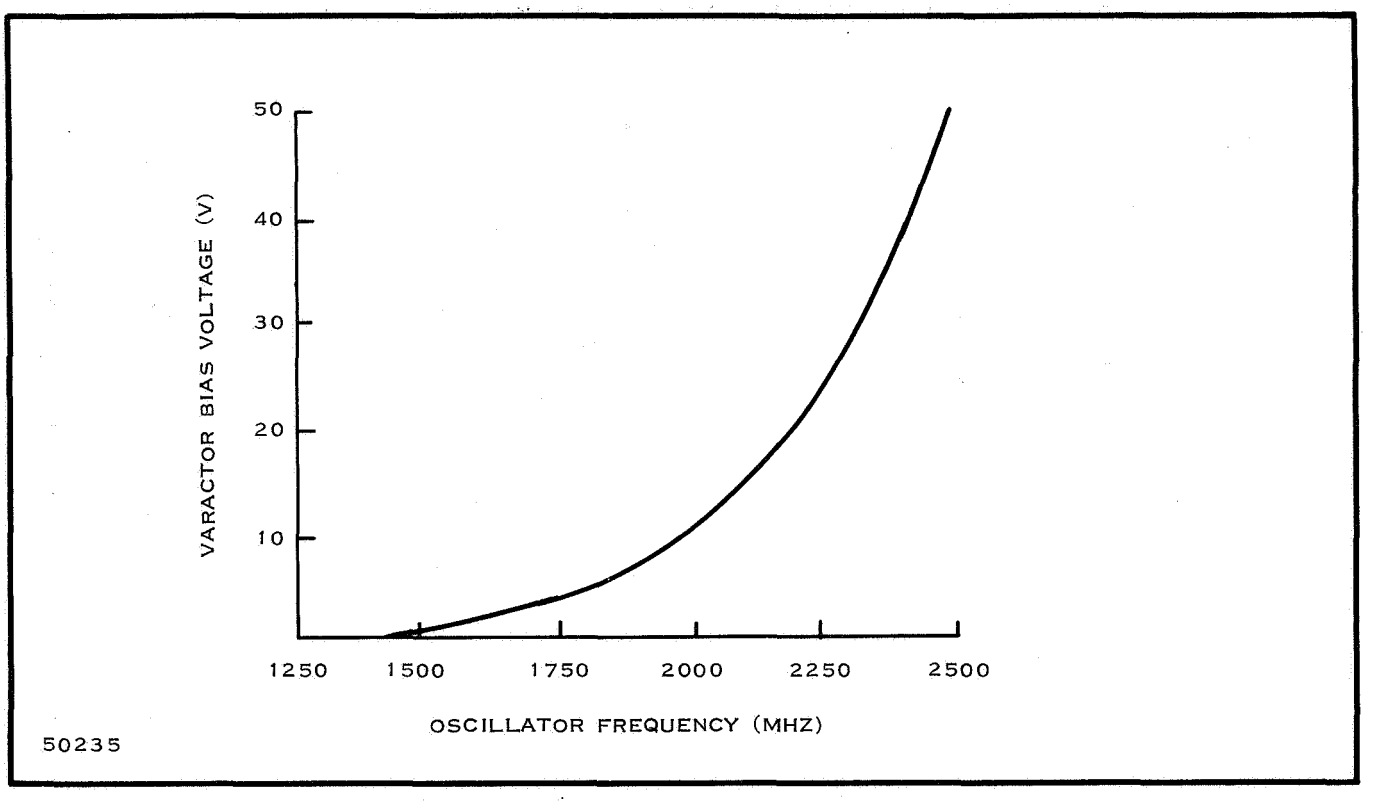

Figure 32. Varactor Bias vs Frequency

Table IX. Schottky Barrier Diode Design Objectives

Parameter	S-Band		X-Band	
	Minimum	Maximum	Minimum	Maximum
Intermediate Frequency Impedance (Z_{IF})	350 ohms	450 ohms	335 ohms	465 ohms
Conversion Loss (L_c)	-	5 dB	-	5 dB
Noise Figure (NF_o)	-	5 dB	-	6 dB
Output Noise Ratio	-	1.2	-	1.2
VSWR		1.3		1.3
Burnout by Single Pulse (B_o)	10 ergs		10 ergs	
Lc Unbalance	-	0.3 dB	-	0.3 dB
X_{IF} Unbalance	-	25 ohms	-	25 ohms

Table X. Gallium Arsenide Gunn Effect Diodes (Texas Instruments Inc.)

Frequency	Type No.	Oscillator Power (mW) (Note 1)	Test Conditions		
			V_{th}	Maximum Operating Voltage	Typical Operating Current
C-Band	L-188	0.1 - 1.0	7 Volts	12 Volts	100 mA - 200 mA
	L-188A	1.0 - 5.0	± 1 Volt		
	L-188B	5.0 -10.0			
X-Band	L-189	0.1 - 1.0	5 Volts		
	L-189A	1.0 - 5.0	± 1 Volt	10 Volts	100 mA - 300 mA
	L-189B	5.0 -10.0			
Ku-Band	L-190	0.1 - 1.0	3 Volts		
	L-190A	1.0 - 5.0	± 1 Volt	7 Volts	100 mA - 300 mA
	L-190B	5.0 -10.0			

OPERATING NOTES:

1. Adequate heat sink must be provided.
2. Current limiting power supply is recommended.

Nearly all the research at Texas Instruments has been done in the frequency range from 4 GHz to 9 GHz. It was felt that the present transistor technology could provide oscillators up to 6 GHz with at least the same power output as the Gunn oscillators. Furthermore, transistor oscillators are more frequency stable.

There are two modes of operation of the Gunn oscillator. In the frequency range from 4 GHz to 30 GHz, the normal Gunn effect mode is used. In this mode, the frequency is determined by the thickness of the chip (i.e., f = the reciprocal of electron transit time), but small frequency changes (10 - 100 MHz) can be made by changing the applied voltage $\pm$1.0 Vdc within the band of oscillation.

The second mode of operation is called Limited Space-Charge Accumulation (LSA). In this mode of operation, oscillation frequency is determined by circuit resonance rather than by transit time. The power output and efficiency are equal to or higher than when the device is operated in the transit time mode. The frequency range for the LSA mode is approximately 30 to 100 GHz.

Very little research has been done in the 2- to 3-GHz range. At these frequencies the chip thickness becomes relatively large and the resonant cavaties become cumbersome. These facts plus the low efficiency (0.5-3%) and the poor frequency stability (one part in 10^4) make it undesirable to use the Gunn devices at 2.5 GHz at this time.

E. THE TUNNEL DIODE

1. General

The tunnel diode offers a unique physical mechanism for semiconductor operation and at the same time offers a unique set of electrical characteristics for improved circuit design. In comparison with transistors, the tunnel diode offers advantages of extremely high frequency operation, low noise, small size, low operating power levels, and high reliability[4].

The tunnel diode is a two-terminal device consisting of single PN junction. The essential difference between it and a conventional diode is that the conductivity of the P and N material is more than 1000 times as high as the conductivity of the material used in conventional diodes.

Because of the very high conductivity of the P and N materials, the width of the junction (the depletion layer) is very small, of the order of 10^{-6} inches. Therefore, it is possible for electrons to tunnel through the junction even though they do not have enough energy to surmount the potential barrier of the junction. Although tunneling is impossible in terms of classical physics, it can be explained in terms of quantum mechanics. For this reason the mechanism is commonly called quantum mechanical tunneling.

Under conditions of reverse bias of a conventional diode there are no free-holes or electrons to conduct charge across the junction. In the tunnel diode, however, a small reverse bias will cause the valence electrons of the semiconductor atoms near the junction to tunnel across the junction into the N region and, thus, the tunnel diode will conduct under reverse bias. In the tunnel diode a small forward bias will cause electrons in the N region to tunnel across the junction to the P region (appearing as valence electrons in the semiconductor atoms), and the tunnel diode will conduct. (Figure 33.) If the forward bias is increased, the energy of the free electrons in the N regions will become greater than the energy of the valence electrons in the P region and consequencly the tunneling current will decrease. This decrease in tunneling current with increasing forward bias causes the negative conductance characteristic which is typical of the tunnel diode. As the forward bias is increased further, the free holes and electrons will have enough energy to flow over the potential barrier of the junction in a manner identical to that of a conventional diode.

Quantum mechanical tunneling has a theoretical frequency limit of 10^7 MHz and is inherently a much higher frequency mechanism than the drift and diffusion mechanisms involved in the operation of conventional diodes and transistors. In practice, the frequency limitation of the tunnel diode is determined by parasitic capacity, inductance, and resistance of the device (Table XI).

The characteristics described in the preceding paragraphs are presented graphically in Figure 33. The portion of the static curve from V = 0 to V = Vp exhibits a low ac positive resistance. The portion from V = Vp to V = V_V is the negative resistance region as the current decreases with increasing voltage. The portion $V > V_V$ is

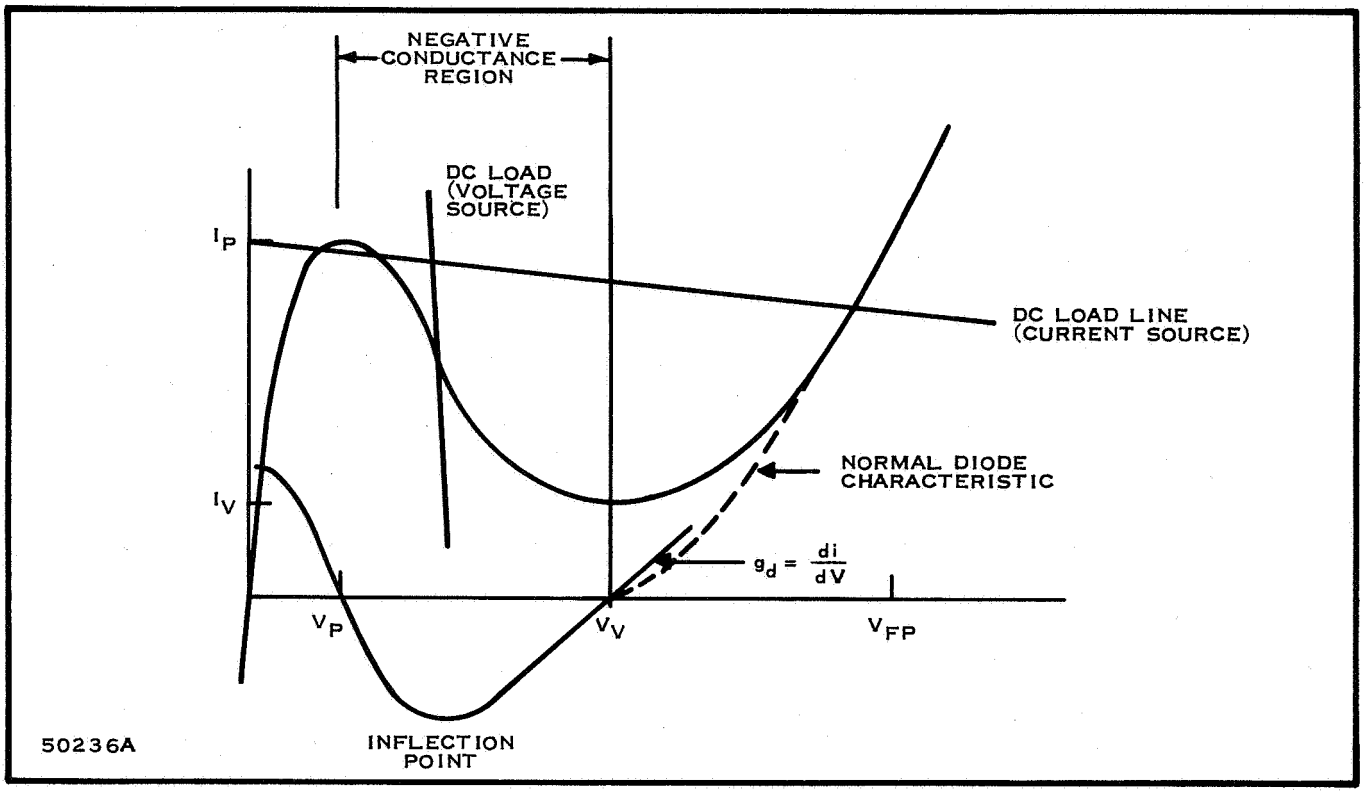

Figure 33. Tunnel Diode V-I Characteristics

Table XI. Tunnel Diode Characteristics

Characteristic	Symbol	Germanium	Gallium Arsenide
Peak Point Voltage	Vp	55 mV	150 mV
Valley Point Voltage	Vv	350 mV	500 mV
Forward voltage at Peak Current	V_{FP}	500 mV	1100 mV
Peak to valley ratio	I_p/I_v	8	15

characteristic of normal diode action. Also shown in Figure 33 is a plot of the conductance, gd = $\frac{di}{dv}$. The voltage at which $\frac{di}{dv}$ becomes negative is called the inflection point. Other parameters are defined as follows:

Ip = the peak current before negative conductance begins

Vp = the voltage at which Ip occurs

I_v = the minimum current at the end of the negative conductance region

V_v = the voltage at which I_v occurs

V_{Fp} = the voltage in the conventional diode characteristic region at which the current is equal in value to I_p.

Tunnel diodes are commonly constructed from two materials, germanium and gallium arsenide, and both exhibit the general characteristics shown in Figure 33. Table XI lists the typical parameters of each type.

The negative conductance region of the tunnel diode has many applications. It may be used for amplification, oscillation, frequency conversion, and switching. To be used as an active device, the tunnel diode must be biased into its negative conduction region with a constant voltage source. A constant current source bias is required in switching applications.

The operational stability of a tunnel diode circuit is determined by the total series resistance, $R_T = R_x + R_s$, as shown by Figure 34.

2. Tunnel Diode Amplifier

A positive conductance by definition dissipates energy; therefore, it follows that a negative conductance will supply energy. This is the basis for negative resistance amplifiers.

Upon examination of the tunnel diode VI characteristics (Figure 33), it becomes evident that for amplifier operation the "operating point" must be in the negative conductance region. Furthermore, to secure a stable operating point, the bias must be from a voltage source. The location of this operating point will depend on the magnitude of the anticipated signal swing, the required signal-to-noise ratio, and the operating temperature range. In most cases it is required to bias the tunnel diode at the point of maximum negative conductance.

The greatest bias problem is that the negative conductance region is nonlinear; thus it is necessary to match the diode conductance closely to the circuit conductance if high gain is to be achieved. Slight variations in the bias point with consequent variations in diode conductance can cause large changes in circuit gain. Consequently, it is very important to ensure a very stable bias voltage. Some possible methods for obtaining stable voltage from low impedance sources are:

the use of mercury cells

the use of forward bias diodes as voltage regulators

the use of zener diodes as voltage regulators.

In oscillators where matching is not required, it is important that, at the lowest operating temperature, the device is driven from a voltage source. Oscillators have been operated successfully over a remarkably wide temperature range from -269°C to 300°C. But in amplifiers, matching must be maintained over the entire operating temperature range. Stable amplification may be accomplished by negative feedback, direct temperature compensation, or by deliberately making the bias network temperature sensitive.

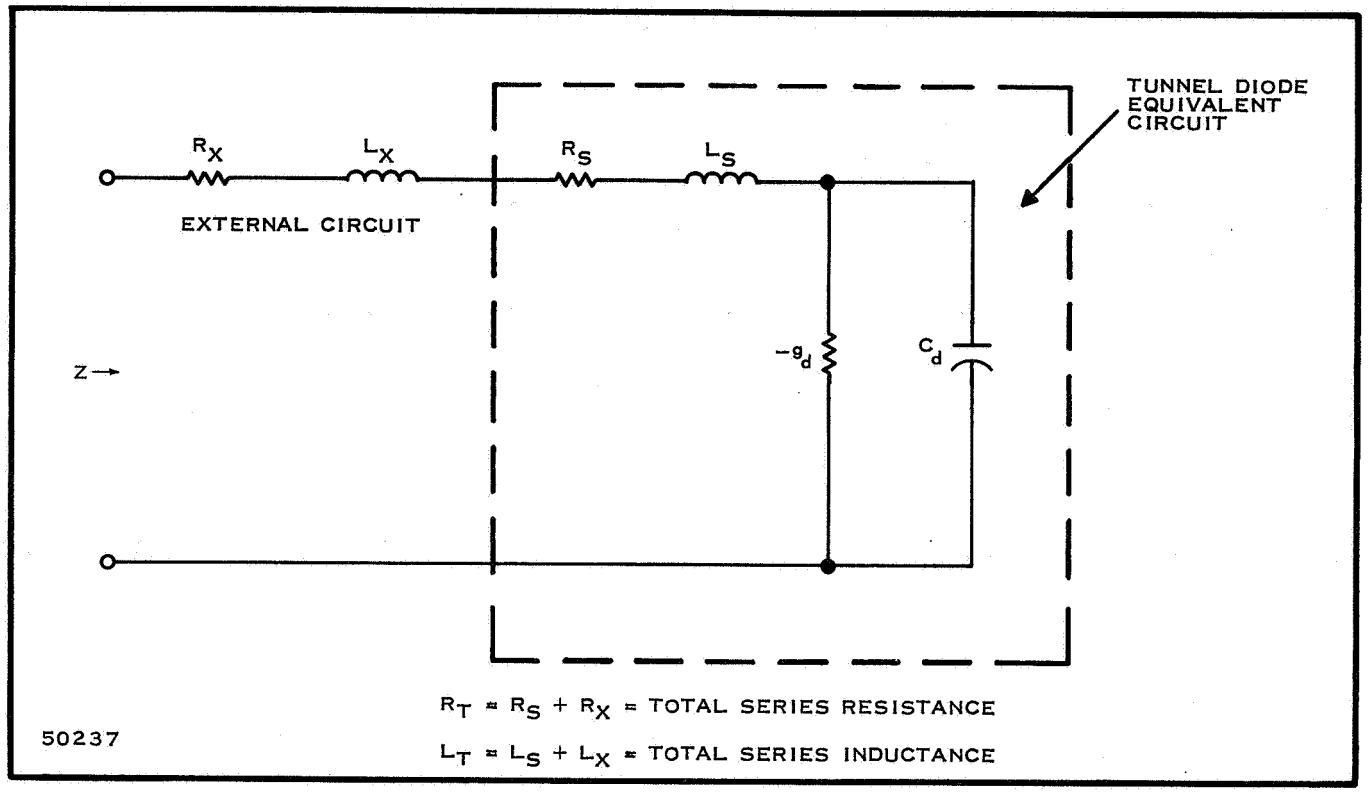

Figure 34. The Tunnel Diode Equivalent Circuit and External Circuit

The tunnel diode will not amplify above its resistive cutoff frequency (f_{ro}) and it should be pointed out that in a physical circuit external components contribute to f_{ro}. In a transistor package, the frequency limit is about 1 GHz, due primarily to lead inductance, but with microstrip and microwave packaging this figure may be increased by an order of magnitude or more.

The tunnel diode may be placed in a parallel circuit to achieve current gain or it may be placed in a series circuit to obtain a voltage gain. It can be seen from Figure 35 that the voltage gain of the parallel circuit is unity. Current gain is accomplished when $g_g + g_l = -g_d$; the current in the $g_g + g_l$ branch increases with voltage at the same rate as the current in the $-g_d$ branch decreases with voltage. The net result is that a large current variation in the $g_g + g_l$ branch is achieved with a very small current variation in the source with a current gain of up to 30 dB. In the series connection shown in Figure 36, the current gain is unity.

Successful linear operation of the tunnel diode amplifier depends on the stability of the complete system, including in particular, the internal impedance of the bias supply and the signal source impedance. The basic amplifier circuit can be reduced to that shown in Figure 37 where $R_T = R_g + R_l + R_s$, $L_T = L_s + L_l$ is the total circuit inductance and $-g_d$ is the negative conductance of the diode at the operating current and voltage.

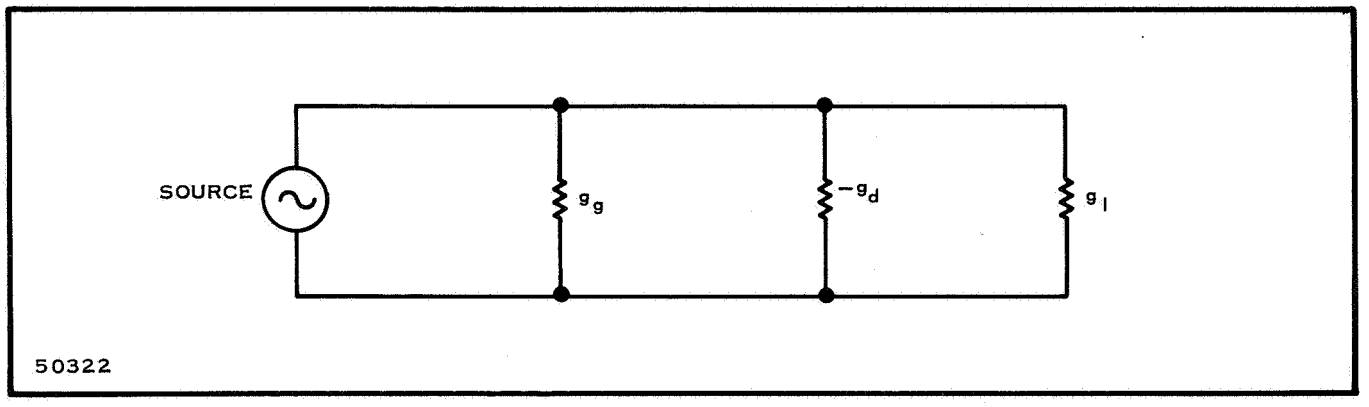

Figure 35. Tunnel Diode Parallel Connection Amplifier Simplified

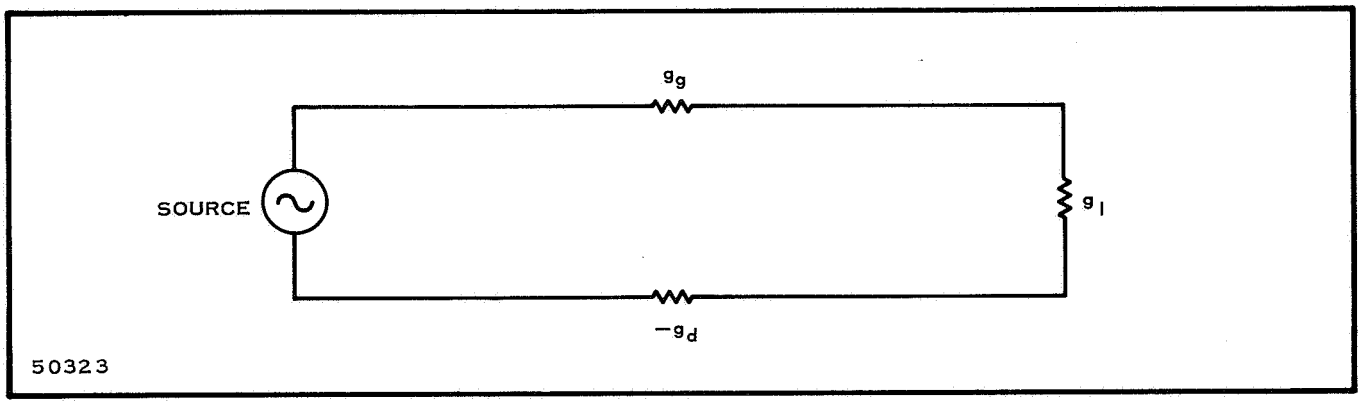

Figure 36. Tunnel Diode Series Connection Amplifier

To determine the system stability, one can examine the distribution of the poles and zeros of the circuit determinant in the complex S-plane. If the zeros seen at the input fall in the right-half side of the S-plane, the system is unstable. Conversely, zeros in the left-half of the S-plane indicate a stable system.

The input impedance is

$$Z_{in} = R_T + S L_T = \frac{\frac{1}{SC}\left|\frac{1}{-g_d}\right|}{\frac{1}{SC} - \left|\frac{1}{-g_d}\right|} \tag{28}$$

By rearranging and collecting terms

$$Z_{in} = \frac{S^2 L_T C + S(R_T C - L_T \left|-g_d\right|) + (1 - R_T \left|-g_d\right|)}{SC - \left|-g_d\right|} \tag{29}$$

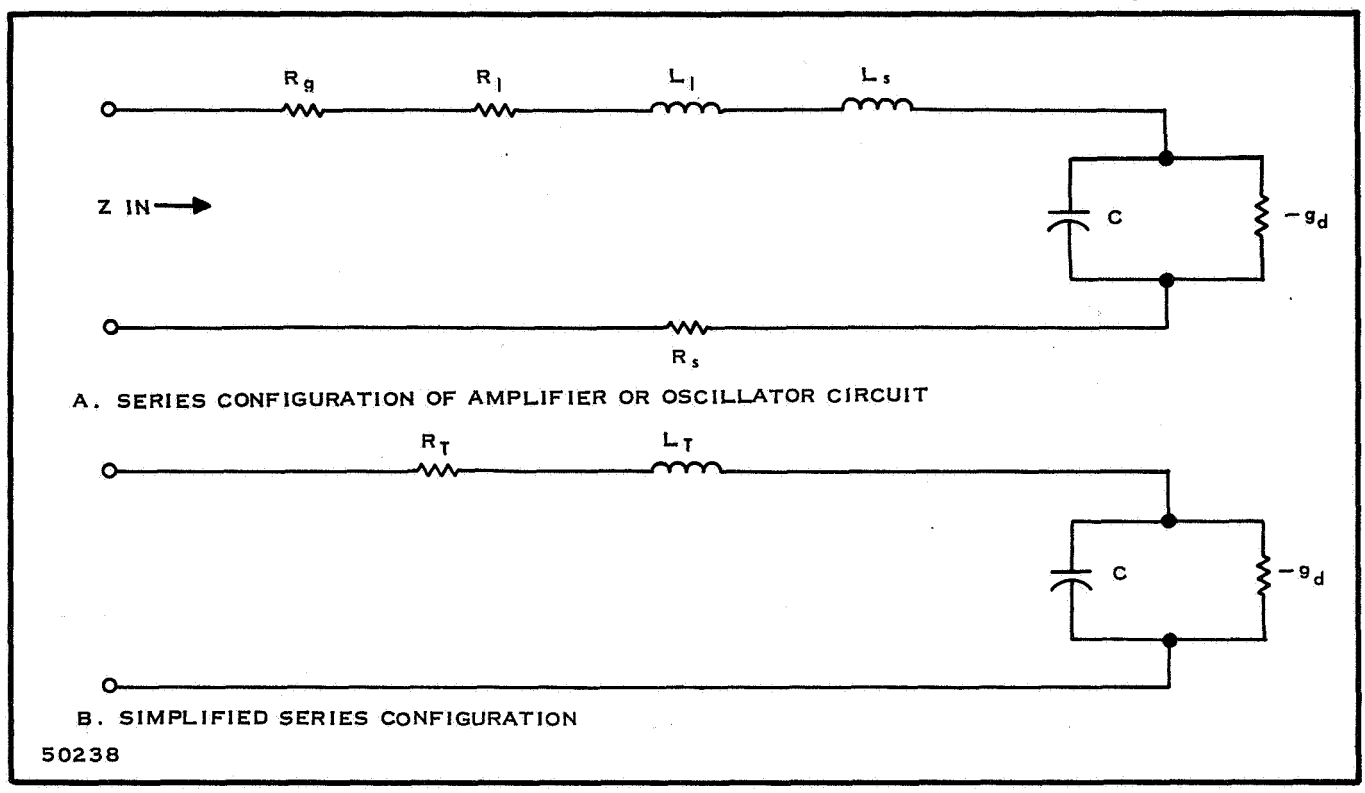

Figure 37. Simplified Schematic for a Tunnel Diode Amplifier or Oscillator

and the zeros are:

$$S = -1/2\left(\frac{R_T}{L_T} - \frac{|-g_d|}{C}\right) \pm \sqrt{1/4\left(\frac{R_T}{L_T} - \frac{|-g_d|}{C}\right) - \left(\frac{1 - R_T\,|-g_d|}{L_T C}\right)} \qquad (30)$$

Then S will have a negative real part only if:

$$\frac{R_T}{L_T} - \frac{|-g_d|}{C} > 0 \qquad \text{and} \qquad 1 - R_T\,|-g_d| > 0 \qquad (31)$$

This can be rewritten as $\frac{1}{|-g_d|} > R_T > \frac{L_T\,|-g_d|}{C}$; and is shown in Figure 38.

In summary, criteria for circuit stability are:

a. The circuit inductance L_T must be less than $\frac{R_T C}{-g_d}$

b. The sum of the positive conductances must be nearly equal to, but always greater than the negative conductance of the diode.

c. The bias must be supplied by a stable voltage source (very low internal impedance).

d. All of the above requirements must remain satisfied over the range of the supply voltages and temperature conditions.

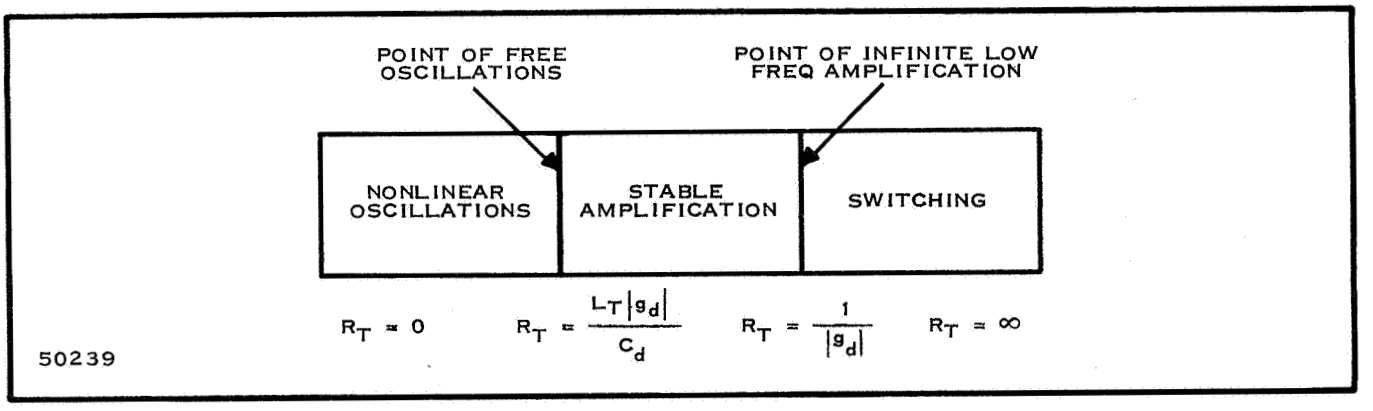

Figure 38. Graphical Conditions for Operating Stability for Tunnel Diodes

3. The Tunnel Diode Oscillator

To operate as an oscillator, the total series resistance (R_T), of the tunnel diode circuit must be less than $\frac{L_T \quad |-g_d|}{C}$ where L_T is the total series inductance, $-g_d$ is the negative conductance of the tunnel diode, and C is the capacitance of the tunnel diode. Oscillators are divided into two groups; the relaxation oscillator and the sinusoidal oscillator. The distinction between these two groups is that sinusoidal oscillators just barely satisfy the criterion for supplying the losses. Relaxation oscillators traverse large loops about the static characteristic (Figure 39).

The desirable features of tunnel diode oscillators include high frequency capability, low power consumption, good frequency stability when properly compensated, low noise, and circuit simplicity. The primary disadvantage is low output power and/or high harmonic content.

a. Relaxation Oscillator

If the real component of the input impedance of the circuit is largely negative, the oscillation amplitude will be large, resulting in significant limiting (i.e., relaxation oscillations). The voltage swing (V_{FP}-V_P) could approach one volt (GaAs units) while the current swing depends on the peak current, I_p, and could be as high as several amperes. The maximum power output for the typical GaAs device (Table XI) is derived as follows:

$$V_{rms} = 1/2 \frac{V_{pp}}{\sqrt{2}} = \frac{1}{2\sqrt{2}} (V_{FP} - V_p) \tag{32}$$

$$I_{rms} = \frac{1}{2\sqrt{2}} (I_p - I_v) \tag{33}$$

$$P = V_{rms} I_{rms} = 1/8 (V_{FP} - V_P) (I_p - I_v) \tag{34}$$

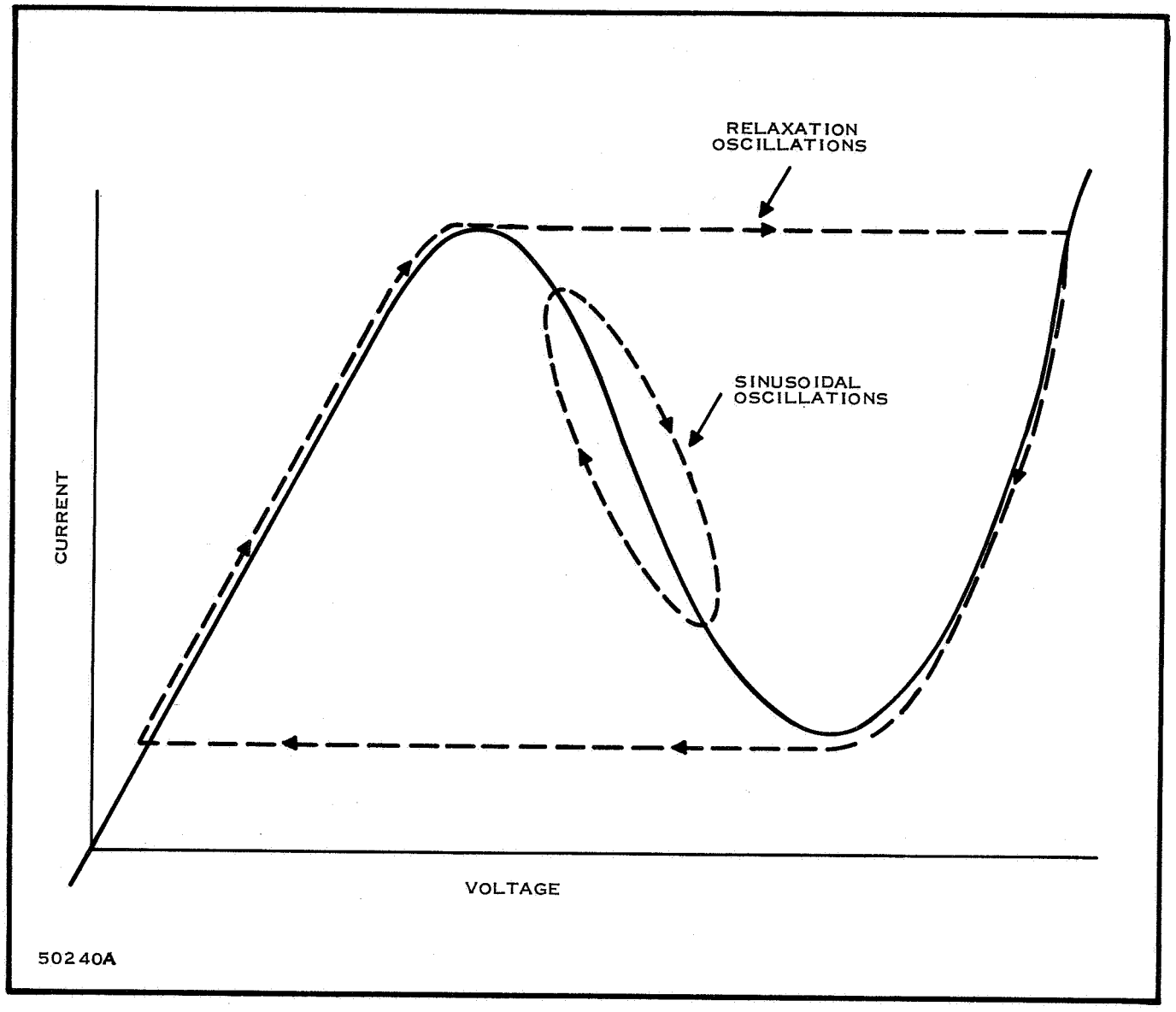

Figure 39. Oscillator Limit Cycles

for GaAs

$$V_{FP} = 1.1 \text{ volts } V_P = 0.15 \text{ volts} \qquad (35)$$

$$I_p = 15\, I_v$$

$$P = 1/8(0.95)(0.933I_p) = 0.113I_p \text{ Watts}$$

b. Sinusoidal Oscillator

The mathematical condition for "free" sinusoidal oscillations requires that the real and imaginary parts of the input impedance equal zero.

$$Z_{in} = R_e(Z_{in}) + I_m(Z_{in}) = 0 \tag{36}$$

If the real part is slightly negative, good sinusoidal oscillations will occur. For this case, the real part of Equation (30) is written,

$$\frac{R_T}{L_T} - \frac{|-g_d|}{C_d} \approx 0 \tag{37}$$

and the resonant frequency is expressed:

$$f = \frac{1}{2\pi} \left(\frac{1 - R_T |-g_d|}{L_T C} \right)^{1/2} \tag{38}$$

The output power is, of course, less than for the relaxation oscillator. Using the same typical GaAs diode, the maximum power output is determined as follows:

$$P = 1/8 \, (V_v - V_p) \, (I_p - I_v) \tag{39}$$

$$P = 1/8 \, (0.50\text{-}0.15) \, (0.933 I_p)$$

$$P = 0.041 \, I_p \text{ watts} \tag{40}$$

Furthermore, in practice, operation would have to be at even less output power because of harmonic distortion due to the nonlinearity of the negative conductance region and because of the danger of shifting into relaxation oscillations.

c. Operating Parameters of the Tunnel Diode Oscillator

The frequency limit of the circuit is determined by the resistive cutoff frequency, f_{ro}, of the device. At microwave frequencies two modes of oscillations are possible. They are above self-resonant frequency, f_{xo}, operation and below self-resonant frequency operation. If the resistive cutoff frequency is less than the self-resonant frequency, only one mode of operation is possible.

The equations for the self-resonant and resistive cutoff frequencies, f_{xo} and f_{ro} respectively, are:

$$f_{xo} = \frac{1}{2\pi} \sqrt{\frac{1}{L_s C_d} - \frac{|-g_d|^2}{C_d^2}} \tag{41}$$

$$f_{ro} = \frac{|-g_d|}{2\pi C_d} \sqrt{\frac{1}{|-g_d| R_s} - 1} \tag{42}$$

Figure 40 shows the Nyquist impedance plots of two tunnel diodes, D1 and D2. Diode D2 reaches its resistive cutoff frequency before it reaches its self-resonant frequency; therefore, only one mode of oscillation is possible. Diode D2, on the other hand may oscillate in the area between where the plot crosses the R axis ($f = f_{xo}$) and where it crosses the $j\omega$ axis ($f = f_{ro}$).

The frequency of operation of the series parallel circuit shown in Figure 41 is

$$fo = \frac{1}{2\pi}\sqrt{\frac{1}{L_T(C + C_1)} - \frac{|-g_d|^2}{C_1\,(C + C_1)}} \qquad (43)$$

It is dependent directly on the junction capacitance, C1, which is in turn dependent directly on temperature and bias. For this reason, the bias and temperature considerations must be closely controlled.

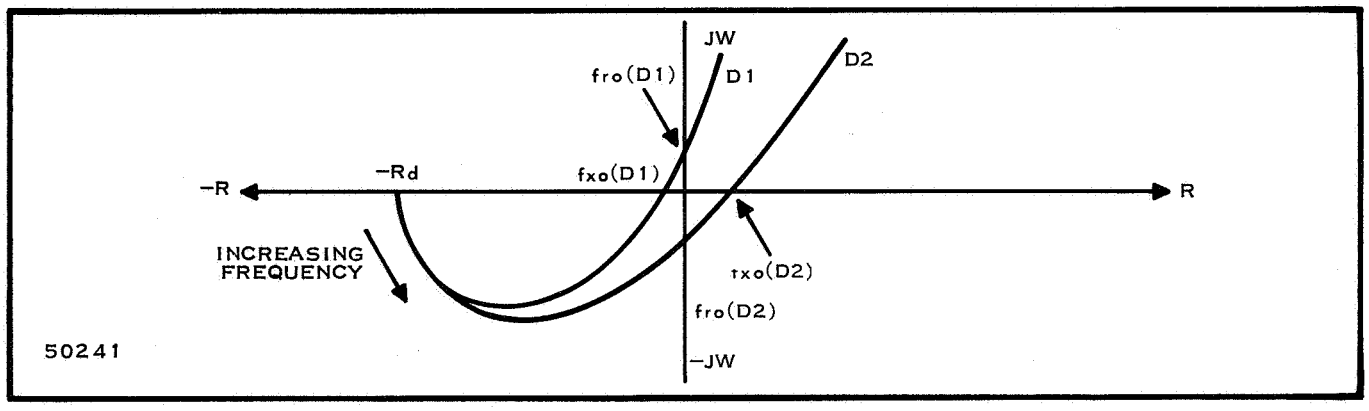

Figure 40. Nyquist Plot of Tunnel Diode Impedance vs Frequency for Two Tunnel Diodes D1 and D2

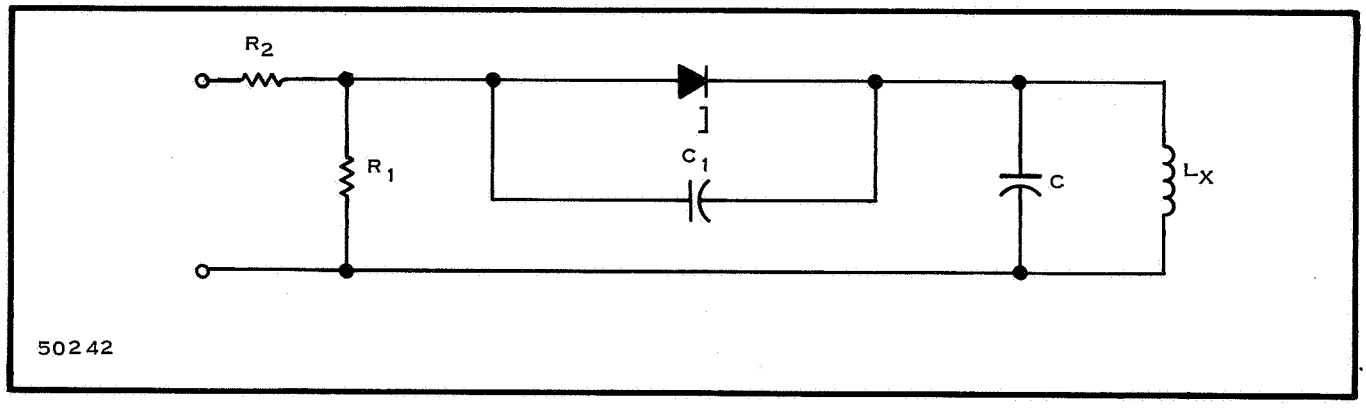

Figure 41. Series - Parallel Circuit for a Tunnel Diode Oscillator

Several approaches have been used to stabilize the frequency. One method is to make the frequency of oscillation relatively independent of junction capacitance. This can be achieved by weakly coupling the tunnel diode to a high Q resonant circuit by tapping the diode into the circuit at a low voltage point on a capacitive voltage divider. If wideband tuning is desired, one capacitor of the voltage divider can be a varactor.

The frequency of operation of the tunnel diode oscillator changes in sharp steps as the bias voltage is varied making it necessary to maintain a very constant bias.

4. The Tunnel Diode Converter

The following simultaneous functions must be performed by a single tunnel diode when it is used as a high gain self-oscillating converter:

a. oscillation at the LO frequency

b. amplification at the RF frequency

c. mixing due to non-linearity

d. amplification at the IF frequency.

On a mathematical basis:

The imaginary part of the external circuit admittance across the negative conductance of the diode should have zeros at the local oscillator and IF frequencies.

The real term of the external circuit admittance, Y, across $|-g_d|$ at the LO frequency must be smaller than the negative conductance of the diode.

The real part of the external admittance across $|-g_d|$ must be larger than the magnitude of $|-g_d|$ at the IF frequency.

The imaginary part of the external circuit admittance is shown plotted against frequency in Figure 42. This condition satisfies (a) above. A possible tunnel diode converter circuit is shown in Figure 43.

5. Tunnel Diode Noise

In the tunnel diode the major contributor to noise is shot-noise. The noise figure equation is:

$$NF = 1 + \frac{20\, I_{DC}}{g_g} + \frac{T_1\, g_1}{T_g\, g_g} \qquad (44)$$

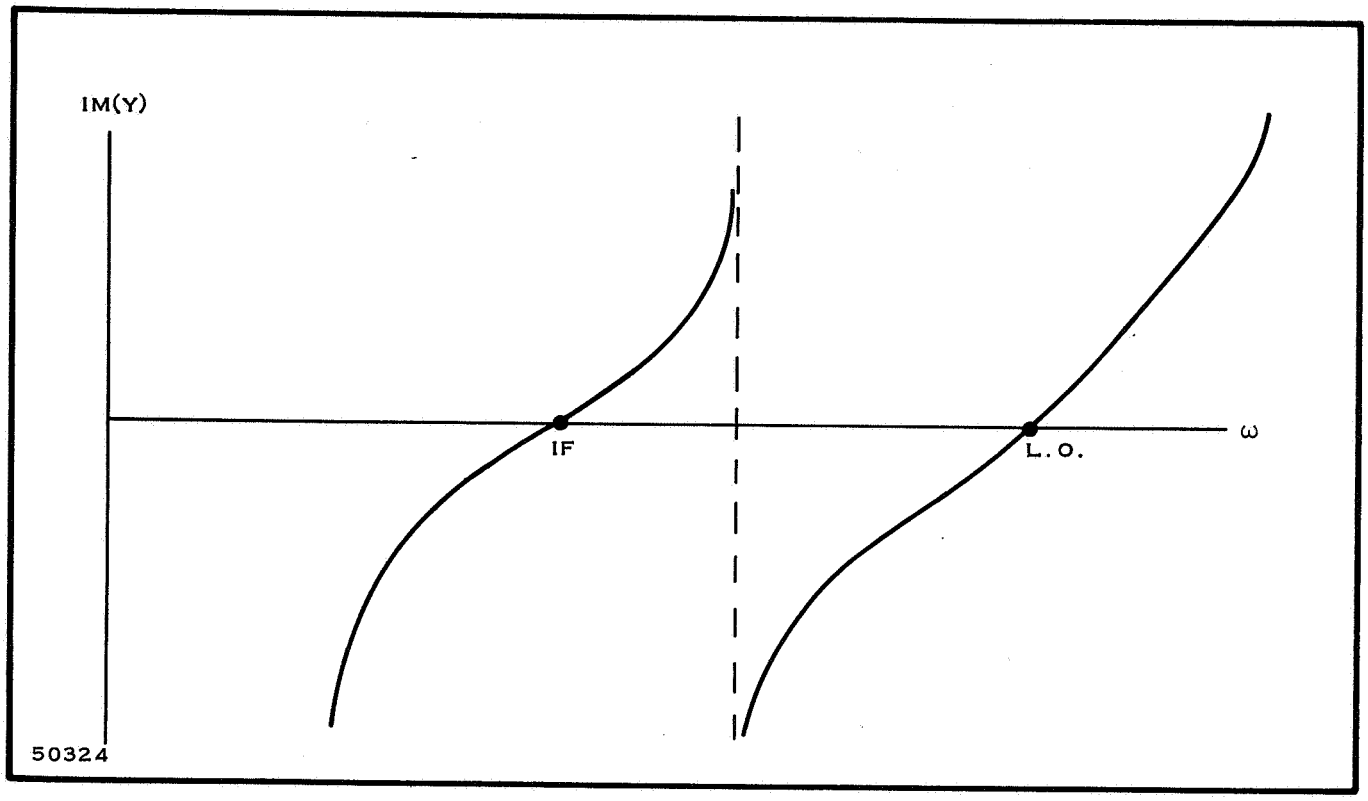

Figure 42. Im(Y) as a Function of Frequency for Two Resonant Circuits

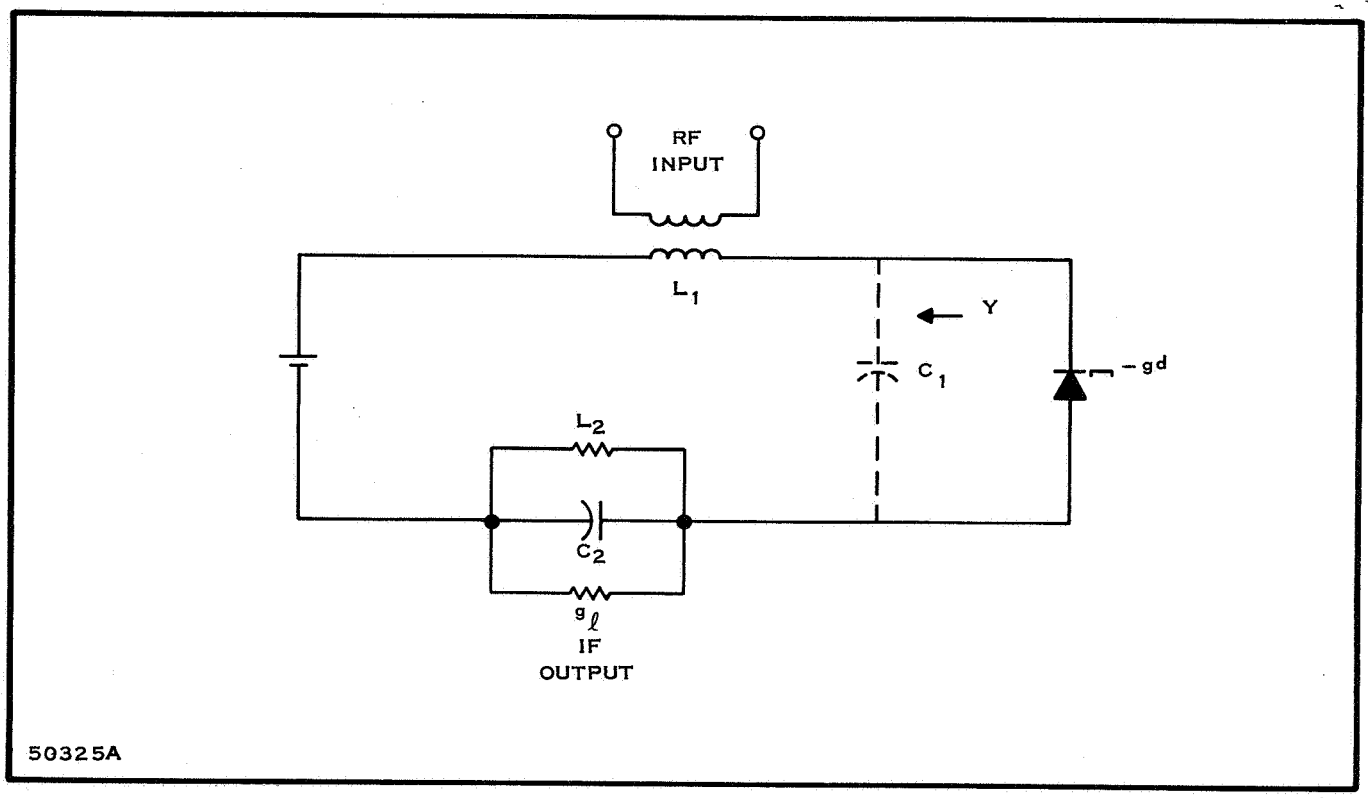

Figure 43. Tunnel Diode Converter Circuit

Where

I_{DC} is DC bias current through the tunnel diode

g_g is the conductance of the generator

g_1 is the conductance of the load

T_1 is the effective noise temperature of the load

It is evident that g_g should be large and g_1 should be small, but for highest gain $g_g + g_1 = |-g_d|$.

Therefore, g_g should be nearly equal to $|-g_d|$.

F. AVALANCHE DIODES

1. General

In 1958, Read[26] predicted microwave oscillations from avalanche diodes. At that time, special doping gradients were recommended in order to achieve a highly localized avalanche zone at one side of a high-field depletion region in a semiconductor diode. Since that time, a great amount of effort has been devoted to the development of solid-state microwave generators. Many diodes, other than Read devices, are showing promise as oscillators and amplifiers when biased into the avalanche breakdown region. In 1965, the generation of substantial power was obtained by avalanching silicon computer diodes. Later, high CW operation with good efficiency was obtained with GaAs varactor diodes and silicon devices[27].

A detailed discussion of how an avalanche diode generates power will not be given here; however, it is pointed out that avalanche effects, induced by reverse-bias, breakdown, and a transit time delay of carriers across the junction combine to yield negative resistance and gain.

Oscillations have been observed in p^{++}-n^{+}-n-n^{++} diodes over a wide frequency range extending to 8 GHz where transit time effects may have been present. However, the absence of a lower cutoff frequency showed that transit time was not essential for the oscillations. Instead they could be attributed to a negative resistance which begins at a critical current density corresponding to carrier concentrations slightly smaller than the impurity concentration in the n^{+} zone. Therefore, space-charge effects must be considered[28]. Inductance (related to the avalanche process), capacitance (related to the depletion layer), and negative conductance and a noise generator is shown in Figure 44. It has been established that a satisfactory small-signal equivalent circuit for the p-n junction avalanche diode is a parallel combination of the above elements. Probably the most serious disadvantage to avalanche diodes is a high noise level.

The problem of frequency stability has not been studied extensively, but it is known that the frequency of operation is dependent on the dc current at the avalanche condition. The characteristic of the avalanche diode illustrated in Figure 45 shows that the current is controlled by limiting rather than by the dc bias voltage. Therefore, currents smaller than the limit current, and the resulting frequency shifts, are probable.

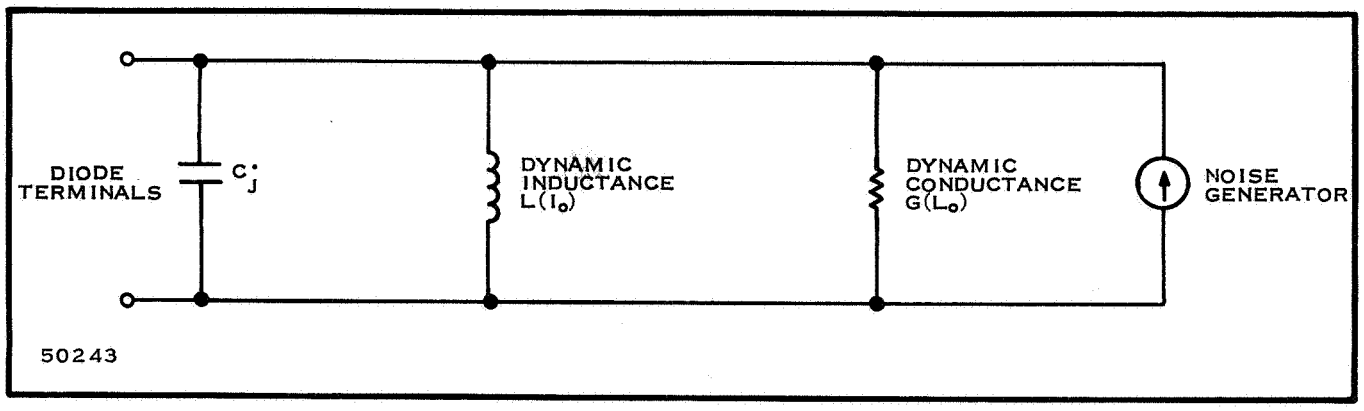

Figure 44. Equivalent Circuit for the Avalanche Diode

2. Operation of an Avalanche Diode

The negative conductance of an avalanche diode is apparent over a wide frequency range; therefore, it can oscillate at several frequencies simultaneously over a wide range. The output at a specific frequency is dependent upon the tuning of the external circuit. Even the most sophisticated filtering techniques are generally unsatisfactory because several fundamentals are present and harmonic and parametric oscillations may exist as well. To determine accurately the power content of any particular frequency component it is essential to use signal substitution methods.

Many microwave oscillators have been built using avalanche diodes. A silicon diode which generates 1.1 watts of CW at 12-GHz with 8-percent efficiency has been constructed.[30] Some GaAs varactors have delivered 25 to 30 mW between 13 — 14-GHz with a 5—6-percent efficiency. The bias current was 10 mA with an avalanche voltage of 45 to 55 volts.

An avalanche diode may also be used to amplify. Avalanched GaAs varactors have given gain when used in a circulator-coupled network which forms a negative-resistance, reflection type amplifier. The amplification was quite stable and oscillations were easily suppressed.

Saturation occurred at levels above 0 dBm and discernable signal levels of -90 dBm were consistently observed. With +10 dBm input, the power gain was more than 5 dB with a 3 dB bandwidth of 100 MHz. At -60 dBm input, the gain was +52 dB with a

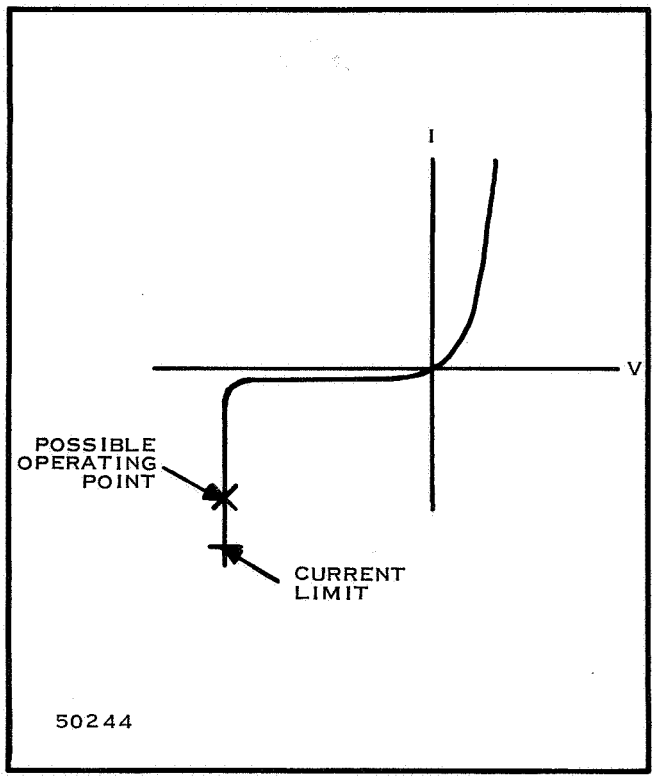

Figure 45. V-I Characteristics of an Avalanche Diode

bandwidth of 10 MHz. The ability to operate with input levels greater than 0 dBm is one of the significant advantages of the GaAs avalanche diode amplifier. Low power requirements is another advantage.

In addition to the noise limitation, the narrow bandwidth may prove to be troublesome in avalanche diode amplifiers. Although, the noise figure of the avalanche diode is prohibitive at the present time, it is very likely that in the near future they will be competitive with, if not better than, Gunn devices and tunnel diodes.

The power output and the high level input make them very attractive. This is a very new and fast growing aspect of solid-state electronics which will bear much attention in the future.

3. Noise Considerations

As stated previously, noise is the major disadvantage of the avalanche process. Studies of avalanche noise in commercially available avalanche diodes reveal large noise variations from diode to diode.[31] The spectral noise density passes through a sequence of maxima and minima with increasing avalanche current.

The maxima and minima are associated with microplasma especially at lower currents (100 μA or less). A microplasma is a localized region of avalanche breakdown. At small magnitudes of current, e.g., of the order of 30μA, the avalanche discharge of the microplasma is unstable and switches on and off. As the current increases, the discharge becomes stable, the on-off switching ceases, and the spectral noise density decreases. Several microplasma may exist at different levels of current, so that as one becomes stable another may become unstable. When all the microplasma are stable (or inactive) the spectral noise density falls off sharply until the noise level of stable discharge is reached.

Microplasma-free uniform avalanche diodes have been prepared by the guard ring technique. The guard ring is a region of high breakdown voltage around the active area of the device. It must have a lower impurity gradient at the junction and a sufficiently large radius of curvature so that the central region breaks down before the surface of the ring. Diodes with diameters from six microinches to 90 microinches and breakdown voltages from 5.9 volt to 46 volt were used. Each wafer also contained a planar n^+p or p^+n diode without the guard ring for capacitance-voltage measurements which are required to determine the width of the depletion layer in the breakdown region[85].

The spectral noise density has three contributors.

$\frac{1}{\sqrt{I}}$ Noise, I is the diode current

Excess noise at low current densities

Excess noise at high current densities

The $1/\sqrt{I}$ noise is independent of temperature from -196°C to 200°C. Any deviation from the $1/\sqrt{I}$ plot is due to excess noise temperature dependence (Figures 46 and 47). It can be seen that it is a linear function of breakdown voltage when plotted on log-log paper.

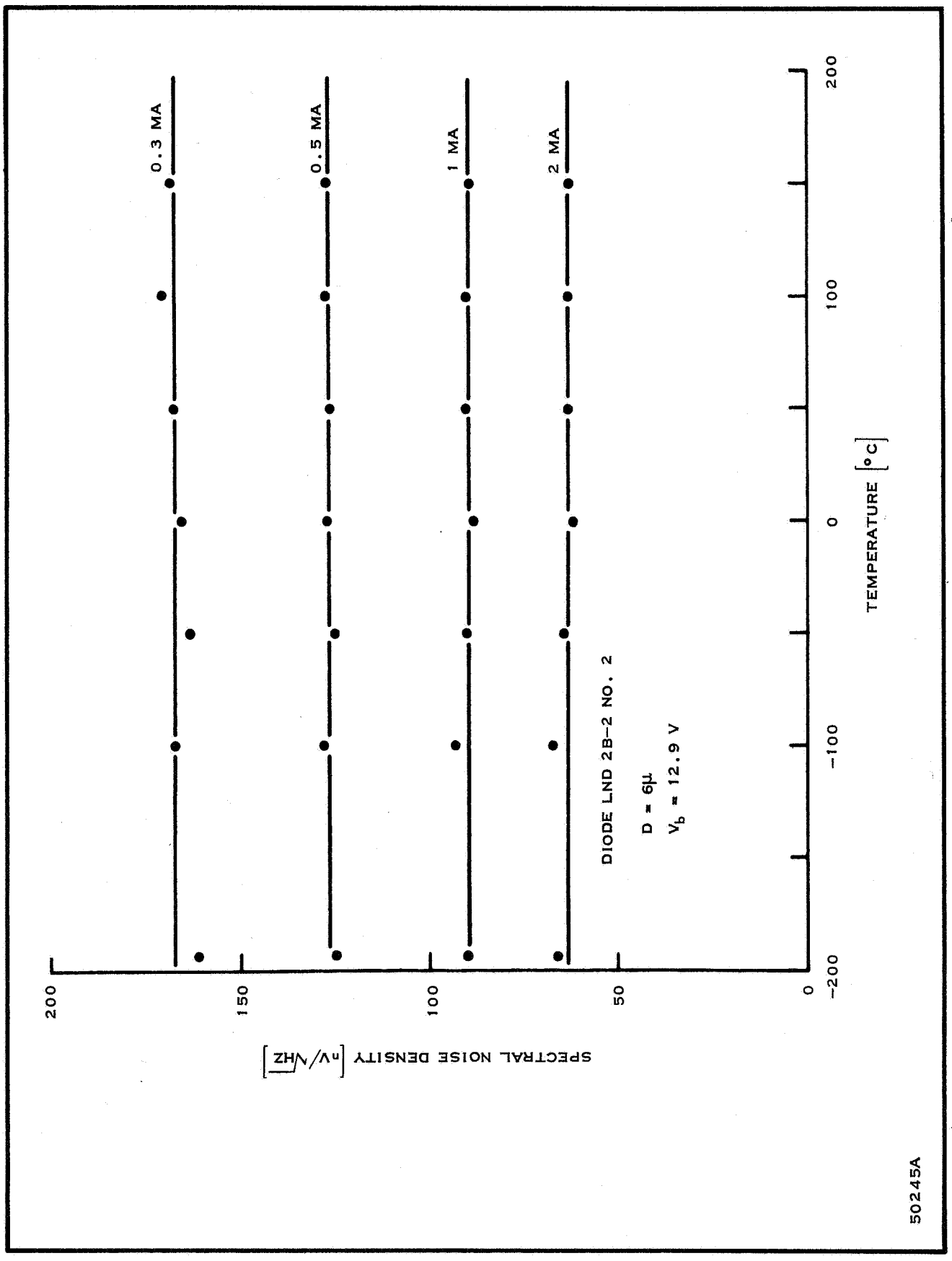

Figure 46. Spectral Noise Density vs Temperature

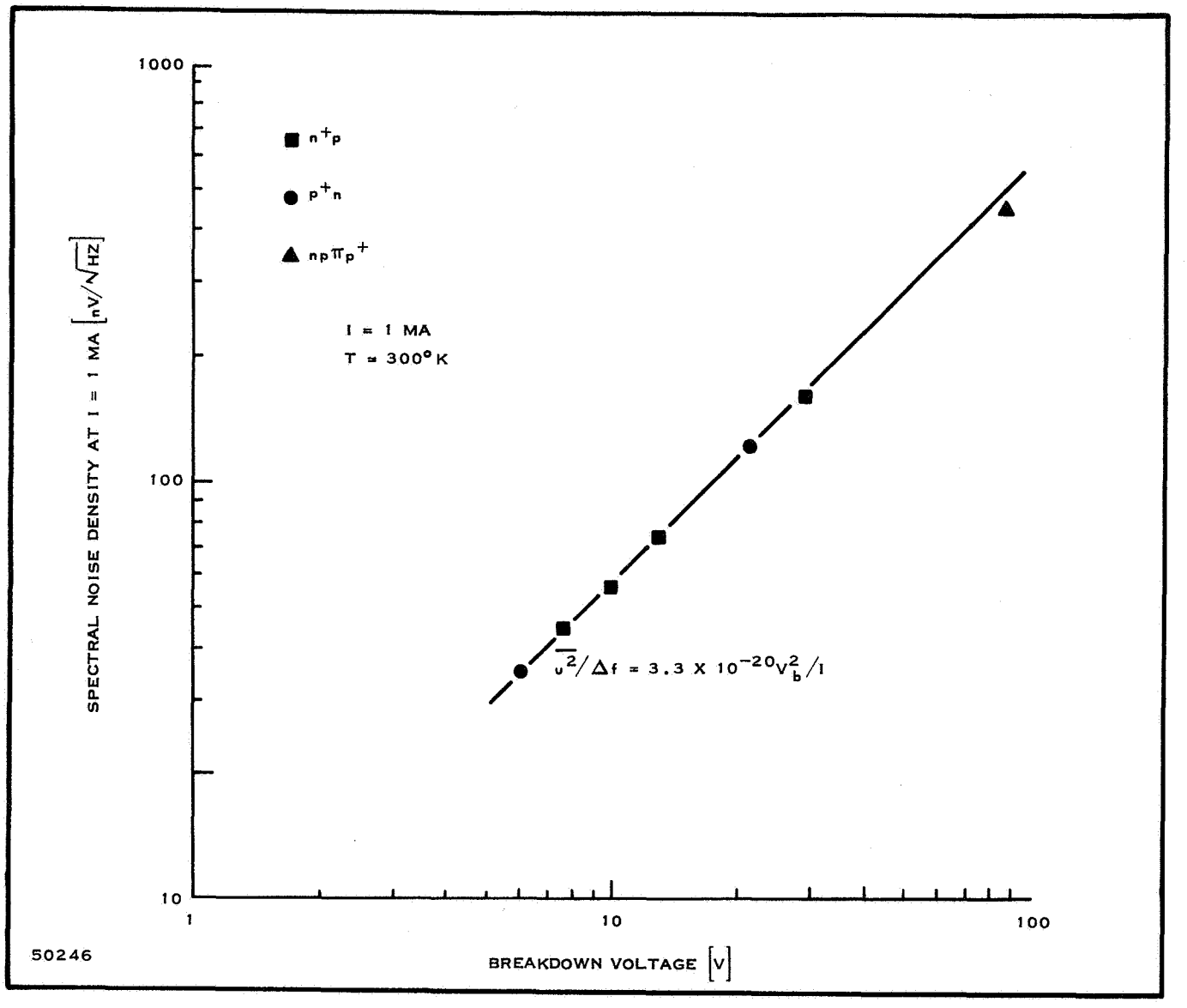

Figure 47. Spectral Noise Density vs Breakdown Voltage

The series resistance (Rs) is in the first approximation, independent of current; however, there is an increase in Rs at high currents. It is an inverse linear function of the breakdown diameter when plotted on log-log paper. This can be seen in Figures 48 and 49.

The excess noise at the higher current densities appears to be associated with thermal effects. This is not surprising since at a current of 20 mA through a 6 μ-inch diode the power density is approximately 10^6 w/cm^2. This corresponds to an estimated temperature rise of 300°C. Therefore, this excess noise can be reduced by improving heat dissipation methods. Experimental studies indicate that the spectral density is not white but increases with decreasing frequency.

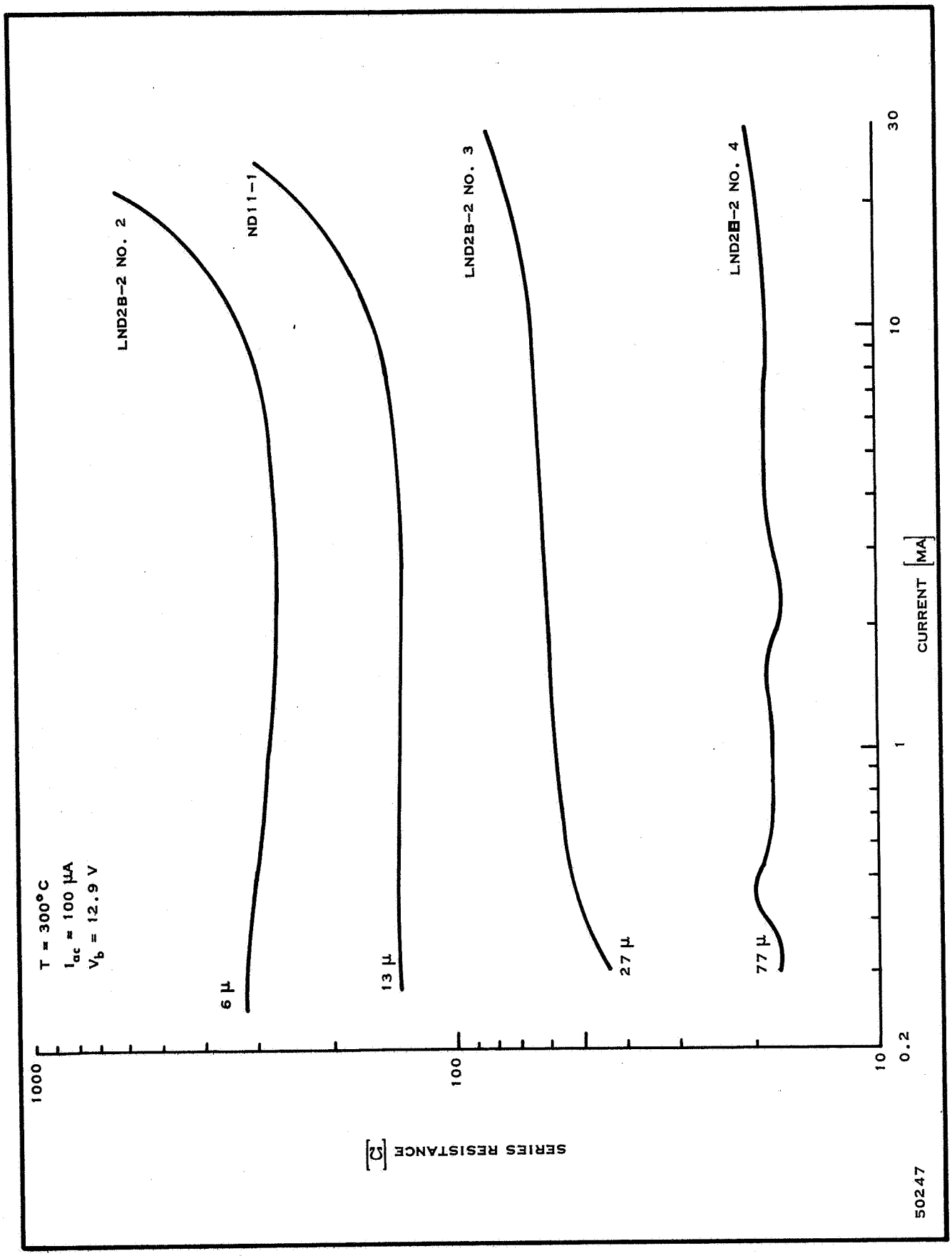

Figure 48. Series Resistance vs Current

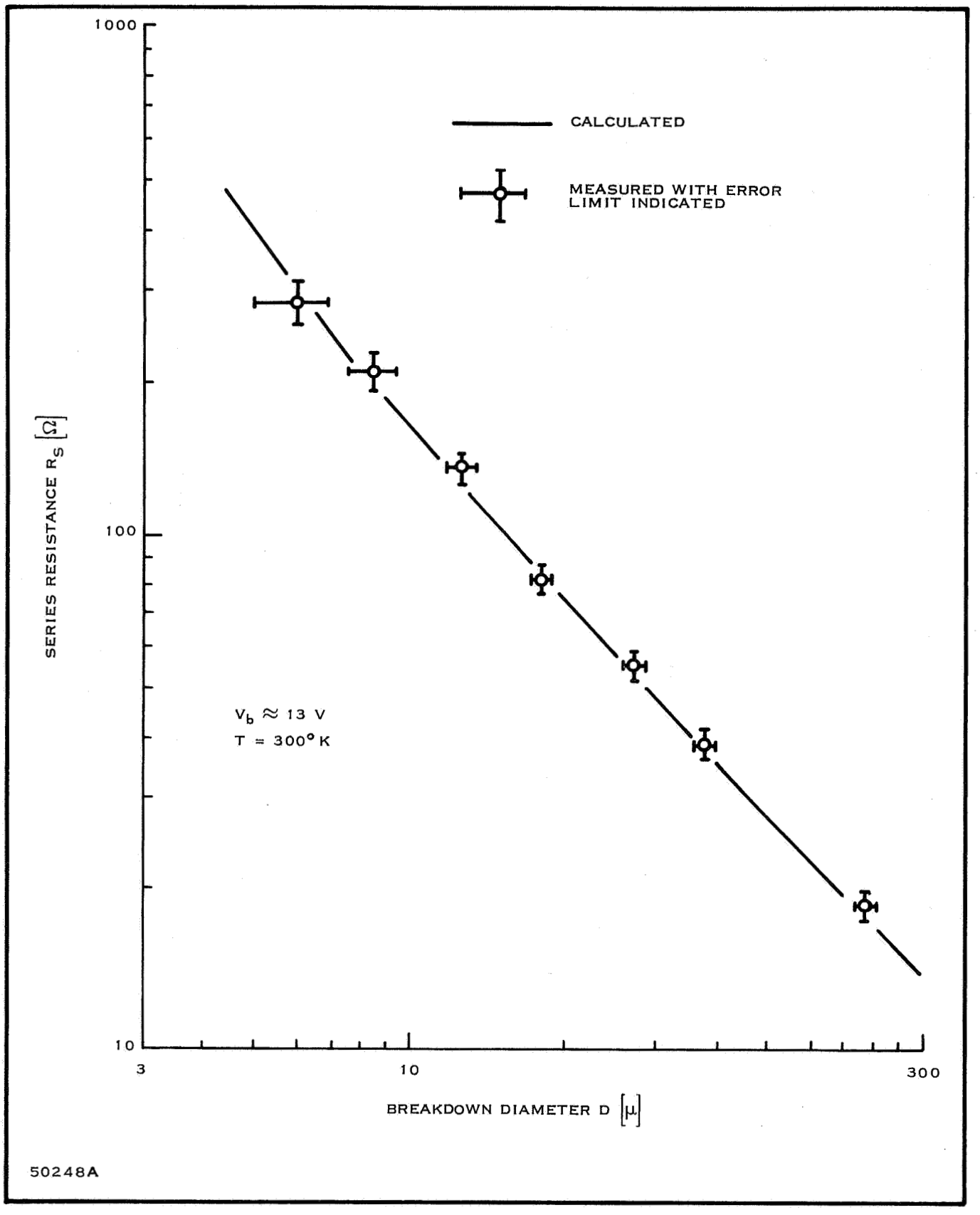

Figure 49. Series Resistance vs Breakdown Diameter

The excess noise at low current densities seems to be associated with non-uniformities of the avalanche breakdown. The non-uniformities causing the noise peaks consist of small variations of V_b which are likely caused by small local variations of the doping concentration in the starting material.

As previously explained, the foregoing analysis was based on diodes made by the guard ring technique. These diodes will not function as oscillators or amplifiers because their capacitance is too high. They will serve as noise generators, low noise avalanche diodes, and low current avalanche diodes.

As noise generators they have several features which make them ideal. Their solid-state design guarantees low weight, small volume, low power consumption, high reliability, and ease of operation. In the case of small diodes, which are free of excess noise at low currents and follow the $1/\sqrt{I}$ low of noise vs current (Figure 50), the reproducibility is considerably improved over conventional solid-state sources. The noise variation from diode to diode from the same batch is less than 5 percent. Their open circuit spectral noise density is flat (+1 dB) from 10 Hz to at least 1-GHz with levels 40 to 50 dB above the thermal noise of Rs. Another feature is the possibility to adjust the noise level by varying the dc current.

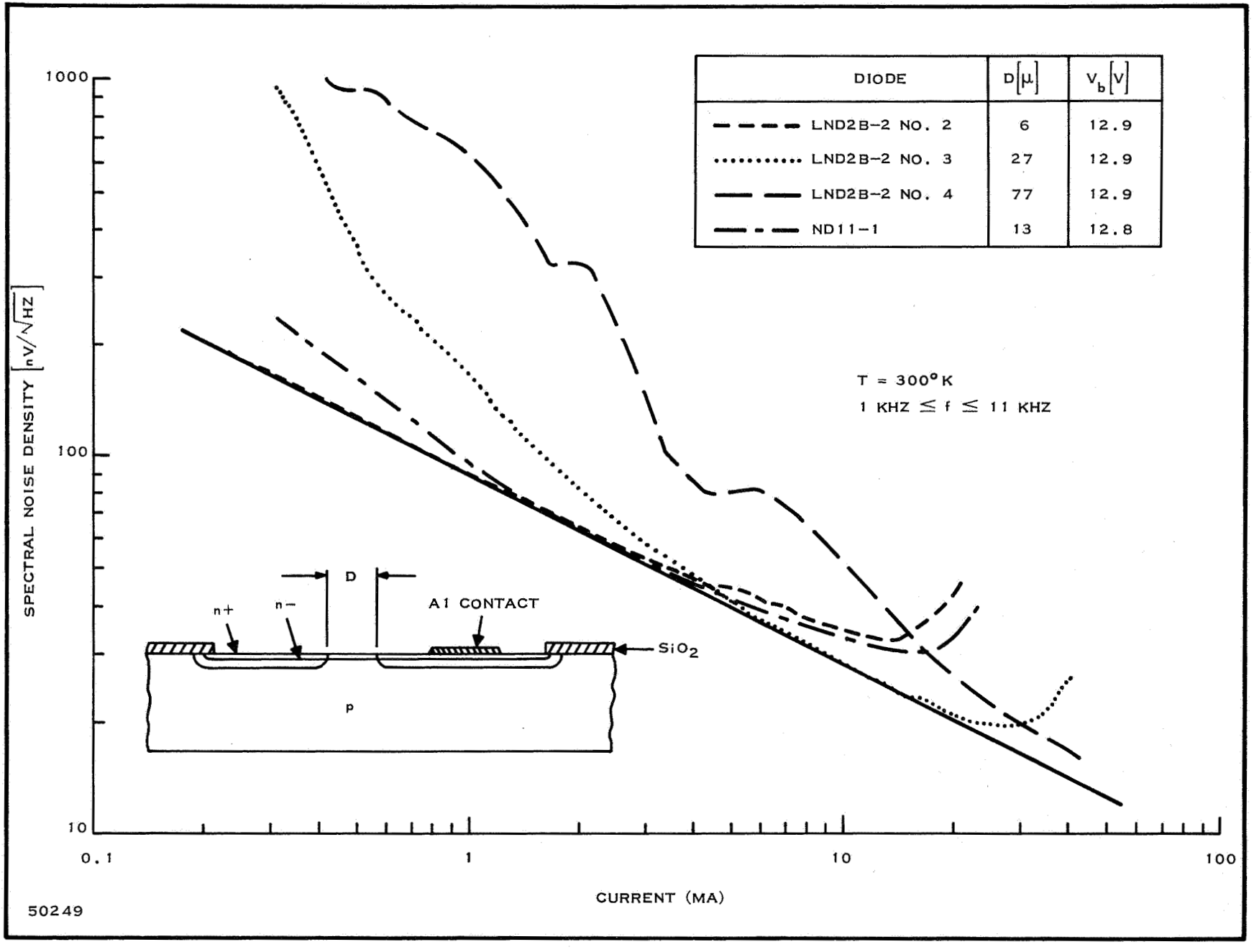

Figure 50. Spectral Noise Density vs Current

SECTION V

LINEAR INTEGRATED CIRCUITS

A. GENERAL

Linear integrated circuits are becoming increasingly available for use up to the VHF region. The use of "off-the-shelf" linear IC's satisfy many requirements applicable to receiver design. The operational amplifier and cascode configurations serve many functions from RF amplification to mixing and detection. These devices were not covered in Scientific Report No. 1 as they were in the state of infancy. Now, however, continued development and applicability to lower frequency integrated stages in a microwave receiver warrants their discussion.

The most common linear integrated circuit today is fabricated by monolithic silicon epitaxial construction and will perform all low level requirements from dc to 200 MHz. In addition to offering the system designer a savings in space and weight, an increased reliability is realized. In systems converted from discrete components to integrated devices, a reliability improvement of six to thirty is feasible.

The present state-of-the-art monolithic transistors have a frequency response extending beyond 1 GHz due to improved photographic techniques which help reduce device geometry and associated capacitances. Nevertheless, integrated circuits encounter special problems in such linear applications as RF and IF amplifiers due to parasitic capacitances between elements in the monolithic substrates, and the lack of frequency selective schemes compatible with integrated structures.

The problems due to parasitic capacitances prevent the full frequency capability of integrated transistor from being fully realized, and the restricted range of component values allowed by monolithic construction in some instances prevents the integrated circuit from performing as well as it's discrete component counterpart.

B. BASIC CIRCUIT CONSIDERATIONS

Monolithic linear integrated circuits are fabricated by the same process which produces digital building blocks for logic systems. That is, the active and passive components are fabricated in a single structure, and all connections are made simultaneously by forming a metal interconnection pattern on the surface of a silicon bar. The forming process is illustrated in Figure 51.

To date, linear integrated circuits for operation at microwave frequencies are not available in monolithic construction. Although in theory, such circuits are possible, hybrid integrated circuits have been more successful. In hybrid construction, high unloaded circuit Q's can be maintained with etched or deposited passive components to which silicon chip transistors or diodes are bonded. The propagation characteristics of a microwave linear circuit requires some form of transmission line circuitry to keep losses low. If the transmission line must propagate energy at microwave frequencies with low losses, the insulating substrate should be a good dielectric. The

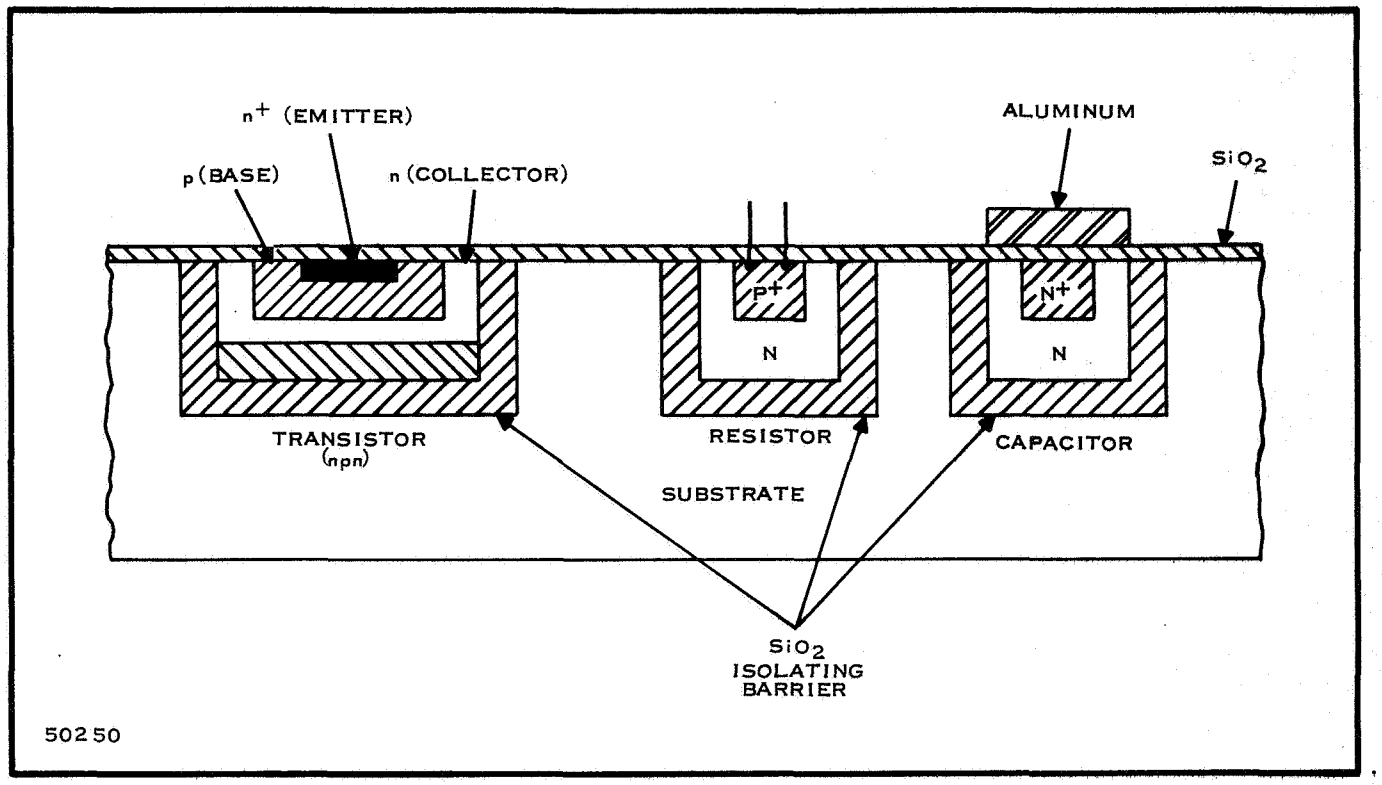

Figure 51. Monolithic Fabrication Process

low resistive semiconductor substrate used in monolithic construction does not serve these needs as well as hybrid techniques which use ceramic or glass substrates.

In Figure 51, it can be noted that each component is completely surrounded by a dielectric material, silicon dioxide (SiO_2). One of the major problems stemming from monolithic construction is that individual components need to be isolated from each other. Several techniques such as using high resistivity substrate or reverse-biased PN junction have been used to achieve the required isolation. The latter method has been more predominant as it is easier to fabricate and provides more complete isolation. However, this method provides capacitive coupling to the substrate. Recent developments seem to indicate dielectric isolation techniques are more advantageous. Dielectric isolation offers the possibility of making and using PNP and NPN devices on the same chip and reduces capacitances as the oxide thickness also controls the capacitance per unit area. The capacitance per unit area is shown in Figure 52 plotted versus oxide thickness. With a two micron dielectric and a typical monocrystalline transistor island, the capacitance would be approximately 0.3 pfd. This is about an order of magnitude less than that obtained for PN junctions.

The only disadvantage of using dielectric isolation over other methods is a slightly reduced power handling capability as silicon dioxide has a lower thermal conductivity than silicon. However, this is not expected to be too great a problem since the total thermal resistance can be controlled by the thickness of oxide used.

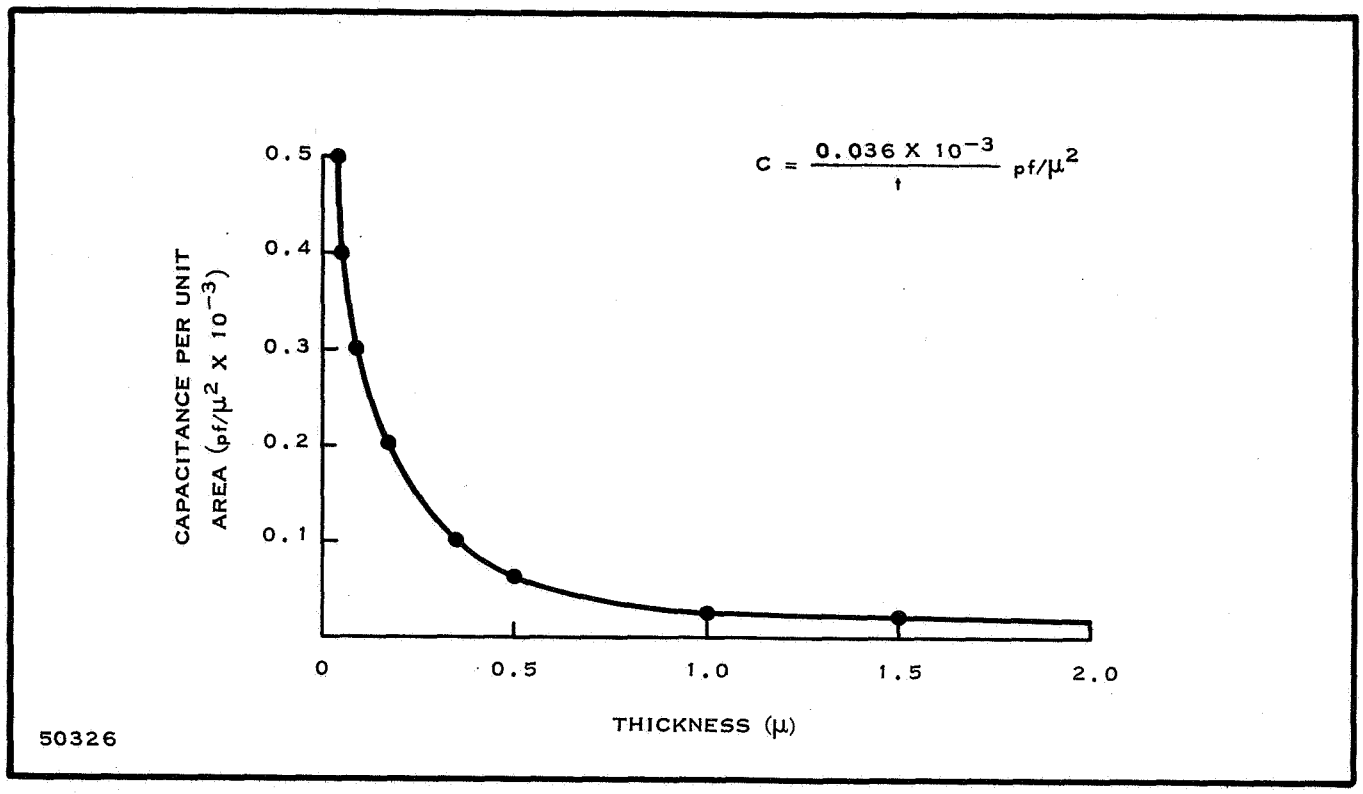

Figure 52. Capacitance per Unit Area vs Thickness

The greater range of circuit design requirements in systems utilizing linear circuits essentially prohibits standardization which is common in logic systems that employ digital building blocks. In many instances, linear circuits are "customized" to meet a particular circuit application.

The nearest thing to standardization is the differential amplifier configuration. Figure 53 shows the basic circuit configuration used for a broad line of multiple functions. The configuration is basically that of a balanced differential amplifier in which the currents to the emitter-coupled differential pair or transistors are supplied from a controlled source. A wide use of linear integrated circuits for analog applications from dc to frequencies into the vhf region such as mixing, limiting, product detection, frequency multiplication, and amplitude modulation in addition to linear amplification can be obtained from such a versatile configuration.

The differential amplifier may be used as a normal operational amplifier by ignoring one of the outputs. The single output and an inverting and noninverting input makes it possible for a positive or negative feedback to be applied. This feedback concept is well suited to integrated circuits because the complete circuit specification is dependent on tolerance of one or two components rather than components of integrated operational amplifier. Many different circuit functions can be performed with an operational amplifier by using different feedback networks around the amplifier as illustrated in Figure 54. Linear integrated circuits with the operational amplifier configuration and utilizing such feedback are ideally suited for instrument and analog use or in control systems.

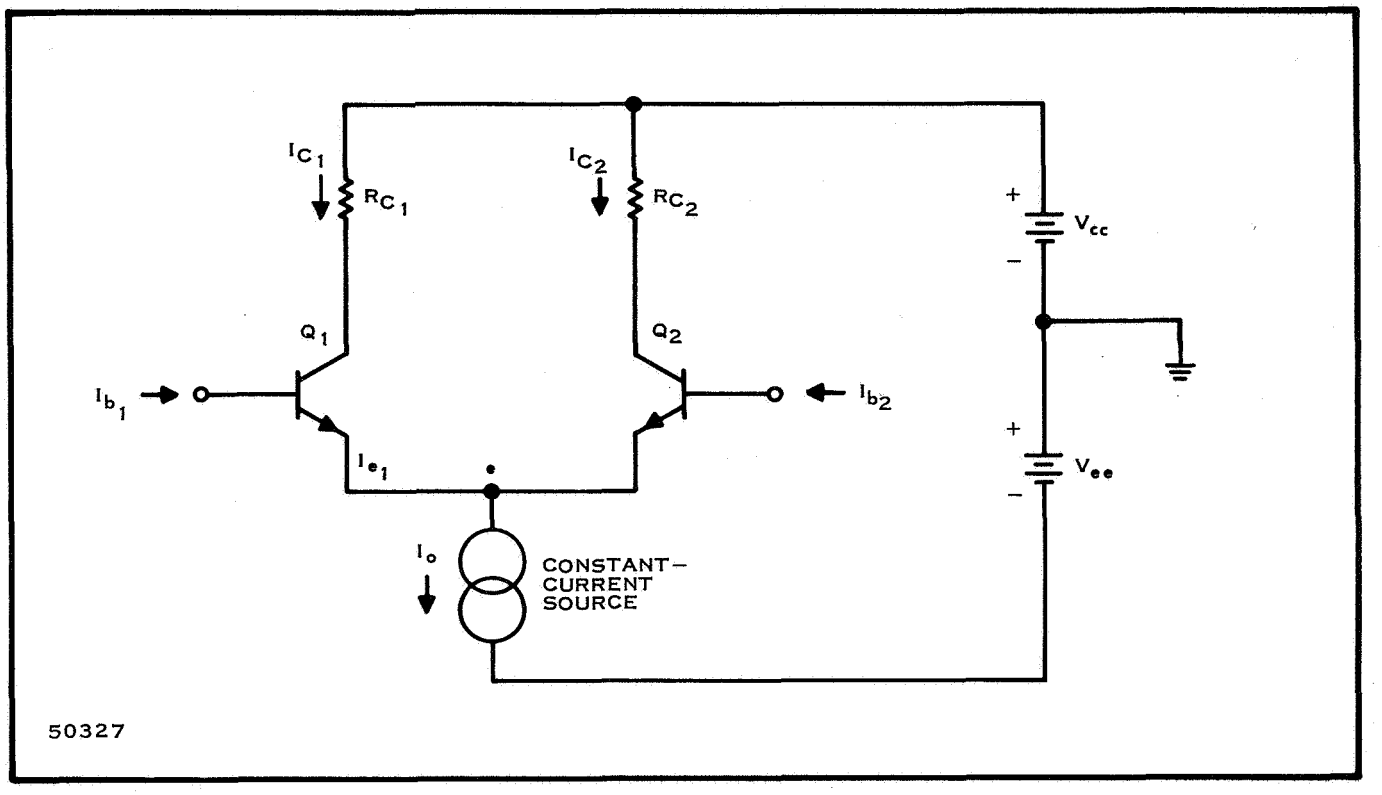

Figure 53. Basic Circuit Configuration for a Differential Amplifier

In Figure 55, a schematic diagram of a video operational amplifier (derived from the differential amplifier), is shown. This operational amplifier is Texas Instrument No. SN5510 which offers medium gain and wide bandwidths. The characteristics of the SN5510 are listed in Table XII. Note that this amplifier has extremely wide bandwidths (40 MHz) and is applicable to wideband-video or tuned circuit applications.

The open loop frequency response characteristic is shown in Figure 56 as well as the input impedance as a function of frequency. A closed loop amplifier frequency response is shown in Figure 57 to illustrate that in various applications it is possible to design 100-MHz amplifiers even though the closed loop gain is relatively low.

C. RF AND IF AMPLIFIERS

The major advantage of integrated circuits is realized when many similar stages can be cascaded in a single package. In receiver applications such advantages can not be fully utilized as each stage of amplification is followed, conventionally, by a tuned coil. The lack of suitable inductive reactance compatible with integrated circuits prevents full realization of cascading similar stages and alternate frequency selective schemes must be considered. One approach has been the use of T-notch filters, composed of lumped RC networks, operating at frequencies below 500-kHz. Another means of providing frequency discrimination is the use of a crystal filter followed by a high gain, wideband (video) amplifier; or at frequencies above 30 MHz, distributed techniques may be used.

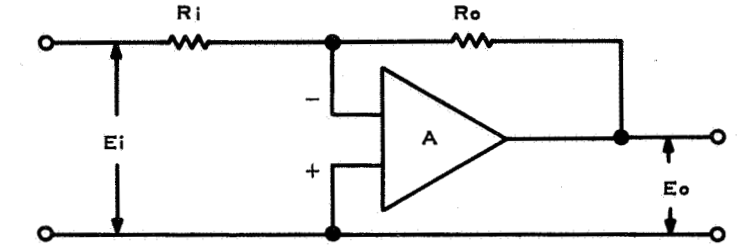

$$E_o = \frac{-R_o}{R_i} E_i$$

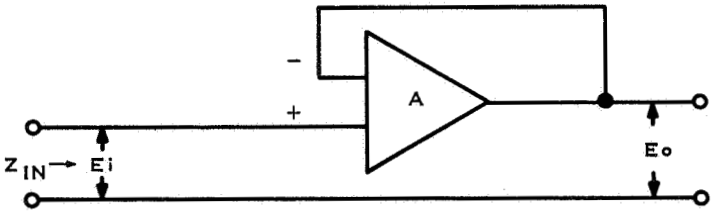

$$E_o = E_i$$

$$Z_{IN} > 10\ M\Omega$$

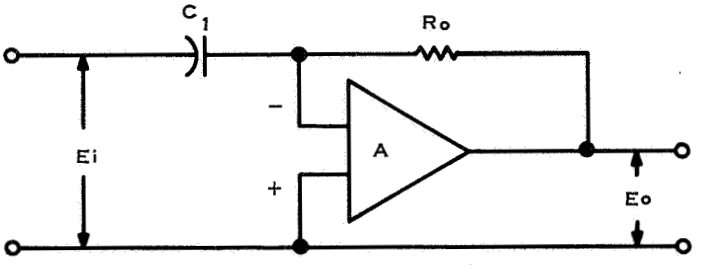

$$E_o = -R_o C_1 \frac{dE_i}{dE}$$

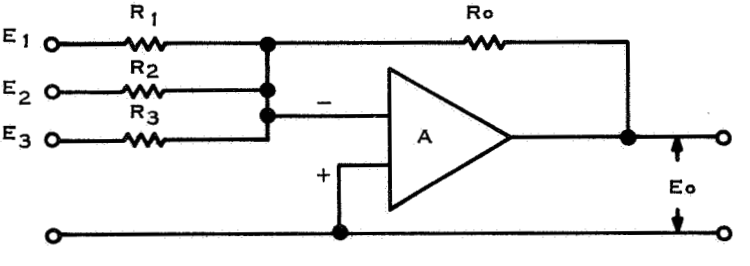

$$E_o = -R_o \left(\frac{E_1}{R_1} + \frac{E_2}{R_2} + \frac{E_3}{R_3} \right)$$

50251

Figure 54. Typical Circuit Functions Obtainable Through Feedback Around a Standard Amplifier

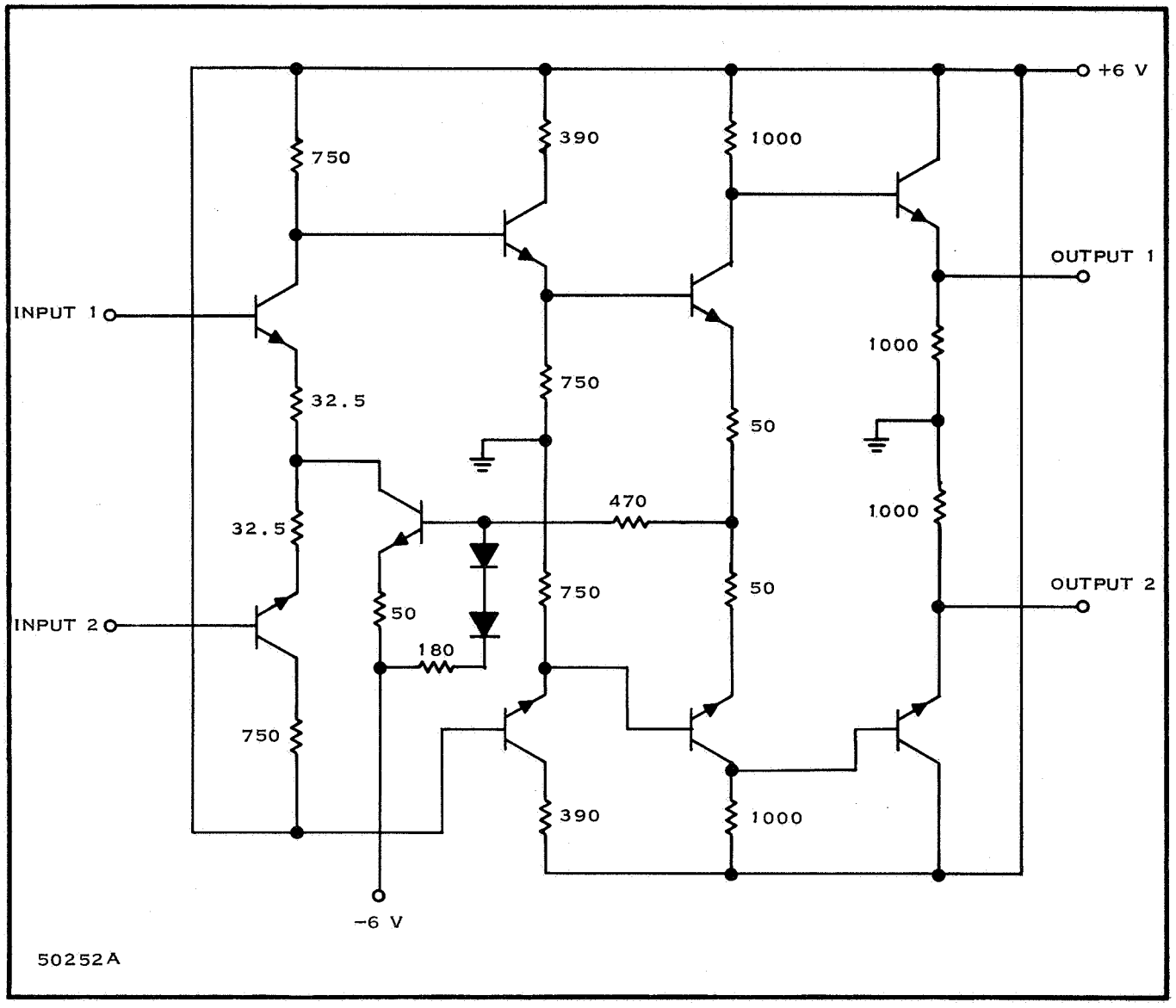

Figure 55. SN5510 Device Circuit Diagram

A typical emitter-coupled, integrated linear amplifier utilizing 2N918 type transistors commercially available for RF and IF amplifiers in the frequency range from dc to 300 MHz is shown schematically in Figure 58. It offers high power gain and increased stability margins. The electrical characteristics of the device are summarized in Table XIII and are shown in Figure 59. This amplifier has been used in a 200-MHz tuned amplifier and as can be seen in Figure 59, noise figures less than 6 dB are possible.

Several linear integrated circuits are available for video application in different circuit configurations. The most applicable for wideband use is the one in which

Table XII. Characteristics of the SN5510

Function	Specification
Open-loop voltage gain	40 dB
3 dB Bandwidth	40 MHz
Input Impedance	6 KΩ
Input capacitance	10 pF
Total power dissipation	165 mW
Maximum linear output voltage	4 V p-p
Output impedance	35 Ω
Common mode rejection	85 dB
Input current	50 μ A

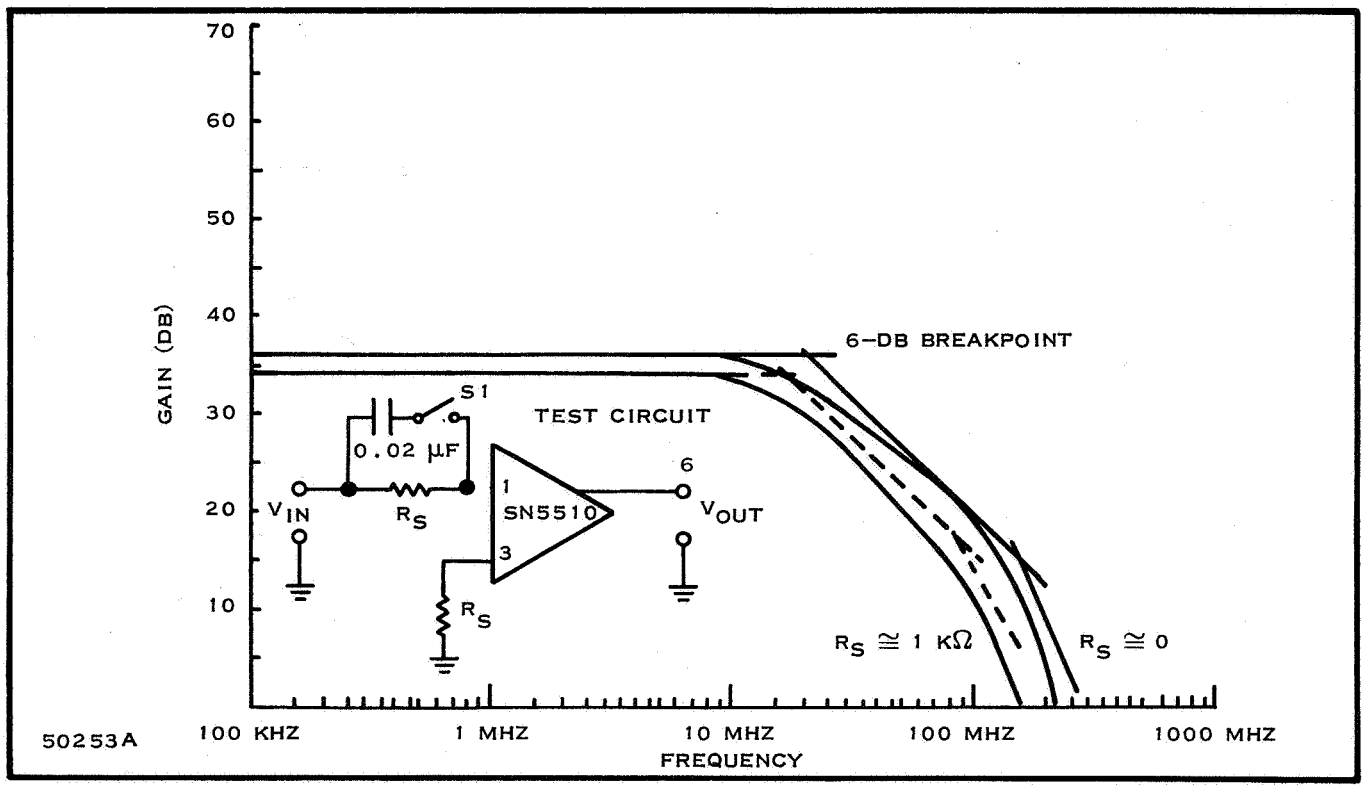

Figure 56. Effect of Source Resistance on SN5510 Open Loop Response

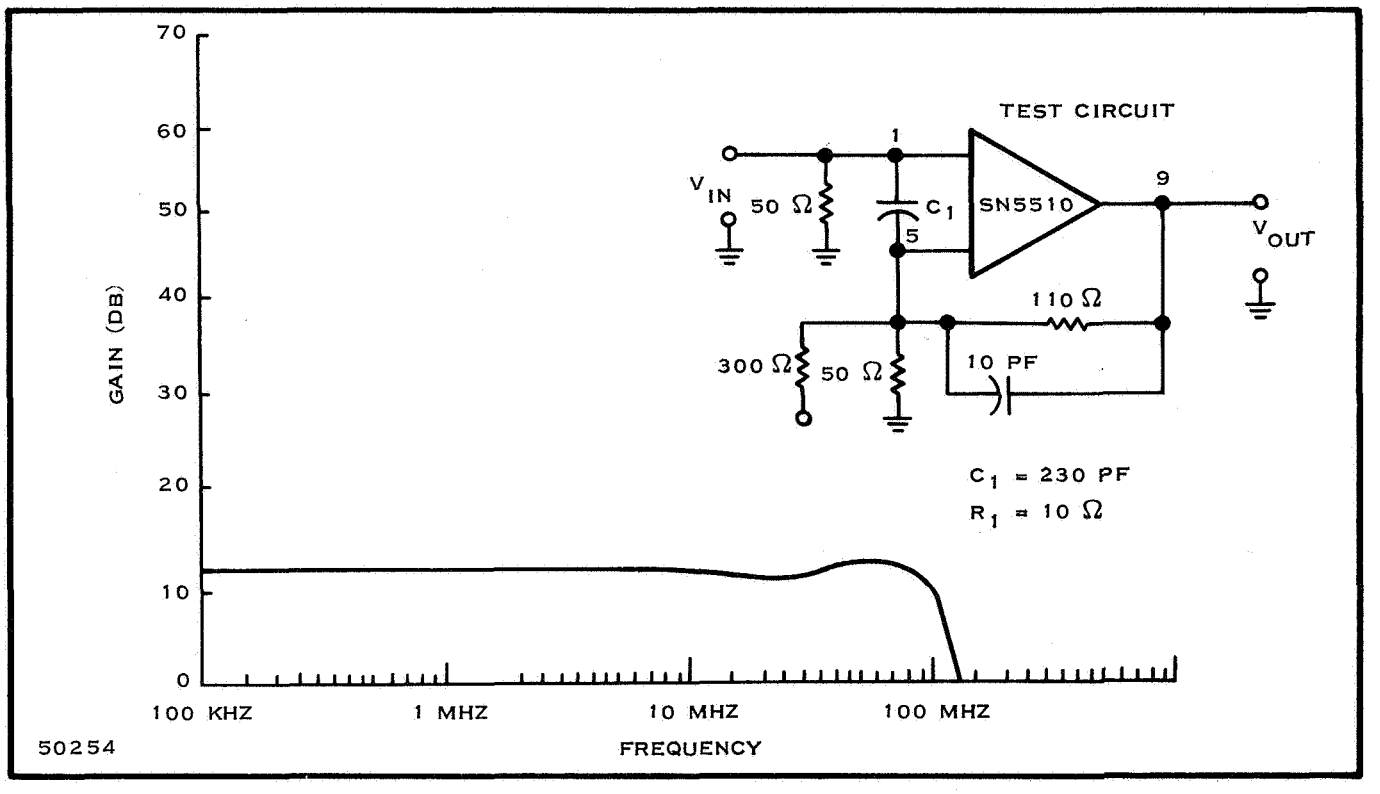

Figure 57. SN5510 10-dB Closed Loop Amplifier

series-parallel feedback pairs are used as building blocks to form the complete amplifier. Such an amplifier is shown in Figure 60; selection of the appropriate RC network in place of Z provides this circuit with two gain ranges, 34 ±1 dB with a 40-MHz bandwidth or 52 ±1 dB with a 35-MHz bandwidth. Either network provides an integrated circuit with a low distortion of 0.2 percent at 200 Hz and a temperature drift ±0.002 dB/°C. The noise figure of either circuit configuration is 5 dB for a 30 MHz bandwidth. The typical gain bandwidth product, f_t, for either circuit is in excess of 2 GHz.

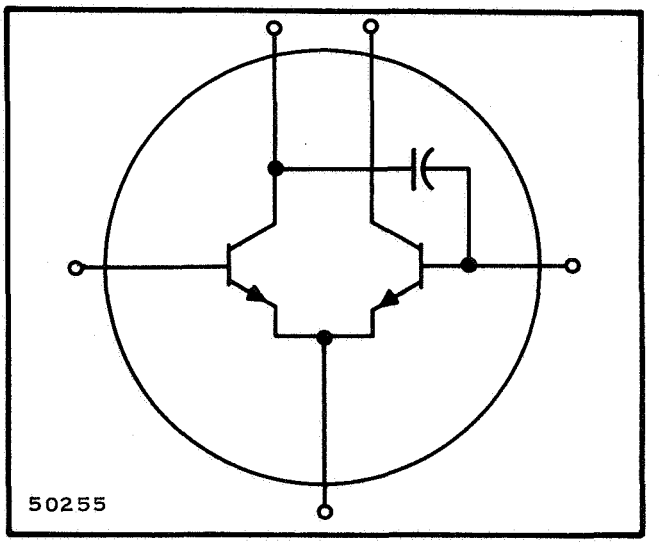

Figure 58. Differential Amplifier Configuration

A balanced differential configuration, consisting of three integrated transistors, is available as shown in Figure 61a. This circuit is basically a single-stage differential amplifier composed of transistors Q_1 and Q_2 driven from a constant-current source Q_3. Each of the terminals must be provided with a biasing network. The circuit may be used in the cascode configuration in which, a common-emitter stage drives a common-base stage. Terminal connections to external biasing networks are shown in Figure 61b and c for a differential amplifier and cascade amplifier with AGC capability.

Table XIII. Typical Integrated Linear Amplifier Parameters

Power Supply Voltage	Vcc	10 Vdc
Power Supply Voltage	VEE	14 Vdc
Total Power Dissipation	Pd	0.5 watt
Operating temperature	^{o}C	-55 to +125
Maximum Input Level (RMS)	$V^{o}in$	2 V(RMS)
Operating Current		
(V_{cc} = 5 Vdc, V_{ee} = -4.7 Vdc, V_{in} = 0)		4 mAdc
Transducer Power Gain		22 dB
(V_{cc} = 5V, V_{ee} = -4V, f = 100 MHz, BN = 3 MHz)		
Noise figure		
(V_{cc} = 5V, V_{ee} = -4V, f = 100 MHz, R_g = RSO)		6 dB

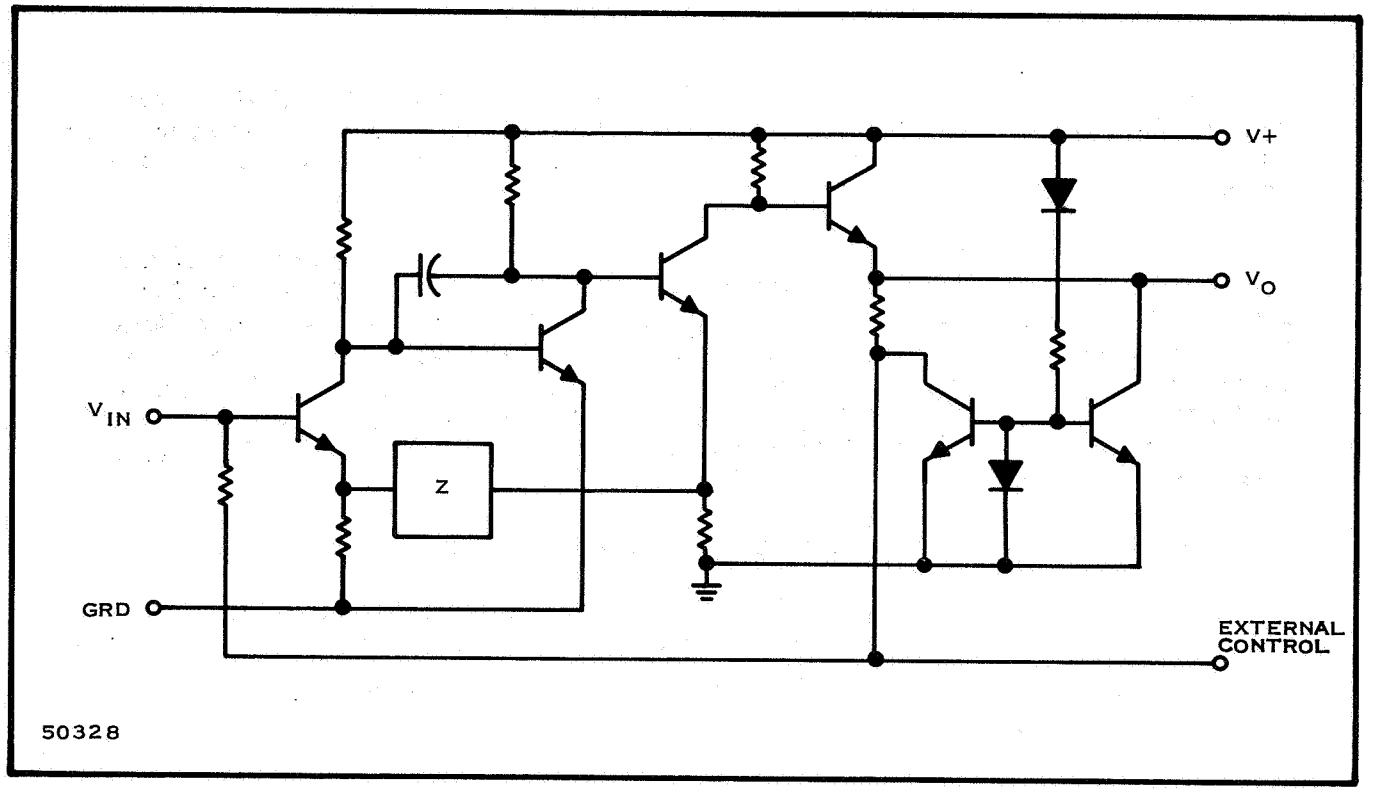

Figure 59. Series-Pair Integrated Circuit

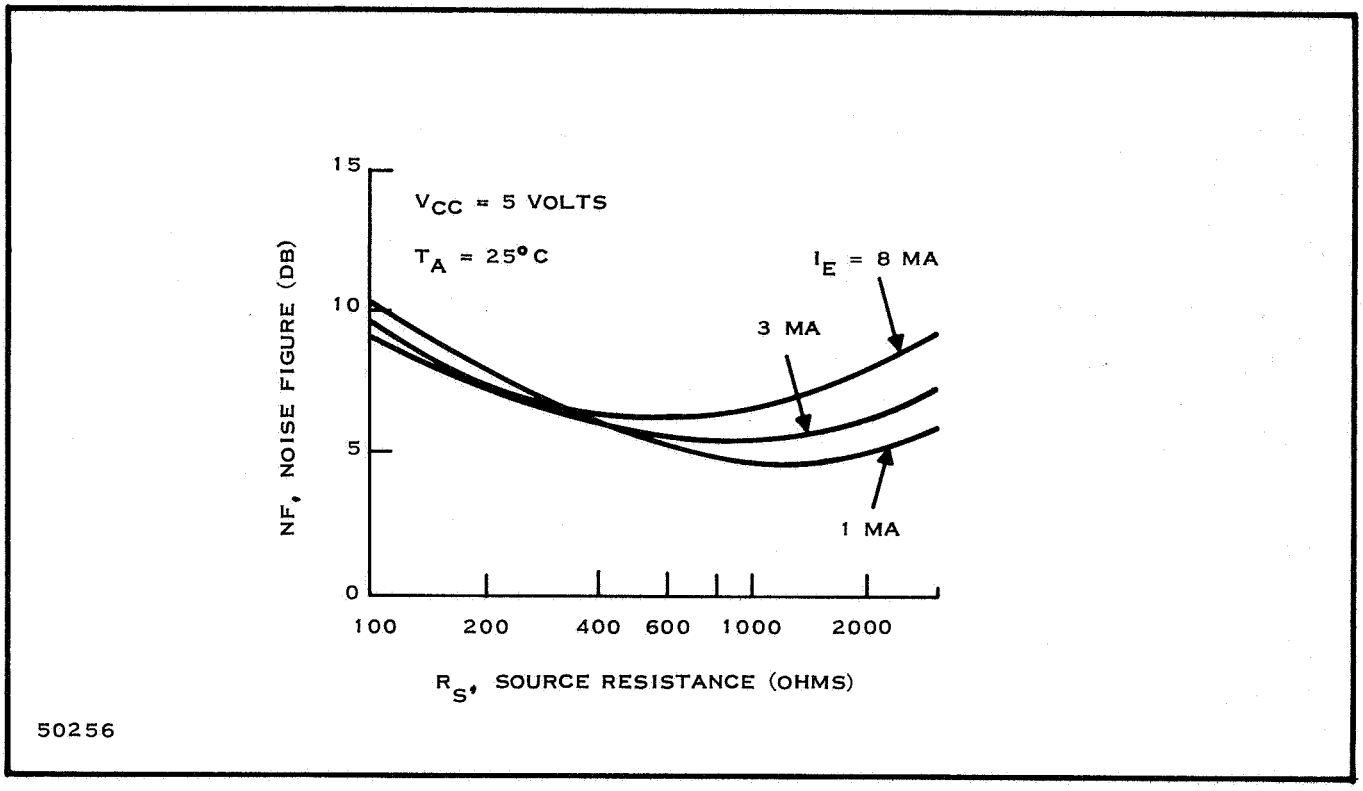

Figure 60. Optimum Noise Figure, Optimum Source Resistance and Available Power Gain vs Frequency

The noise figure of typical RF amplifiers employing the differential circuit or cascode configuration is dependent upon the dc operating current and frequency. The noise figure increases both with an increase in current and with an increase in frequency.

Figures 62 and 63 show representative noise figure data for tuned amplifiers in the differential and cascode configuration respectively. In each case, the input and output are tuned, and the input is conjugately matched to a 50-ohm noise diode. The curves show that for optimum single-stage noise performance, the operating current should be low, which results in low gain. Thus, in system applications of the tuned amplifiers, the operating current in each stage should be adjusted to obtain optimum over-all noise figure by considering the gain and noise figure of the first stage and the noise figure of the second stage.

Gain control to differential stages may be provided in two ways:

the negative voltage applied to the base-bias resistor R, can be adjusted to vary the current in transistor Q_3, or

a differential offset voltage can be applied to transistors Q_1 and Q_2.

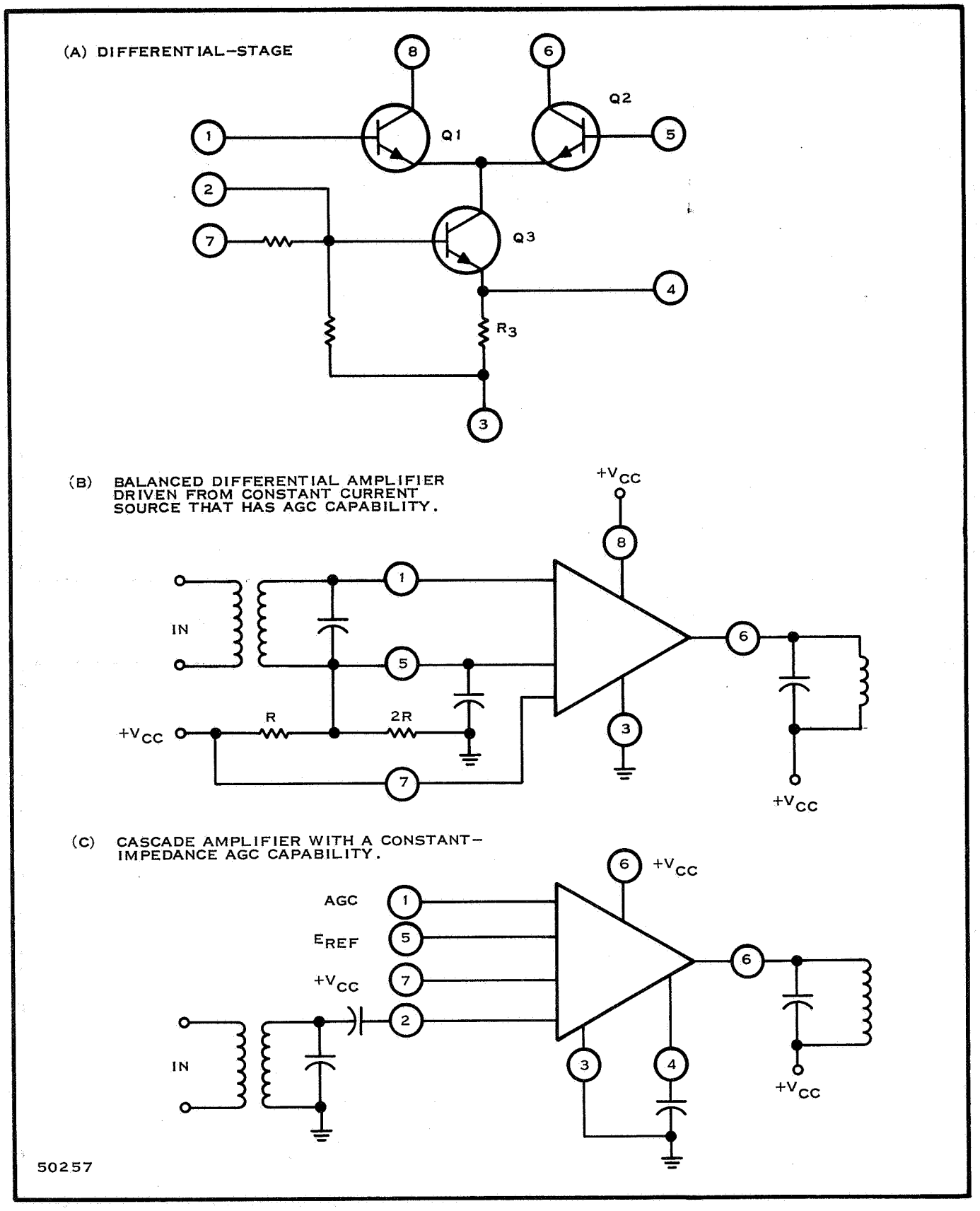

Figure 61. Differential Stage, Balanced Differential Amplifier, and Cascode Amplifier Circuit Diagram

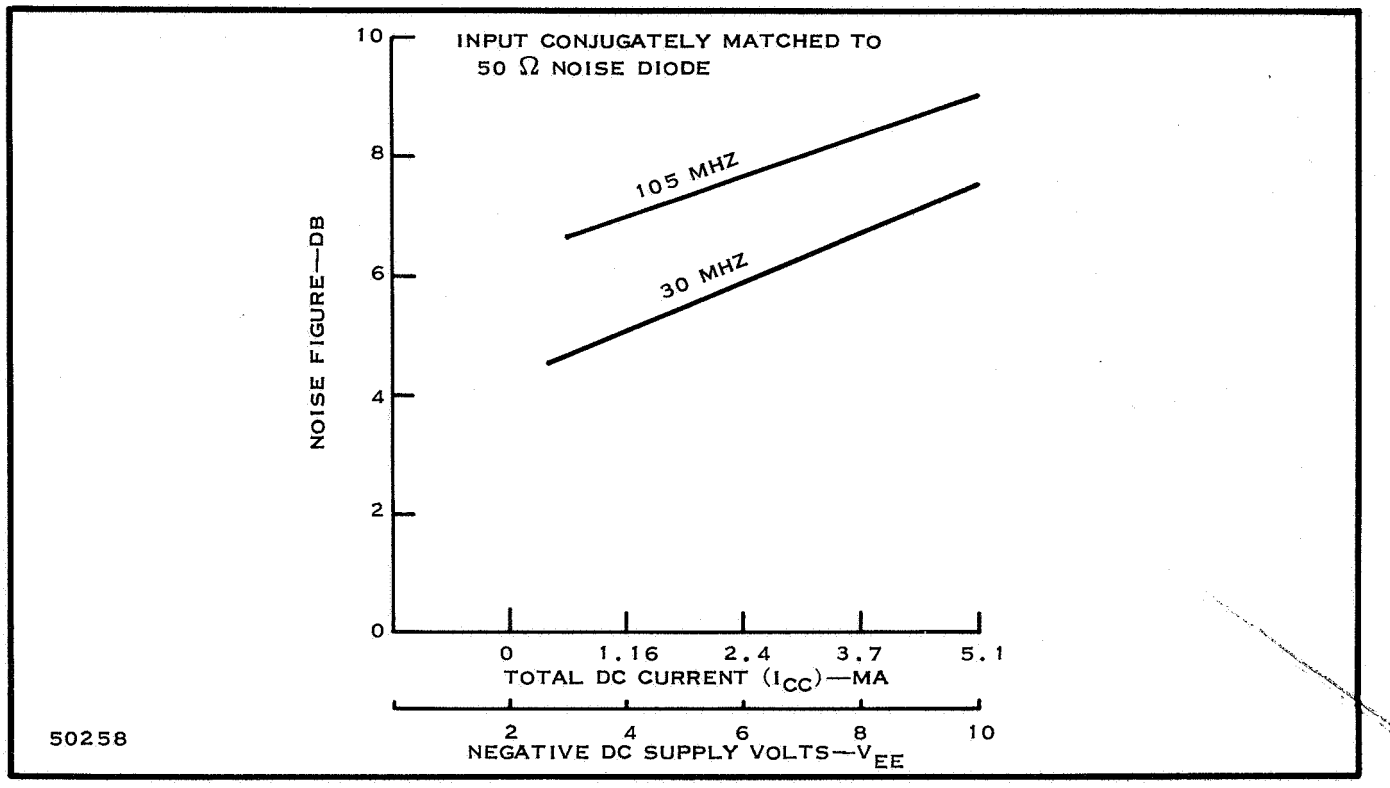

Figure 62. Representative Noise Performance When Operating in a Differential-Amplifier Configuration

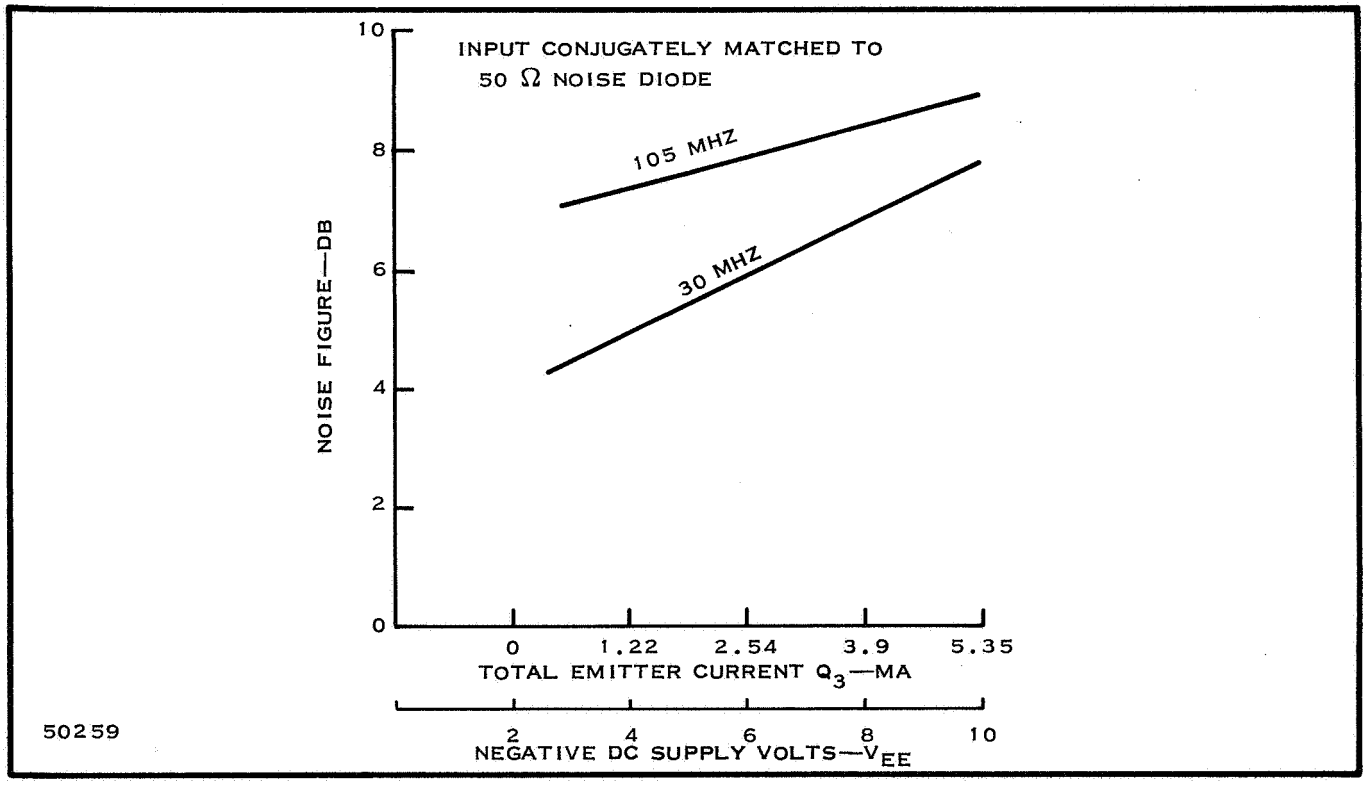

Figure 63. Representative Noise Performance When Operating in a Cascode-Amplifier Configuration

In both cases, maximum gain is obtained at zero volts. The first method provides greater gain-control range, but also requires more control voltage than the second method. Figure 64 and 65 show the typical gain control as a function of voltage for the two methods. The maximum gain-control range that can be obtained is dependent on the full gain used, the circuit loading, and the external-circuit layout. The maximum range varies with frequency as shown in Figure 66.

Cross modulation and modulation distortion are important considerations in the selection of an amplifier for use in AM systems. Figure 67 and 68 shows the cross-modulation distortion of a typical integrated circuit as a function of their gain-control characteristics. The amount of cross-modulation distortion is determined by the two-generator method with the input of the circuit under test driven from a 50-ohm source and with its output tuned to the frequency of the desired carrier. The amplitude of the undesired carrier input voltage is that necessary to produce 10 percent cross-modulation distortion for each manually determined gain-control setting. Cross-modulation data for cascode configurations is shown in Figure 68 where the gain control may be provided by either of two methods:

a negative voltage applied to the base of Q_3 , or

a negative voltage applied to the base of Q_1. In the latter case, the required AGC range is greater, but there is no improvement in cross-modulation characteristics.

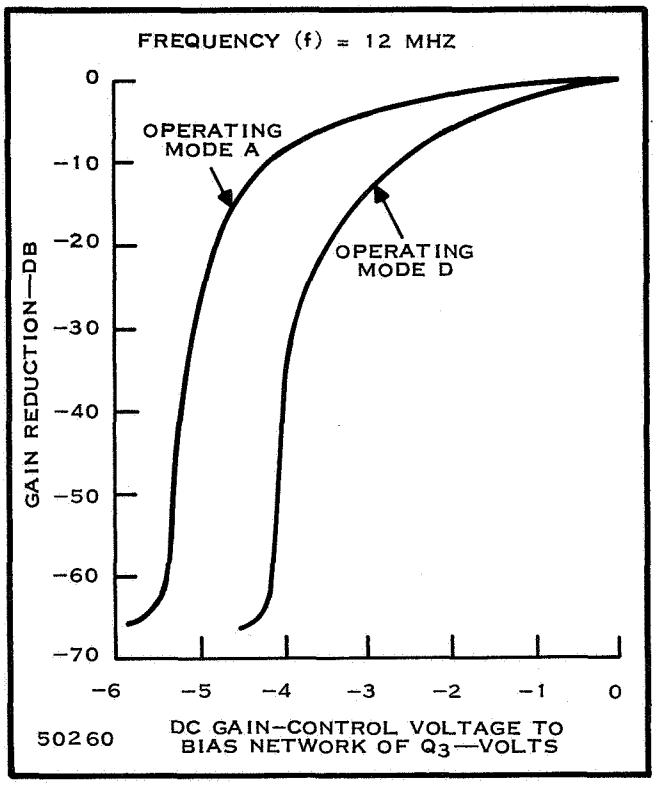

Figure 64. Gain Control Characteristics as a Function of the DC Gain Control Voltage Applied to the Bias Network of Transistor Q_3

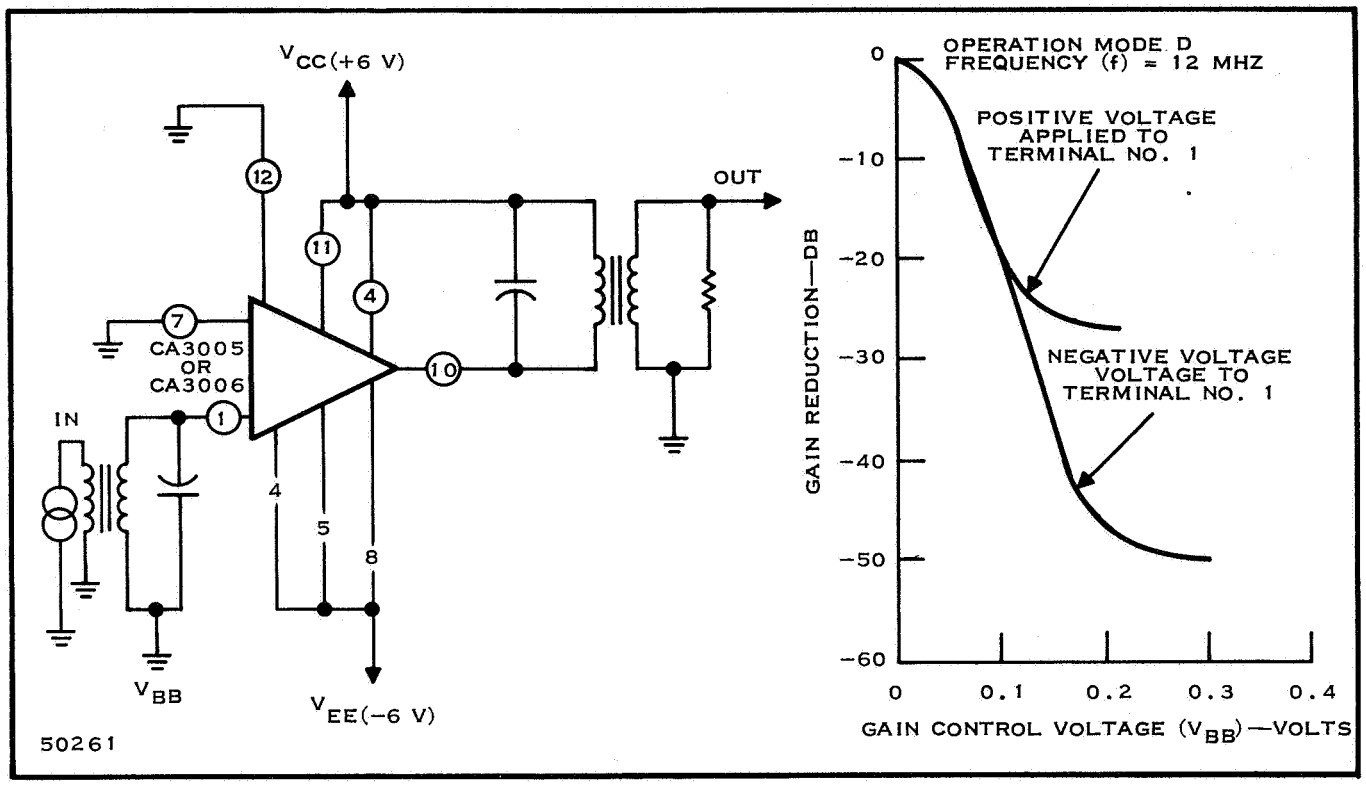

Figure 65. Gain Control Characteristics as a Function of the DC Offset Voltage, V_{BB} Applied to the Differential Pair of Transistors Q_1 and Q_2

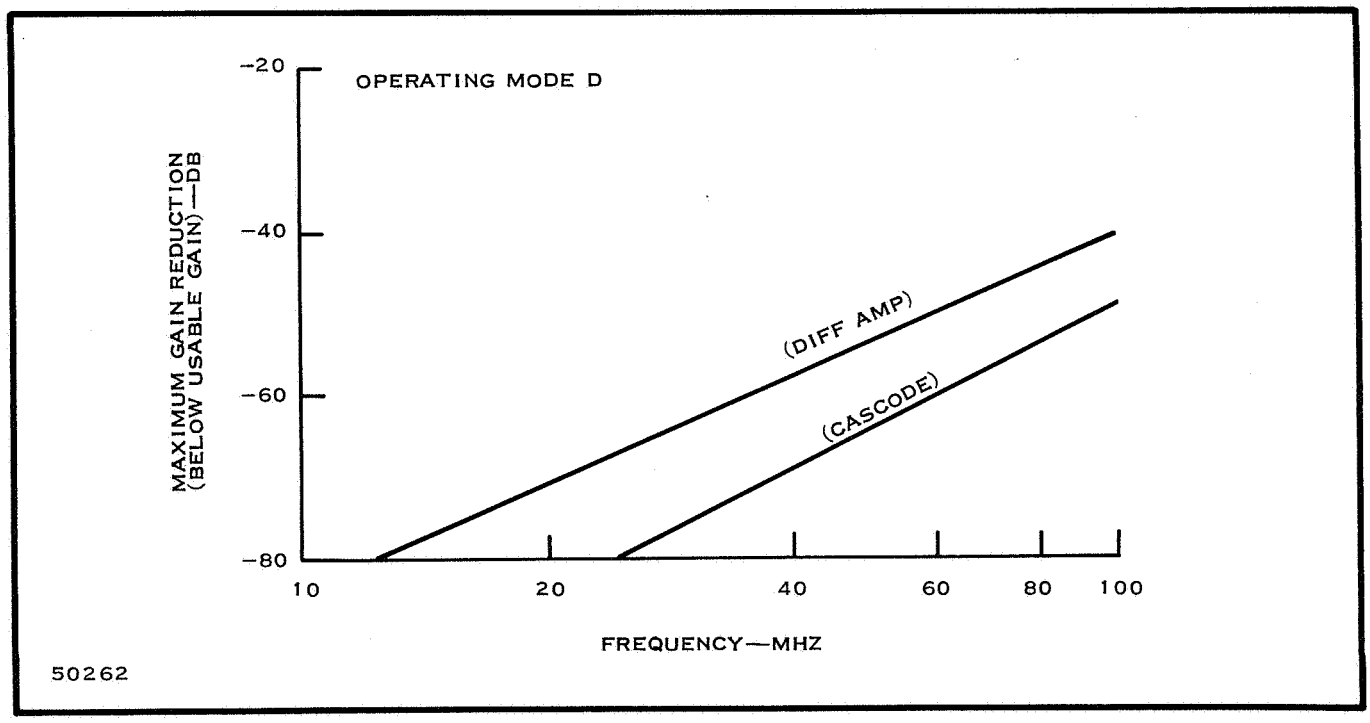

Figure 66. Maximum Gain Control Provided by Variations in the Current through Transistor Q_3 as a Function of Frequency

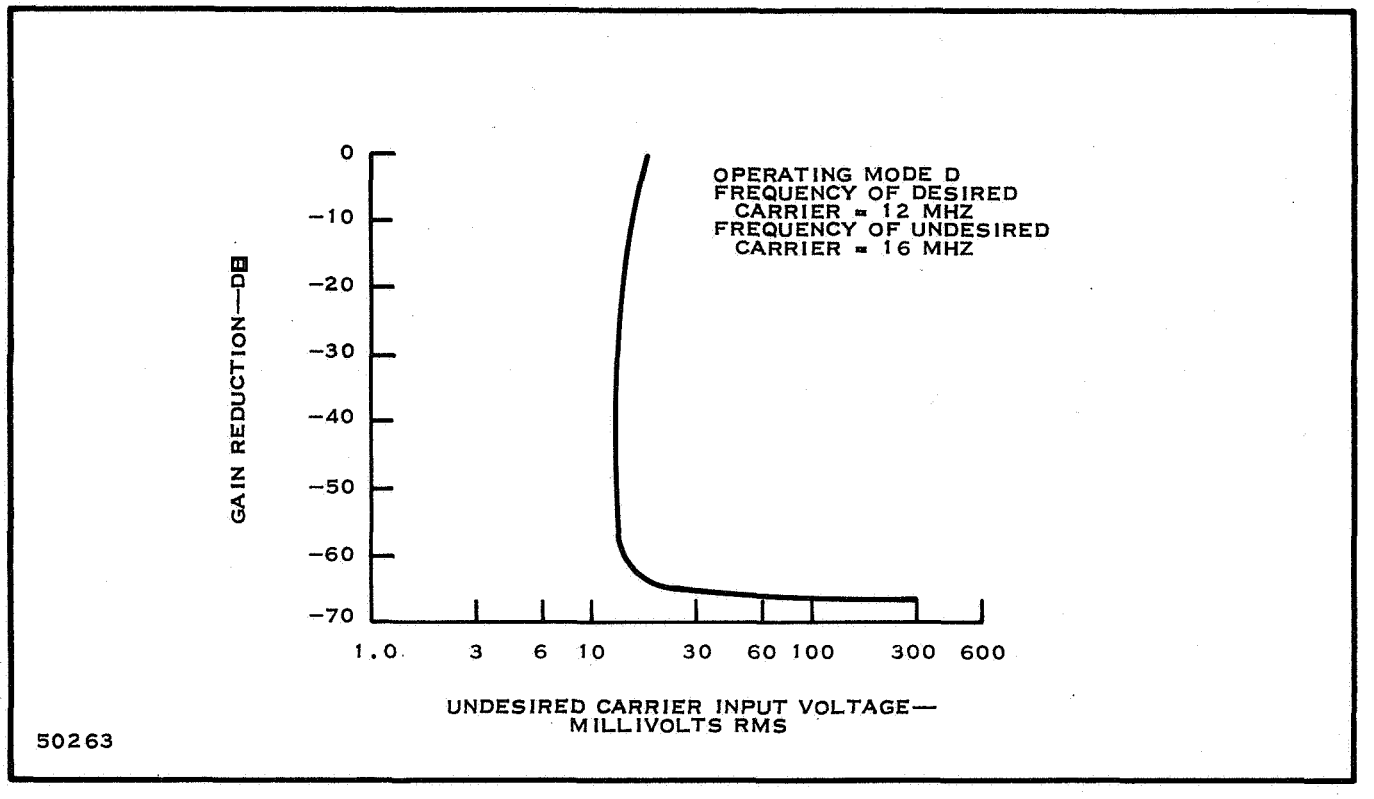

Figure 67. Gain Control as a Function of the Input Voltage from an Undesired Carrier that will Produce Cross-Modulation Distortion of ten percent for Balanced Differential Amplifier Operation. The gain-control voltage is applied to bias network of the constant-current transistor, Q_3.

Figure 69 shows the power gain and noise performance for either the differential or cascode amplifier configuration as a function of AGC voltage. From this figure, it may be noted that a typical integrated RF amplifier can achieve a 5.5 dB noise figure and a 15 dB power gain at 100 MHz.

D. LIMITERS

Linear integrated circuit also function well as limiters in both the differential-amplifier and cascode configurations. The advantage of the differential configuration is that collector saturation of either transistor Q_1 or Q_2 can be avoided because of the action of the constant current transistor Q_3. The transfer characteristics of Figure 70 show the excellent limiting capabilities achieved because the constant-current transistor, Q_3 limits the operating current so that the collectors of the differential-pair do not saturate. As saturation must be prevented for good limiting, the load resistance and low level voltage gain are limited for a given bias current and supply voltage.

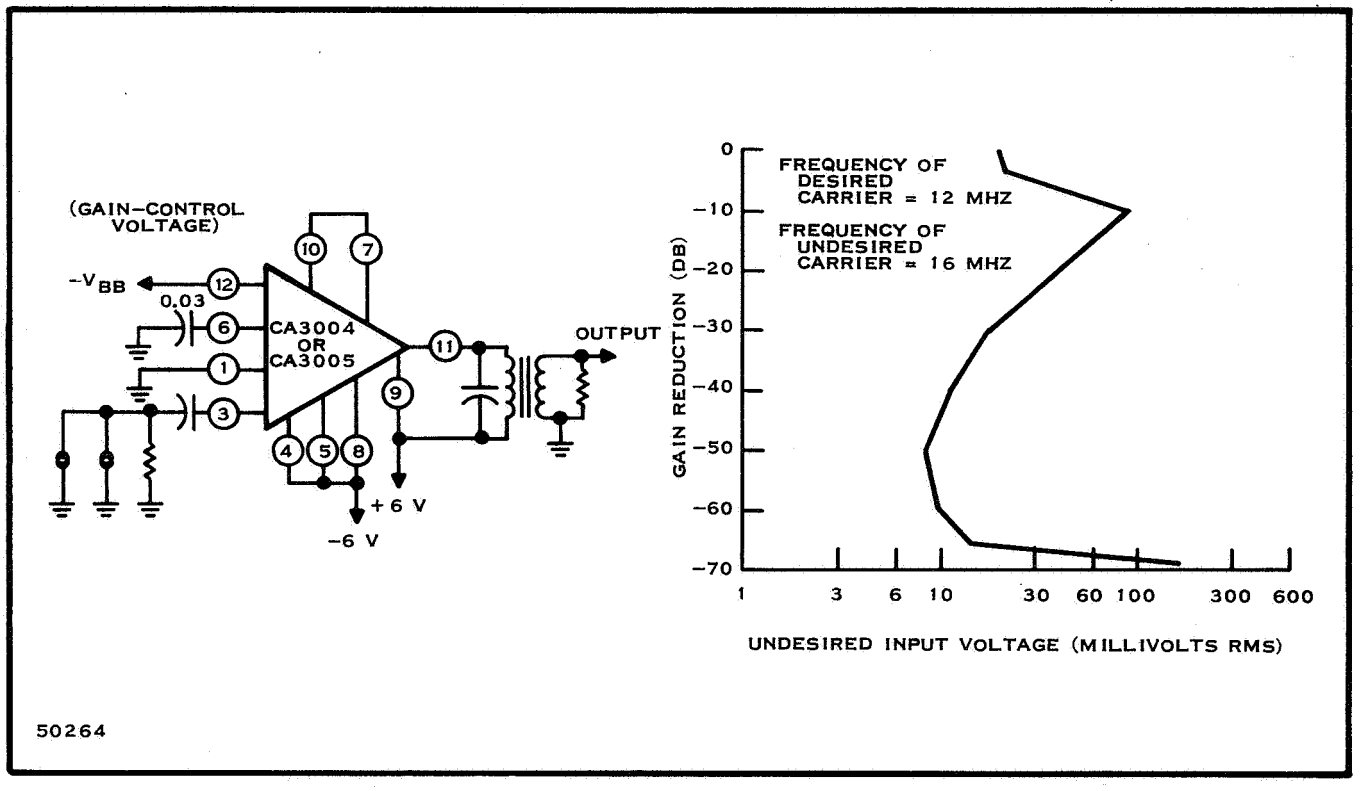

Figure 68. Gain Control in a Cascode Configuration, as a Function of the Undesired Carrier Voltage that will Produce ten percent Cross Modulation Distortion when the Gain is Controlled by a Negative Bias Voltage Applied to the Base of Transistor Q_3. The Schematic diagram illustrates the circuit configuration.

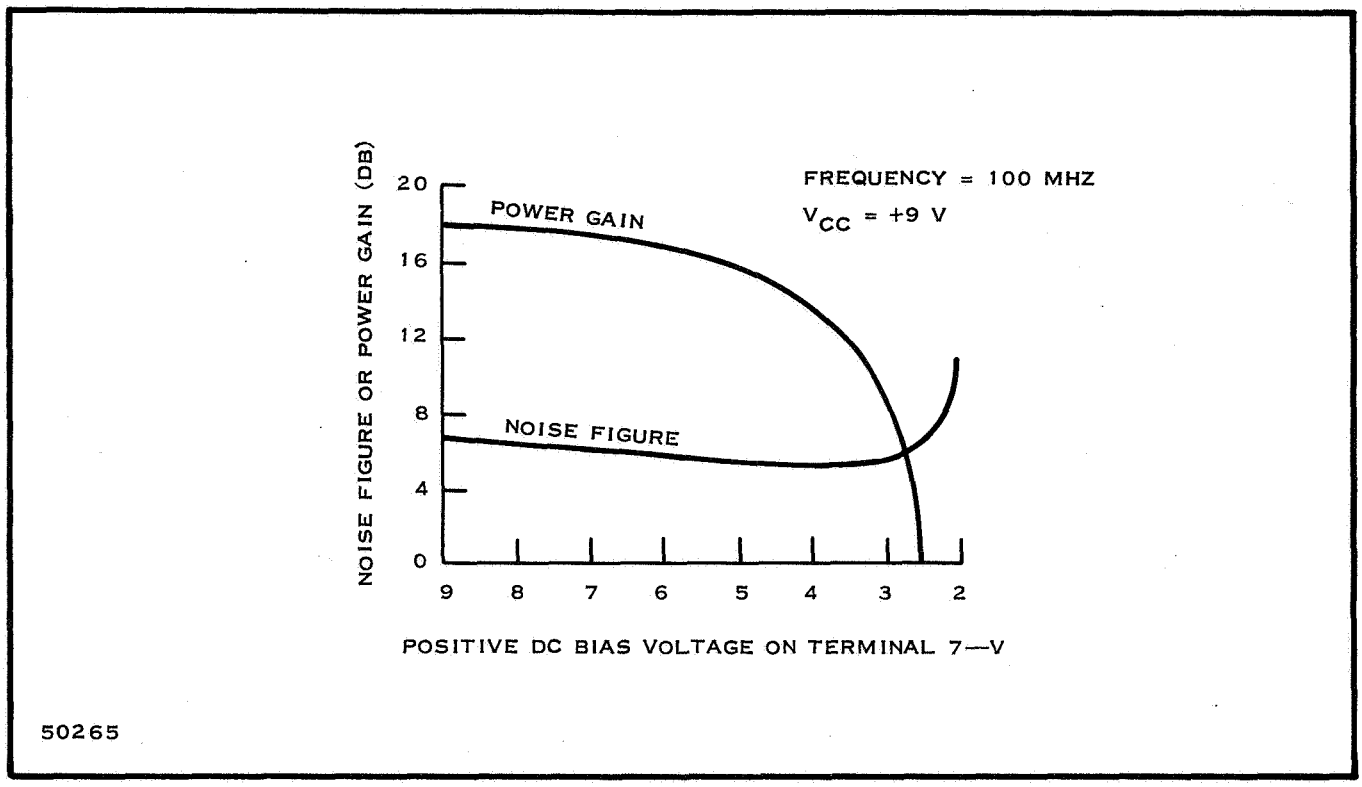

Figure 69. 10.7-MHz Transfer Characteristics in the Cascode or Differential Connection

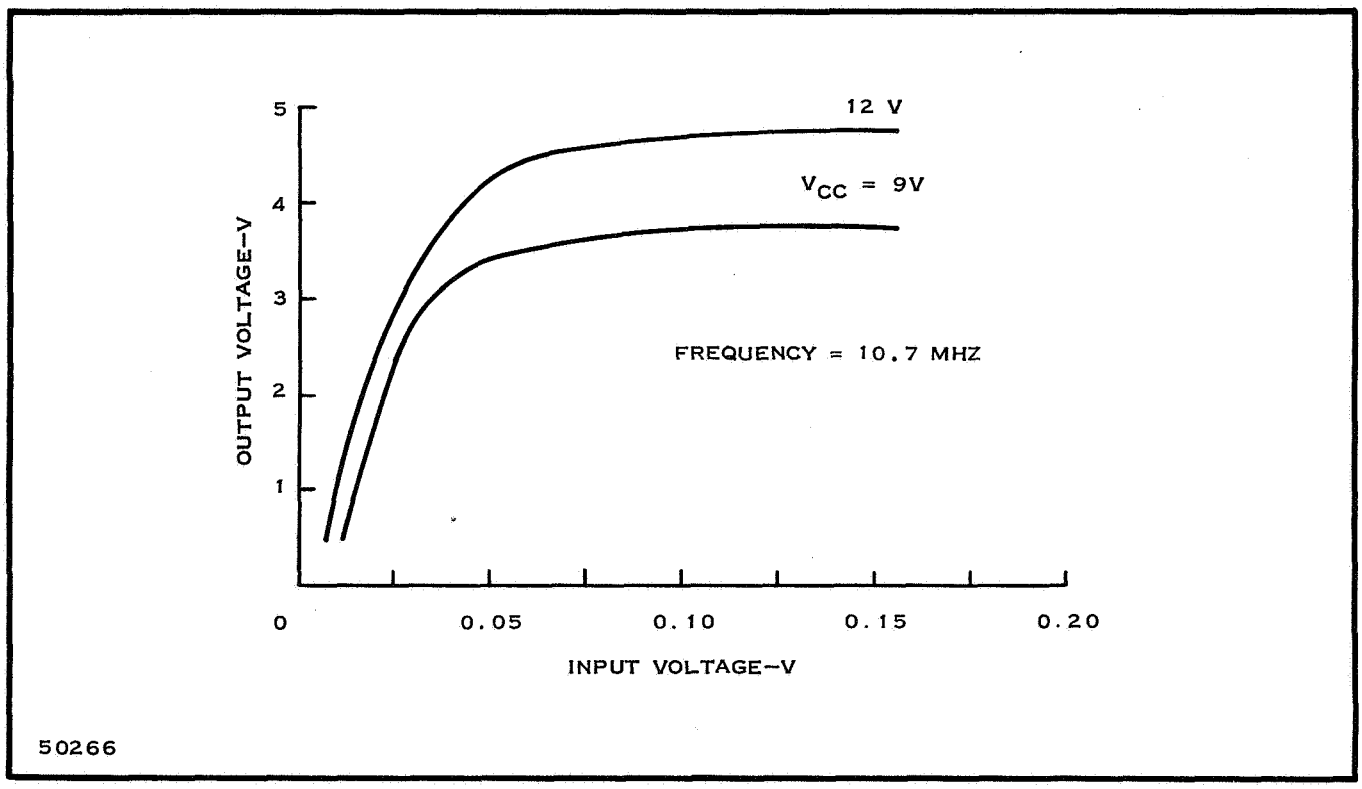

Figure 70. Limiting Characteristics of a Linear Integrated Circuit

SECTION VI

THIN FILMS

A. GENERAL

Scientific Report No. 1 discussed the subject of thin film from the aspect of materials, process methods, parameter limits, and resistor and capacitor characteristics. This report discusses the usefulness of microstrip circuits, the relative merits of various substrates, and the applications of lumped element components.

B. MICROSTRIP

1. Theory

The parameters of strip line has been fairly well established for several years. However, because of its non-symmetrical nature (Figure 71), microstrip has been somewhat neglected. Even now an exact theoretical analysis of the microstrip mode is lacking, but this medium can be accurately characterized by suitable measurement techniques. The characteristic impedance, Zo, wavelength, λg, and loss per wavelength can be determined as a function of frequency and other pertinent parameters for microstrip lines.

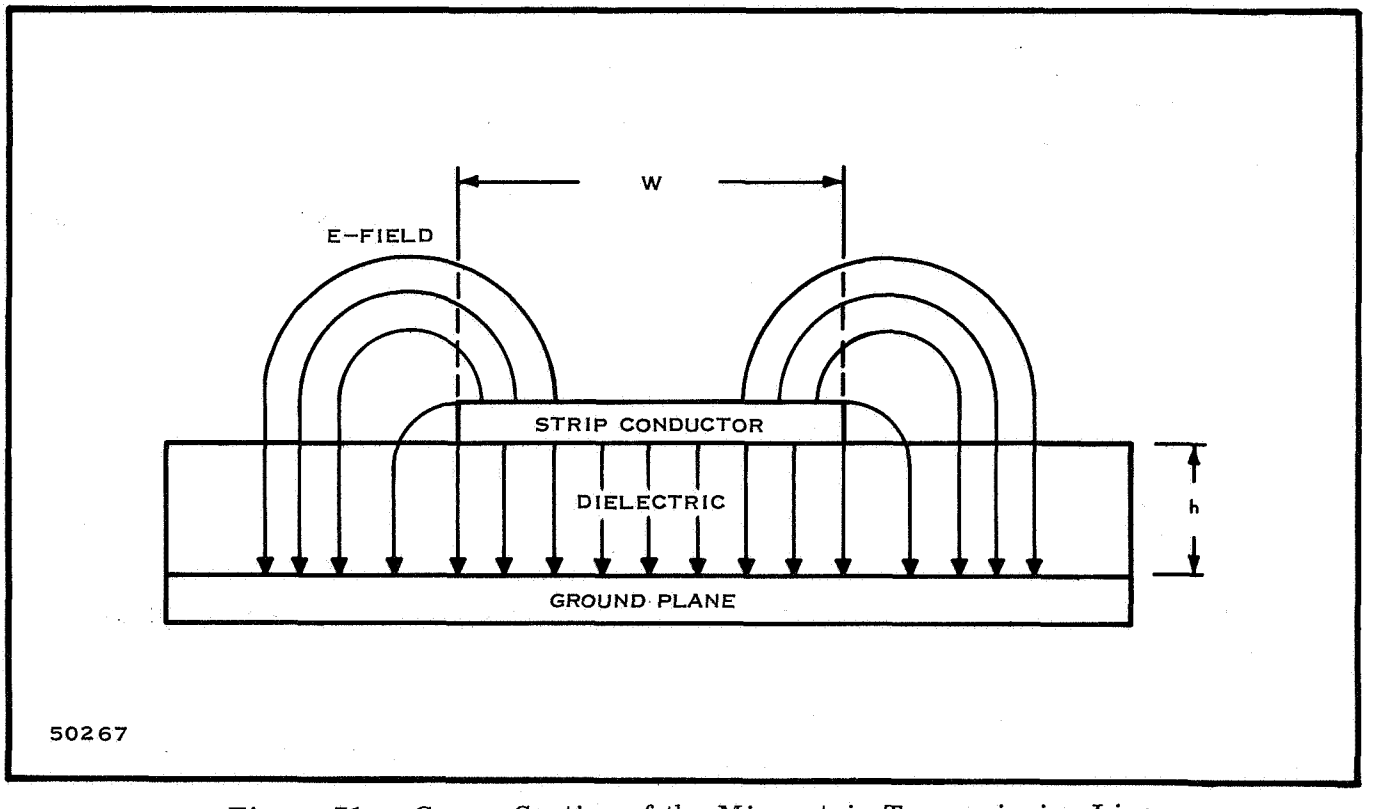

Figure 71. Cross-Section of the Microstrip Transmission Line

Recently formulas have been developed which fit experimentally obtained results [32]. The characteristic impedance of the unshielded microstrip line is given by

$$Z_o = \frac{377h}{\sqrt{\epsilon_r}\, W \left[1 + 1.735\ \epsilon_r^{-0.0724} \left(\frac{W}{h}\right)^{-0.836}\right]} \tag{45}$$

and the wavelength by $$\frac{\lambda g}{\lambda TEM} \approx \left[\frac{\epsilon_r}{1 + 0.6\ (\epsilon_{r-1})\ \left(\frac{W}{h}\right)\ 0.0297}\right]^{1/2} \tag{46}$$

when $\frac{W}{h} \geq 0.6$

where λg = guide wavelength

λo = free space wavelength

$\lambda TEM = \lambda_o / \sqrt{\epsilon_r}$

ϵ_r = relative dielectric constant of insulating layer

W = width of conductor

h = thickness of dielectric substrate

The attenuation due to conductor loss is approximately

$$\alpha_c = \frac{\sqrt{\pi f \mu}}{2 Z_o W} \left[\frac{1}{\sqrt{\sigma_1}} + \frac{1}{\sqrt{\sigma_2}}\right] \quad \text{nepers/meter} \tag{47}$$

where f = frequency in hertz

$\mu = 4\pi X 10^{-7}$ h/m

σ_1 = conductivity of strip in (ohm - m)$^{-1}$

σ_2 = conductivity of groundplane in (ohm - m)$^{-1}$

In the limiting case, as the impedance approaches a low value (when $W/h \gg 1$), Equation (47) becomes

$$\alpha_c = \frac{\sqrt{\pi f \epsilon_o \epsilon_r}}{2h} \left[\frac{1}{\sqrt{\sigma_1}} + \frac{1}{\sqrt{\sigma_2}}\right] \quad \text{nepers/meter} \tag{48}$$

and from this equation it may be seen that large h (obtained by thick substrates) is required to minimize α_c.

The losses due to the insulating substrate can be neglected for hybrid circuits on ceramic. However, losses on silicon can not be neglected and may be approximated by

$$\alpha_{d\ SEMICOND.} \approx 1/2\ \frac{Z_o W}{\rho h}$$

where ρ = Substrate resistivity in ohm-cm.

Calculated losses of lines on ceramic and silicon are tabulated in Table XIV.

Table XIV. Losses of 50-Ohm Microstrip Lines in Microwave Integrated Circuits

Line	Conductor	Dielectric		ϵ_r	Loss dB/cm		Q of a $\frac{\lambda}{4}$ Resonator	
		Material	Thickness		2 GHz	10 GHz	2 GHz	10 GHz
A	Gold	Ceramic	10 mils	9.9	0.098	0.22	48	106
B	Gold	Ceramic	25 mils	9.9	0.039	0.088	120	265
C	Gold	Si(150 Ω CM)	10 mils		1.3	1.44	2	9
D	Gold	Si(1500Ω CM)	10 mils		0.24	0.38	14	50

Another source [33] shows resistivity of silicon substrate versus line loss (Figure 72). However, as the temperature increases, charge carriers are thermally excited, lowering the resistivity of the material. Even at lower temperatures, the resistivity decreases due to the increase in mobility of the charge carriers with decreasing temperature. This curve is shown in Figure 73.

For circuits not requiring extremely high Q, microstrip on silicon can be very useful. If a higher Q is necessary it can be achieved, up to a limit, by using a higher dielectric substrate such as ceramic. A hybrid IC will then be necessary.

The characteristic impedance of straight line segments of microstrip transmission line of various widths was measured by slotted line and time domain reflectometer techniques[34]. The lines were made from gold, silver or aluminum. The substrate was either glazed Al_2O_3 or unglazed Al_2O_3. The characteristic impedance versus the width to height ratio is given in Figure 74.

The results of these measurements are given in Figure 75. Note that λ_o / λ_g is nearly independent of frequency, but is dependent on the characteristic impedance Z_o, and the substrate material. This is in agreement with Equations (45) and (46).

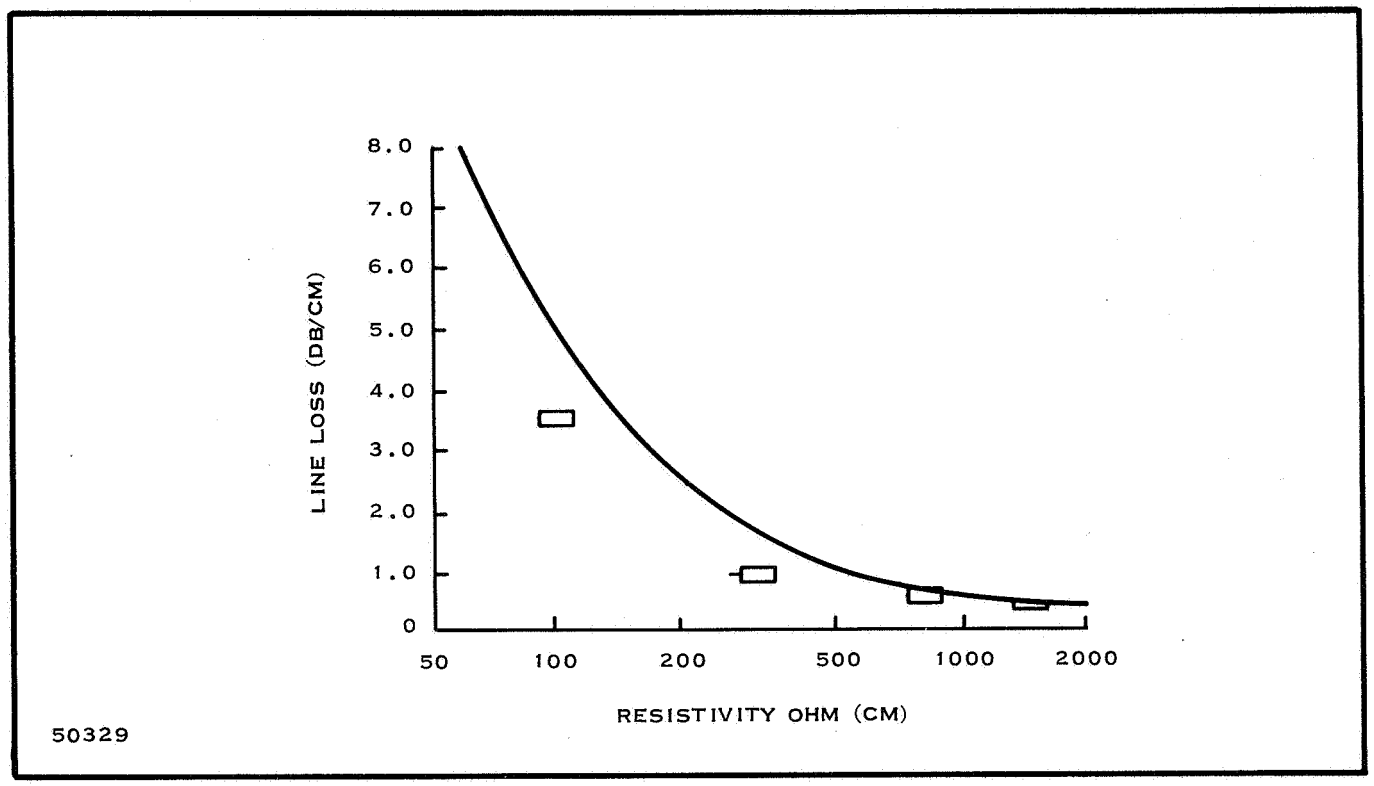

Figure 72. Microstripline Loss as a Function of Dielectric Resistivity

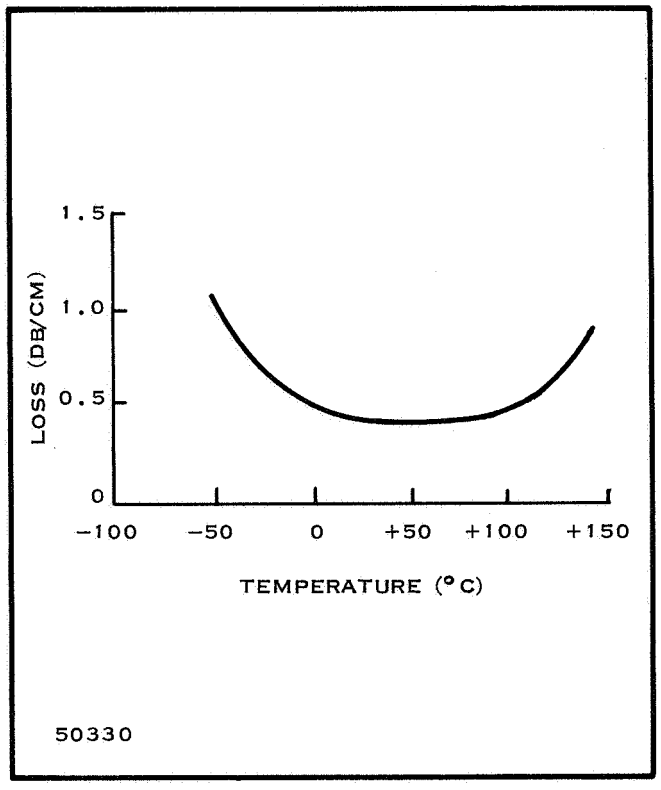

Figure 73. Microstripline Loss on 1500 Ohm Silicon Substrate

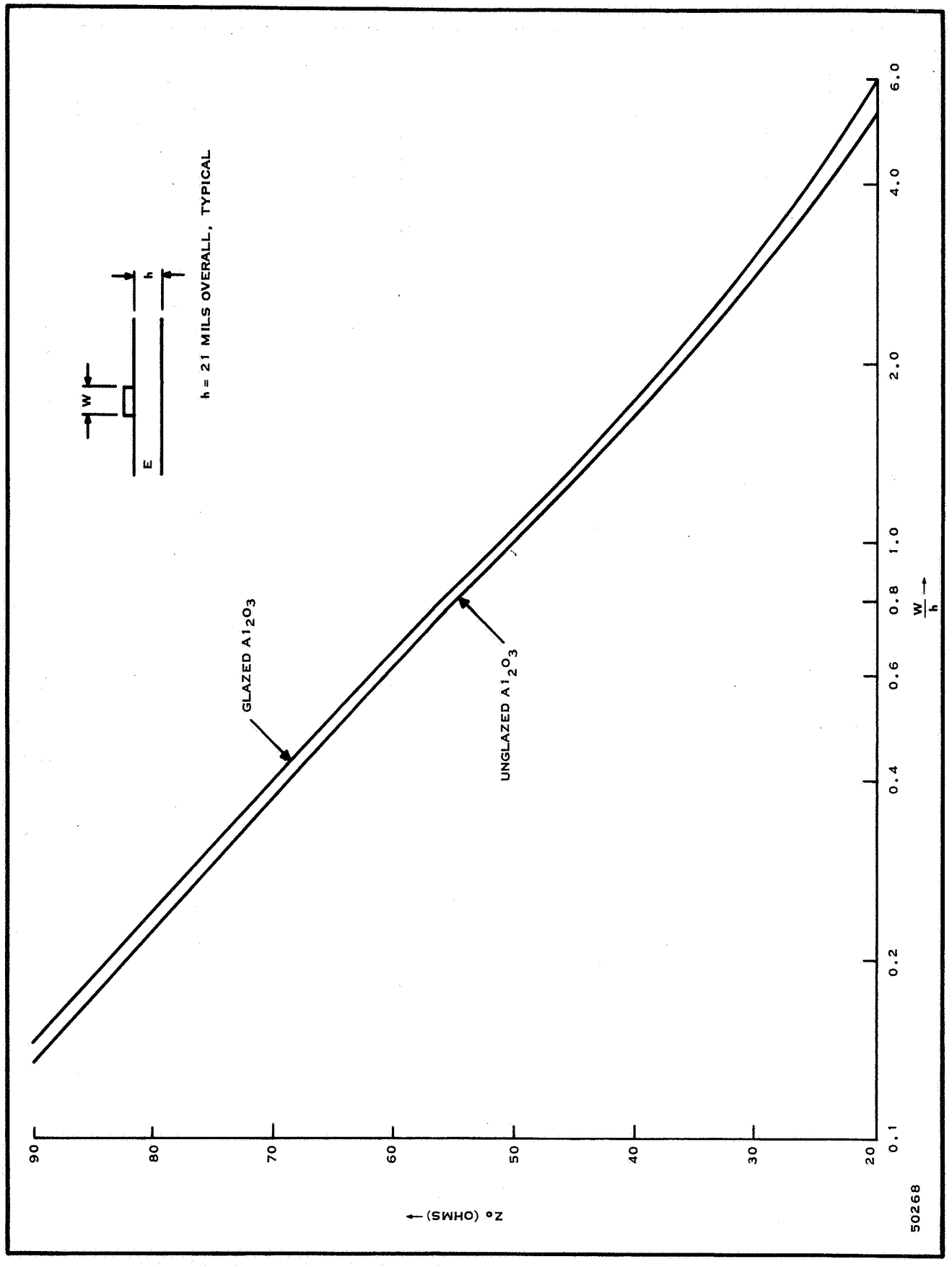

Figure 74. Characteristic Impedance vs W/h Ratio for Microstriplines on Aluminum Oxide

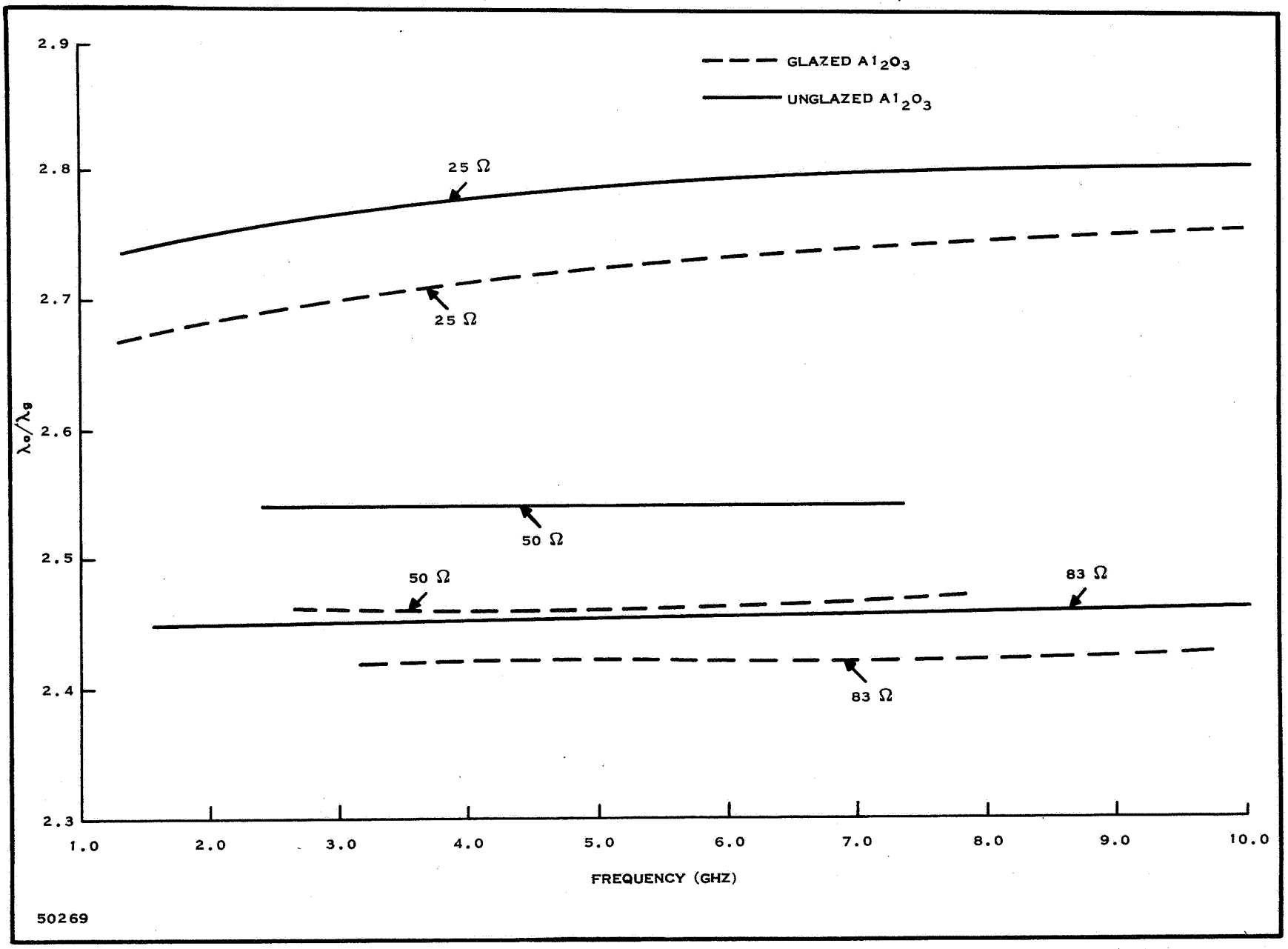

Figure 75. Free Space to Microstrip Wavelength Ratio ($\lambda o/\lambda g$) vs Frequency for Microstrip on Aluminum Oxide Substrates

The Q (quality factor) of a microstrip resonator is an important design consideration. If the microstrip is an open or shorted section, the unloaded Qu of a quarter-wavelength resonator is $Qu = \frac{QdQc}{Qd+Qc}$ where Qc is the Q of the conductor and Qd is the Q of the substrate. If all the conductors are of the same material

$$Qc = 1/6 \quad \frac{\lambda TEM}{\lambda g} \quad \frac{W}{h} \quad Z_o \quad \sqrt{\epsilon_r} \quad h \sqrt{F_{GHz}} \quad \sqrt{\sigma_c}$$

The Q of the substrate, (Q_d), is approximately the Q of the dielectric; for semiconductor substrates $Qd \approx w\rho \epsilon r \epsilon o$

The calculated values of Q from Table XIV show that microstrip resonators have lower Q's than conventional cavity resonators and that the penalty in performance is greatest in the monolithic IC type of microstrip.

2. Selection of Substrates

Selection of a microwave IC substrate is critical in that the substrate is an integral part of the circuitry and must be chosen for low dielectric loss. The chosen substrate must be homogeneous both within itself and from batch to batch. The thin-film must strongly adhere to the substrate, and even if the substrate is only 10 to 50 mils thick, neither the substrate nor the conductors should deform by temperature cycling. The substrate thermal conductivity should be high and its surface must be free of pits for uniform transmission lines and short free capacitors to be deposited. Usually substrate thickness is a tradeoff between conductor Q and the maximum allowable thermal resistance of the substrate.

3. High Dielectric Substrates

The primary advantage of a substrate having a higher dielectric than ceramic ($e_r \geqq 9.6$) is size reduction. By increasing the dielectric constant of the substrate from 10 to 100, the guide wavelength of a 50-ohm microstrip line can be reduced by a factor of 0.35 and low loss and microstrip lines can be fabricated[35].

The measured and calculated impedance is plotted in Figure 76 as a function of geometry and dielectric constant. The calculated impedance is based on the conformal mapping solution given by Wheeler [36]. Notice that the high dielectric substrates require smaller values of w/h for high impedance levels because of the higher transmission line capacitance. Since the width is restricted by thin film technology limitations, thicker substrates will be required for high-impedance microstrip circuits.

The measured and calculated ratio of free space-wavelength to microstrip wavelength is plotted in Figure 77 as a function of dielectric constant and geometry. This ratio has been computed also from a conformal mapping solution given by Wheeler [35,36].

High-dielectric substrates, consisting of a temperature-compensated titanium dioxide homogeneous mixture, have been shown to have the properties

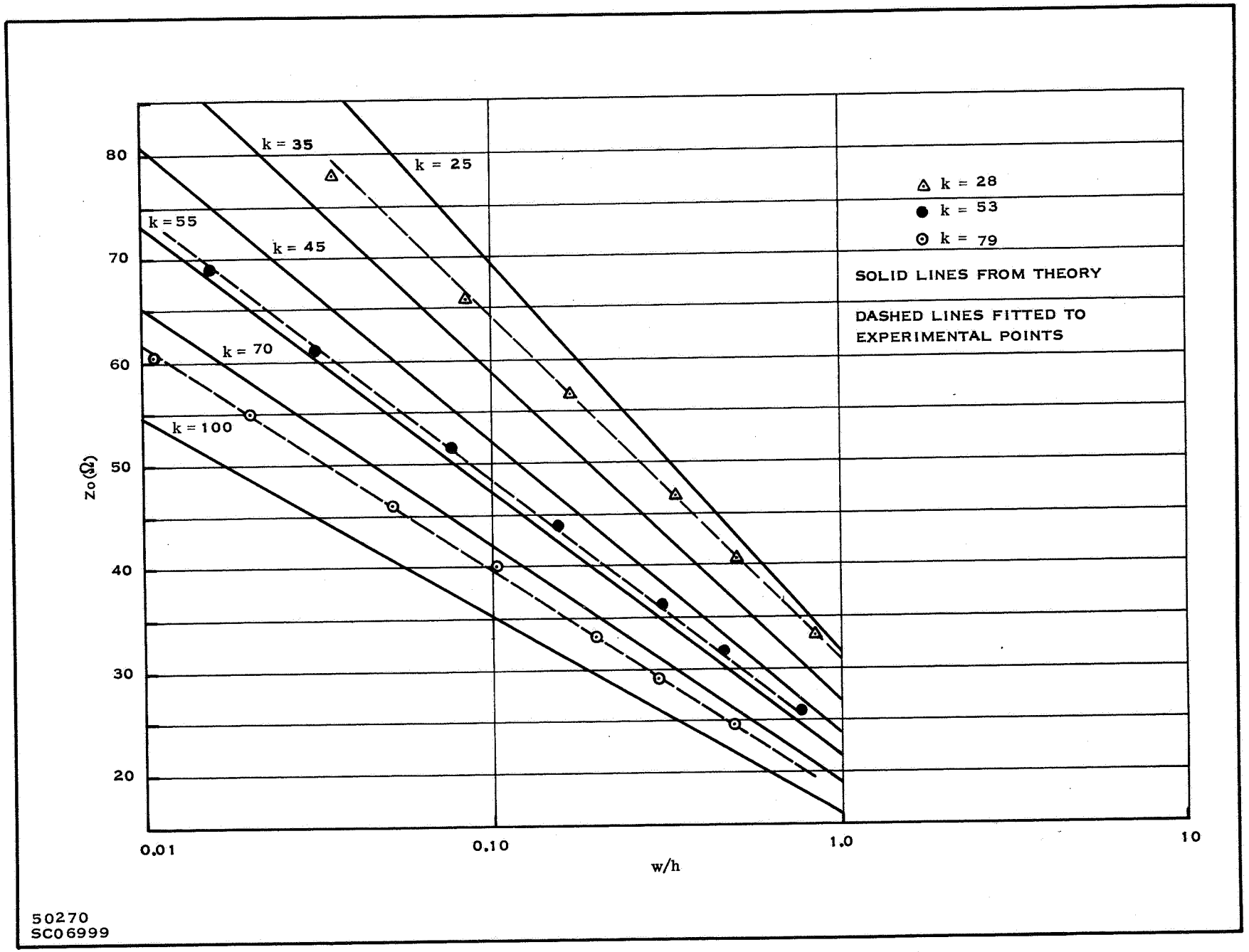

Figure 76. Characteristic Impedance vs Dielectric Constant and Geometry

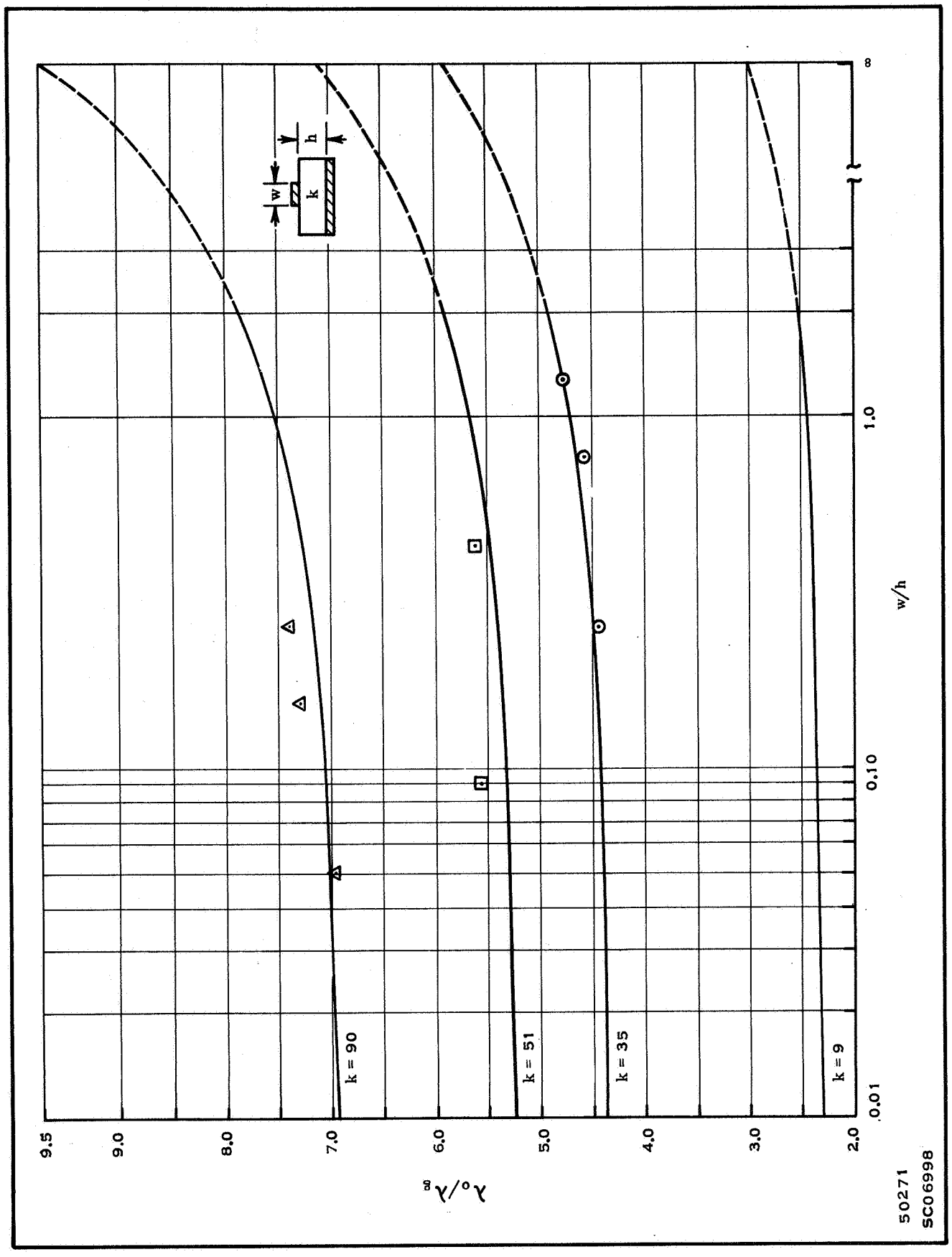

Figure 77. λo/λg vs Dielectric Constant and Geometry

required for reduced-size microwave integrated circuits. The variations of microstrip wavelength, characteristic impedance, and attenuation with geometry and dielectric constant are in good agreement with the theory. The low values of attenuation and guide wavelength make this material particularly attractive for low loss microwave circuitry.

At the present state-of-the art, only smaller physical size justifies using high dielectric materials because other factors tend to discourage its use. The rough surface of titanium dioxide makes it impossible to form thin film capacitors without shorting. The very small circuit dimensions makes it difficult to make external connections. In order to get characteristic impedances at the higher levels, a thick substrate is required, and to add to the problem the temperature conductivity is quite low: 0.05 for TiO_2, 0.15 for ceramic, and 1.0 for silicon. And finally there is a problem with energy lost from surface waves which are independent from the TEM wave of the Microstrip.

4. Circuits

Printed microstrip has made possible a variety of integrated components such as directional couplers. One type of directional coupler is shown in Figure 78a which uses the fringing effect to accomplish coupling. Tight coupling requires very close spacing between conductors (e.g. less than 0.5 mm) or very long sections (e.g. several wavelengths). It is possible that the circuit will resonate in the balanced twin strip mode. Another disadvantage of this type of coupling is the difficulty of controlling both the phase change coefficient and the coupling factor in a prescribed manner [37].

A second type of coupler, shown in Figure 78b, is known as the branched arm coupler. It has certain advantages over the parallel-line coupler, but if a high value of directivity over a large bandwidth is required, the number of branches becomes rather large (e.g. more than 3) and the impedance of the outer arms tends to become higher than can be realized in this or any similar form of construction (e.g. more than 150 ohms).

A third method (Figure 78c) employs two microstrip conductors back to back over a common ground plane. Coupling is accomplished by slotting the ground plane between the two strips. By the proper choice of slots, a wide variation in coupling strength is possible and either forward or reverse directivity can be obtained.

Microstrip filters may be one of three types. The parallel coupled resonator, shown in Figure 79, employs half wave sections which overlap adjacent section by one-quarter wave. (These sections need not be in a straight line. They can be in the form of a semicircle to conserve space.) The large amount of overlap results in both electrostatic and electromagnetic coupling. The coupling affects the image impedance of the lines so it is necessary to adjust the width of the sections to control the characteristic impedance. The insertion loss vs. frequency of three experimental filters is shown in Figure 80. Responses were also observed at $2\omega_o$ and $3\omega_o$. The VSWR characteristics are shown in Figure 81.

The direct-coupled filter, (Figure 82), has sections which are approximately one-half wave length long and are coupled to each other at each end by gap capacitances.

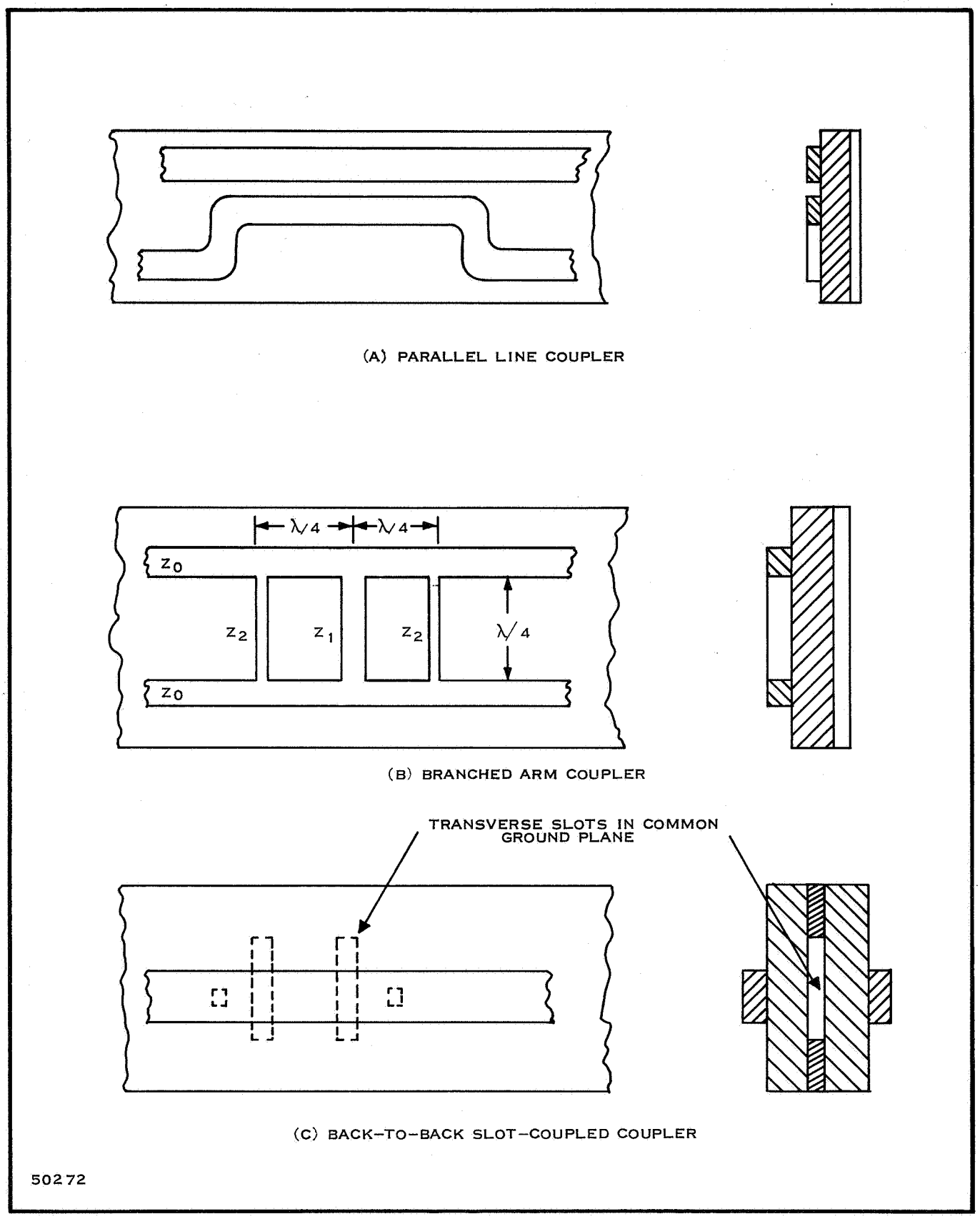

Figure 78. Differential Forms of Microstrip Directional Coupler

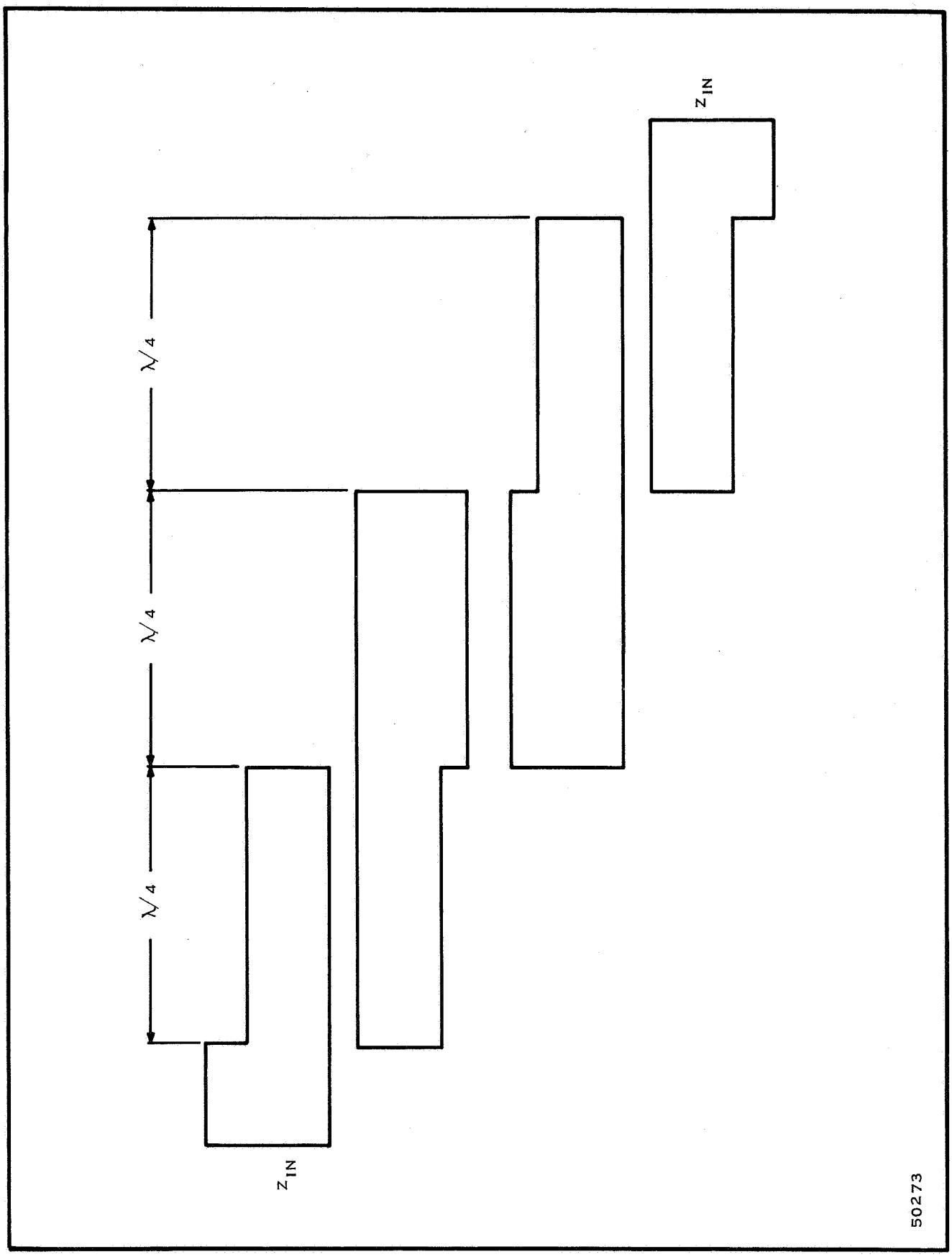

Figure 79. Two-Section Parallel Coupled Resonator Filter

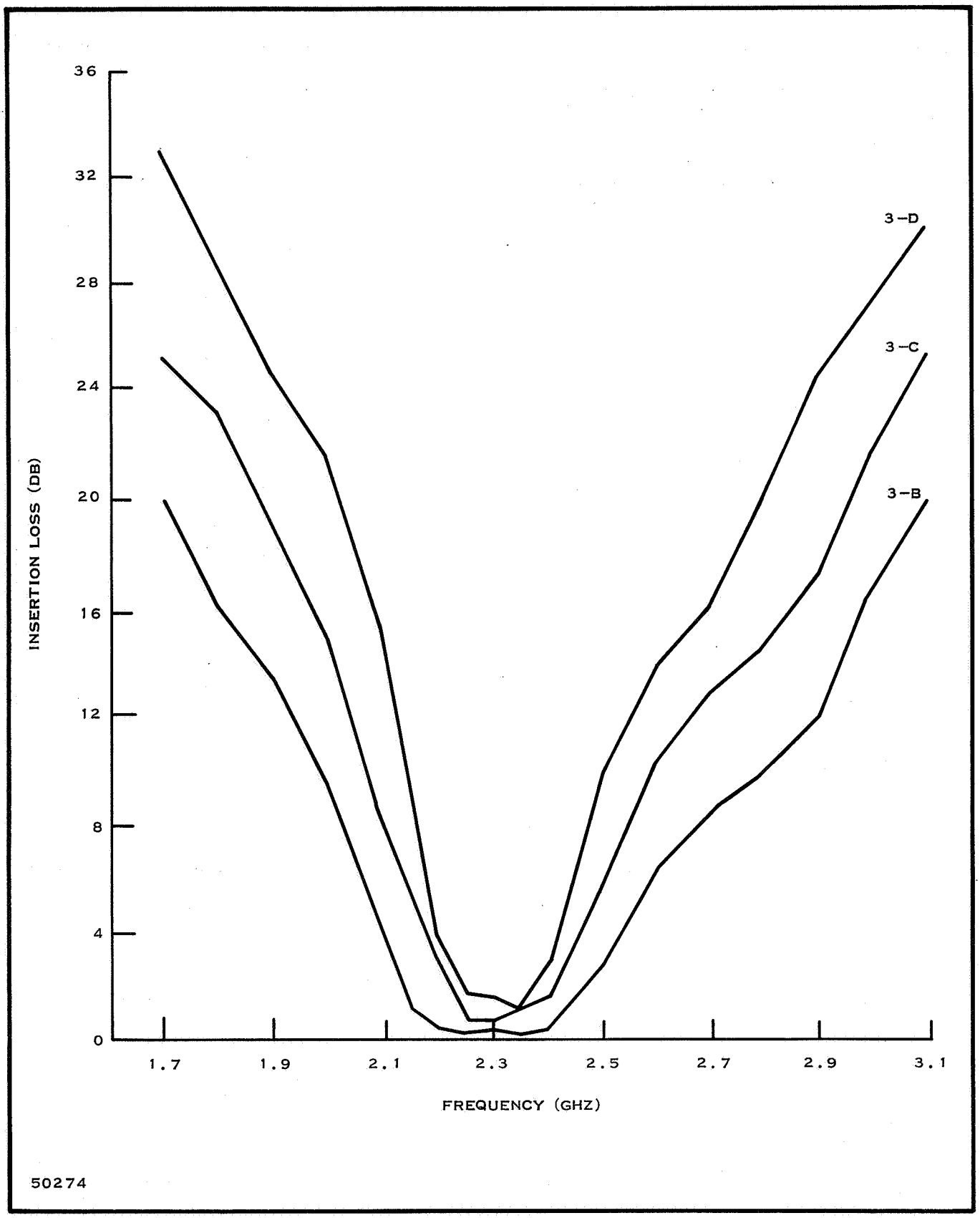

Figure 80. Insertion Loss vs Frequency of Parallel Coupled Filters

VSWR CHARACTERISTICS

FREQUENCY GHZ	3-B	3-C	3-D
2.15	3.30	7.0	18.0
2.20	1.75	3.05	6.70
2.25	1.37	1.83	2.85
2.30	1.42	1.56	2.40
2.35	1.43	1.65	2.65
2.40	1.54	2.40	5.10
2.45	2.1	4.50	10.23

50275A

Figure 81. VSWR Characteristics of Parallel Coupled Filters

A computer program using equations by Matthaei [38] was written to determine gap widths and conductor lengths. The resulting filter characteristics are shown in Figures 83 and 84.

The third type filter uses either open or shorted tuning stubs. The characteristics of some thin-film filters using stubs and parallel coupling are shown in Figures 85, 86, 87, and 88.

Couplers, filters, and transforming sections must be fabricated from transmission line sections having low loss and well defined characteristic impedance properties using process and materials compatible with other circuitry components.

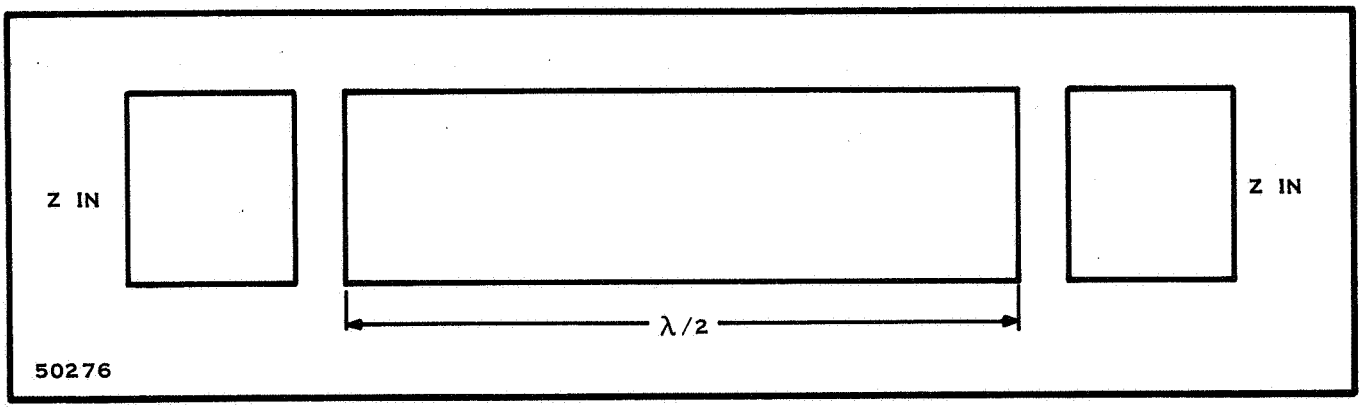

Figure 82. One-Section Direct Coupled Resonator Filter

One problem is the loss characteristics. For short interconnection of 50-ohm circuits, a loss of 3 - 5 dB/cm can be tolerated. The design of filters and couplers requires that the loss be no greater than 0.5 to 1.0 dB/wavelength. Bandpass filters require a few hundredths of a dB per wavelength for steep skirts and low insertion loss.

An additional advantage can be gained by using microstrip on the same substrate as the active components. By using high resistivity silicon, microstrip transmission lines loss can, at room temperature, approach conducter losses only.

C. LUMPED ELEMENTS

If the dimensions of a circuit element are so much smaller than a wavelength that distributed effects play no part in its operation, it is called a lumped element. At microwave frequencies lumped elements are very small. It has been more practical to build large distributed circuits of waveguides and coaxial cables because the circuits have higher Q due to a higher storage volume. But in IC's these elements are not practical; consequently minute lumped elements are now being fabricated with exacting precision. The phase shift over the element is zero because they are so short. If extra amplification stages do not circumvent the low Q problem, the idea of using IC's for circuits requiring high Q may have to be abandoned. Lumped elements in hybrid or monolithic IC's may be practical up to 3 GHz.

In the microwave region, inductors may be fabricated by thin-filming a spiral, loop, or a meandor line on a high dielectric substrate. At 2 GHz, a 5-turn spiral, 0.040 inch in diameter, on glass has an inductance of 10 nh and a Q of 45. A 0.060-inch coil has an inductance of 25 nh and a Q of 60. Figure 89 shows a plot of Q^2 versus f for such an inductor (the linear variation is expected for a true inductor).

The results for a series LC circuit are shown in Figure 90. The straight line response shows the absence of distributed effects; therefore, the circuit behaves like a lumped series LC circuit across the band 0.5 to 2.5 GHz. The element values shown were determined from circuit response and are close to design values [39].

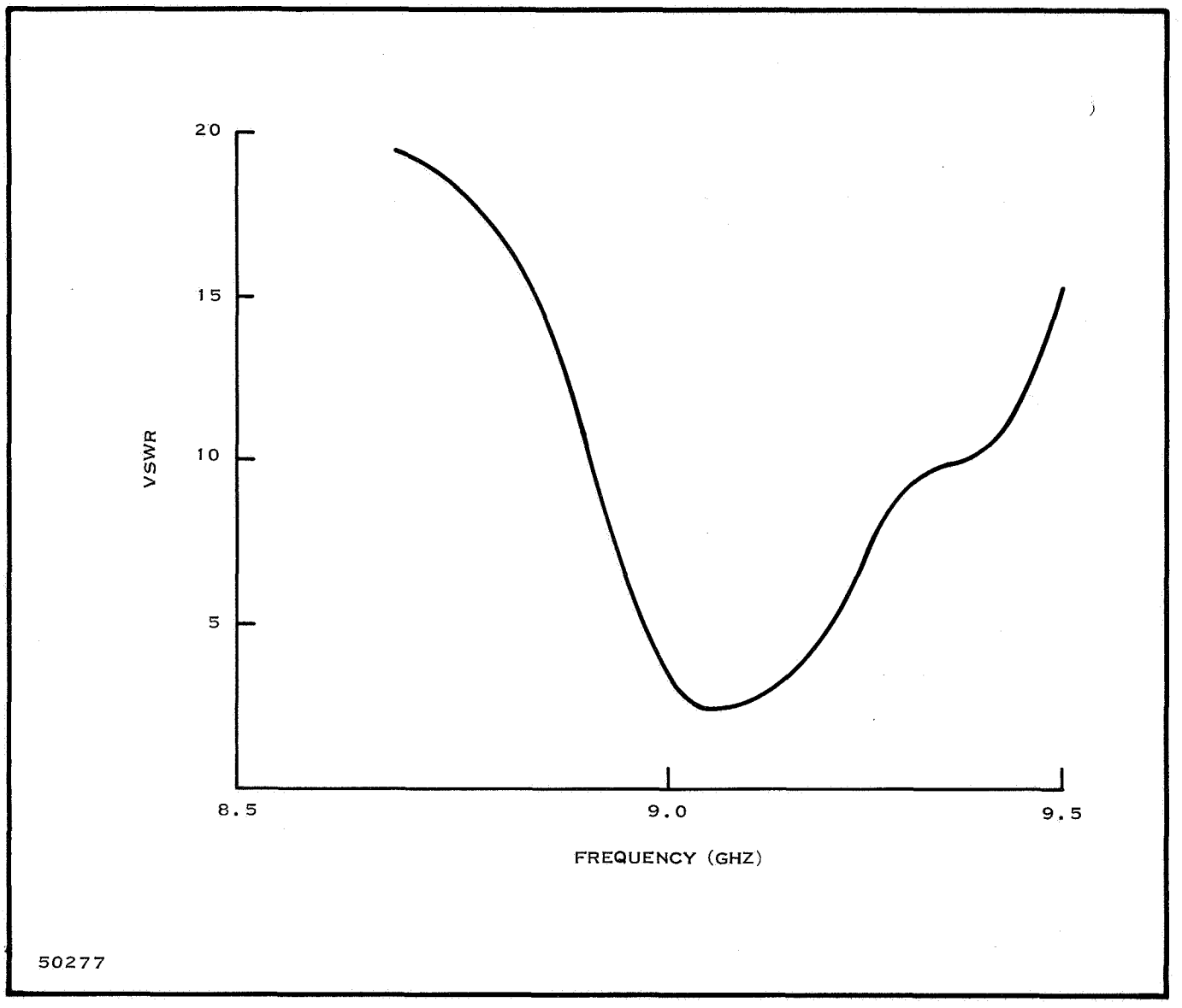

Figure 83. Two-Section Direct Coupled Filter - VSWR vs Frequency

Figure 91 is a thin-film lumped element circuit to match an experimental transistor pellet to 50-ohm transmission lines. The entire amplifier occupies an area 130 mils by 110 mils. This amplifier yielded 2.4 dB of gain at 1.86 GHz. Using stub tuners to compensate for faulty input match, the gain was increased to 4.4 dB. In other circuits with stub tuners to adjust for parasitic reactances introduced by the breadboarding, gains as high as 3.8 dB have been achieved at 2 GHz with 0.5-watt output power and 25 percent collector efficiency. Thin-film lumped elements might also be used as chokes and bypass capacitors in distributed stages.

Figure 92 illustrates the relative sizes of the different circuit elements of an integrated 2 GHz lumped element amplifier. A 2 GHz microstrip amplifier using the same transistor and designed for minimum size is about 10 times as large. As a

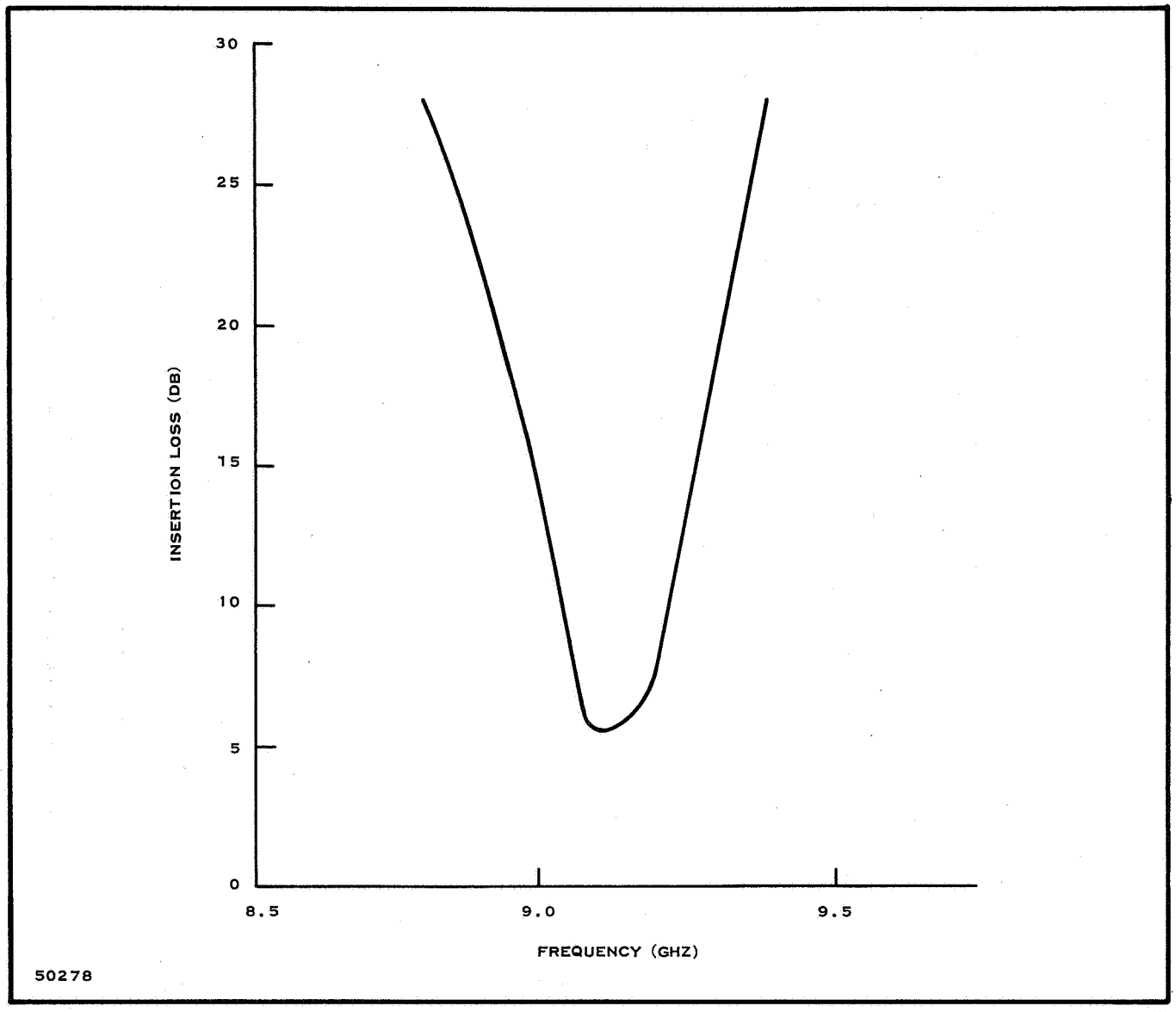

Figure 84. Two-Section Direct Coupled Filter - Insertion Loss vs Frequency

further indication of relative size, a 10-nh coil and a 0.636-pf film capacitor form a simple LC resonator with a Q of 25 at 2 GHz in about 2000 square mils. In contrast, a microstrip resonator constructed from a 50-ohm line in a 25 mil thick alumina substrate will have a Q of 120, but its area is about 15,000 square mils. Thus, the designer is faced with an area vs. Q tradeoff.

Thin-film capacitors are suitable to microwaves and an extensive report on construction and characteristics is available[7]. Thin-film resonant circuits are not subject to variable tuning so correct values must be fabricated initially. Tuning may be possible using active filters; however, this field is as yet relatively unexplored.

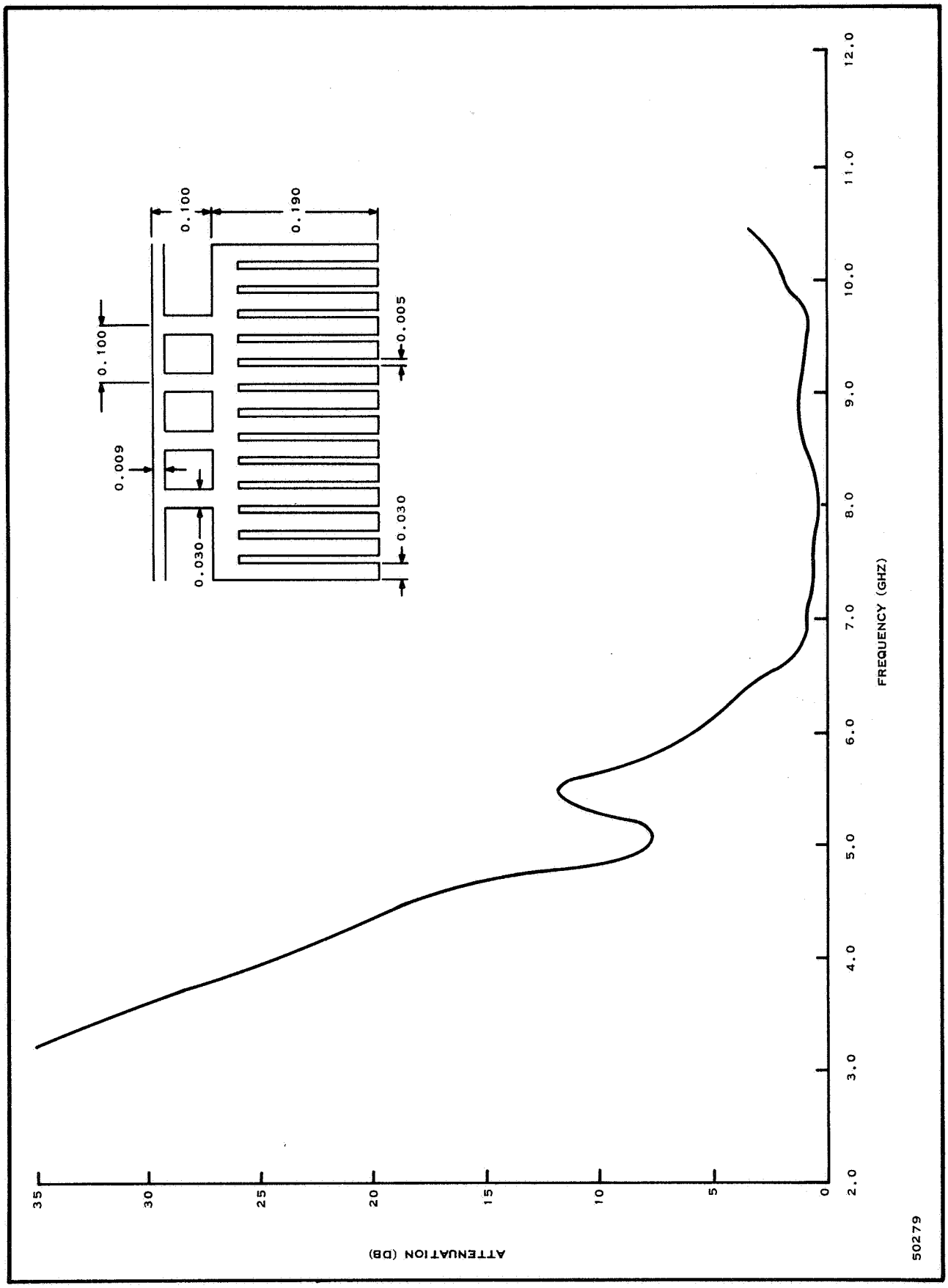

Figure 85. High Pass Filter, 10-mil Ceramic

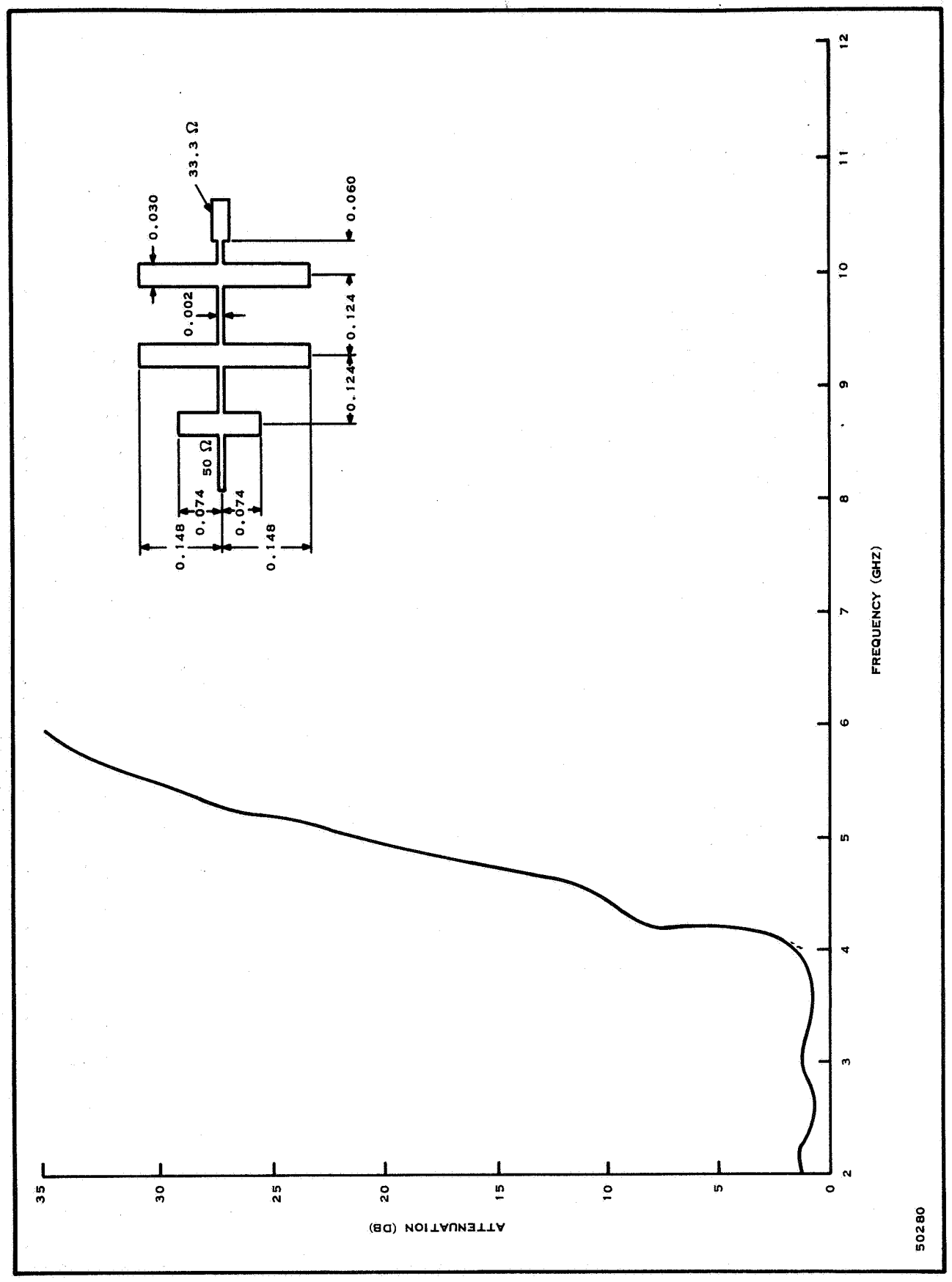

Figure 86. Low Pass Filter, 10-mil Ceramic

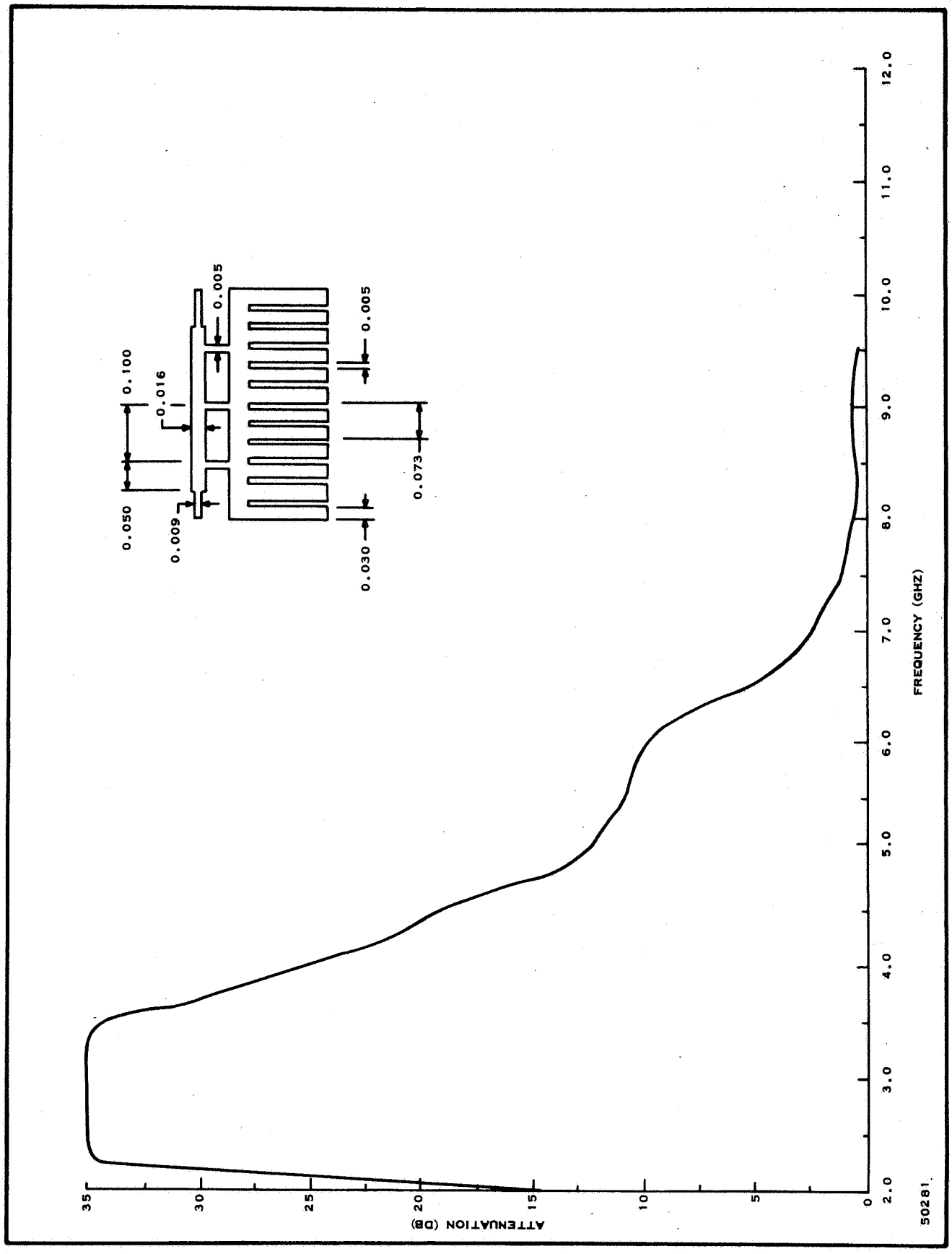

Figure 87. Different Configuration of a High Pass Filter, 10-mil Ceramic

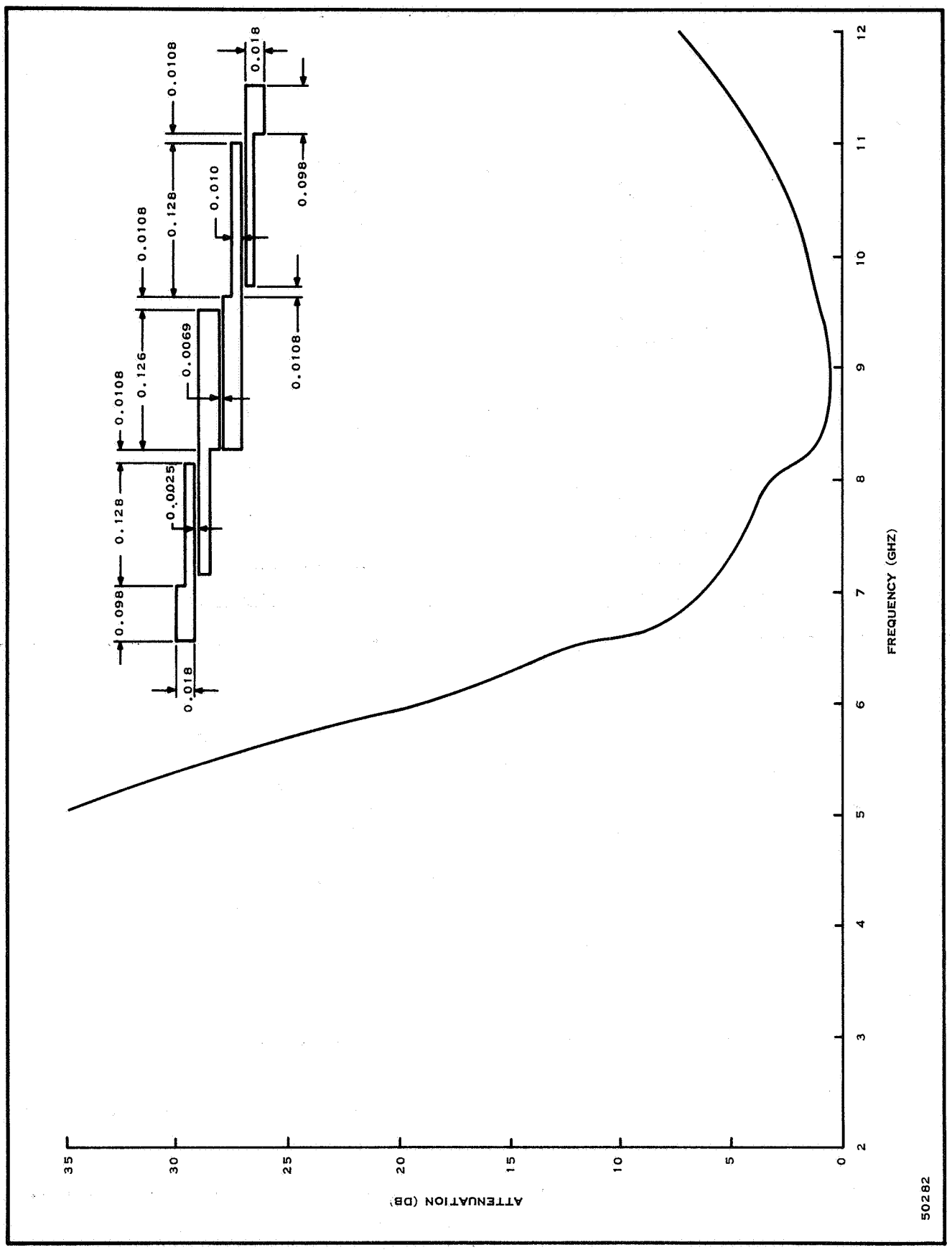

Figure 88. Bandpass Filter, 20-mil Ceramic

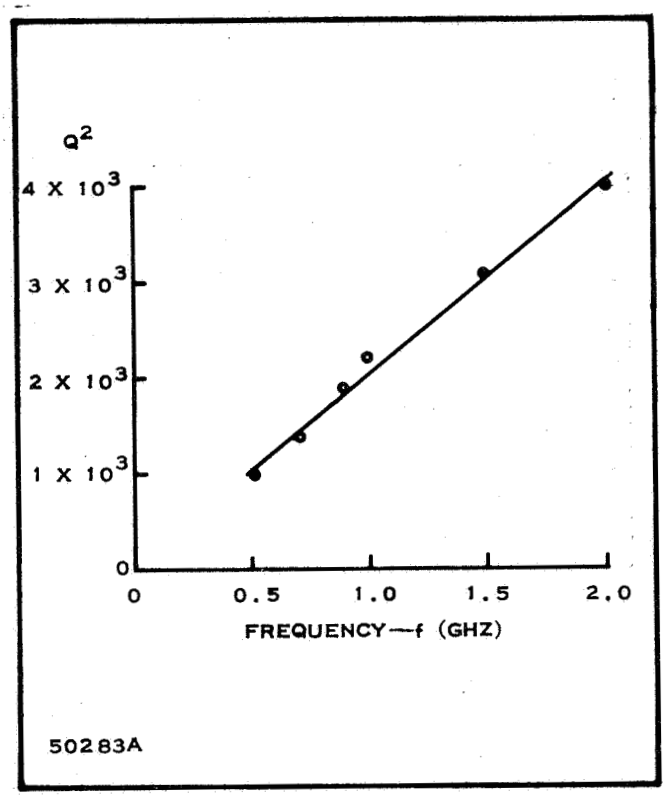

Figure 89. Measured Frequency Variation of Inductor Q

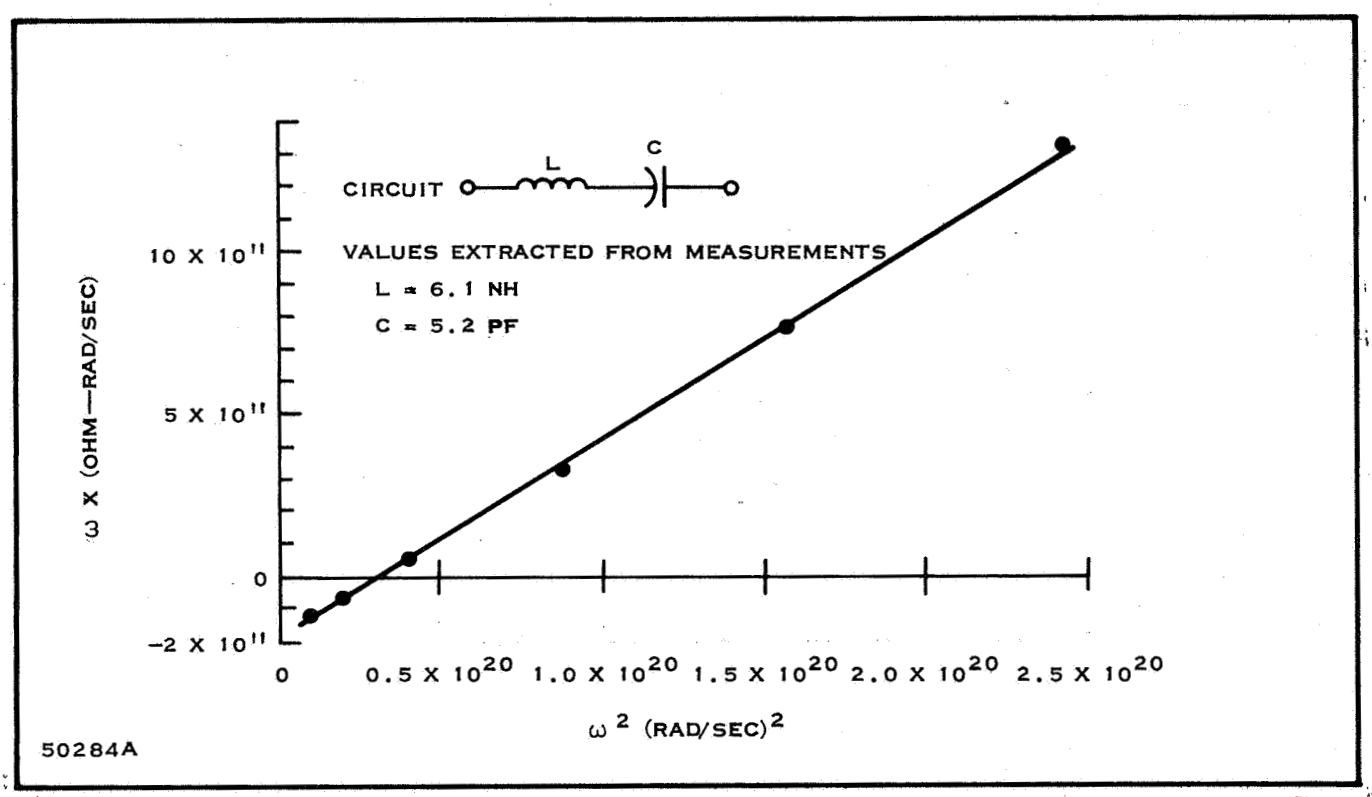

Figure 90. Measured Frequency Response of the Reactance of a Lumped LC Circuit

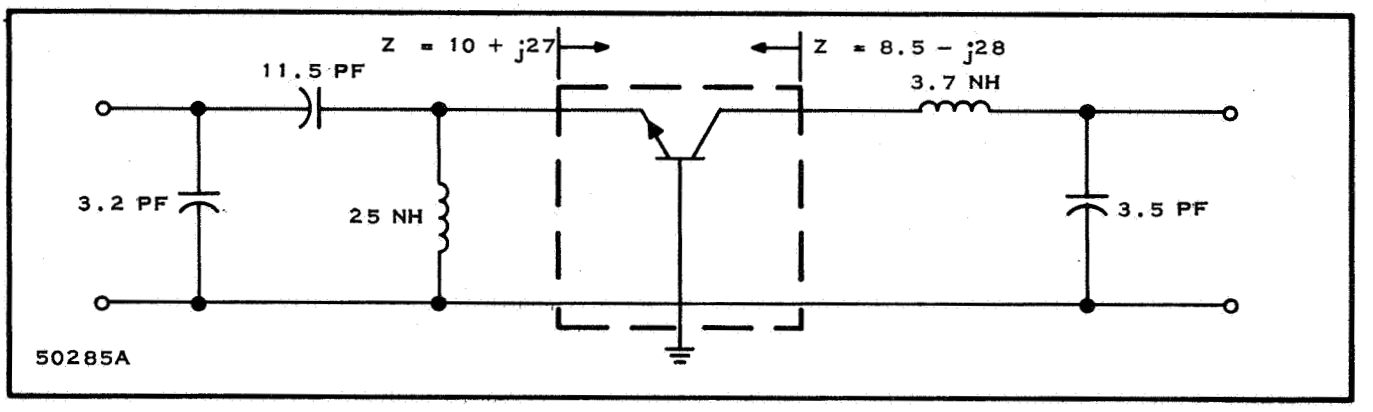

Figure 91. RF Circuit Diagram for Power Amplifier

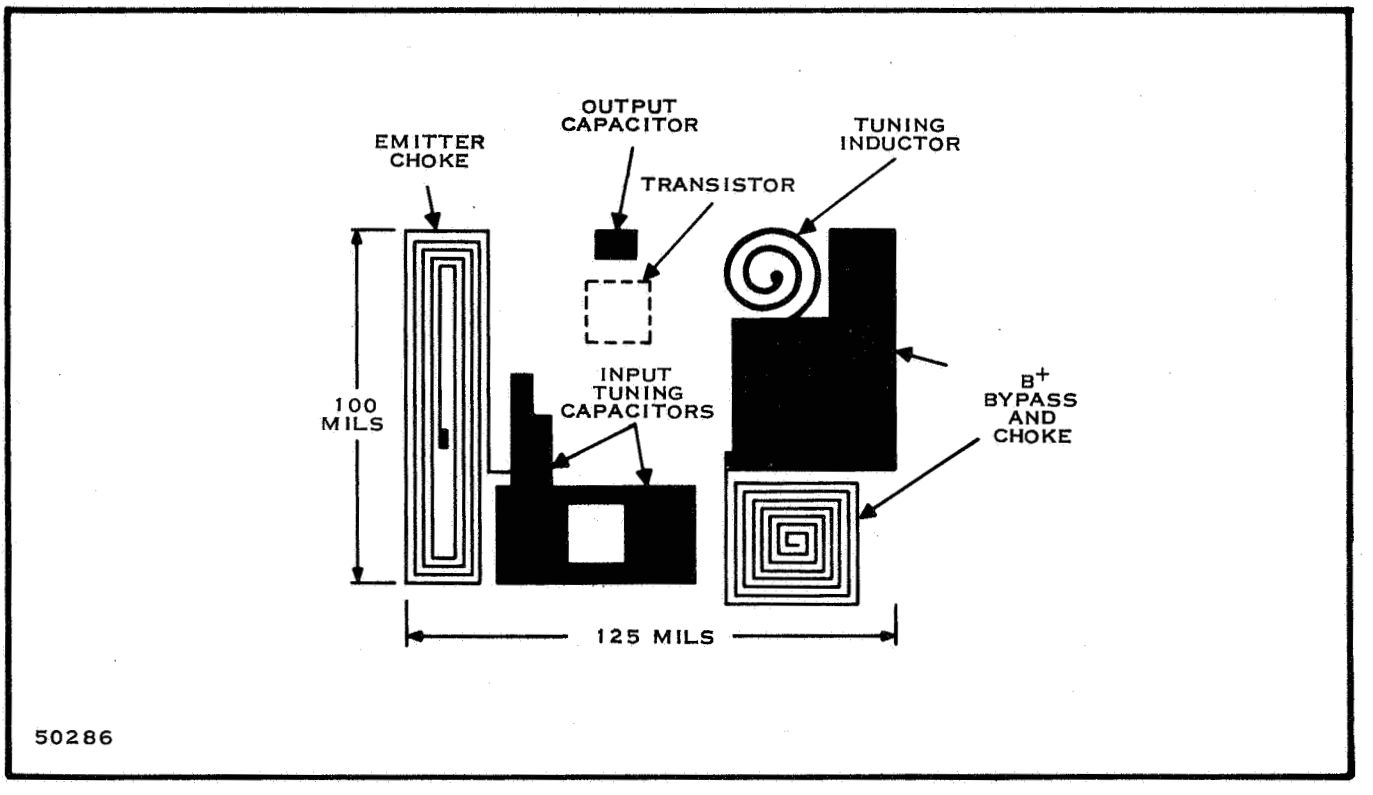

Figure 92. Layout of 2-GHz Integrated Lumped Circuit Amplifier

SECTION VII

FERRITES

A. INTRODUCTION

The first scientific report considered the general ferromagnetic properties of ferrite materials. In this report, these properties are further described and their application to microwave components is extended.

The unilateral transmission properties of ferrite materials are well suited for use in circulators and isolators where the propagation characteristics must differ for different directions of propagation. At higher frequencies, ferrites are easily integrated into microstrip fabrication of these devices.

Better understanding of the behavior of the intrinsic properties of ferrite materials have resulted in such nonlinear applications as frequency doublers, power limiters, and modulators. Difficulties which have been experienced in the past such as high dielectric constant, operation at high power levels and large insertion loss at ultrahigh frequencies are being reduced by better preparation of ferrite materials.

The principles underlying the ferromagnetic behavior of ferrite materials is well documented [40,41] but are briefly reviewed below along with a discussion of recent developments in ferrite materials and devices.

B. MICROWAVE PROPERTIES

The electrical characteristics of ferrites are specified by their complex permeability which may be written as

$$\mu^* = \mu_o [u' - ju''] \tag{49}$$

where

μ' = real part which determines phase shift

μ'' = imaginary part which is the loss component of permeability

μ_o = permeability of free space ($4\pi \times 10^{-7}$ h/M)

The response of a ferrite sample to a circular polarization wave is shown in Figure 93 where it is seen that the loss and phase shift through a ferrite sample is different for opposite wave polarization.

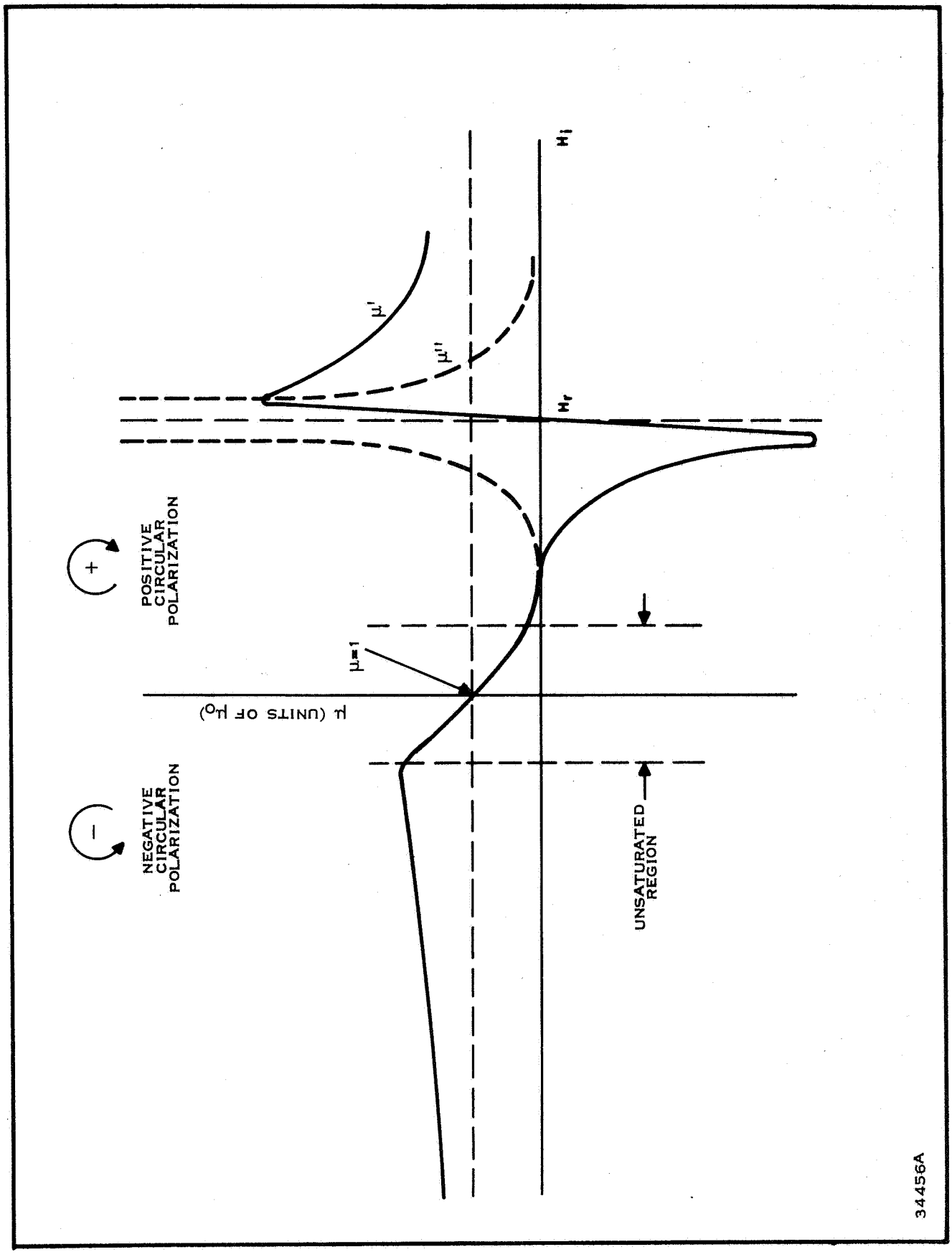

Figure 93. Ferrite Permeability for Circularly Polarized Waves as a Function of Internal Magnetic Field

The magnetization properties of ferrites is the result of the separate ferrite electrons spinning about their own axis as they orbit the nucleus of their parent atom. Electron spin is the principal contributor to the magnetic properties which arise mainly from the magnetic dipole moment associated with the electron spin. The total magnetic moment of the ferrite atom is given

$$\mu = J_g \mu B \tag{50}$$

where J is the quantum number associated with the total angular momentum resulting from the spin and orbital moment, μB is the magnetic dipole moment of the electron and equal to 9.27×10^{-21} ergs/gauss and g is the Lande spectroscopic-splitting factor. When the ferrite material is placed in a dc magnetic field (Hdc), the spin axis of the electrons become aligned in the direction of the applied magnetic field, and the magnetic dipoles tend to align themselves parallel to the applied field. Consequently, a net magnetization results which is the sum of the separate magnetization contributed by each electron. The magnetization of a ferrite specimen is then given as the density of magnetic dipoles per unit volume

$$\vec{M} = N\mu \quad . \tag{51}$$

For a large external magnetic field which saturates the ferrite sample, $\vec{M}$ becomes $\vec{M}s$. The whole sample behaves in the same fashion as a large single magnetic dipole. The saturation magnetization, Ms, for common ferrites is given in Table XV.[42]

Table XV. Saturation Magnetization of Ferrites

Material	Saturation Magnetization Ms (oersteds)
Nickel Zinc Ferrite	5000
Nickel Aluminate	500—1700
Nickel Cobalt Aluminates	1500– 3000
Manganese—magnesium Ferrite	2100
Manganese- magnesium Aluminate	600—1700
YIG	1780
Substituted YIG	300—1200

When subjected to an RF magnetic field alternating at a microwave frequency superimposed upon a dc magnetic field, the magnetization vector $\vec{M}$ of the ferrite sample will precess as a gyroscope about the axis of the applied dc magnetic field.

The precessional frequency is proportional to the externally applied dc field and may be written,

$$W_o = \gamma \vec{B}_o \quad . \tag{52}$$

This frequency is commonly referred to the gyromagnetic resonance frequency as it is dependent upon the gyromagnetic ratio, γ. This ratio is the ratio of the magnetic moment of the ferrite material to the angular momentum of its magnetization vector, $\vec{M}$. The gyromagnetic ratio may be expressed as

$$|\gamma| = 1.4 \text{ g MHz/oe} \tag{53}$$

where g is the Lande spectroscopic-splitting factor and is normally taken to be equal to 2 for most ferrite materials.

The magnetic induction vector, $\vec{B}$, shown in Equation (51) relates the permeability tensor, the magnetic field intensity vector, $\vec{H}$, and the magnetization vector, $\vec{M}$, as seen in the relation[43,44]

$$\vec{B} = \mu_o \left[\vec{H} + \vec{M}\right] = \mu_o \, [\mu] \, \vec{H} \tag{54}$$

where μ_o $[\mu]$ is the complex permeability tensor in rationalized mks system, and μ_o is the permeability of free space ($4\pi \times 10^{-7}$ h/M).

The applied magnetic field required for ferromagnetic resonance in an infinite ferrite medium is given as

$$H_o = \omega/|\gamma| \quad . \tag{55}$$

If the microwave frequency is held constant and the magnetic field is varied around the value required for resonance, the -3 dB points in the response will define the magnetic field "line width," ΔH. Narrow linewidth then corresponds to high Q material, since linewidth represents the "bandwidth" of a material [40,45]. This relationship may be expressed

$$\Delta f \approx \gamma \, \Delta H \quad . \tag{56}$$

Linewidth is a function of frequency as well as temperature. At a room temperature of 300°K and at 9.34 GHz, linewidth may range from 0.1 oersteds (Oe) to 10 Oe for highly polished YIG garnets. Impure samples of YIG may have linewidths of 100 Oe. In this sense any substitution such as gallium is an impurity and accounts for the relatively larger linewidths of substituted (GA YIG) specimens.

The manner in which various operating regions for ferrite materials yields different microwave devices is shown in Table XVI.

Table XVI. Classification of Microwave Ferrite Devices

Gyromagnetic Effect	Biasing Field	
	Variable	Fixed
Linear		
Faraday Rotation	Switch Variable Attenuator	Isolator Circulator
Field Displacement	Switch	Isolator Circulator
Resonance Absorption	Switch	Isolator
Variation of RF Permeability	Phase Shifter Modulator Tuned Filter Tuned Cavity	Circulator
Nonlinear		
Nonlinearity of Magnetic Characteristics		Ferromagnetic Amplifier Oscillator Power Limiter

Pure magnetic ferrites are those metallic oxides which have the general composition of $MO \cdot Fe_2O_3$, where M is any divalent metal ion such as iron, cobalt, manganese, zinc, copper, barium or any mixture of these. A commonly "mixed" ferrite composition for microwave applications is magnesium-manganese ferrite. Substitution of such trivalent metals as aluminum, gallium, chromium for some of the Fe^{3}_{+} ions of the crystal structure yields "substituted" ferrites which exhibit reduced magnetic losses in the UHF region. The general formula for a magnetic garnet is $M_3 \cdot Fe^{2} \cdot (FeO_4)$, where M may be nonmagnetic trivalent yttrium, lutetium[40] or one of the rare-earth ions from lanthanum through ytterbium. Polycrystalline garnets such as Calcium Vanadium Bismuth (CVB) has a crystal uniformity which results in lower required magnization to achieve resonance. Thus, allowing devices to be designed in a lower frequency region. The use of rare-earth and yttrium-free garnets have also been reported used in lower frequency devices as their low linewidth property results in low insertion loss [46].

It is found that it is easier to magnetize the crystal along certain directions than others. The crystal axis in which the smallest amount of applied magnetic field is required to saturate the specimen is called the easy axis or easy direction of magnetization. Along other directions, a larger field is required for saturation, and is called the hard axis. The difference between the energy required to magnetize the sample to saturation along the hard direction and the easy direction is called anisotropy energy. This energy results in an internal anisotropy field within the ferrite sample. This

internal field, in addition to the internal field resulting from the porosity of the material, will effect the resonance frequency of the ferrite. The dependance of the ferromagnetic resonance frequency upon the applied magnetic field and the anisotropy field is expressed for a spherical ferrite sample

$$f = \gamma [Hdc + Ha] \tag{57}$$

where Ha is anisotropy field and Hdc is the external applied field.

Ferrites have specific resistivities that may be as much as 10^6 or 10^8 ohm-cm at microwave frequencies. The loss tangent of a typical ferrite may range from 5×10^{-2} to 5×10^{-4} and the relative dielectric constant may range from 10 to 20 at microwave frequencies. Such high dielectric constants give rise to difficulties in proper matching in microwave circuits[47].

Ferrites and garnets for microwave applications have polycrystalline grain size between 10 and 20μ in which spin waves having wavelengths as short as 0.1μ can exist. Careful preparation of varied ferrite compounds have resulted in samples with grain structure of 1.0 and 2.0μ[48]. The grain boundaries provide sufficient discontinuities to break up spin waves in much the same manner as surface roughness breaks up uniform propagation in single-crystal YIG spheres since spin waves do have a definite frequency. Such preparation processes increased the microwave power absorption threshold, P_{crit} by an order of magnitude without an increase in low power insertion loss. The increase in threshold is the result of an increased spinwave linewidth. These materials with grain size down to 1.0μ permit the realization of dielectric loss tangents(ϵ''/ϵ') = 0.0005 at 9.3 GHz. The comparison of the properties of small grain ferrite to commercially available ferrite is given in Table XVII.

Table XVII. Effects of Grain-Size Variation at 9.4-GHz for Magnesium Manganese

Characteristic	Standard	Fine Grain
Grain size (microns)	10 - 12	1 - 1.5
ϵ''/ϵ'	0.00025	0.00025
ΔH (linewidth,Oe)	560	550
g	2.83	2.86
$4\pi M_s$ (Gauss)	2188	2029
h_{crit} (Oe) sphere	7.63	38.0
P_{crit} (kW) rod	2	50

Synthesized hexagonal ferrite of polycrystalline compounds tested for ferromagnetic resonance at room temperature were found to have useful microwave properties.[49] The linewidth of such structures were found to vary between 100 and 1200 Oe and the anisotropy field varied from 0 to 40,000 Oe. Such compounds also have easy and hard directions of magnetization which required different magnetic fields values to achieve ferromagnetic resonance. One consequence of hexagonal structures is that high values of magnetic anisotropy can be attained with some substitutions. Thus, smaller external fields are required for saturation and operation of ferrite at lower frequency ranges are more easily obtainable, as Equation (57) demonstrates. Previously, the small external fields required to achieve resonance would not saturate the ferrite sample and operation in the UHF range was impractical. The different impurity substituted compounds in hexagonal ferrite structures have a marked effect on the magnetic anisotropy and linewidth.[49] If narrower linewidths could be achieved, useful microwave devices at frequencies above 10 GHz could be constructed.

Materials for use in cryogenic circulators need to have a low saturation magnetization, 400-600 Gauss together with small anisotropy fields. Undoped and aluminum doped yttrium iron garnets (YIG, YIG - AL), mixed gadolinium-yttrium iron garnets (Gd - YIG) and calcium-vanadium bismuth garnets (CVB) are compared at room temperature and 4.2°K (Table XVIII). CVB is shown to have the smallest low field losses of the materials compared. The data in Table XVIII was obtained for disc-shaped samples magnetized normally to the plane of the disk, and at a frequency of 4.2 GHz.

Table XVIII. Parameters of Materials Used in Cryogenic Circulators (Sample 10 mm x 1 mm)

	T = 300°K		T = 4.2°K	
	H (Oe)	$4\pi M_o$ (KG)	H (Oe)	$4\pi M_o$ (KG)
YIG	86	1.77	190	2.44
YIG - AL	52	0.58	1030	0.80
GD - YIG	50	0.58	510	0.68
CVB	225	0.41	625	0.43

C. RF ATTENUATORS

RF attenuators constructed with Per malloy films offer possible application where controlled attenuation is required[50]. An electrically controllable attenuator has been fabricated from two pairs of film, identical in properties and geometry, which are sandwiched into two segments of a strip line with the film surfaces making contact with the ground plane as shown in Figure 94. Films prepared by evaporation of

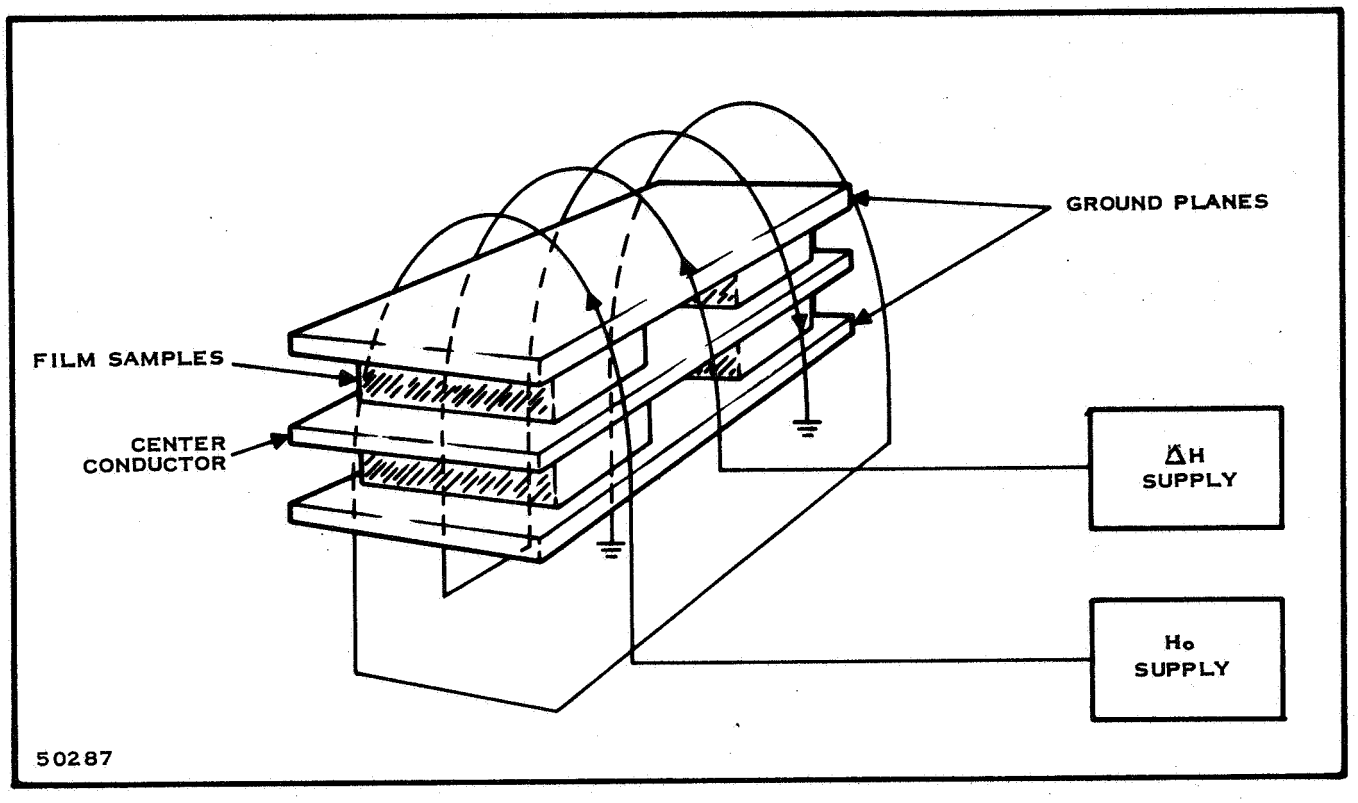

Figure 94. Electrical Controlled Attenuator

81/19 NiFe onto heated 0.15 mm glass substrates yielded an attenuation-range that varied almost linearly with frequency. The attenuation ranged from 15 dB at 1-GHz to 27 dB at 2.7 GHz while insertion loss decreased from 9.8 to 3.5 dB. The attenuation is proportional to the film thickness and length and inversely proportional to the glass thickness.

D. CIRCULATORS

Ferrite Y-junction or three port circulators offer many advantages in communication systems operating from L-Band to X-Band. In addition to their use as duplexers in Radar systems, circulators work fine in microwave relays or transponders since the transmitter and receiver usually operate at different frequencies. The circulator also enables simultaneous use of the transmitter and receiver with a single antenna. Because of its low loss, circulators may be utilized in low noise receivers without contributing to receiver noise. In such applications, two 3-port circulators, with one terminated by a matched load, are used with parametric preamplifiers or Helium-cooled masers. Four-port circulators may also be used in this application, but they are inherently more narrow band. The use of two to three port circulators to provide the proper matching impedances is shown in Figure 95.

A circulator is a three or four-port device in which energy introduced at one port circulates only to a second port while energy introduced at the second port circulates only to the third port. The third port is connected to but isolated from the first port.

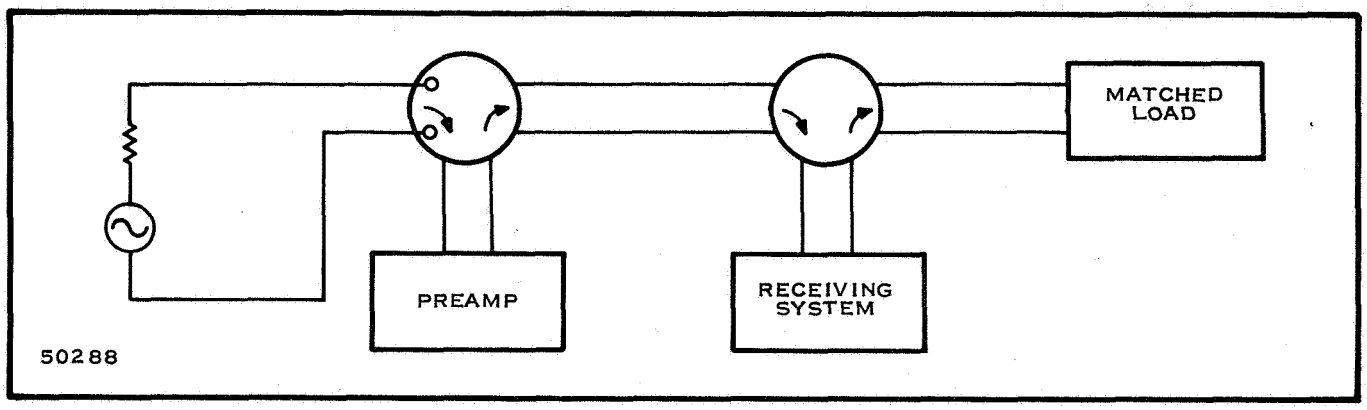

Figure 95. Two 3-Port Circulators

Circulation will occur in a symmetrical stripline junction that is loaded with ferrimagnetic material when all three ports are matched to the characteristic line impedances, if the magnetic biasing field is between the field required for saturation (H_{sat}) and the field required for resonance (H_o), where

$$H_o = H_{dc} \pm H_a + (N_t - N_z)\, 4\pi M_s \tag{58}$$

and

H_{dc} = applied dc field

N_t, N_z = demagnetization factors, in tranverse and tuning direction (59)

and

$$H_{sat} = H_a + (4\pi M_s), \tag{60}$$

and

H_a = anisotrophy field. (61)

The theory of the stripline circulator as described by Bosma[51] and by Fay and Comstock[52] shows that operation of the device is dependent upon the phase relationship of the three ports. This in turn is dependent upon the total differential phase shift between the input at one port and the output at the other two ports. At X-band, the size required to achieve the necessary phase relationships is compatible in size with the microwave integrated circuit functions.

The microstripline y-junction circulator consists of a conducting metallic disc on a ferrite substrate, which in turn is on a conducting ground plane. The structure has a resonant frequency; it is essentially at this resonant frequency that maximum isolation and minimum insertion loss occurs. When no magnetic field is applied, the standing-wave field pattern for the lowest frequency resonance of the circular disc structure is shown in Figure 96a. The electric field vectors inside the ferrite are

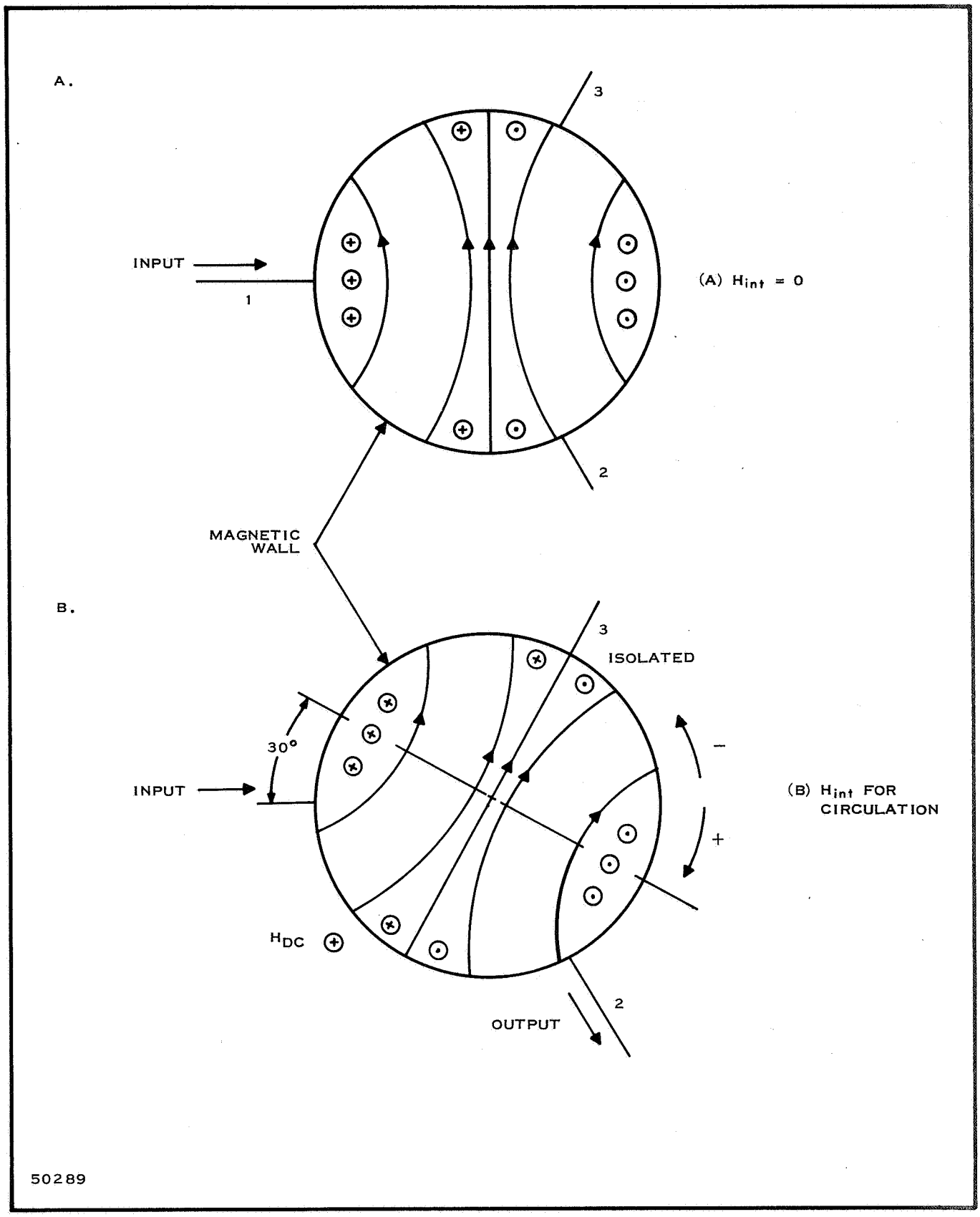

Figure 96. Bipolar Mode of a Dielectric Disc with and without Magnetization

perpendicular to the plane of the disc and the RF magnetic field vectors are parallel to the plane of the disc. Ports 2 and 3, if open-circuited, will see voltages which are 180 degrees out of phase and approximately half the magnitude of the input voltage. If the field pattern is rotated, as in Figure 96b, port 3 is at the voltage null position of the disc while the voltages at ports 1 and 2 are equal.

Small circulators have been constructed using strip transmission line conductors and ferrite discs to provide the circulator action. One such integrated circulator was fabricated recently at Texas Instruments. This circulator was of the y-junction type and was designed to utilize microstrip lines with a small disc of YIG ferrite 216 mils in diameter and 20 mils thick. This circulator had good isolation (>35dB maximum); however the bandwidth was less than desired. The bandwidth is primarily determined by the matching or coupling into the ferrite media. No attempt was made to optimize this in the initial design. This circulator also used an external magnet and no attempt was made to optimize the magnetic path or integrate the magnetic structure.

Of the possible circulator configurations, the symmetrical junction circulator appears the most attractive for application at X-band. It should result in the smallest size, the simplest construction and also the lowest insertion loss. Figure 97 illustrates an integrated circulator using a ferrite substrate. The design of the magnetic return path may be improved for compactness; a return path is virtually necessary in order to minimize fringing fields which could couple strongly to the outside world.

A 4-port circulator could be obtained by putting two 3-port circulators end to end, as shown in Figure 98, in which case the magnetic path may be closed in a useful way.

E. ISOLATORS

Ferrites are used in many various types of isolators such as:

Faraday—rotation type

Resonance—isolator

Field displacement

The nonreciprocal electrical properties of ferrite material in which the transmission coefficient is not the same for different directions of propagation is employed in microwave isolators. Isolators of several types, depending upon their region of operation regarding the resonance absorption curve, have been constructed utilizing the nonreciprocal property. Such devices allow transmitting a microwave signal with a minimal amount of transmission loss and prevents reflections from the load from interacting with the generating source. The advantages these devices offer are to minimize power output variations from power amplifiers and frequency pulling of an oscillator as variations in load impedances occur.

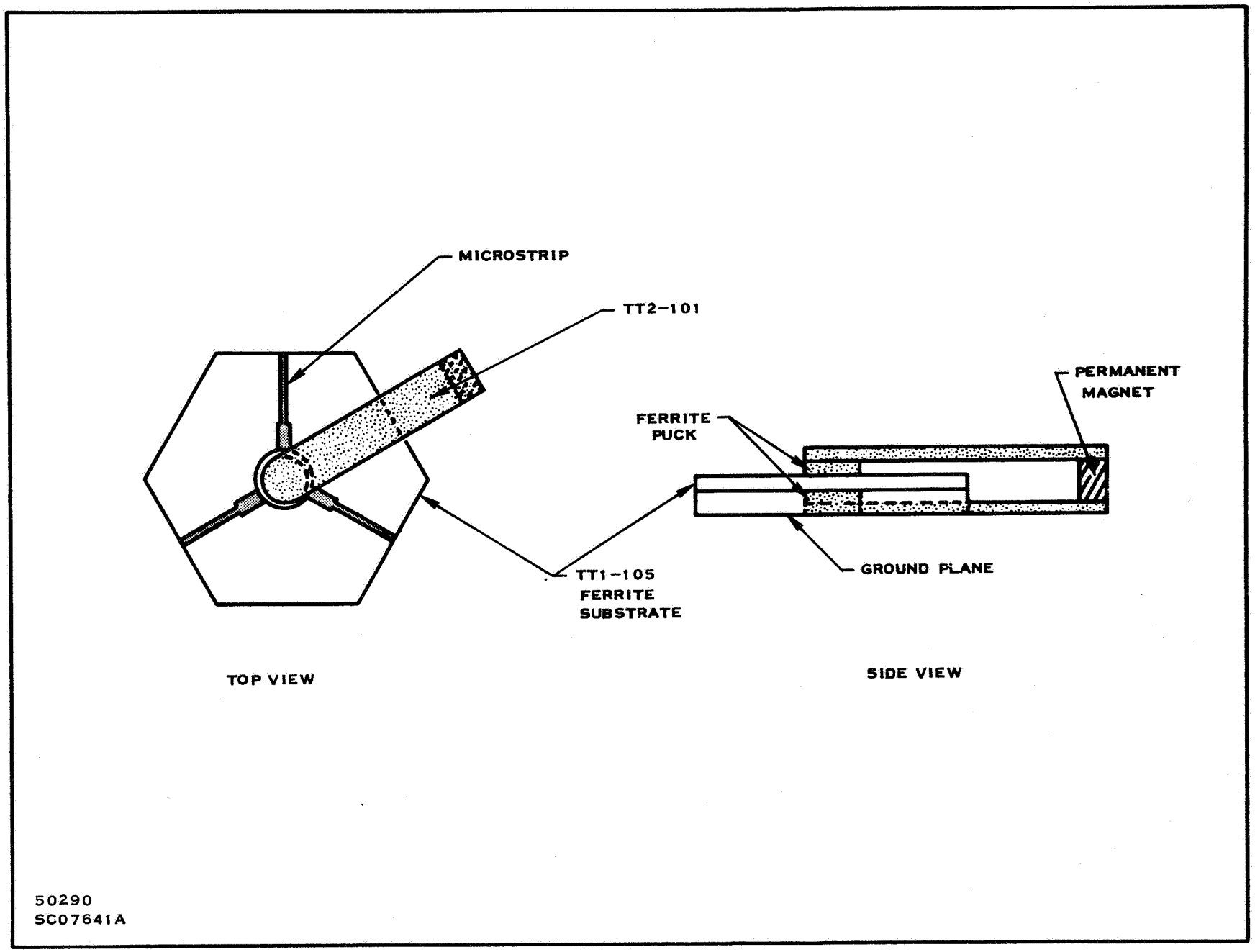

Figure 97. Three-Port Integrated Circulator

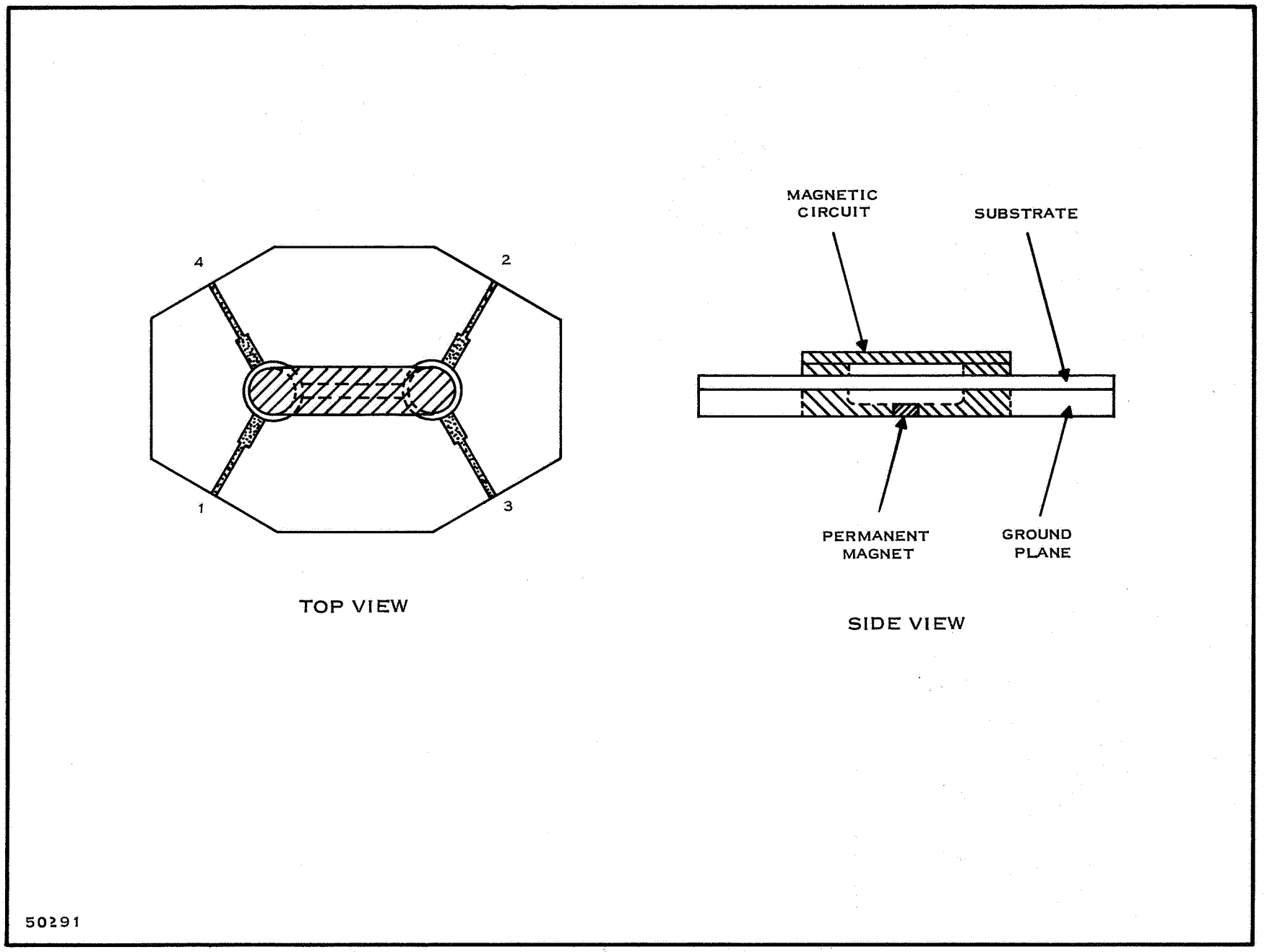

Figure 98. Four-Port Circulator with Closed Magnetic Path

An isolator that is a one-way transmission device or absorption device is the Faraday-rotation isolator which is essentially a four-port circulator where two ports are terminated with matched loads. Practical isolators of these types omit the two extra ports by mounting resistive elements internally within the devices. The resistive elements are separated by a cylindrical ferrite rod which is magnetized along its axis by an external field (Figure 99). The resistive elements are aligned to permit unaffected Faraday rotation of the plane of the propagated wave. This rotation principle results in the reverse wave being rotated 45 degrees counterclockwise by the ferrite rod with the electric vector parallel to the second resistive element; thus the reflected energy is completely absorbed. This type if isolator is referred to as an absorption isolator and it is a low power device because the amount of RF power absorbed is limited by the resistive element. Faraday-rotation type of isolators normally will provide about 30 dB of isolation over a 10 percent bandwidth with less than a 0.58 dB insertion loss at X-band.

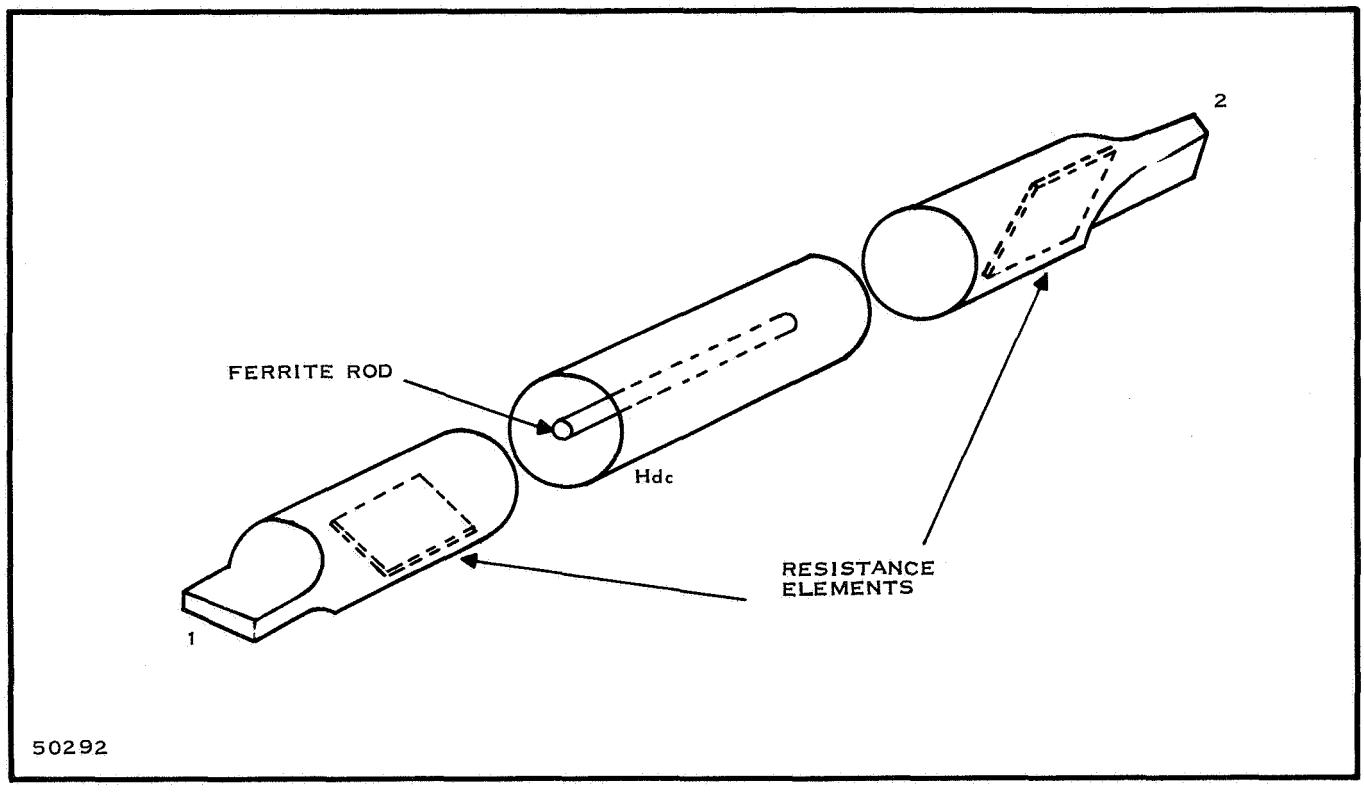

Figure 99. Faraday Rotation Isolator

SECTION VIII

FILTERS

A. INTRODUCTION

1. General

The first scientific report discussed several types of non-tunable transmission line filters which were compatible with integrated circuits and their passband characteristics could be maintained in microstrip construction. In this report, the discussion of parallel-coupled filters is continued and recent attempts to reduce the size of these filters at S-Band are examined. In addition, magnetically tunable YIG filters, which are finding wide spread use in modern microwave receivers, are discussed.

Good RF selectivity and a high degree of spurious rejection in microwave receivers requires the use of bandpass filters as preselectors. Ideally, the preselector affords perfect transmission for all frequencies which fall within the passband and infinite attenuation of signals and noise within the stop band. Such characteristics as these are obtained in basic bandpass filters employing multiple resonators or in structures that superimpose bandpass and band reject filters to obtain the desired composite characteristics. Generally, the bandpass characteristics are obtained from transmission line filters which exhibit periodic response as shown in Figure 100. The desired bandpass frequency performance of this type of filter is designed from lowpass prototypes using insertion-loss methods. The design techniques are well documented for the basic classes of filters such as lowpass, highpass,and bandpass. This section is restricted to a discussion of fixed tuned and electrically tuned bandpass filters which would normally function as a component of a microwave receiver.

2. Fixed Tuned Filters

Lumped-constant LC resonators at microwave frequencies are impractical, so out of necessity, desired frequency characteristics are synthesized from distributed parameter elements such as that offerred by transmission line techniques. The present day use of microstrip makes such techniques applicable to integrated structures in which the desired LC resonant properties are obtained by open or shorted transmission lines. These filters are discussed in Section VI. However, such filters fabricated in microstrip as an integrated circuit may not be tuned.

3. Variable Tuned Filters

Filters can be tuned electronically or by a magnetic field. Magnetically tunable filters using single-crystal yttrium iron garnets (YIG) obtain high unloaded Q at microwave frequencies making it possible to build bandpass filters with relatively low insertion loss. The lowest frequency at which a pure YIG sphere will resonate is about 2 GHz. A pure YIG disk sample can be tuned to much lower frequencies, but have the disadvantage of being difficult to machine and are fragile. For this reason, operation at lower frequencies generally employ gallium substituted ferrite resonators, (GaYIG). The substituted material has a reduced saturation magnetization which permits operation down to a few hundred megacycles. However, such substituted materials reduces the unloaded Q which results in increased filter losses.

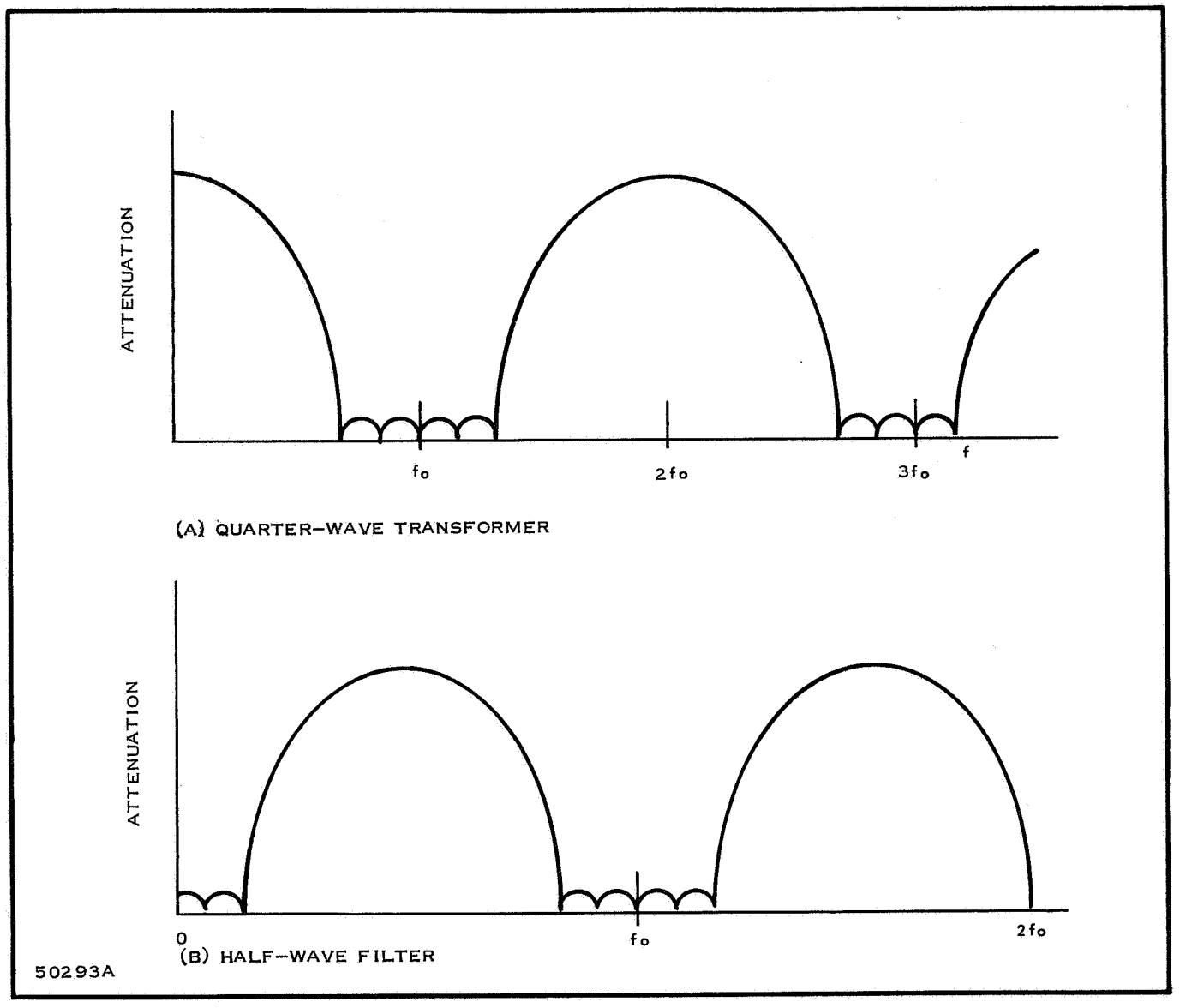

Figure 100. Periodic Nature of Transmission Line Filter

Materials possessing high dielectric constants may be used as dielectric resonators in the construction of tunable filters. The use of small volumes of such material which have dielectric constants on the order of 80, allow high unloaded Q's of 10^4 to be obtained. These filters can be tuned by adjusting the spacing between resonators, or if ferroelectric material is used, by tuning the resonance electrically by application of a high electric field. The chief disadvantage of high-dielectric constant resonators constructed of present day materials is the excessive dependence of the resonant frequency on temperature.

B. STRIPLINE FILTERS

The conventional design of the parallel-coupled filter at lower microwave frequencies gives a physical configuration that is long and narrow. When such a configuration is constructed on microstrip ceramic cracking and mechanical instability results. To minimize the size of the filter, two different designs where attempted, (1) "folding", and (2) a vertical parallel-coupled filter. These configurations are shown in Figures 101 and 102. The insertion loss charateristic of these filters is shown in Figures 103 and 104.

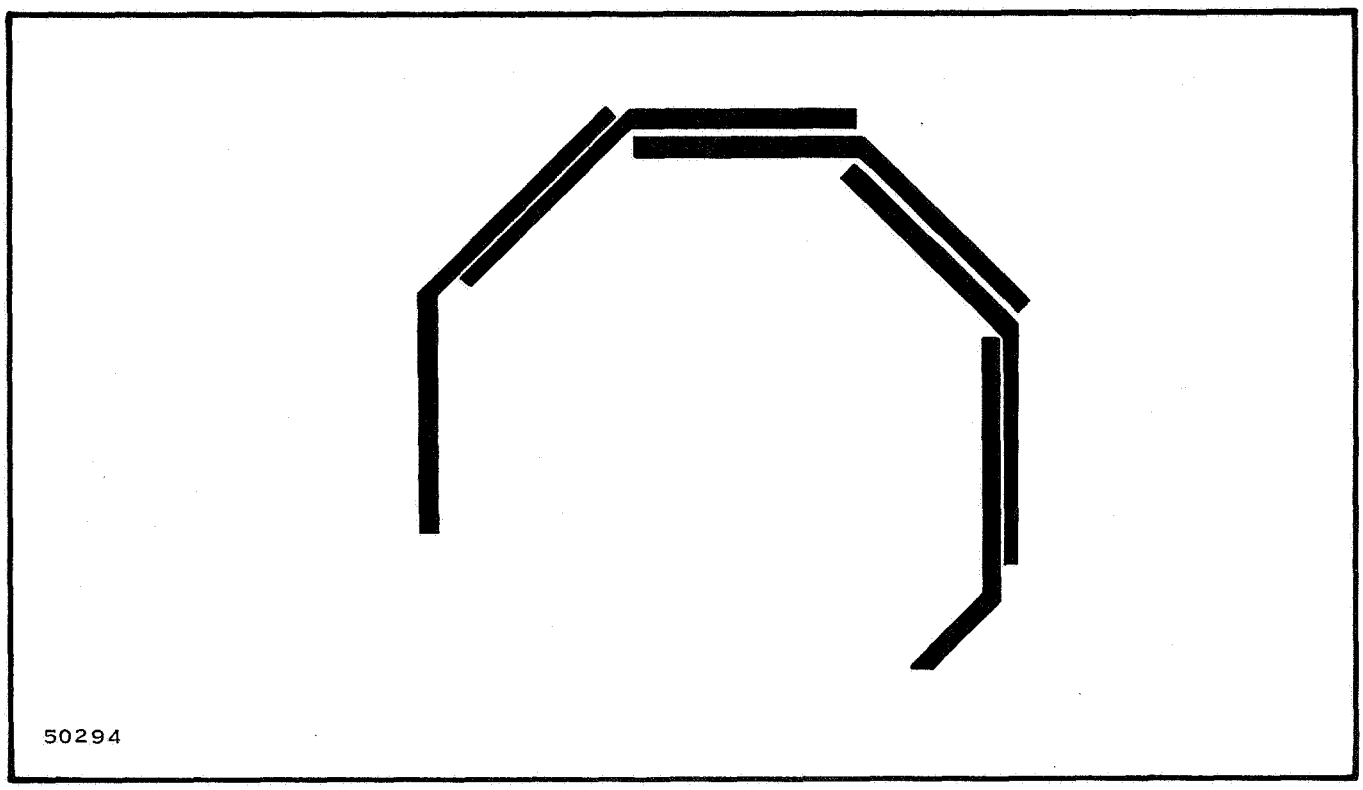

Figure 101. Parallel Coupled (Folded) Filter

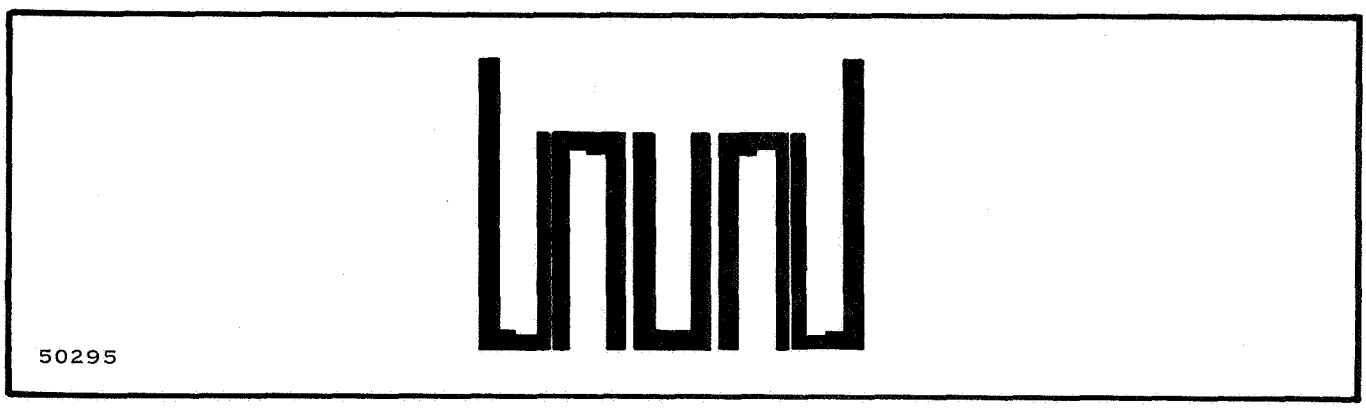

Figure 102. Vertical Parallel Coupled Filter

Both filters were constructed on stripline and designed as a 3-pole network with a center frequency (f_o) of 1.6 GHz and a desired skirt response which would result in a greater than 30-dB insertion loss at 200 MHz from f_o. Figures 103 and 104 illustrate that the filters center frequency differs slightly from the design center frequency; other than that, the effects of folding appear negligible.

Since the effective coupling area of each filter is reduced from a quarter wavelength, it was necessary to compensate the gap coupling while maintaining the overall element length at one-half wavelength. This was accomplished by decreasing the gap in an amount proportional to the decreased coupling length.

Considering briefly the adaptation of the stripline bandpass filter design to microstrip circuitry on ceramic, it is important to note that of the basic design differences, the most significant change in the design procedure results from the absence of the upper ground plane and corresponding dielectric material. Utilizing design information and calculations of gap capacitance based on the normal filter equations, it is possible to progress from a stripline design to the desired microstrip of thin-film design. However, it may be necessary to compensate the coupling and redesign the filter.

Bandpass filters exhibiting low passband insertion loss and extremely steep rejection skirts can be realized by means of a composite bandpass, bandstop filter structure. A pair of band reject filters, each one exhibiting the desired rejection at the portion the frequency spectrum corresponding to their designated reject frequencies, coupled with a bandpass filter determines the overall pass band characteristic. One of the direct advantages of such a structure is that the number of resonators needed to achieve a given response is reduced. In addition, lower midband insertion loss is obtained and lower Q resonators are required. A typical attenuation response for a composite bandpass, band reject filter is shown in Figure 105. As is seen from the figure, the band reject filters independently set the slope or skirt selectivity.

The optimum design for the composite filter is one which uses the fewest number of resonators to achieve the desired slope and utilizes a large number of stagger-tuned band reject filters to achieve the rejection bandwidth as dissipative losses occuring at the lower edges of the band reject filter slope, have the effect of rounding the edges of the passband response. Thus, the required unloaded Q needed for a slope filter is determined by the permissible rounding at the passband edges.

A composite bandpass, band reject interdigital filter has been designed which successfully offers frequency separation in a multiplexer unit. The stripline configuration is illustrated in Figure 106. Both the bandpass and the band reject filter had the same number of elements in order to accomplish a constant-resistance input that equalled the generating source resistance. This arrangement permitted a number of filters to be cascaded without harmful interaction effects.

The design center frequency of the filter combination was 1.5GHz with a desired bandwidth of 5 percent. The measured VSWR was better than 1.25 in the passband; and insertion loss at band center was 0.38dB. The performance characteristics are shown in Figure 107.

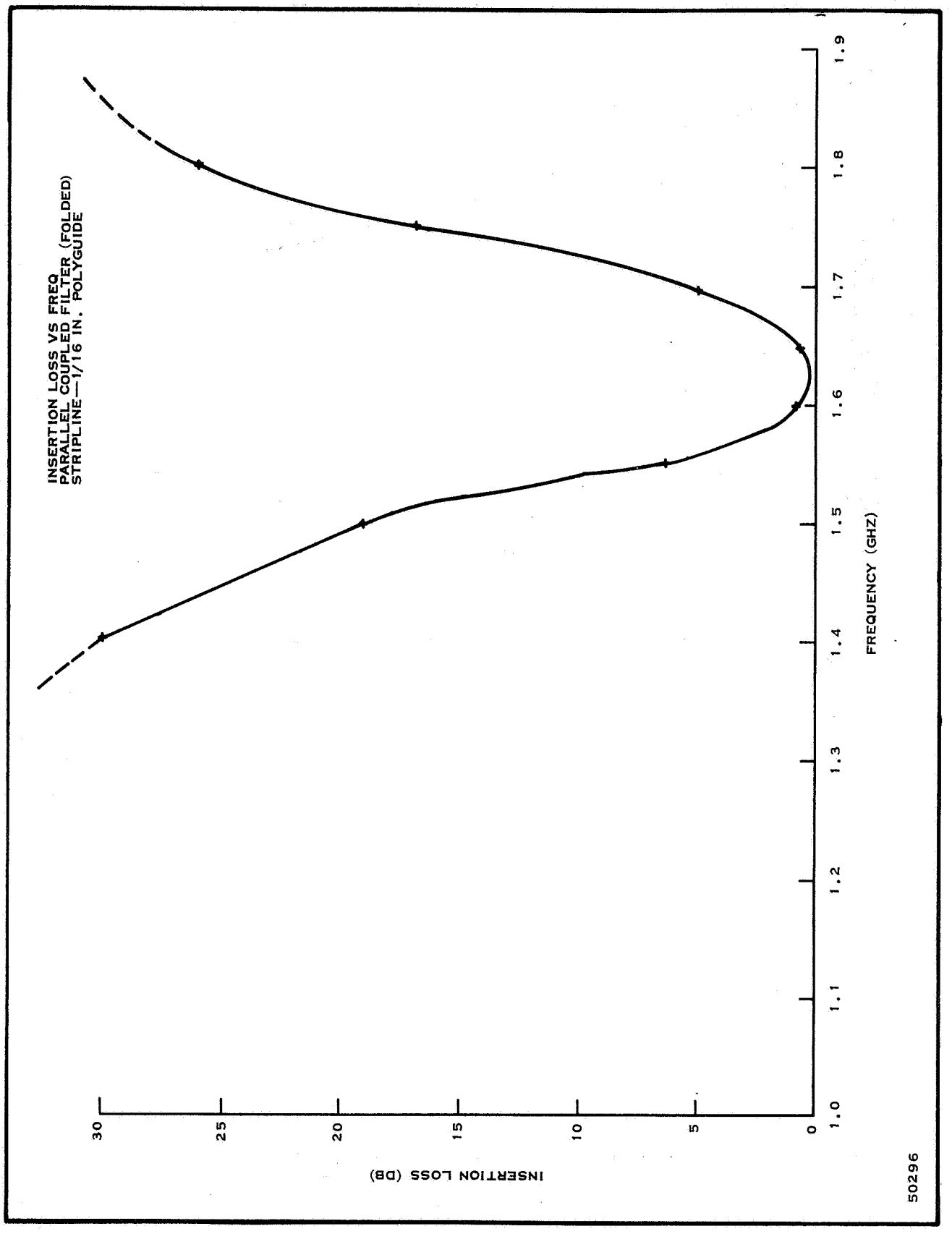

Figure 103. Parallel Coupled Filter - Insertion Loss vs Frequency

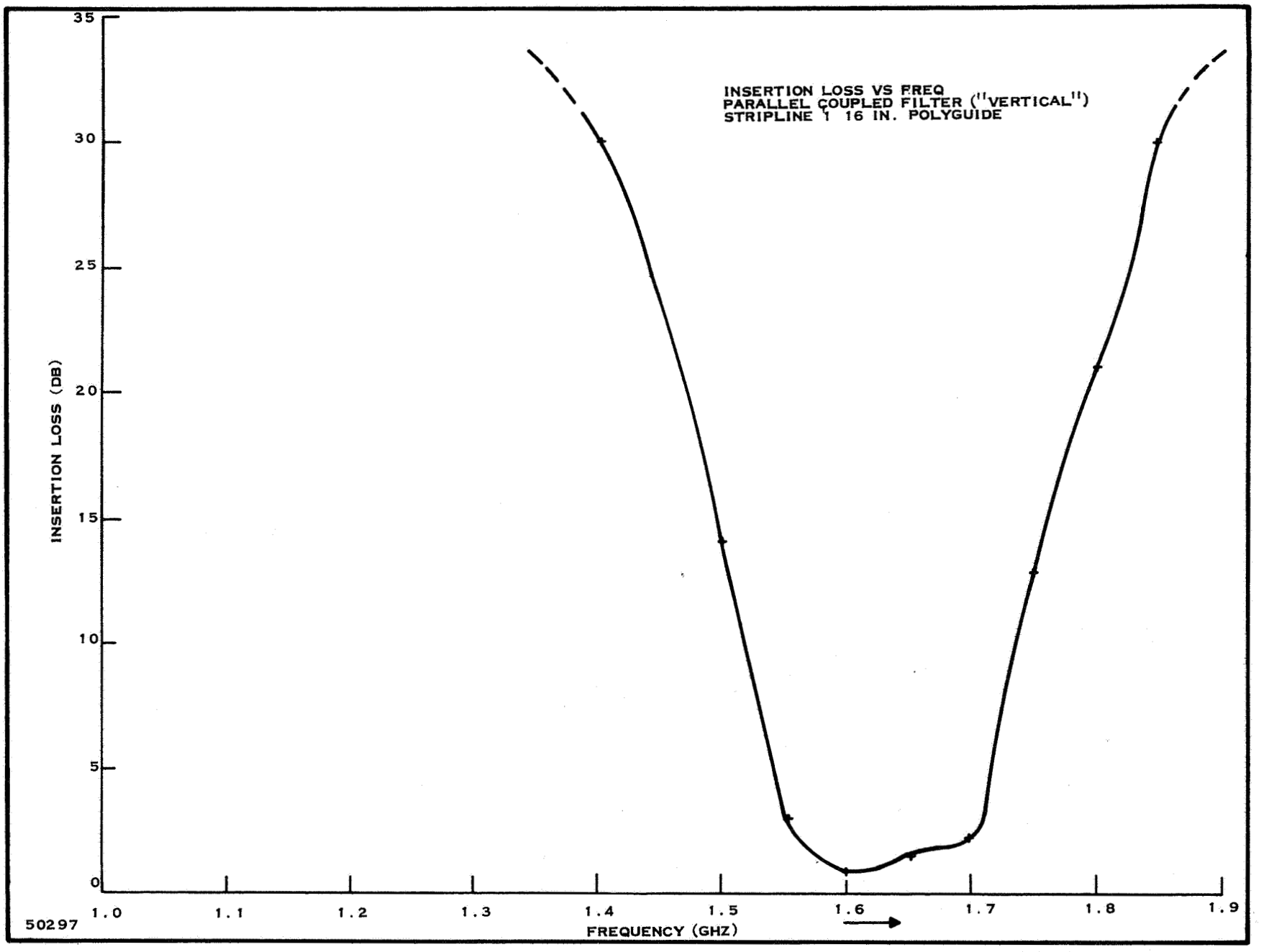

Figure 104. Finished Stripline Filters

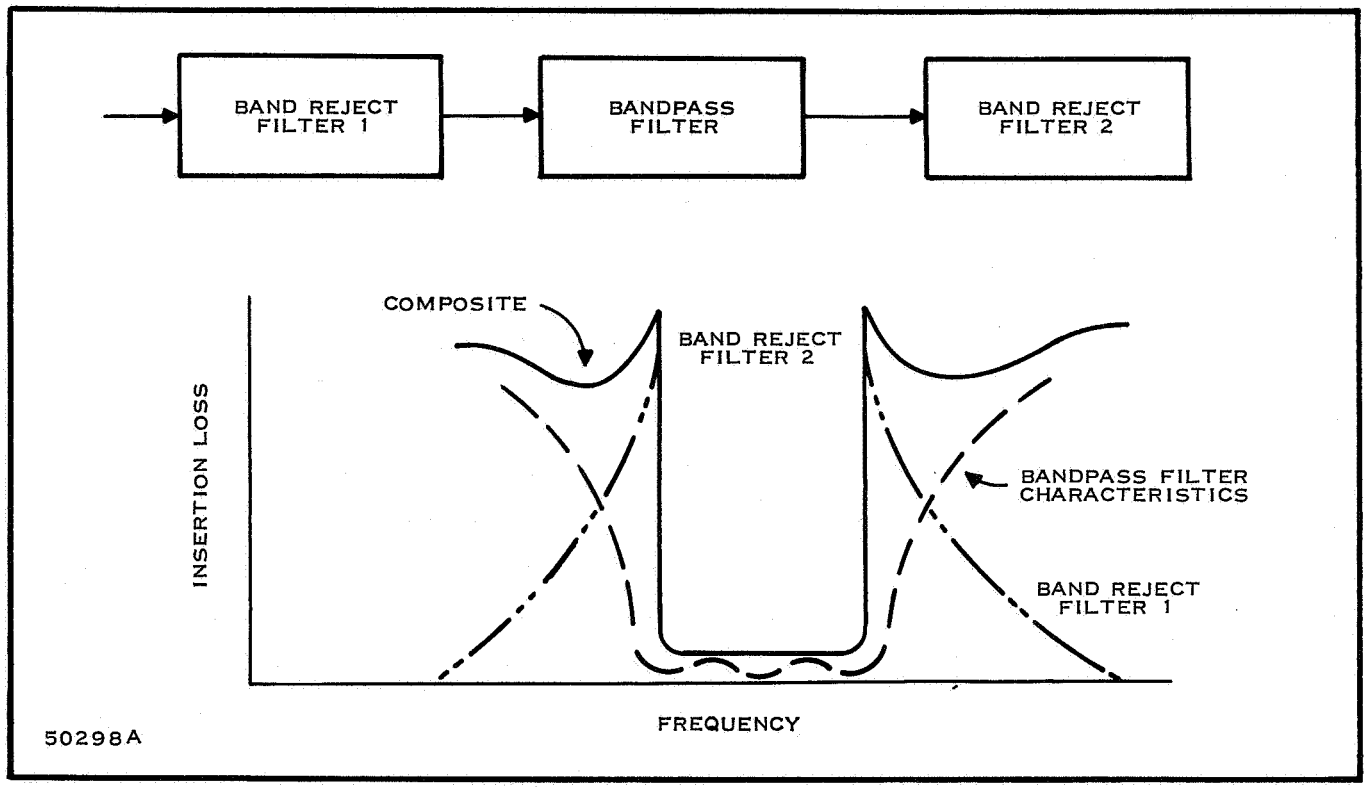

Figure 105. Composite Bandpass — Band Reject Filter

C. YIG MAGNETICALLY TUNABLE FILTERS

In recent years attention has been given to bandpass and bandstop filters constructed with highly polished spheres or discs of ferromagnetic materials such as yttrium iron garnet (YIG) and gallium substituted YIG (GAYIG). The magnetic properties of such materials have been incorporated into microwave devices which offer unique advantages as resonators and preselectors. These devices have unloaded Q's greater than 1500 in a 600-MHz to 12GHz frequency range which results in narrow bandwidths with high-offband rejection and are capable of being electronically tuned by an external magnetic field [53].

The principle of operation of a single YIG sphere is shown in Figure 108. In this figure, it may be seen that an uniform dc magnetic field Hdc is applied in the z direction and an RF magnetic field is applied in the x direction. A gyroscopic effect results in which the magnetic moment vector $\vec{M}$ precesses about the Z axis causing RF energy to be coupled out of the coils in the y direction. Maximum energy is coupled to the load when ferromagnetic resonance occurs. This resonance is expressed simply as

$$f\ (\text{megahertz}) = 2.8\ \text{Hdc}\ (\text{Gauss}) \qquad (62)$$

Coupling of energy from the RF source to the load at frequencies away from resonance is typically 50dB down due to the orthogonal arrangement of the coil loops [45].

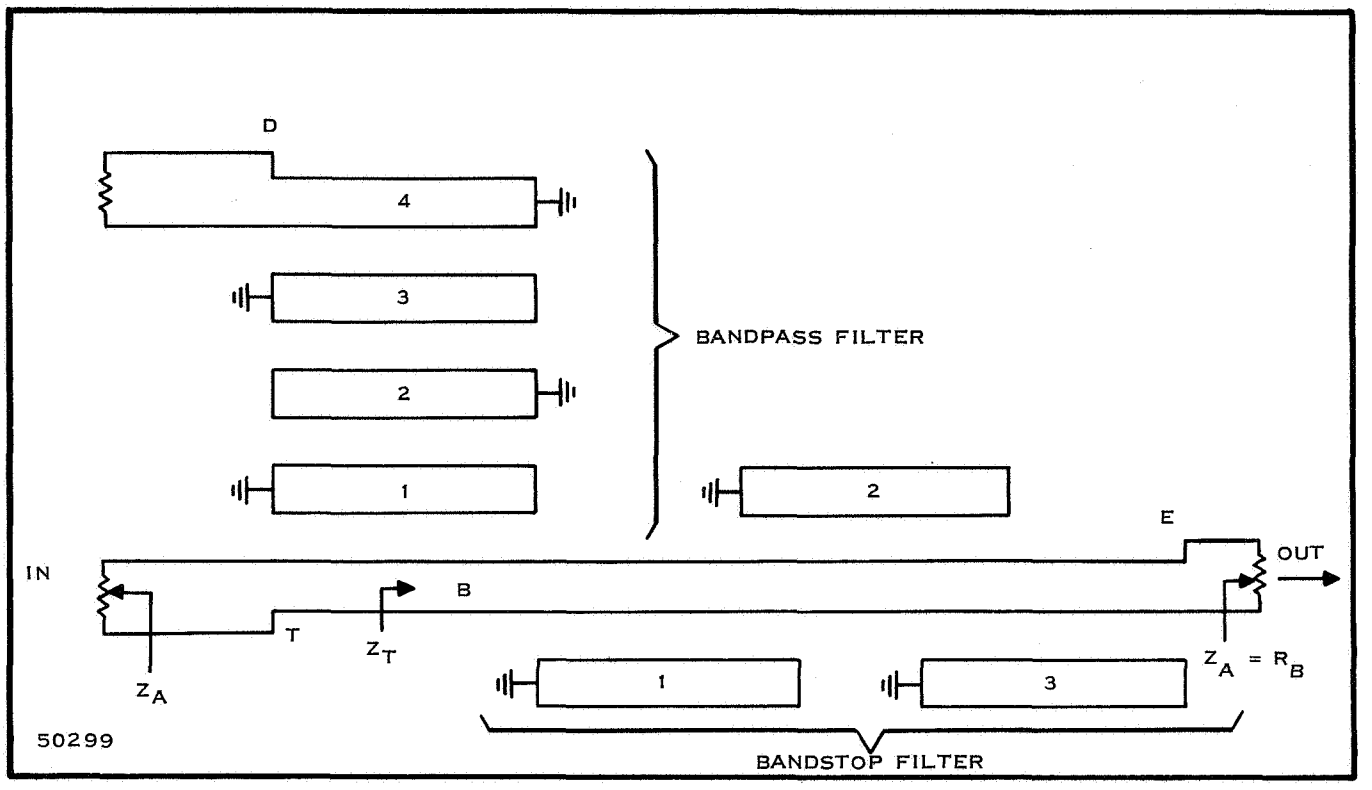

Figure 106. A Composite Bandpass — Band Reject Interdigital Filter

YIG filters are operated from 2.0-GHz to mm wave bands. The upper frequency is limited to available magnetic fields. The low frequency limitation is due to poor coupling and low values of unloaded Q. Extending YIG filters to VHF regions requires the use of YIG disc ferromagnetics instead of spheres or the use of GAYIG which has a lower saturation magnetization. The lower frequency limitations may be seen from Equation (63) which defines the unloaded Q of a sphere as

$$Qu = \frac{Hdc - M/3}{\Delta H} \tag{63}$$

where ΔH is the intrinsic line width, and M the saturation magnetization of the material. For YIG, M = 1785 gauss and $\Delta H = 0.5$ oersteds at room temperature. Consquently, Qu becomes zero for an applied magnetic field of 595 gauss. This corresponds to a frequency of approximately 1700 MHz. The unloaded Q characteristic as a function of frequency is shown in Figure 109.

Measurements of YIG and GAYIG bandwidths as a function of temperature indicate that a change of 10 percent may be expected over a -50°C to +70°C temperature range. The worst frequency drift is experienced at colder temperatures, but can be minimized if the YIG resonator temperature is maintained as high as possible. For a fixed magnetic field, the frequency shift about the center frequency of the passband of the resonator may be written as

$$\Delta f = 3.7\Delta\frac{K_1}{M} \tag{64}$$

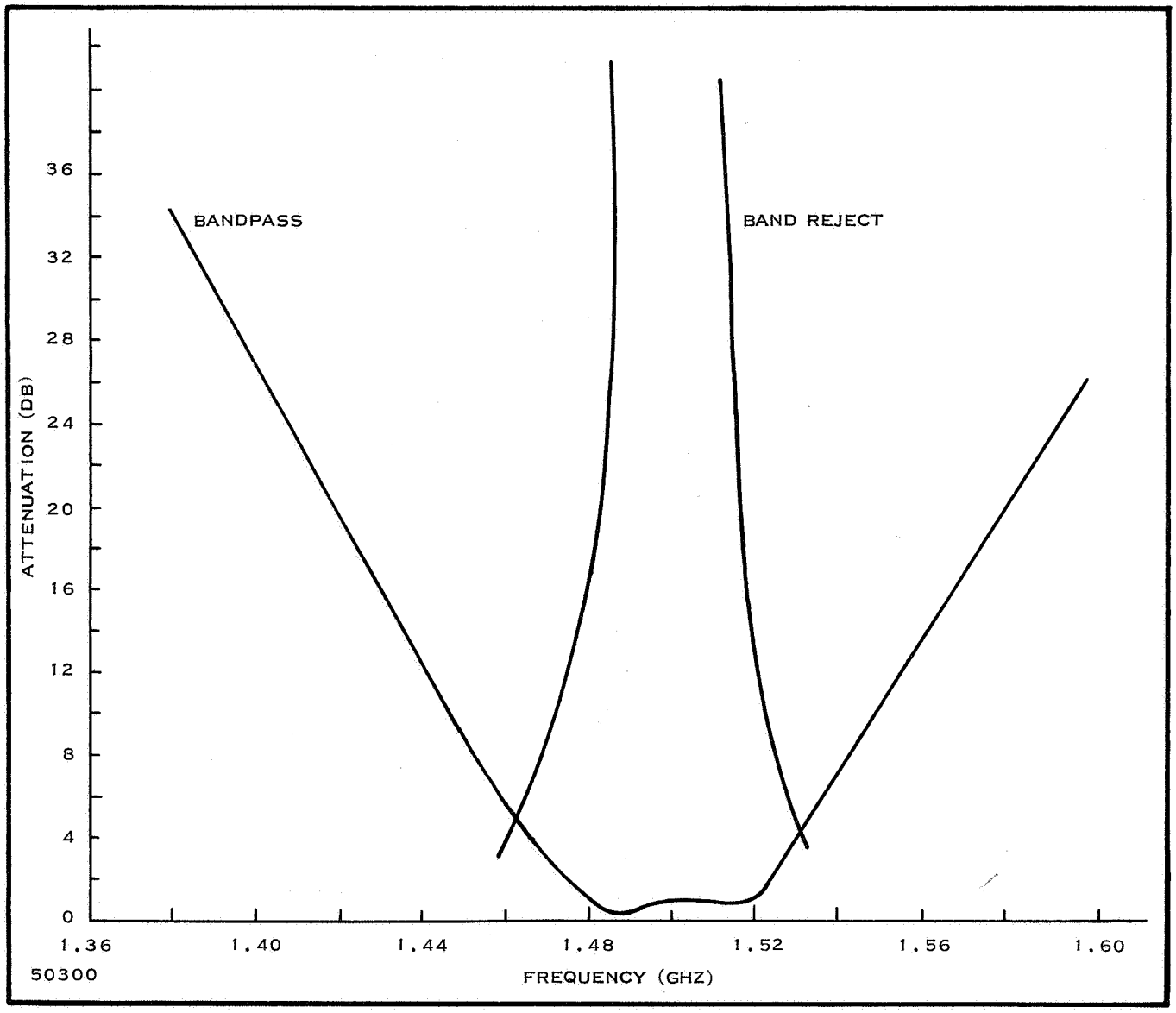

Figure 107. Attenuation vs Frequency for Bandpass and Band Reject Sections of the Interdigital Filter

where K_1/M is the first order magnetic anisotropy. This quantity is the dominant temperature dependent term which is responsible for any temperature drift encountered. The variation of the first order magnetic anisotropy versus temperature is plotted in Figure 110.

From Equation (63) it may be seen that a single YIG sphere operating from 2- to 12-GHz requires an applied magnetic field of 700 to 4000 gauss. In order for electromagnets to efficiently provide magnetic fields, a small air gap must be presented by the microwave structure. This is due to the fact that the power required to establish a given magnetic field is proportional to the square of the air gap. Large air gaps are undesirable as they lead to saturation of the magnet iron causing nonlinear tuning and the requirement of a large number of ampere-turns which would result in increased

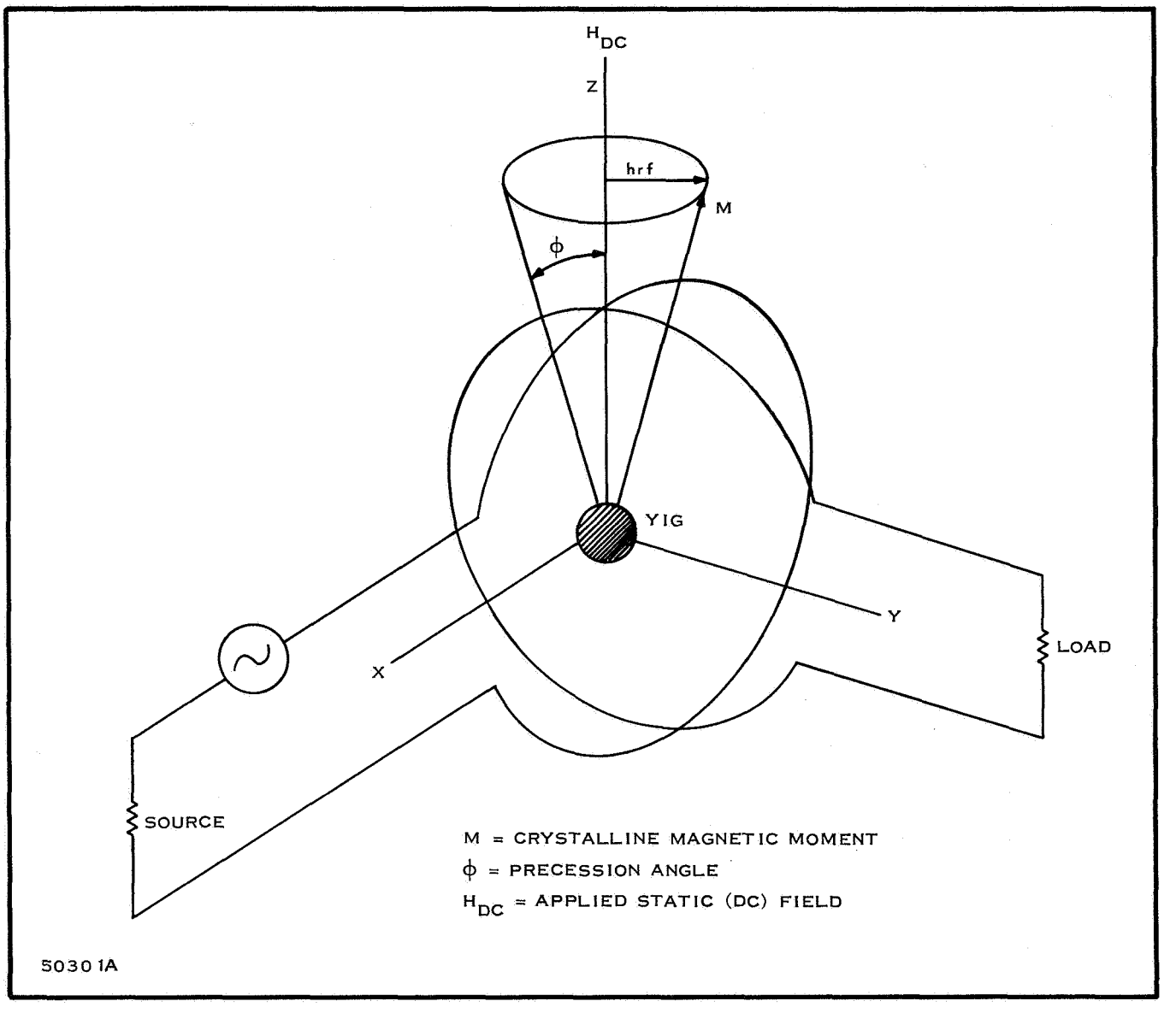

Figure 108. Single YIG Sphere

inductance and flux leakage. A very homogeneous magnetic field is required for tuning the YIG to resonance. To provide such a field and to minimize gradients that exist in the air gap, cylindrical re-entrant magnet cores are used in the construction of the electromagnetics.

The geometry of the microwave device determines the size of the magnet gap and the amount of isolation and coupling between the loops. Stripline circuits provide high offband rejection, good coupling, and allows filters to be reproduced by photoetching in addition to providing structures that utilize small air gaps. Frequency-independent coupling may be obtained by using transmission lines shorted at the YIG so that the only connection between the perpendicular loops is through the YIG itself which fills a small hole piercing the ground plane at the junction of the transmission lines[7] such a structure is shown in Figure 111.

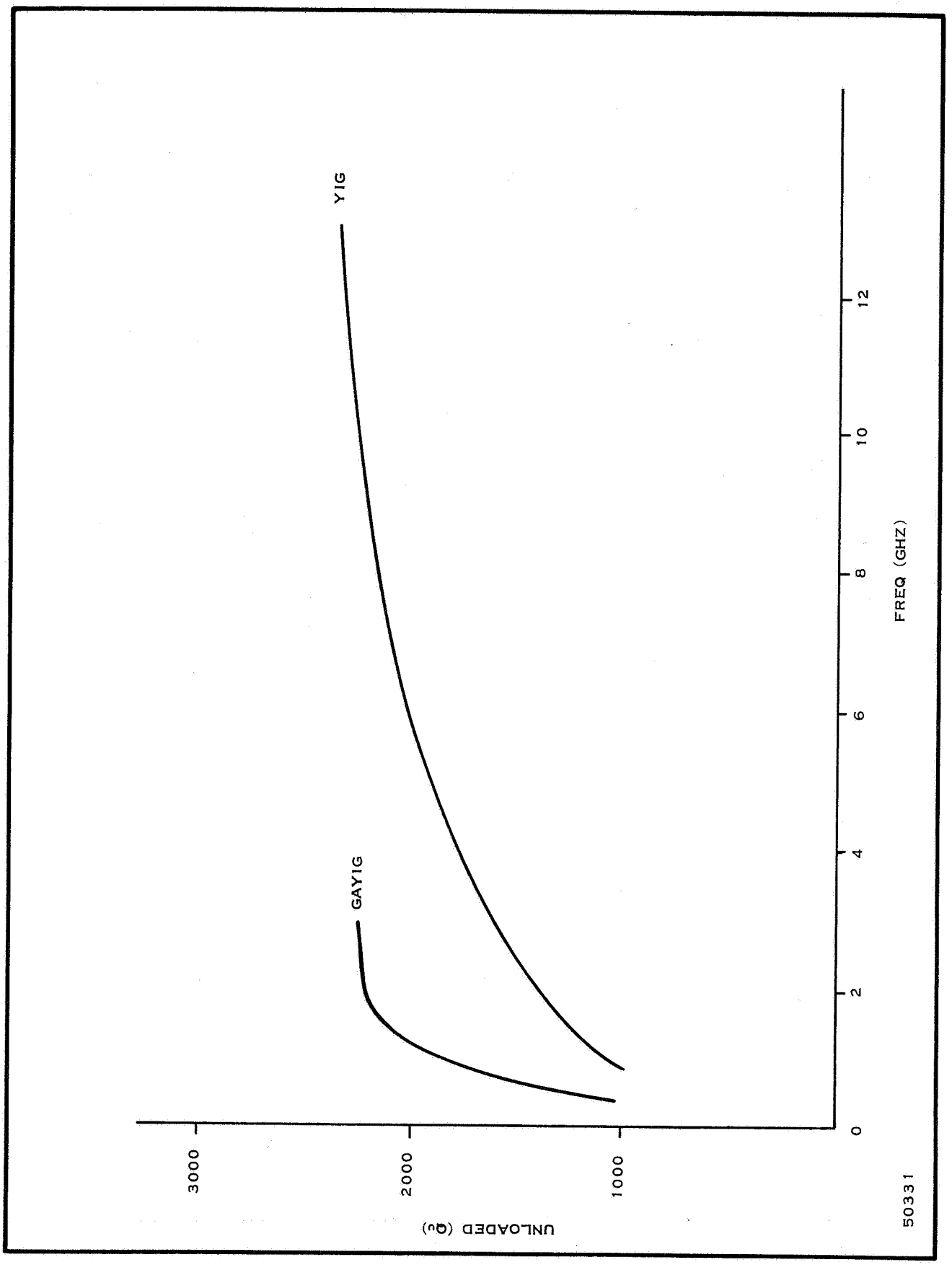

Figure 109. Unloaded Q of YIG

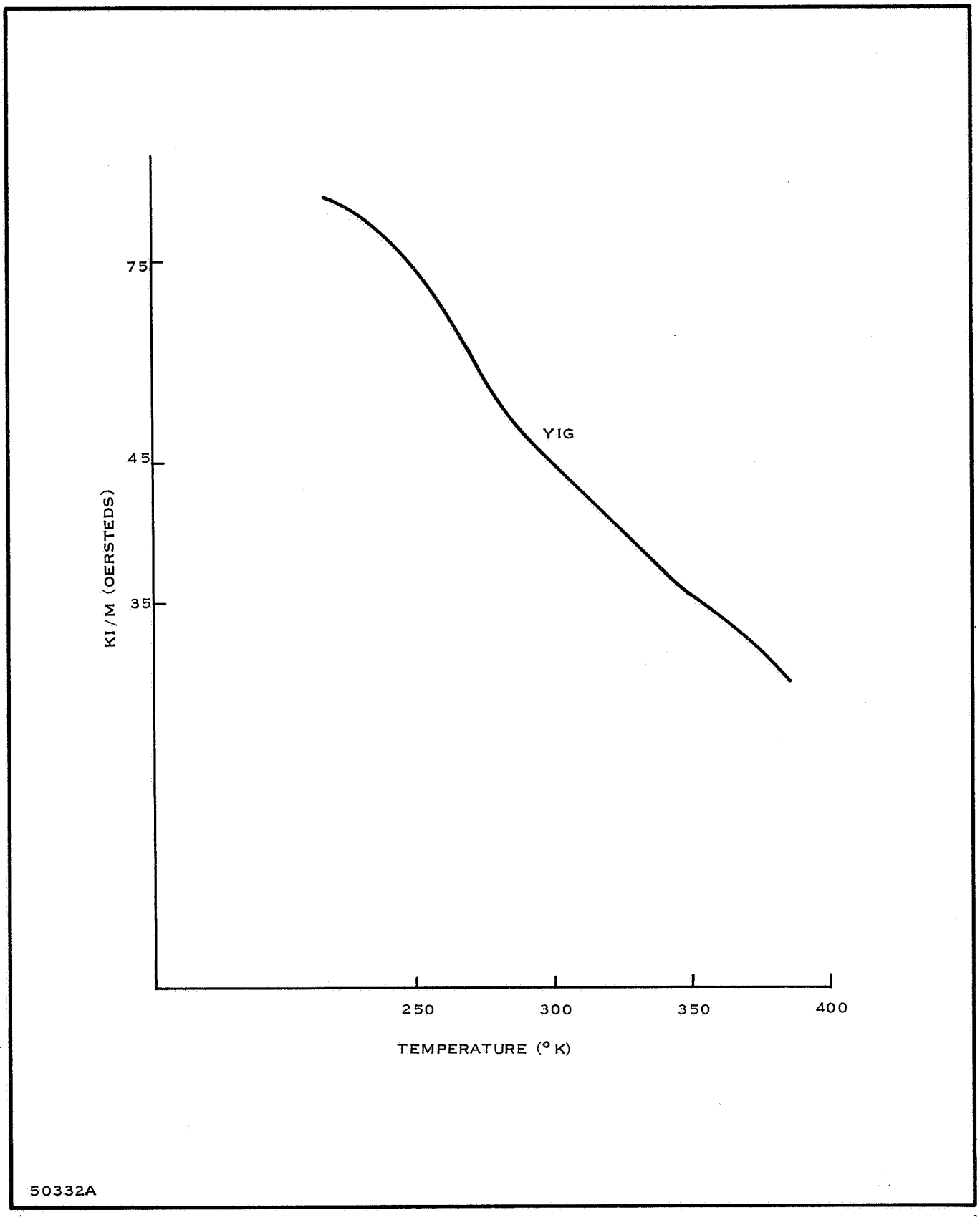

Figure 110. Variation of the First Order Magnetic Anisotropy vs Temperature

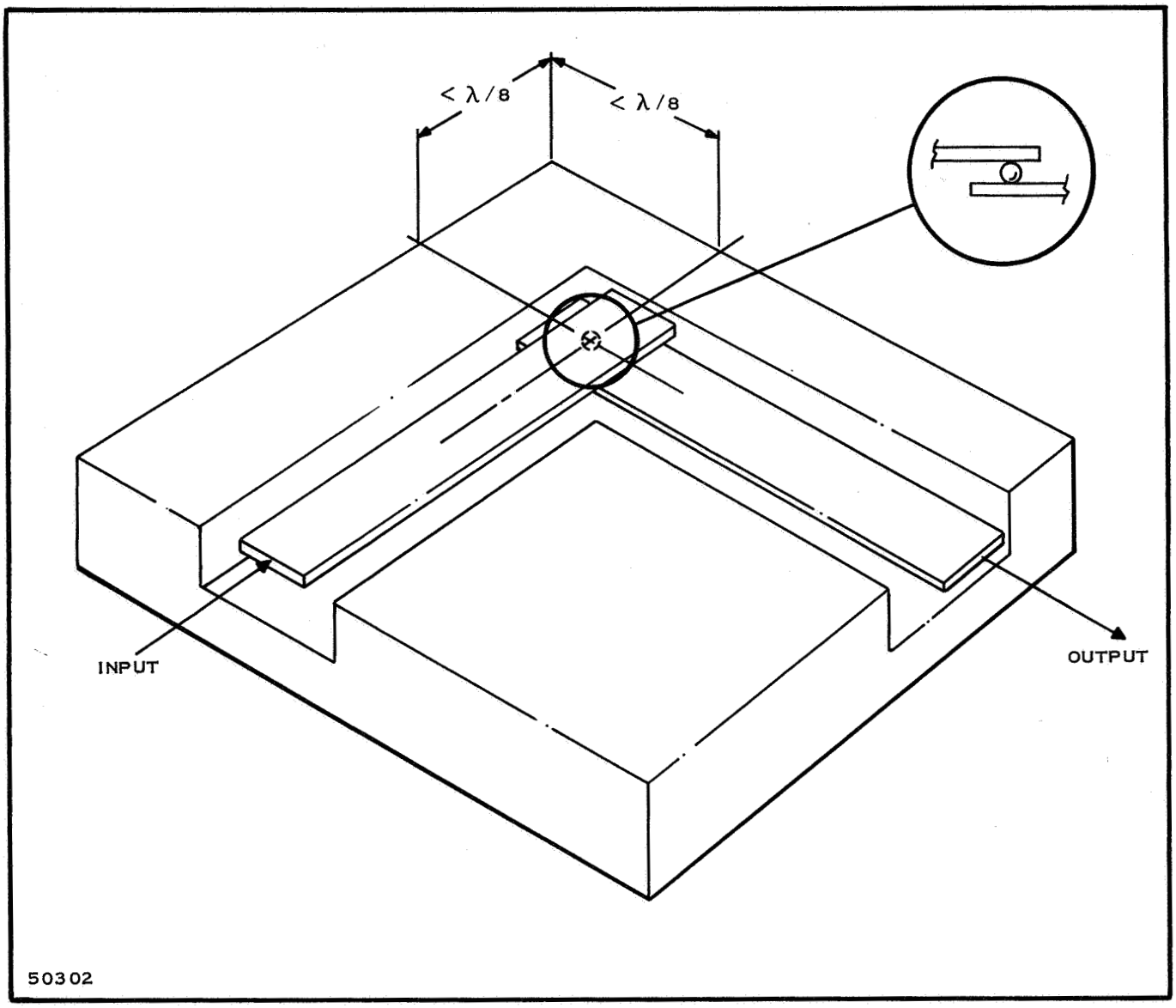

Figure 111. YIG Filter

In the case of two-resonator filters, the transmission lines are not necessarily placed at right angles but may be in parallel as illustrated in Figure 112.

The length of the magnet air gap required for this arrangement is increased proportionally by the number of resonators used. When two or more resonators are multiple — coupled to provide a magnetically tunable band-pass filter characteristic, a coupling slot in the common side wall between two strip-transmission lines will result in the smallest possible air gap [55]. This arrangement is shown in Figure 113.

Figure 114 gives curves of the theoretical Qe plotted against the diameter of spherical resonators for various line dimensions for a short-circuited symmetrical strip line transmission line. The curves can be used for ellipsoidal resonators by

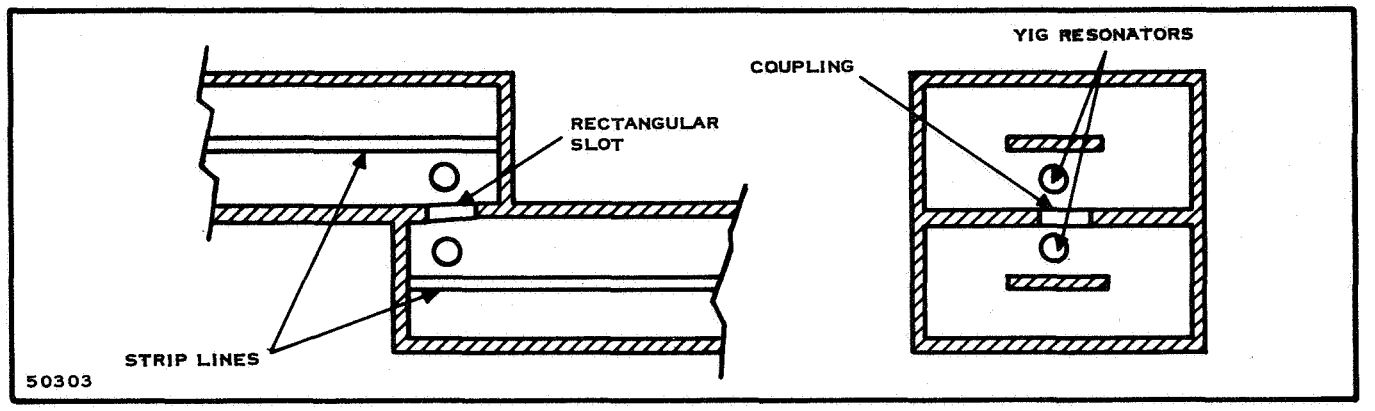

Figure 112. Parallel YIG Filter

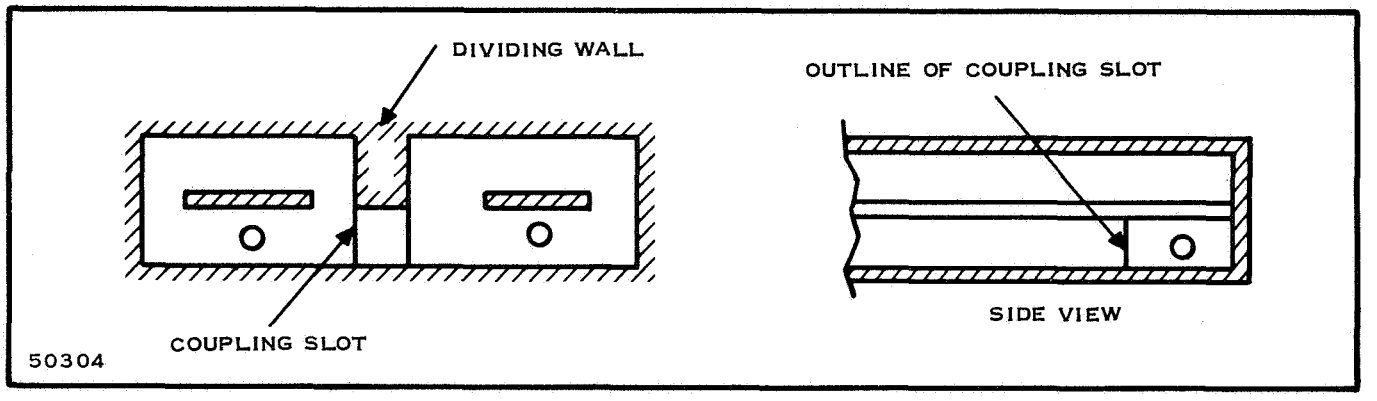

Figure 113. Multiple-Coupled Magnetically Tunable Bandpass Filter

replacing Dm with Dm^E where

$$Dm^E = 2(abc)^{1/3} \tag{65}$$

in which a, b, and c are the semi-axes of the ellipsoid. The curve can be used for materials other than YIG by means of the following formula

$$Q^{om} = \frac{M_s^{YIG}}{M_s^{om}} \quad Q^{YIG} \tag{66}$$

where Q^{YIG} = external Q for YIG,

Q^{om} = external Q for material other than YIG

M_s^{YIG} = Saturation magnetization of YIG (1750 gauss at room temperature)

M_s^{om} = Saturation magnetization of other material

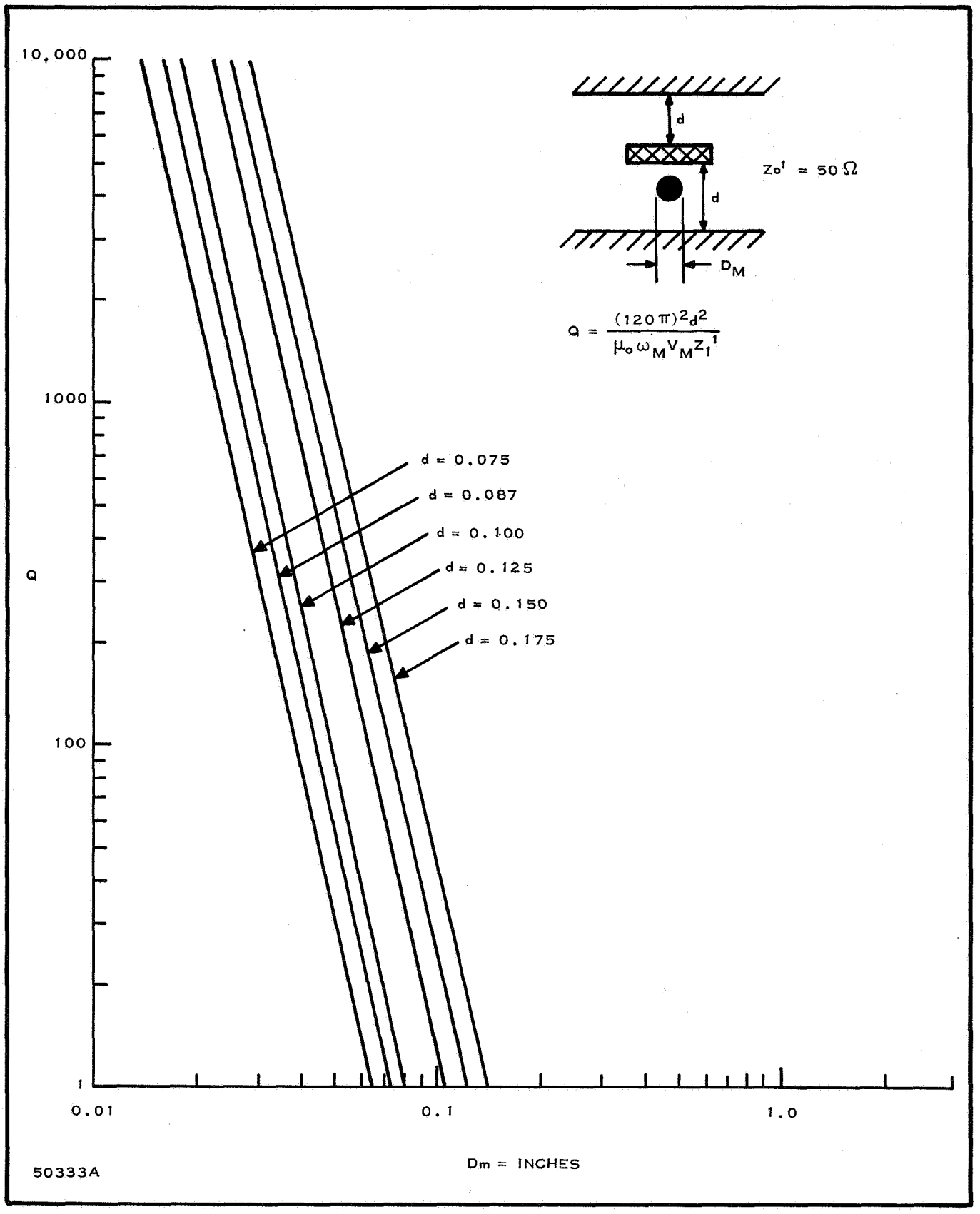

Figure 114. Theoretical Q_e vs Resonator Diameter

The dimensions of the coupling slot and the spacing between resonators are determined largely by experiment.

Figure 115 summarizes the performance of the two-resonator sidewall-coupled YIG filter constructed with a center frequency of 2.0 GHz. Insertion loss at band center varies between 2.4 dB for a center frequency of 2.0 GHz and a minimum value of 1.2 dB at a center frequency of 3.0 GHz. The 3 dB and 30 dB bandwidths of the filter varied only slightly as the center frequency was tuned over the 2- to 4-GHz range.

The use of YIG resonators as preselectors in a superheterodyne receiver is shown in Figure 116. This figure illustrates the many uses of YIG filters which were employed in an S-Band superhet receiver built by LORAL. A YIG filter selects the desired harmonic output and provides the matching structure between the oscillator and the first mixer. A microwave discriminator utilizes a YIG filter to compensate for the nonlinear tuning of the varactor tuned VCO.

Another tunable filter is the dielectric-loaded microwave cavity. A single or double-ended cavity filled with a high dielectric material will support high Q resonances, and movable shorting plungers at one or both ends allow frequency tuning. Tuning may be accomplished over an octave or more. These structures may be used as microwave resonators in solid-state communication equipment; however, integration of the cavity resonator itself into an "integrated" or thin-film component is unlikely; therefore, it will not be discussed in this report.

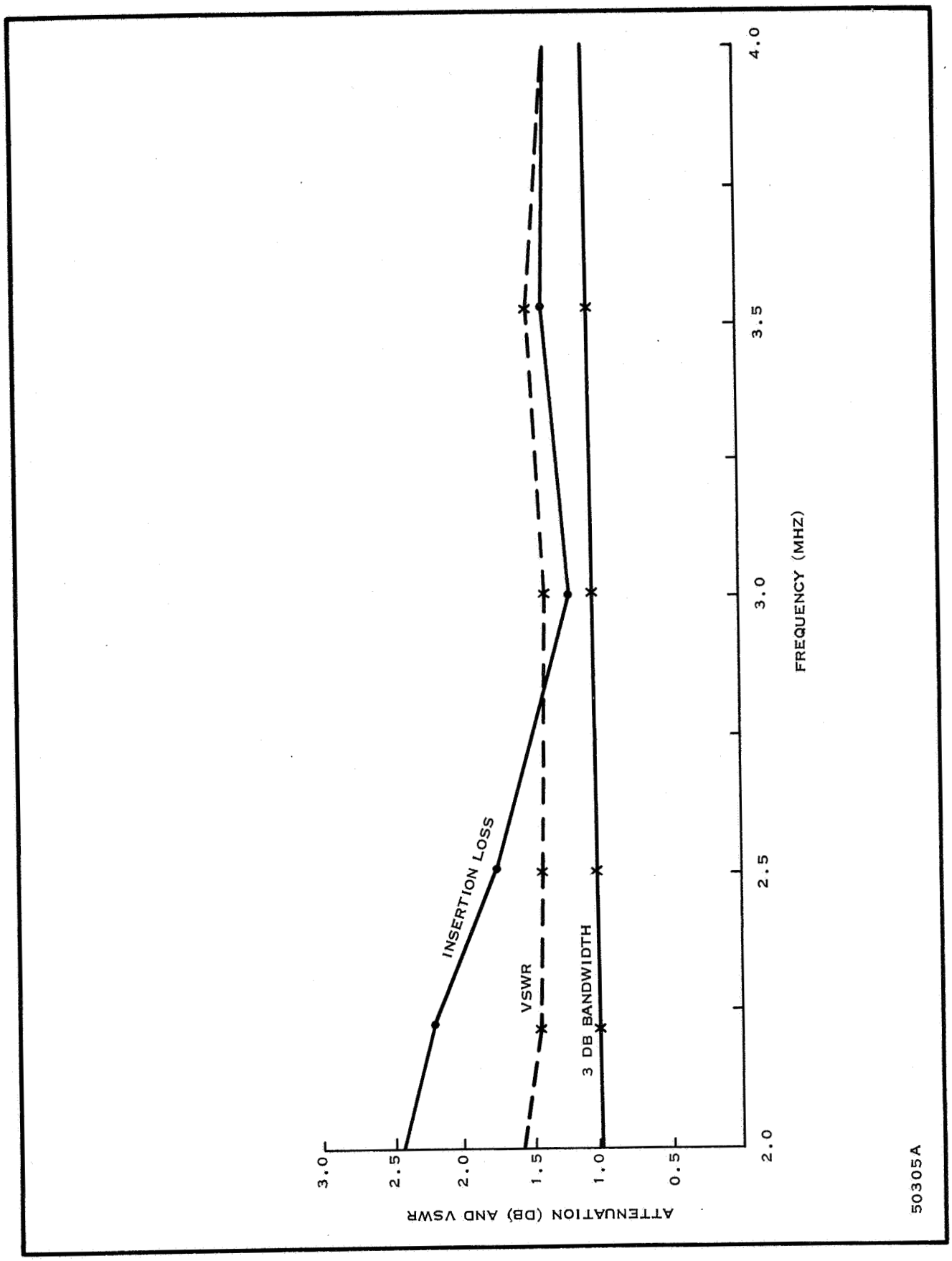

Figure 115. Characteristics of the Two Resonator Sidewall Coupled YIG Filter vs Frequency

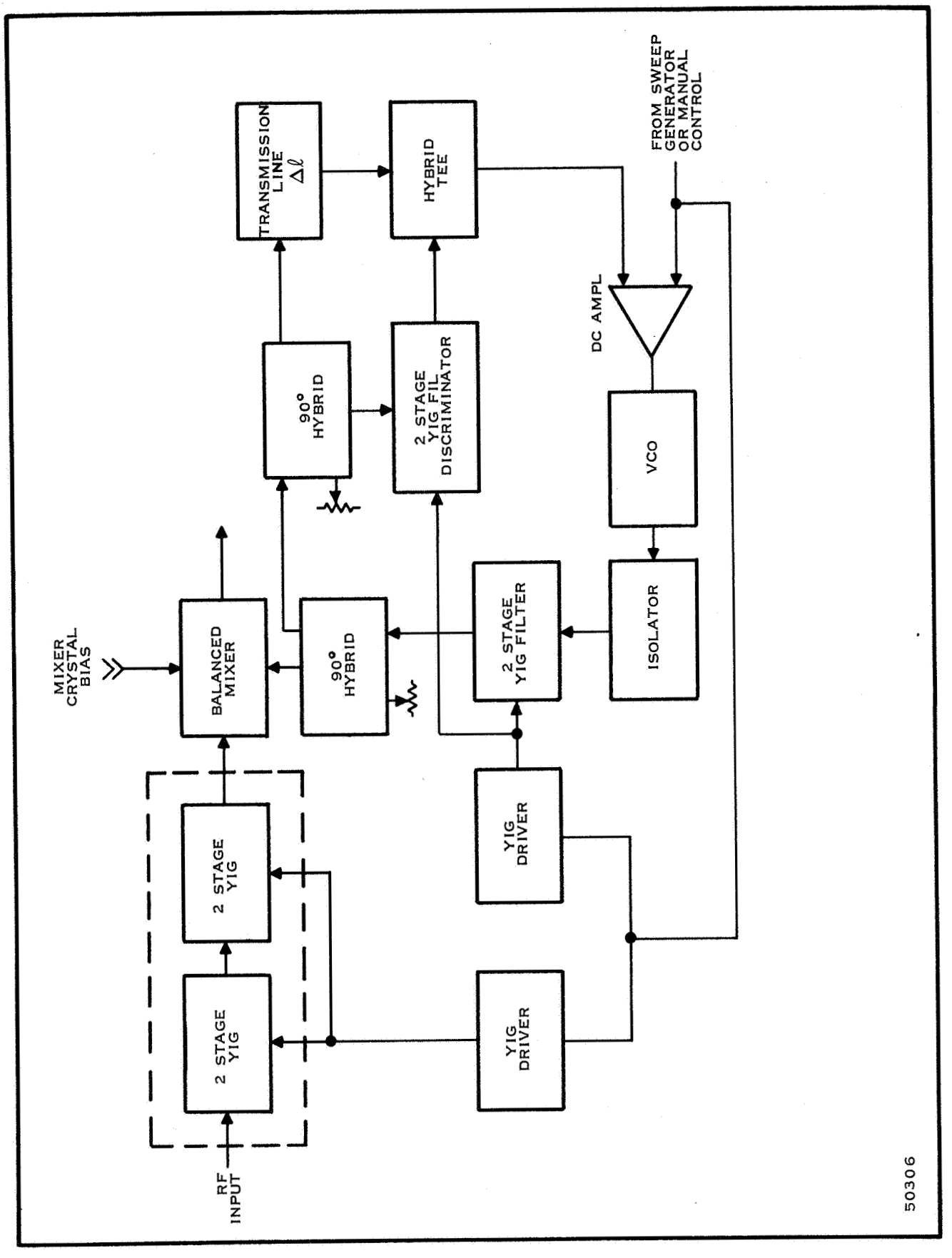

Figure 116. S-Band Receiver

SECTION IX

MIXERS

A. GENERAL

Scientific Report No. 1 reviewed the basic characteristics of Schottky barrier diodes. In this section, the discussion presented earlier is extended to cover the conversion loss and noise figure characteristics of these devices. The application of these diodes in integrated balanced S and C-band mixers and the mixing process required for superheterodyne detection are reviewed.

B. THE MIXING PROCESS

The mixer stage in a superheterodyne receiver is essentially a frequency converter which translates the received signal frequency to a relatively lower intermediate frequency where amplification may be more readily achieved. Where it is desired to further remove spurious input signals from the local oscillator signal, more than one mixer stage may be used to transform one intermediate frequency to one lower in frequency as in the case of multiple conversion receivers. Such use of mixers is referred to as heterodyne detection and will form the subject of this section, although the mixing process may be employed in other applications such as sideband generation in suppressed carrier systems.

At lower UHF regions where RF amplification is realizable, RF amplifiers commonly precede the first mixer stage and the noise figure of the mixer has almost insignificant bearing upon overall noise performance of the receiver if the amplifier gain is sufficiently high. In this case, where the mixer is preceded by RF gain, the overall noise figure of the receiver may be expressed in terms of cascaded networks which are representative of the RF stages preceeding the mixer, the mixer itself and the following IF amplifier. This relationship is given in Equation (67)[58] .

$$NF_o = F_1 + \frac{F_2}{G_{11}} + \frac{F_3}{G_{12}} \qquad (67)$$

where NF_o is the overall noise figure

F_1 is the noise factor of the first stage

F_2 is the noise factor of the second stage

F_3 is the noise factor of the third stage

G_{11} and G_{12} are the power gains associated with the corresponding stages.

Equation (69) is expressed as a numeric and is normally given in dB by taking the product of 10 times the $\log_{10}$ NF.

In receivers where RF amplification does not precede the mixer, the overall noise figure is usually written[59].

$$NF_o = 10 \log Lm \left[F_{if} + tm-1\right] \quad (68)$$

where

Lm is the effective noise conversion loss expressed as a ratio

tm is the effective mixer noise temperature

F_{if} is the noise factor (a numeric) of the IF amplifier.

Frequency translation is accomplished in the mixer stage by means of a local oscillator (LO) which is combined with the received RF signal in a nonlinear element. Under these conditions, the nonlinear device generates a complex frequency spectrum that contains the sum and differences of the frequencies of the originally applied signals in addition to infinite beat frequencies resulting from the harmonic generation of the local oscillator frequency.

The basic single-ended mixer stage using one diode as the nonlinear element is shown in Figure 117[60].

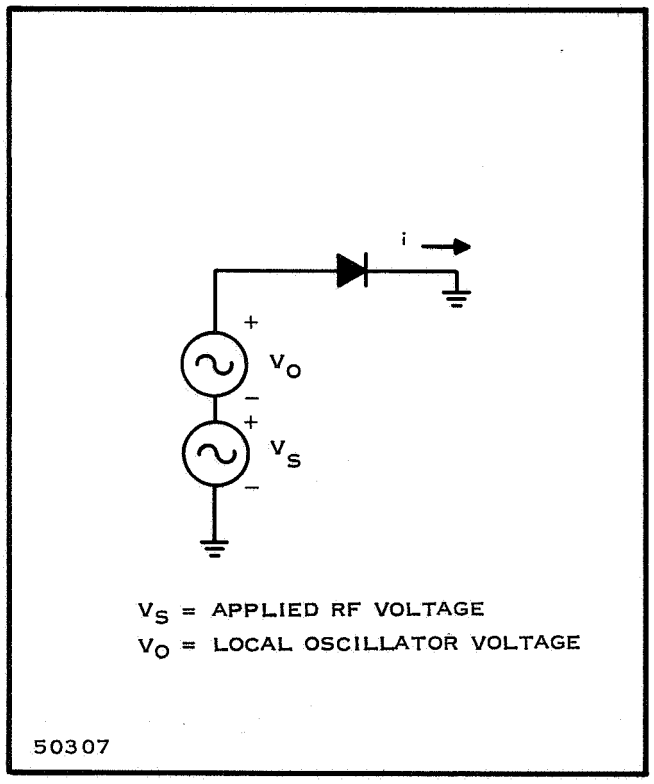

Figure 117. General Circuit of Single End Diode Mixer

In the majority of diode mixer circuits, the diode is biased to minimize conversion loss. Thus, the applied RF and local oscillator voltages combine with the DC biasing voltage in an additive manner, such as

$$e = Vdc + V_o \cos w_o t + V_s \cos w_s t \quad (69)$$

where

Vdc is the bias voltage

V_o is the peak amplitude of the local oscillator voltage

V_s is the peak amplitude of the received RF signal.

The characteristic of the diode are dependent upon the applied voltage, i.e.,

$$i = f(e) \quad (70)$$

which is a continuous function that may be expanded into a power series,

$$i = a_o + a_1 e + a_2 e^2 + a_3 e^3 + \ldots + \tag{71}$$

In the literature, this expansion, with Equation (69) substituted, has been carried out to the fifth order term and a representative account of the IF frequency spectrum is obtained[61]. In sensitive receivers, the amplitude of the local oscillator voltage is normally much greater than the received signal voltage. Operating the local oscillator at high levels has the advantage of optimizing the mixer's performance by expanding the mixer's dynamic range and improving intermodulation rejection.

The nonlinearity of the mixing element causes harmonics of the local oscillator frequency to appear in the IF outputs which beat with the signals present in the input, thereby creating new frequencies. These frequency components fall into three categories:[64]

Spurious mixer products are the extraneous frequency components in the mixer output other than the desired sum or difference terms.

"Crossovers" are undesired frequency components that fall within the passband of the mixer outputs and may be heard in the audio portion of the receiver.

Intermodulation is frequency components that result from two signals, one desired, the other undesired being impressed upon mixer input and combining with the local oscillator.

Of these spurious response, intermodulation is the worst in superheterodyne receivers. It is the direct result of the third and higher order characteristics of the mixer element and can not be completely eliminated by preceding the mixer with a narrowband filter. Reduction of these frequency components can only be obtained by making effective use of the mixer element and by making proper choice of the dc operating point. Such steps, in turn reduces the magnitude of the higher ordered terms in the power series.

It has been recently published that applying different biasing voltages to two diodes in a balanced mixer have resulted in intermodulation response ratios greater than 100 dB and ratios of 80 dB or better in the case of single-ended stages[63]. The biasing scheme reported reduces the magnitude of the 4th and 6th order terms of the power expansion thereby reducing the interaction of these components within the mixer[69].

Some of these spurious frequencies in the input are subharmonics of the IF frequency and fall within the IF passband. The general expression for the case of two spurious input frequencies is

$$mf_2 - nf_1 = p\, f_{LO} \pm f_{IF} \quad . \tag{72}$$

The spurious signals that are separated from the local oscillator by submultiples of the IF is given when n = o, m = p

$$pf_2 = pf_{LO} \pm f_{IF} \quad . \tag{73}$$

The strongest of these signals is separated from the tuned frequency of the receiver by 1/2 of the difference frequency (IF) and it can not be entirely rejected by filtering.

The mixer will also respond to the image frequency. That is a signal separated from the desired signal by twice the IF frequency. This frequency is important in mixer design since power consumed at this frequency is taken away from the available signal power and results in lower conversion efficiency. Proper termination of the image frequency ensures minimum power dissipation and conversion loss of the mixer. The image frequency may also be generated within the mixer as a result of the direct beat between the desired signal and the second harmonic of the local oscillator frequency, and also as a result of the beat between the intermediate frequency and the local oscillator frequency.

A substantial improvement in integrated mixer performance may be obtained by properly terminating the image frequency as seen in Table XIX. In broadband mixers, this response to the image frequency may degrade the mixer noise figure by as much as 3 dB.

Table XIX. Schottky Barrier Diode Noise Figures

Frequency	Image-Terminated		Broadband	
GHz	Si	GaAs	Si	GaAs
2.93	3.2	2.6	5.0	4.7

C. MIXER DIODES

Diodes employed in mixer applications are usually point-contact or true Schottky barrier diodes. In some instances, tunnel diodes and backward diodes have been reported in mixer applications, and at higher frequencies of millimeter wavelengths experiments with bulk indium antimonide InSb have been reported. Investigations into the use of quantum effects to provide the mechanism for mixing have been explored in an X-band system utilizing a maser and a ruby crystal as the mixing element [69].

The crystal point-contact and Schottky barrier diodes are quite similar in operation, but contrast markedly in their construction. Both devices use a metal-semiconductor rectifying contact or Schottky barrier in their fabrication, and are based upon majority-carrier conduction. However, in silicon and gallium arsenide diodes, the contact is a planar junction as compared to the sharp metal whisker used in the point contact diode.

Both devices exhibit a square law forward response in their dc or static current-voltage characteristic for low values of forward voltage. Above a few tenths of a volt, the response becomes linear and the current-voltage characteristic is determined mainly by the bulk or spreading resistance, Rs, of the semiconductor material used in the fabrication of the diode. Both types of devices have physical limitations to high frequency performance resulting from the parasitic or barrier capacitance of their rectifying junctions. The barrier capacitance is somewhat lower in the Schottky barrier

devices because of its planar construction. Nevertheless, the shunting effect of this barrier capacitance at the rectifying contact becomes important at higher frequencies.

Other advantages of the Schottky barrier are that they are readily adaptable to integrated circuit structures and yield better reproducibility during fabrication. For the latter reason they afford economical selection of matched pairs for use in balanced mixer circuit configurations. In addition, the planar area contact between the metal and the semiconductor results in uniform contact potential and uniform current distribution throughout the junction. This, in turn, results in low series resistance and greater resistance to transient pulse burnout.

The high frequency attributes of the diode and its characteristic behavior become evident in mixer applications where diode noise figure, conversion losses and IF and RF impedances are critical factors.

The diode parameters are related to the materials used in the construction [65, 72]. For example, if a circular area of contact is assumed, the spreading resistance RS, is related to the geometry of the diode by

$$Rs = \frac{1}{4 \sigma a} \tag{74}$$

where σ is the conductivity of the semiconductor and "a" is radius of the circular area of contact between the rectifying junction and the semiconductor. The barrier resistance, Rb, is derived from the theoretical expression of an ideal diode I-V characteristics of the junction [71]. Typically, the current of a rectifying unit increases exponentially for applied voltages of a few tenths of a volt in the forward direction and may be expressed,

$$i = I_S \left[\epsilon^{q\, v/nkT} - 1 \right] \tag{75}$$

where I_S is the saturation current and is dependent upon the junction area and type of metal and semiconductor material used. The remaining parameters are defined:

q is the electron charge = 1.6×10^{-19} coulombs

T is the temperature in degrees Kelvin (°K)

k is Boltzman's constant = 1.38×10^{-23} joules/°K

v is the voltage applied across the diode junction. That is the applied RF voltage minus the drop across R_S

n is the diode ideal factor. In Schottky Barrier diodes it is close to one—approximating the ideal diode characteristics. For point contact diodes it is somewhat higher.

From this expression, the barrier resistance, Rb may be derived

$$Rb = \frac{dv}{di} = \frac{26}{i} \tag{76}$$

where i is the RF signal current in milliamperes. Since a biasing current I_o normally exists, the above definition of Rb may be rewritten as

$$Rb = \frac{26}{i + I_o} \tag{77}$$

where I_o is expressed in milliamperes. The capacitance rising from the storage of charge in the boundary or depletion layer for diodes fabricated with uniform impurity density is given

$$C_B = \frac{C_o}{\left[1 + \frac{V}{V_b}\right]^{1/2}} \quad . \tag{78}$$

This capacitance is referred to as the barrier capacitance of an abrupt junction. It is nonlinear in that it is dependent upon the thickness of the barrier layer which in turn is a function of applied voltage. The other parameters are defined:

V is the applied voltage

C_o is the zero bias junction capacitance

V_b is the barrier potential, usually about 0.7 volts.

At higher frequencies the shunting effects of this capacitance reduces the RF voltage across the barrier.

The dynamic or barrier resistance, Rb, is associated with either the point contact or Schottky barrier diode. In the case of small signal applications, this resistance is dependent upon the current flow through the diode. In practice this current is the sum of the quiescent current and the current generated by the local oscillator.

The aforementioned parameters and the package parasitic parameters may be combined into an equivalent circuit representing a typical microwave diode as shown in Figure 118.

The equivalent circuit has been found to be valid to approximately 600 GHz. The parasitic elements Rs and Cb limit the upper frequency range, however, below 1 GHz, the shunting effect of the nonlinear barrier capacitance may be neglected as well as the package parasites. The remaining two resistive elements Rs and Rb are summed into what is normally termed the video resistance, Rv. Thus,

$$Rv = Rs + Rb \quad . \tag{79}$$

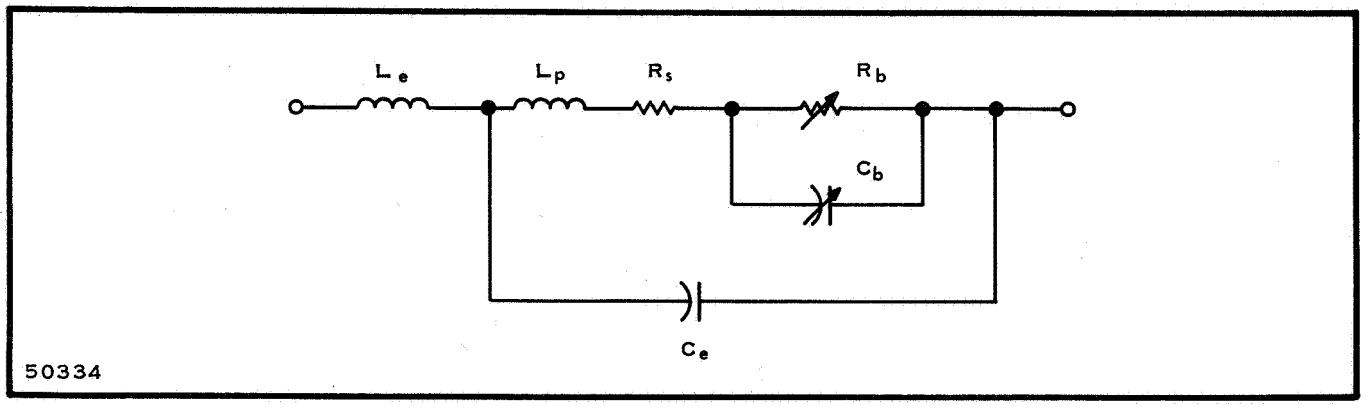

Figure 118. Complete Equivalent Circuit of Microwave Mixer Diode

As seen from Equation (77), the barrier, resistance is determined by the drive level furnished by the local oscillator. At higher drive levels, the linear relationship no longer holds and the static characteristic curve falls away from a straight line relation since electron mobility is a decreasing function of electric field strength. Hence, the series or spreading resistance increases with current instead of remaining constant. At still higher voltages the current tends to saturate at a value determined by the scatter limited velocity of the majority carriers in the semiconductor.

The forward response for several mixer diodes are plotted in Figure 119 for comparison. As it is seen from the curve, Schottky barrier diodes exhibit a much lower series resistance than do conventional point contact diodes. As may be expected, this results in smaller circuit losses. The parasitic series resistance is typically 3.3 ohms for silicon and 1.8 ohms for gallium arsenide at zero bias voltage.

The major source of conversion loss in mixer diodes is the effect of the series resistance. If it were not for the R_S, as shown in Figure 118, the noise figure of a mixer using an ideal p-n junction could be reduced to 0 dB. Modern Schottky barrier silicon and gallium arsenide diodes have sizeable reductions of their parasitic resistance which measures typically 3.3 ohms for silicon and 1.8 ohms for gallium arsenide at zero bias voltage. Thus, presently available diodes have conversion losses which are so low that operational single sideband noise figures as low as the measured double sideband performance can be obtained.

D. MIXER PERFORMANCE

Careful control of losses and careful control of out-of-band impedances can yield noise figures for mixers followed by low noise state-of-the-art IF amplifiers of less than 2 dB up to at least 3 GHz and probably less than 3 dB from K-band down.

Typical noise figures for silicon, Si, and Gallium arsenide, GaAs, diodes at S- and X-band, plotted as a function of local oscillator power, is given in Figure 120. This figure indicates that the silicon barrier diodes offer an advantage when used with local oscillator powers below 1 mW. The GaAs diodes have a slighter advantage for oscillator driving power greater than 10 mW.

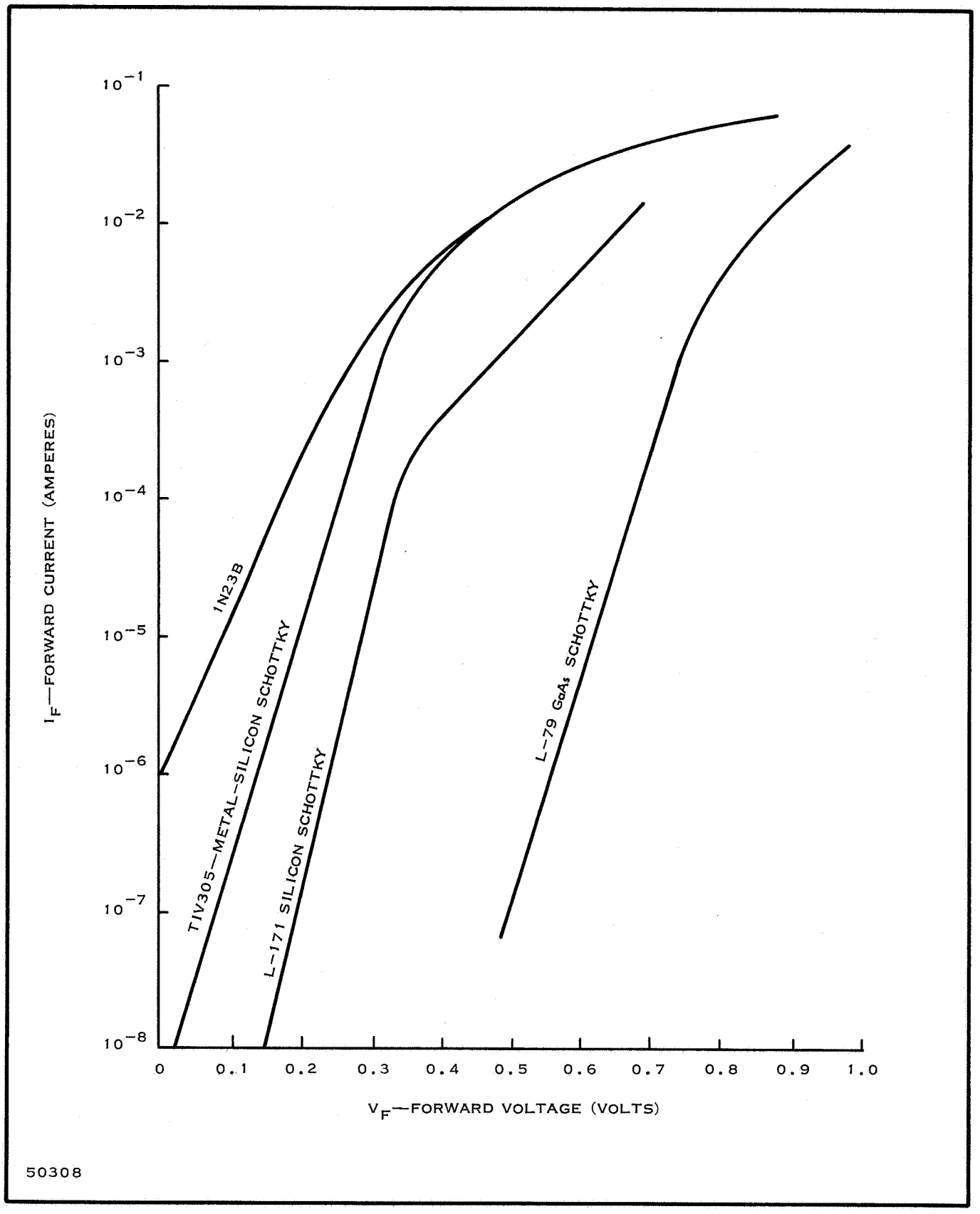

Figure 119. Forward Response of Mixer Diodes

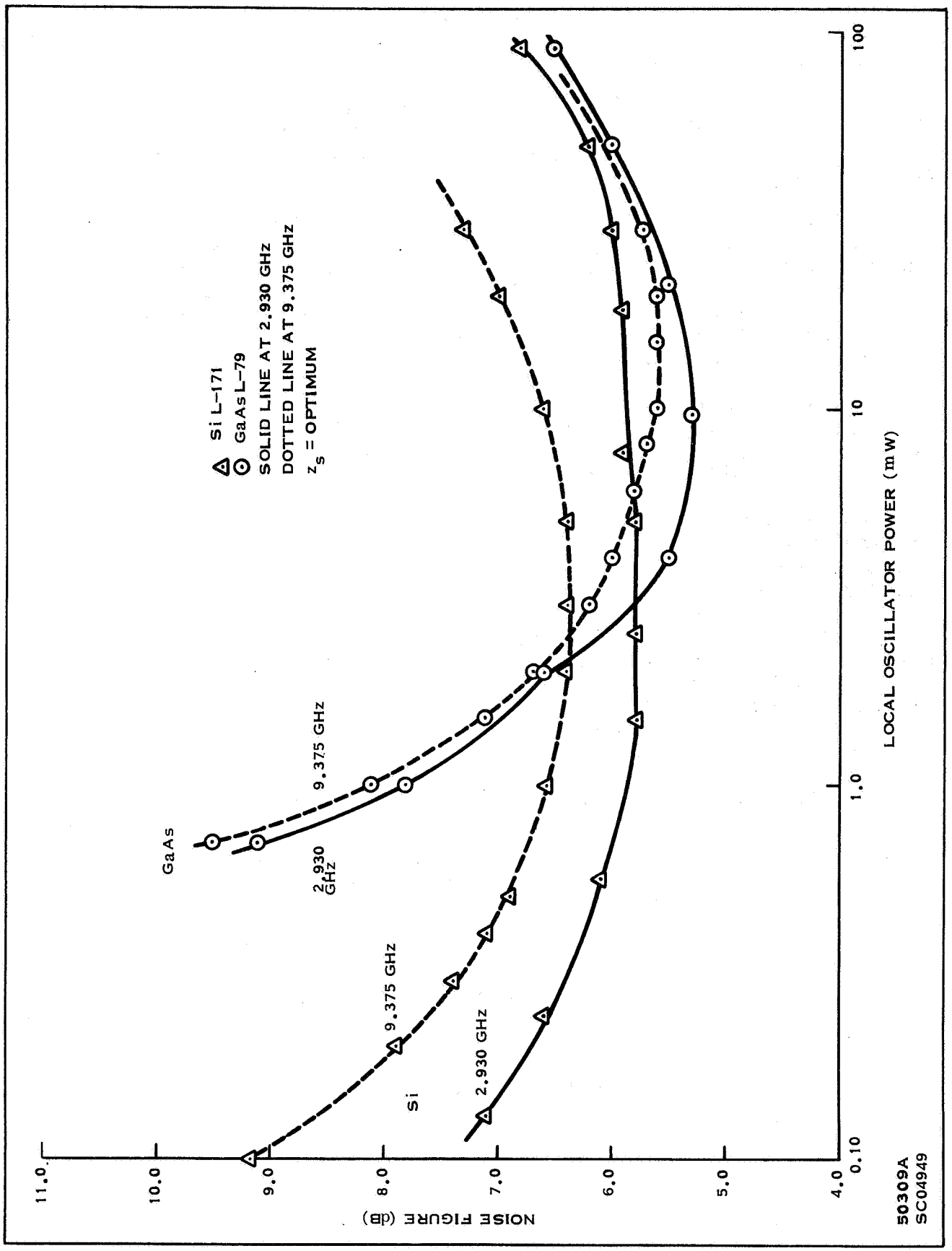

Figure 120. Schottky Barrier Noise Figure vs Local Oscillator Power

Another diode parameter which must be considered in design of the complete receiver is its IF impedance. The IF impedance of the mixer diode is strongly dependent on the termination of the image frequency.

It has been found that the IF loading of the mixer stage is not independent of the admittance of the signal source. Thus, to minimize conversion loss, requires the proper matching of the input and output terminals of the mixer stage with the signal source and the input of the IF stage.

The diode IF impedance also depends strongly upon the local oscillator power, the frequency, and the RF tuning of the mixer circuit. The IF impedance of a pair of silicon Schottky barrier diodes measured over a signal range in a ceramic S-band balance mixer is shown in Figure 121. The measurement was taken using a 30-MHz IF amplifier and shows a source impedance of 60-125 ohms over a signal range of 1.7 to 2.4 MHz for a local oscillator power of 1.0 mW. The impedance measured is for two diodes; the IF impedance for one diode would be one-half of that indicated.

As noted in Equation (68), the overall noise performance of a receiver not employing RF gain before the mixer is dependent upon the noise figure of the IF amplifier. The noise figure of the IF amplifier is a function of the IF impedance of the mixer; thus image termination will determine the noise figure of the IF amplifier.

A mixer stage is sometime referred to as being "broadband." This designation implies that the RF circuit attached to the mixer RF terminals is broadly enough tuned so that the load admittance presented to the image frequency is that which is normally available to the signal frequency.

The noise figure of a diode may commonly be specified as a double-sideband (DSB) noise figure. This signifies the operation of a mixer when it is receiving usable signals in both the signal and image bands. The single-sideband (SSB) noise figure is obtained by adding 3 dB to the double sideband noise figure which is measured with a 1.5-dB noise figure IF amplifier. The single sideband operation is more commonly the normal configuration, and requires terminating the image frequency.

The single-sideband noise figure of a mixer may be given:

$$NF = \left[1 + \frac{L\ signal}{L\ image}\right] \left(1 + \frac{T_e}{T_o}\right) \qquad (80)$$

where

L image = conversion loss at image frequency

L signal = conversion loss at signal frequency

T_e = effective input noise temperature of the mixer

T_o = ambient temperature (290°K).

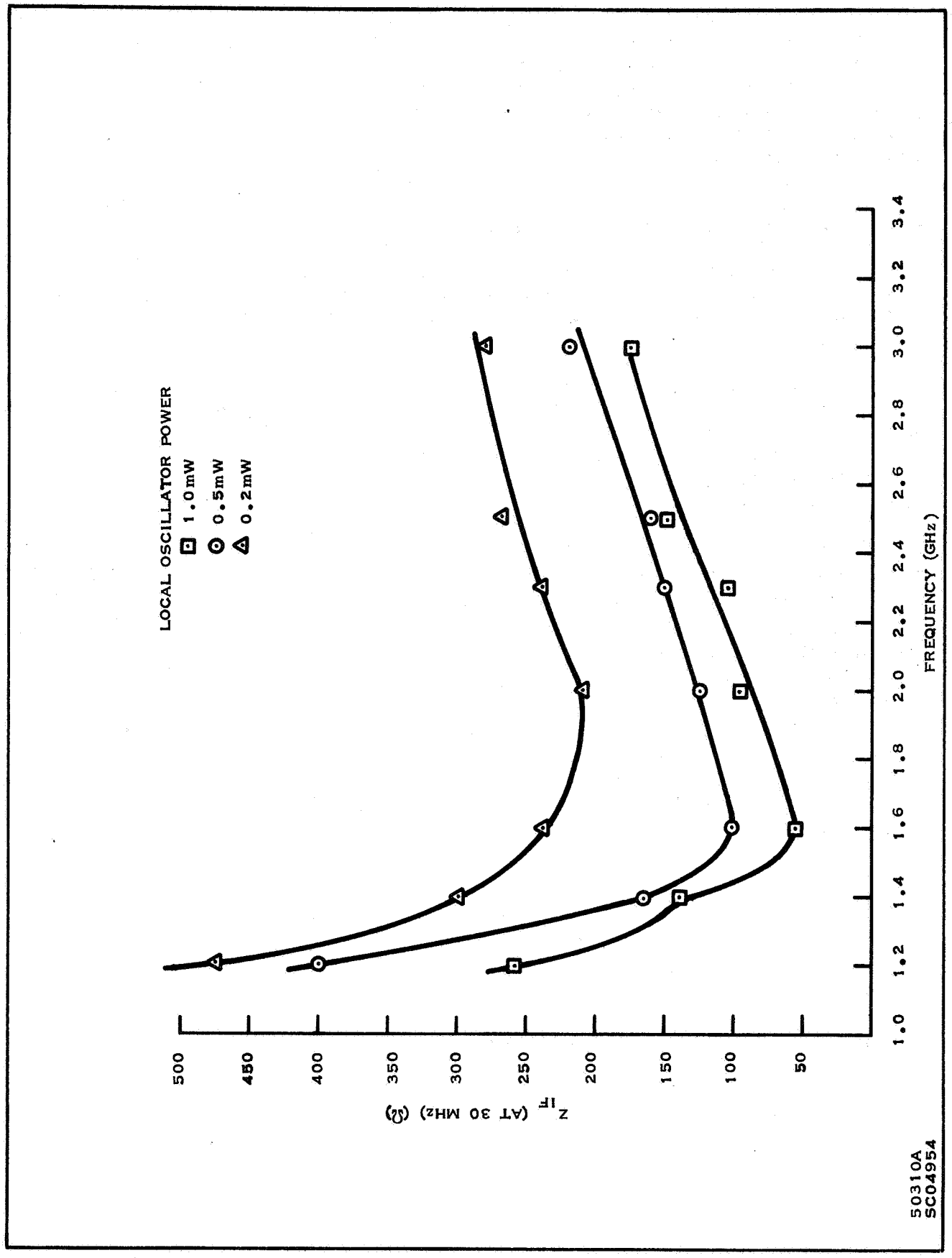

Figure 121. Silicon Schottky Barrier Intermediate Frequency Impedance at 30 MHz

For the broadband mixer, L image = L signal and the noise figure is degraded by 3 dB. If the conversion loss of the diode is assumed to be essentially constant at the signal and image frequencies, the ratio of L signal to L image is equal to the ratio of the mismatch losses at the signal and image frequencies. Using this ratio, mismatch losses in the above expression gives an indication of the manner in which the noise figure of the mixer is increased over the case where the mismatch loss at the image frequency is infinite.

The image-terminated mixer reduces signal power loss by preventing any of the signal power, which is converted by the mixer diode to frequencies other than the IF, from being dissipated in the source or any other termination. By presenting an open circuit to the mixer diodes, the noise temperature of the diode is reduced because the noise currents generated by the image frequency are prevented from flowing and can not be converted to appear as noise at the IF. The open circuit image termination will reflect back the image signal produced by the mixing action of the diode.

An image-terminated mixer requires a frequency selective matching network which provides the desired impedance to the image frequency. Care must be taken to match the local oscillator and signal source to the mixer diode. These matching conditions propose a restriction upon the tuning range of the image terminated mixer, as narrow-band tuning range is required in order to simultaneously match the signal, L.O. and image frequencies.

Very low noise microwave mixers using gallium arsenide diodes in a hybrid-ring configuration and in which the image frequency was terminated into an open circuit has been built at 2.7 GHz. A 30-MHz IF amplifier with a noise figure of 0.78 dB followed the mixer [80]. The hybrid-ring losses were less than 0.1 dB, the VSWR was below 1.15 and this isolation was greater than 30 dB from 2.5 to 2.9 GHz. The measured single-sideband noise figure of the mixer was 2.09 ±0.05 dB after losses of the RF filter were subtracted.

The effective mixer conversion loss as shown in Equation (68) determines the noise figure of a mixer for any given IF and bandwidth. The conversion loss, Lm, in Equation (68) is the effective loss realized in a specific mixer. It is really a sum of three types of losses. The first type of loss depends on the degree of match obtained at the RF and IF ports. It can be expressed as: [59]

$$L_1 = 10 \log \frac{(S1 + 1)^2}{4S_1} + 10 \log \frac{(S_2 + 1)^2}{4S_2} \qquad (81)$$

where S_1 is the RF VSWR and S_2 is the IF VSWR.

The second loss represents a loss of signal power due to the diode parameters and can be evaluated from the diode's equivalent circuit. This loss is the ratio of

$$L_2 = 10 \log \left[1 + \frac{Rs}{Rb} + \omega^2 C_B R_S R_B \right] . \qquad (82)$$

The third factor affecting the overall conversion loss is the actual conversion loss at the diode junction. For the image terminated case, the loss is

$$L = \left(1 + \frac{\sqrt{1+\gamma_2 - 2\gamma_1^2}}{1+\gamma_2}\right)\left(\frac{1+\gamma_2}{\gamma_1^2}\right) \tag{83}$$

where

$$\gamma_1 = \frac{\left(\frac{\bar{x}-1}{2}!\right)^2}{\frac{\bar{x}^2}{2}!\,\frac{\bar{x}-2}{2}!}$$

$$\gamma_2 = \frac{\left(\frac{\bar{x}-1}{2}!\right)^2}{\frac{\bar{x}+1}{2}!\,\frac{\bar{x}-3}{2}!}$$

$$\bar{x} = \log^{i2/i1} \Big/ \log^{V_2/V_1} .$$

The value of $\bar{x}$ is the slope of the log-log plot of the static or V I characteristic.

The noise temperature of a mixer diode is defined as the output noise ratio of the noise power developed by the diode to the thermal noise of an equivalent resistance at 290°K.

For the Schottky barrier diode, the noise temperature of the diode is defined.

$$td = tw + \frac{Kn\ Id}{f} \tag{84}$$

where f is operating frequency

Id is the biasing current flowing through the diode

tw is a constant representing shot and thermal noise

Kn is a constant .

In the case of planar functions such as that for Schottky barrier Kn is 1.8 Hz/μa and tw is typically 0.8. The noise temperature over a given band of frequencies is

$$td = tw + \frac{Kn\ Id}{B}\ \ell n\ \frac{f_2}{f_1} \tag{85}$$

where B is the bandwidth ($f_2 - f_1$)

f_2 is the upper frequency

f_1 is the lower frequency.

Equation (85) is plotted in Figure 122 to illustrate the superiority of the planar junction as contrasted to the performance of a crystal point-contact diode. This figure also illustrates that the diode noise temperature depends upon the quiescent current in the diode and the chosen intermediate frequency. It can be noted from this figure that the diode noise temperature has a finite value at higher frequencies equal to thermal noise and the thermal noise is lower in a planar junction than in point-contact diodes.

The noise spectrum of the diode is not uniform as it is high in the audio range and varies inversely with frequency up to about one megacycle. Above this frequency it tapers off and approaches thermal noise. The diode noise temperature, and the two noise temperatures are interrelated as follows:

$$tm = \frac{2}{Lm}\left[t_d\left(\frac{Lm}{2} - 1\right) + 1\right] \text{ for image terminated} \qquad (86)$$

$$tm = \frac{1}{Lm}\left[t_d\,(Lm-1) + 1\right] \text{ for image open or shorted} \qquad (87)$$

where

tm is effective mixer noise temperature

td is effective diode noise temperature

Lm is effective mixer conversion loss.

Quite commonly, balanced mixers are used in microwave receivers as they offer the advantage of suppressing local oscillator noise and spurious intermodulation components. In solid state receivers, the balanced configuration employs two diodes and a stripline hybrid junction; either a quadrature edge-coupled or branch-line hybrid couplers or a hybrid ring. In either case, the balanced mixer provides a push-pull output signal at the intermediate frequency in which the odd order terms in the power expansion given in Equation (71) are cancelled.

The hybrid-ring balanced mixer configuration is illustrated in Figure 123, in which two mixer diodes are driven in shunt by the local oscillator signal and in push-pull by the RF signal. The local oscillator signal applied at port A divides into two paths traveling around the ring, combining in phase at port D and out-of-phase at C. Similarly, the RF signal applied at arm C divides and arrives in phase at B and D and out of phase at A. Hence, at arms B and D, the in-phase local oscillator voltage and the RF signal voltage and the 180 degree phase relationship between the local oscillator and

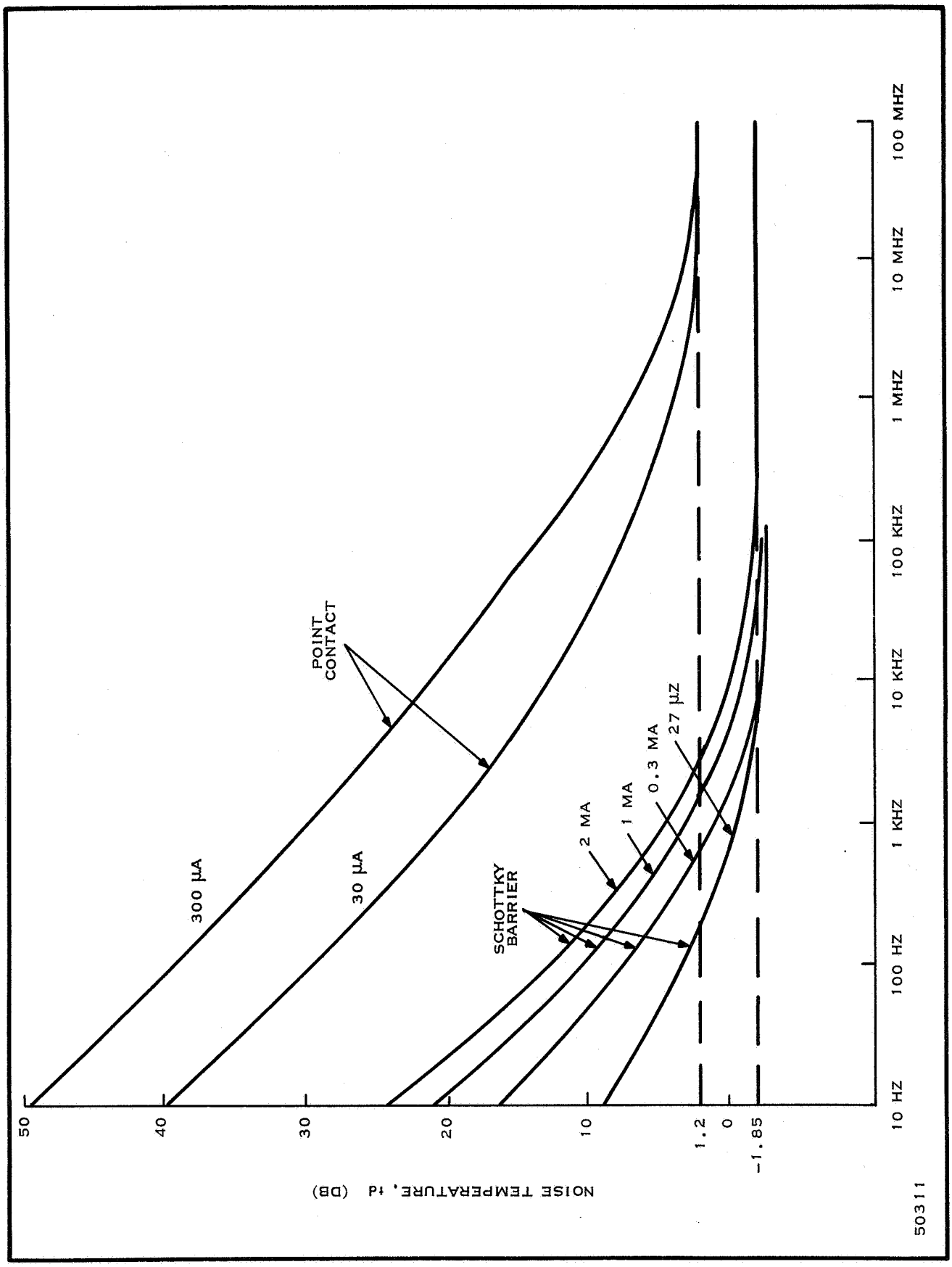

Figure 122. A Plot of Noise Temperature vs Frequency

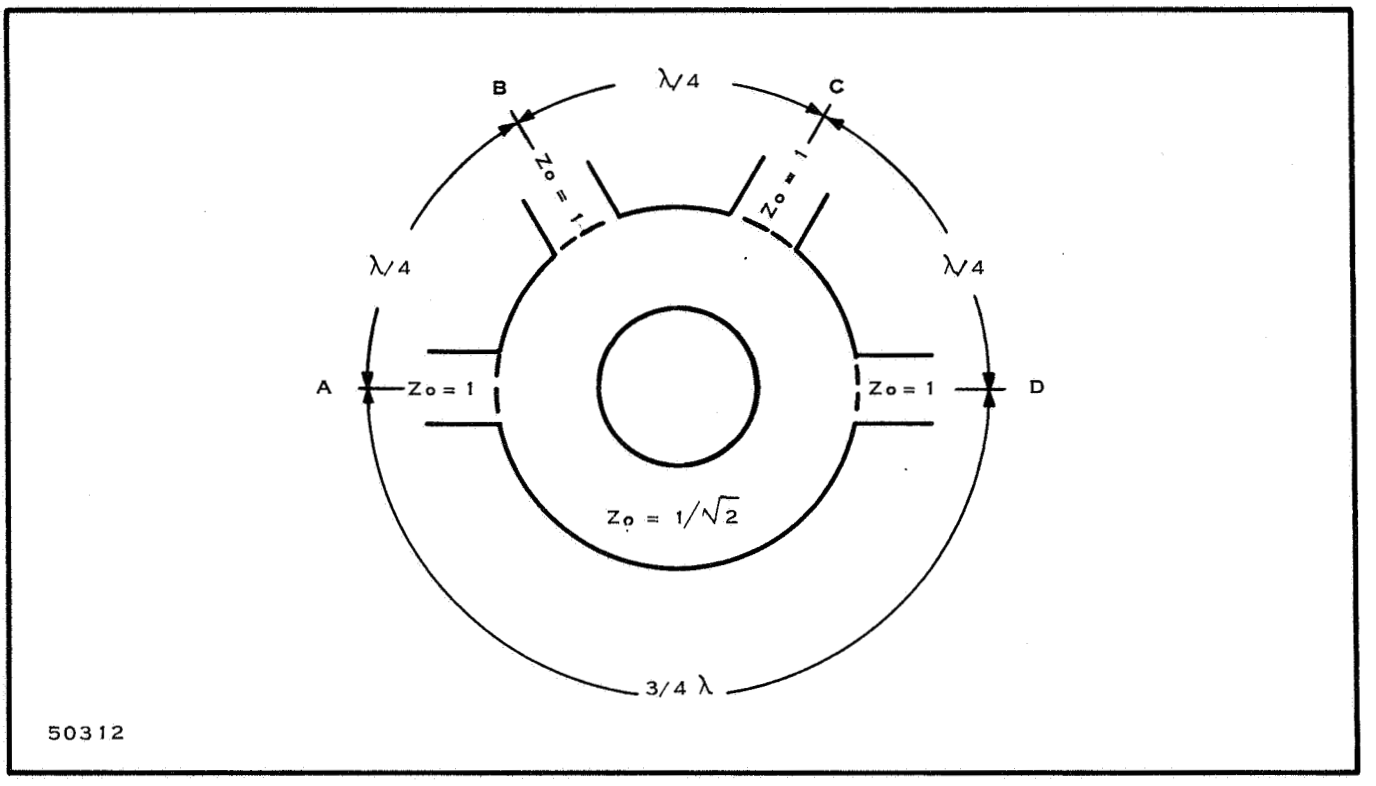

Figure 123. The Hybrid Ring Circuit

signal voltage produce opposing IF signals. The IF signals are added together in push-pull in a balanced input circuit of the following IF stage. The amplitudes of the IF voltages are equal if the conversion losses of the diodes are matched. The decoupling between the local oscillator and the RF signal arms of the hybrid-ring circuit makes possible the use of a oscillator with relatively low power as compared to the single diode mixer.

The noise figure performance of an experimental S-band balanced mixer using silicon Schottky barrier diodes is given in Figure 124. The same characteristics for gallium arsenide barrier diodes is shown in Figure 125. In comparing the noise properties of the silicon diodes to the gallium arsenide diodes it is seen that the silicon circuit gives equivalent noise figures with one-tenth the local oscillator drive required for the gallium arsenide diode mixer. The optimum noise figure for the silicon mixer occurs for a local oscillator power between 2 to 4 mW.

The performance of an experimental S-band balanced mixer using silicon Schottky barrier diodes mounted on an Al_2O_3 substrate is shown in Figure 126. The mixer was constructed using 90 degrees branch hybrid line couplers. The couplers required high impedance lines to obtain a broad bandwidth (Z = 90 ohms) so 0.7-mil line widths were used in the high dielectric Al_2O_3 substrate.

The performance of a stripline image-terminated mixer using an external band-pass filter is given in Figure 127. The mixer shows a 3-dB improvement in noise figure over the broadband mixer model. The mixer was constructed for use at C-Band using 1/16 inch Teflon fiber glass board. The circuit consists of an RF matching network, a

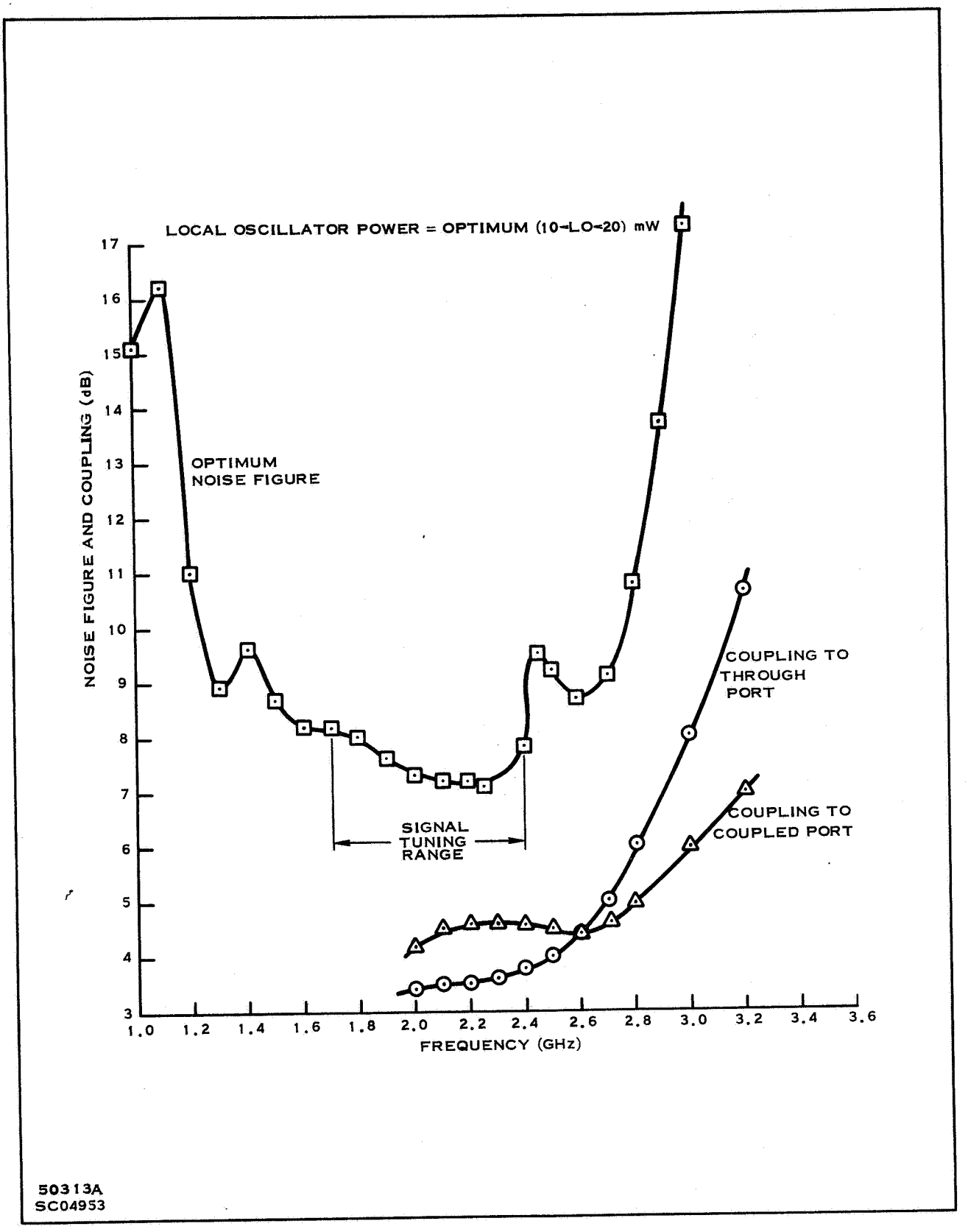

Figure 124. Noise Figure vs Frequency of S-Band Ceramic Balanced Mixer with Gallium Arsenide Schottky Barrier Diodes

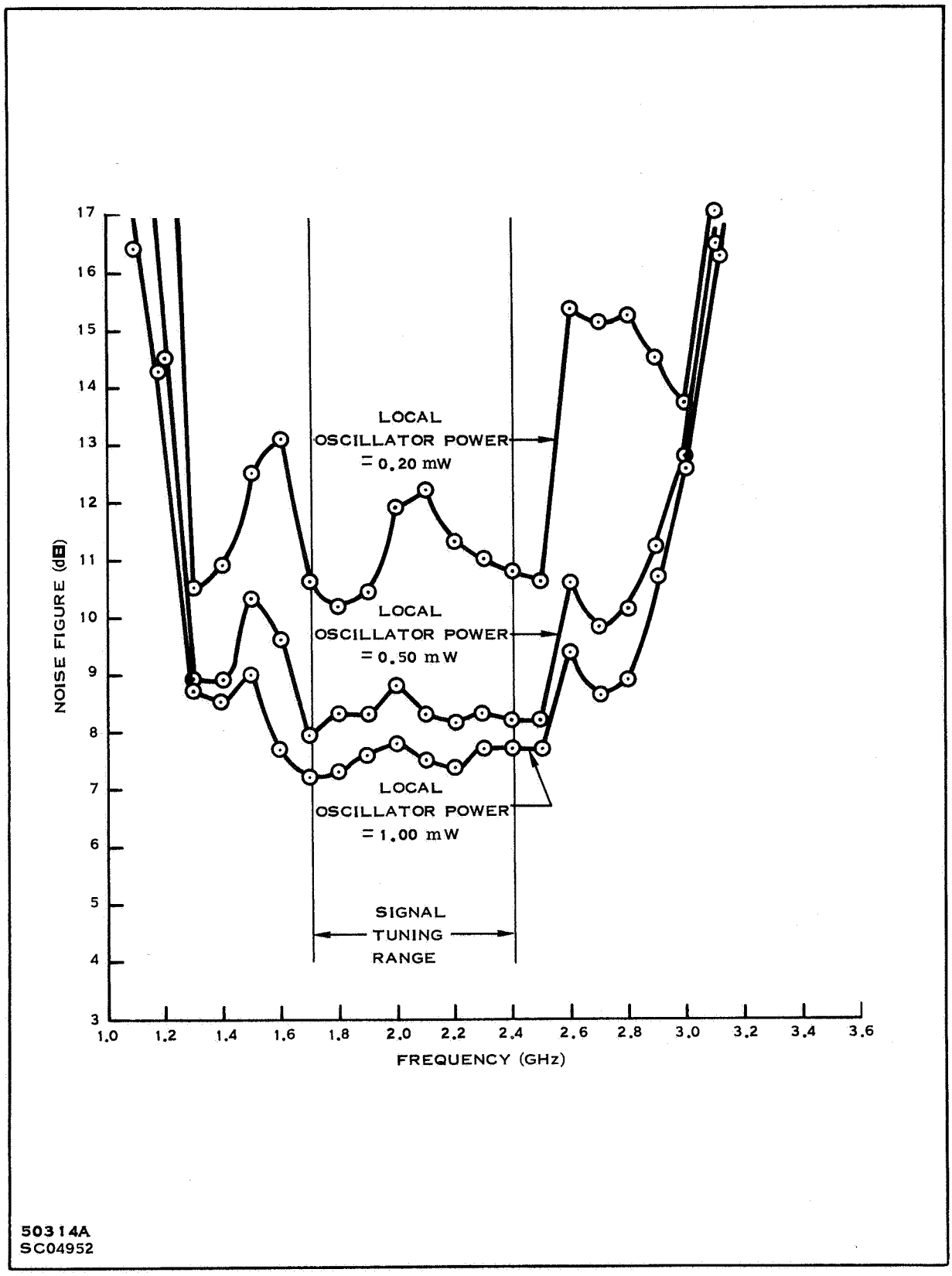

Figure 125. Noise Figure vs Frequency of S-Band Ceramic Balanced Mixer with Silicon Schottky Barrier Diodes

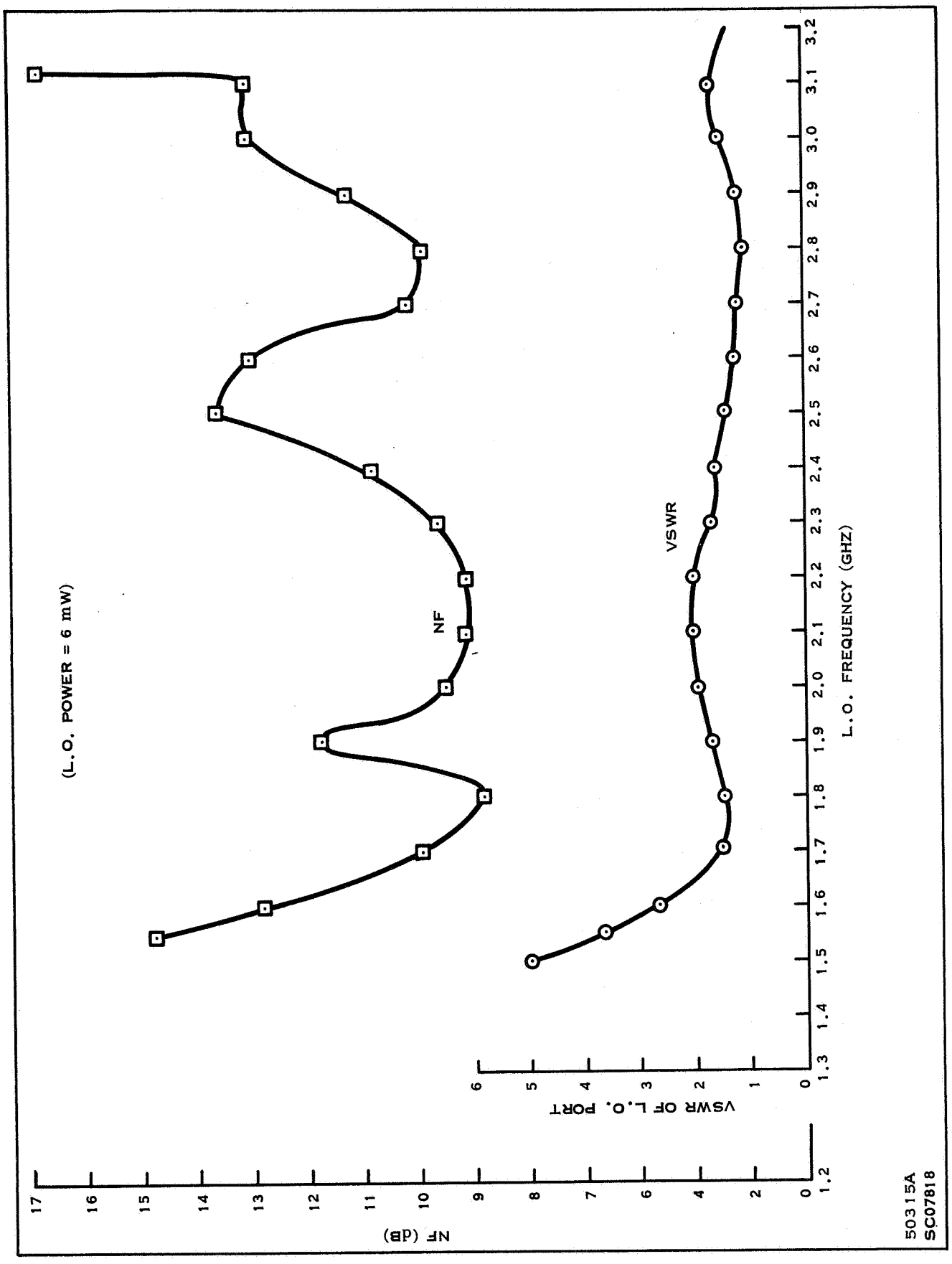

Figure 126. Performance of High Dielectric S-Band Balanced Mixer vs Local Oscillator Frequency

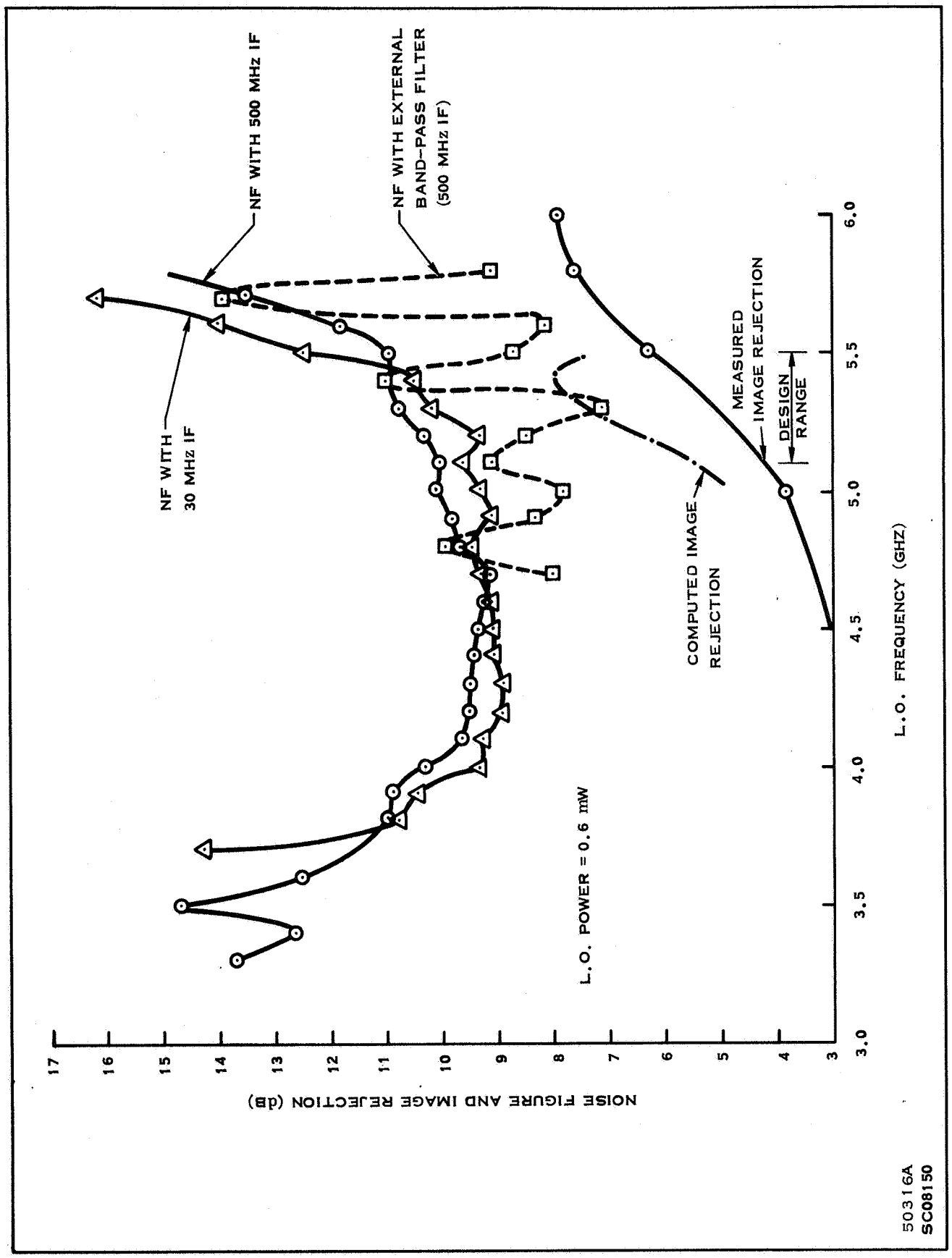

Figure 127. Performance of C-Band Image Terminated Mixer vs Local Oscillator Frequency

1/4 open-circuit stub for RF ground and a silicon Schottky barrier diode. The signal and local oscillator were coupled by an external 10 dB coupler. A VSWR of 30 existed at the image frequency, reflecting back 88 percent of the image power to the diode. The circuit operated with a 500-MHz IF over a signal range of 4.6 to 5.0 GHz with a image termination giving a calculated mismatch loss of 9 dB at the image frequency f_I. A local oscillator power of 0.6 mW gave the best noise figure.

The ordinary microwave balanced mixer will respond to either of two signals which are displaced from the local oscillator by the intermediate frequency. One signal is normally the desired signal and the other is the image signal. The inability of a balanced mixer to distinguish between the proper signal may be enhanced by combining two balanced mixers, four diodes, into an image suppression mixer which readily provides some 20 dB reduction to the image response of a receiver. Such a configuration is shown in Figure 128.

Two balanced mixers used with a quadrature hybrid and a hybrid tee for coupling the local oscillator and the RF input signal to the mixers comprise the microwave circuit of a common form of the image suppression mixers. The two balanced mixers are connected so that the IF components produced by the image are of such a phase to add at the output port where they can be resistively terminated.

Figure 128 illustrates a low frequency version of the ring image-suppression mixer. In this circuit, the diodes connected in a bridge configuration is driven by two broadband transformers more than 100 mc wide. The use of the double-balanced circuit cancels higher order products and reduces the primary signal giving a wide dynamic range.

D. FIELD EFFECT TRANSISTOR

In some instances, double conversion may be applicable to the overall design of a given microwave receiver. In such a case, the use of a FET as the second mixer offers many advantages. The FET operates well in the VHF/VHF, offering conversion gain as well as high immunity to spurious response and extremely low noise figures. Operating as a mixer with gain, eliminates the low noise requirement for the following IF amplifier. The cross-modulation characteristics of diode mixers is almost completely eliminated in the FET by its nearly perfected square law transfer function.

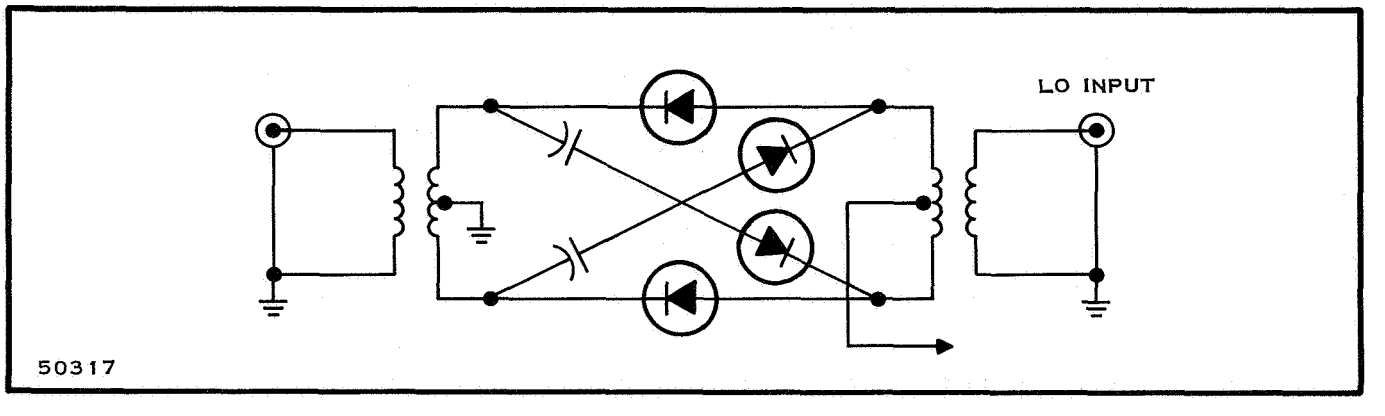

Figure 128. Combination of Two Balanced Mixers

Maximum gain is obtained by applying the RF signal to the gate and good isolation is achieved with the local oscillator signal feed into the source. The input impedance of the mixer varies with different levels of LO injection and with sufficient oscillator drive into the source, the impedance into the gate is well below 100 ohms.

The optimum operating point where the transfer characteristic are almost square law is very near pinch-off bias of the FET where the drain current, Id = 0. However, conversion gain of the IF signal results when Id is increased because the transconductance, gm, is increased. The dilemma of these two different considerations is resolved by self-biasing the FET well below I_d = 1 mA with a suitable source resistor, then applying a large LO signal to drive the FET on during positive half-cycles at the LO frequency. The effective, gm, at the IF will then be sufficient to provide gain.

A FET mixer constructed with stripline is illustrated in Figure 129 which has the performance characteristics as listed below.

RF input	575 MHz
LO input	620 MHz
IF output	45 MHz
Conversion gain	9 dB
IF Bandwidth	9 MHz
Noise Figure	6.5 dB

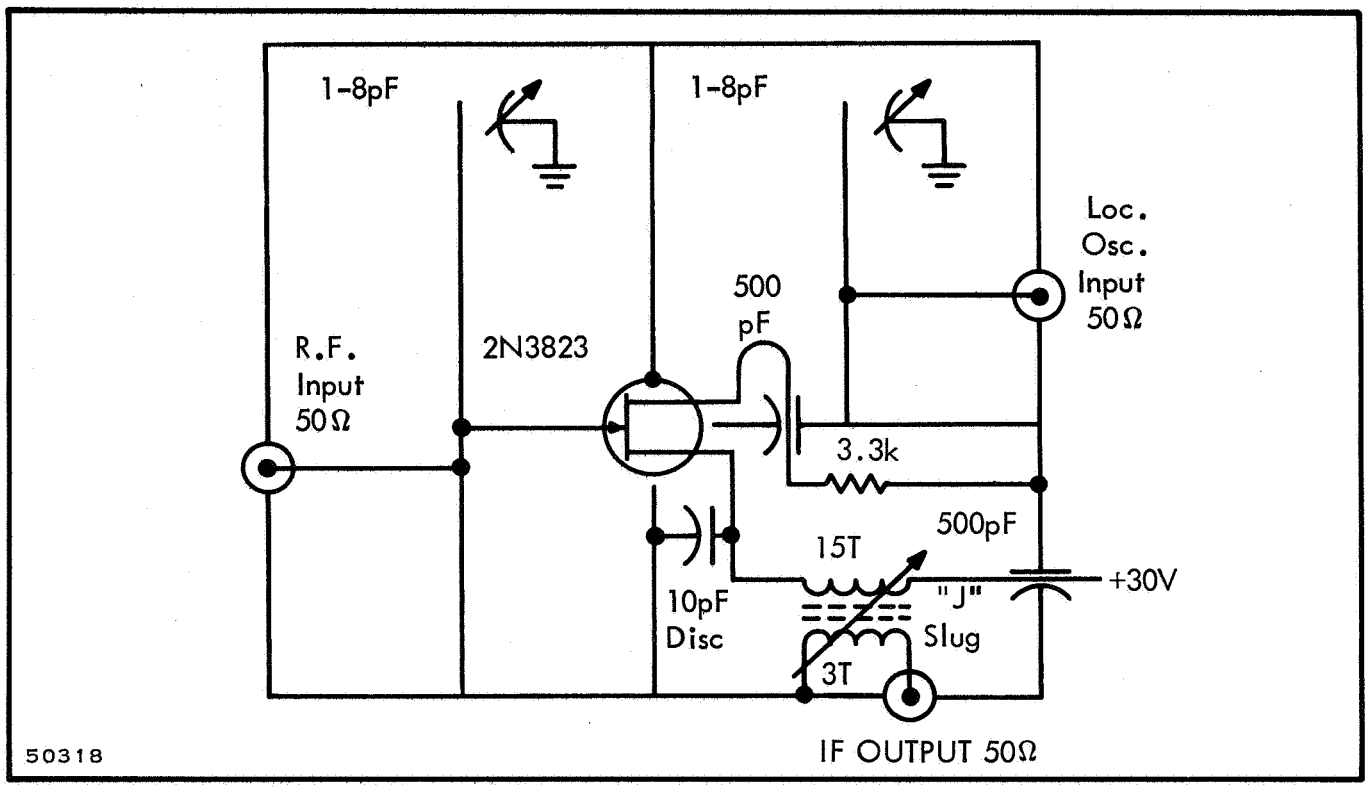

Figure 129. FET Mixer Circuit

SECTION X

PROGRAM PERSONNEL

Name	Title
Ben S. Skinner	Project Engineer
Charles T. Johnston	Engineer
Eldon Gordon	Engineer

SECTION XI

CONCLUSION

This study was performed under item 9 of the work statement which required that an analytical study of solid-state integrated microwave circuits, techniques and components be undertaken prior to the development of an S-band FM telemetry receiver subsystem. The results of this study indicate that sufficient semiconductor microwave technology exists to make the development of a receiver in the 2200- to 2300-MHz frequency region feasible. This study considered microwave components, devices and techniques applicable to receiver applications. Correlated with the phase II study of telemetry receiver configurations, these data will be used to provide specific circuits within current technology to meet this design objective. As time passes, it may be necessary to up-date this report due to continued research in microwave semiconductor technology. Nevertheless, the current state-of-the-art will be utilized in subsequent work performed under this contract.

BIBLIOGRAPHY

1. Private Communication with Harry Cooke, Texas Instruemtns Incorporated

2. Private Communication with A. J. Anderson, Texas Instruments, Incorporated

3. Editorial, "Low-Noise Germanium Transistors Priced to Win Phased-Array Market", Microwaves, Vol. 5, No. 3, March 1966, pp. 114-116

4. Texas Instruments Incorporated, Study of Solid-State Integrated Microwave Circuits, Scientific Report No. 3, 30 June 1967

5. Texas Instruments Incorporated, Microwave Transistors Technical Report ECOM-01371-5, by George Johnson, David Boone, Julius Lange, Quarterly Report No. 5, Contract No. DA 28-043 AMC-01371(E), DA Project No. 1P6-22001-A-056, Task 04, Jan. 1967

6. E.O. Johnson, "Physical Limitations on Frequency and Power Parameters of Transistors", RCA Review Vol. 26, June 1965, pp. 163-177

7. Texas Instruments Incorporated, Study of Solid-State Integrated Microwave Circuits Scientific Report No. 1, 31 Dec. 1965

8. Harry F. Cooke, "Microwave Transistor Circuits", Microwaves, Vol. 3, No. 8, Aug. 1964, p. 28

9. Texas Instruments Incorporated, Microwave Transistors Technical Report ECOM-01371-6, by George Johnson, David Boone, Julius Lange, Quarterly Report No. 6, Contract No. DA 28-043 AMC-01371(E), DA Project No. 1E6-22001-A-056, Task 06, April 1967

10. Donald R. Carley, Patrick L. McGeough, and Joseph F. O'Brien, "The Overlay Transistor", Electronics, Vol. 38, No. 17, Aug. 1965, p. 70

11. H. C. Lee and George Gilbert, "Overlay Transistors Move Into Microwave Region", Electronics, Vol. 39, No. 6, 21 March 1966, p. 93

12. Robert Minton, "Semiconductor High-Frequency Power-Amplifier Design", WESCON Record, 23 Aug. 1966

13. H. C. Lee, "Microwave Power Generation Using Overlay Transistors", RCA Review, Vol. 27, June 1966, pp. 199-215

14. Paul Kolk, "MOS-FET High Frequency Amplifiers," WESCON Record, 23 Aug. 1966

15. Joe Schurmann, "Junction FET Revises VHF Tuner", The Electronic Engineer, Vol. 26, No. 4, April 1967, p. 63

16. J. B. Compton, "Junction FET High Frequency Applications", WESCON Record, 23 Aug. 1966

17. G. C. Luettgenau and A. R. Brand, "Circuit Simplification with IGFETS", WESCON Record, 23 Aug. 1966

18. Texas Instruments Microlibrary, Communication Handbook, Part II, 1965, Chapter 6

19. Texas Instruments Incorporated, Molecular Electronics for Radar Applications, by T. M. Hyltin and L. R. Pfeifer, Jr., Interim Engineering Report No. 4, Contract AF 33(615)-1993, BPSN 4-6399-415906, MERA No. 3 and S-674159-415906, Jan. 1967

20. Rodger R. Webster, "Microwave Transistors", Microwave Journal, Vol. 9, No. 7, July 1966, pp. 99-102

21. Private Communication with Bernie Landress, Texas Instruments Incorporated, Dallas, Texas

22. Texas Instruments, A Proposal to Develop, Produce, and Deliver Schottky Barrier Microwave Mixer Diodes, Part I Technical Discussion, 15 September 1966, 57SC66, prepared for Department of the Air Force Headquarters Systems Engineering Group (AFSC), Wright Patterson Air Force Base, Ohio, in response to RFP No. F3361567R1153, Aug. 15, 1966

23. "Record Gunn Effect Power Levels and New Tube Techniques", Reported at British Microwave Conference, Microwaves, Nov. 1966, p. 12

24. D. Cawsey, MA "Design of Wide Range Varactor Tuned Microwave Tunnel Diode Oscillators", Proc. of the IEEE, Vol. 113, No. 6, June 1966, pp. 943-947

25. C. H. Manney and H. H. Doemland", A Tunnel Diode Discrete-Frequency Oscillator" IEEE Trans. on Circuit Theory, Vol. CT-13, No. 1, March 1966, pp. 71-73

26. W. T. Read, Jr., "A Proposed High Frequency, Negative-Resistance Diode" Bell System Technical Journal, Vol. 37, March 1958, pp.401-446

27. "A Bit of History", Microwaves, Vol 5, No. 8, Aug. 1966, pp.26

28. B. Hoefflinger, "High Frequency Oscillations of p^{++}-n^{+}-n-n^{++} Avalanche Diodes Below the Transit-Time Cutoff", IEEE Trans on Electron Devices, Vol. ED-13, No. 1, Jan. 1966,pp.151-157

29. V. Higgins, J. Baranoski, and M. McCormick, "Avalanche Transit-Time Diodes", Microwaves, Vol. 5, No. 8, Aug. 1966, pp. 24-29

30. T. Hasty, P. Cunningham, and W. Wisseman, "Microwave Oscillations in Epitaxial Layers of GaAs", IEEE Trans on Electron Devices, Vol. ED-13, No. 1, Jan. 1966, pp. 114-117

31. R. Haitz, Noise of a Self-Sustaining Avalanche Discharge in Silicon, Part I Low Frequency Noise Studies, Texas Instruments Incorporated, Dallas, Texas

32. H. Soboa, "Extending IC Technology to Microwave Equipment", Electronics, Vol. 40, No. 6, 20 March 1967, pp. 112-124

33. R. Ciarametaro, Microstrip Filters and Gap Capacitances, 1966 Summer Development Program Report, Texas Instruments Inc., Dallas, Texas, 25 Aug. 1966

34. B. Vincent, "Ceramic Microstrip for Microwave Hybrid Intergrated Circuitry", 1966, IEEE G-MTT Symposium, Palo Alto, California

35. G. Vendelin, "High Dielectric Substrates for Microwave Hybrid Integrated Circuitry", G-MTT Symposium Digest Cat. No. 17C66, 1967, pp. 125-128

36. H. Wheeler, "Transmission Line Properties of Parallel Strips Separated by a Dielectric Sheet", IEEE Trans. on Microwave Theory and Techniques, Vol. MTT-13, No. 3, March 1965

37. J. Dukes, "Broadband Slot Coupled Directional Couplers", The Institution of Electrical Engineers, Paper No. 2402R, Aug. 1957

38. G. Mathhaei, L. Young, E. Jones, Microwave Filters, Impedance Matching Networks, and Coupling Structures, McGraw-Hill, 1964

39. P. Daly, S. Knight, M. Coulton, and R. Ekholdt, "Lumped Elements in Microwave Integrated Circuits", G-MTT Symposium Digest Cat. No. 17C66, 1967, pp. 139-141

40. B. Lax and K. Button, Microwave Ferrites and Ferrimagnetics, McGraw-Hill, 1962

41. ITT, Reference Data for Radio Engineers, Fourth Edition, 1966

42. Dwight Caswell, "Understanding Circulators", Microwaves, Vol. 2, No. 8, Aug. 1963, p. 24

43. W. H. VonAulock, "Theory of Linear-Ferrite Devices for Microwave Applications", Journal of Applied Physics, Vol. 37, No. 3, March 1966, pp. 939-946

44. W. H. VonAulock, "Selection of Ferrite Materials for Microwave Device Applications", IEEE Transactions, Vol. MAG-2, No. 3, Sept. 1966, pp. 251-255

45. George H. Thiess, "Theory and Design of Tunable Y1G Filters", Microwaves, Vol. 3, No. 9, Sept. 1964, p. 14

46. Kenneth A. Lehman, "L-Band Properties of Single Crystal 600G Calcium Vanadium Bismuth Iron Garnet", Journal of Applied Physics, Vol. 37, No. 3, March 1966, pp. 1087-1089

47. R. N. Chase, Microwave Circuit Theory and Analysis, McGraw-Hill, 1963

48. A. C. Blankenship and R. L. Huntt, "Microwave Characteristics of Fine-Grain High Power Garnets and Spinets," Journal of Applied Physics, Vol. 37, No. 3, 1 March 1966, pp. 1066-1068

49. R. A. Braden, I. Gordon, R. L. Harvey, "Microwave Properties of Planar Hexagonal Ferrites", IEEE Transactions, Vol. MAG-2, No. 1 March 1966, pp. 43-54

50. D. T. Ngo, "Constant-Phase Electrically Controllable RF Attenuator Using Permalloy Film at Resonance", Journal of Applied Physics, Vol. 37, No. 3, March 1966, pp. 1077-1078

51. H. Bosma, "On Stripline Y - Circulation at UHF," IEEE Trans. on Microwave Theory and Techniques, Vol. MTT-12, Jan. 1964, pp. 61-72

52. C. E. Fay and R. L. Comstock, "Operation of the Ferrite Junction Circulator", IEEE Transactions on Microwave Theory and Techniques, Vol. MTT-13, No. 1, Jan. 1965, pp. 15-27

53. Robert Blau, "Y1G Microwave Electronically Tunable Preselectors", Microwave Journal, Vol. 5, No. 5, May 1962, pp. 98-102

54. R. V. Pound, Microwave Mixers, Vol. 16, Radiation Laboratory Series, McGraw-Hill, 1950

55. Philip S. Carter, "Side-Wall-Coupler, Strip-Transmission Line Magnetically Tunable Filters Employing Ferrimagnetic YIG Resonators", IEEE Transactions on Microwave Theory and Techniques, Vol. MTT-13, May 1965, pp. 306-315

56. V. Uzunoglu, Semiconductor Network Analysis and Design, McGraw-Hill, 1964

57. B. T. Vincent, Jr., H. F. Cooke, and A. J. Anderson, "Microwave Power Generation and Amplification Using Transistors", The Microwave Journal, Vol. 9, No. 7, July 1966, pp. 63-68

58. William A. Rheinfelder, Design of Low-Noise Transistor Input Circuits, Hayden Book Company, 1964

59. HP application note 907, "The Hot-Carrier Diode, Theory, Design, and Application"

60. Earl L. Cummins, "Overloading and Spurious Responses in Transistor FM Tuners", Fairchild Application Note, TP-24, Nov. 1963, Presented at IEEE Spring Conference of PGBTR, Chicago, Illinois, July 1963

61. Herbert W. Pollock and Morris Engelson, "An Analysis of Spurious Response Levels in Microwave Receivers", Microwave Journal, Dec. 1962

62. L. Becker and R. L. Ernst, "Nonlinear-Admittance Mixers", RCA Review, Vol, 25, Dec. 1964, pp. 662-691

63. J. H. Lepoff and A. M. Cowley, "Improved Intermodulation Rejection in Mixers", IEEE Transactions on Microwave Theory and Techniques, Vol. MTT-14, No. 12, Dec. 1966, pp. 618-623

64. E. W. Pappenfus, Warren B. Bruene, and E. O. Schoenike, Single Sideband Principles and Circuits, McGraw-Hill, 1964

65. Henry C. Torrey and Charles A. Whitmer, Crystal Rectifiers, Vol. 15, Radiation Laboratory Series, McGraw-Hill, 1950

66. A. M. Cowley and H. O. Sorensen, "Quantitative Comparison of Solid State Microwave Detectors", IEEE Transactions on Microwave Theory and Techniques, Vol. MTT-14, No. 12, Dec. 1966, pp. 588-602

67. C. A. Burrus and D. T. Young, "Formed Point-Contact Gallium Arsenide Backward Diodes for Millimeter Wave Applications", Solid-State Electronics, Vol. 9, No. 1, Jan. 1966, pp. 49-58

68. T. Oxley and F. Hilsden, "The Performance of Backward Diodes as Mixers and Detectors at Microwave Frequencies", Radio and Electronic Engineer, Vol. 31, No. 3, March 1966, pp. 181-191

69. F. Arams, C. Allen, B. Peyton, and E. Sard, "Millimeter Mixing and Detection in Bulk in Sb.", Proc. of IEEE, Vol. 54, No. 4, April 1966, p. 612

70. Walter H. Higa, "Low-Level Microwave Mixing in Ruby" - Correspondence, Proc. of IEEE, Vol. 54, Oct. 1966, p. 1453

71. G. C. Messenger and C. T. McCoy, "Theory and Operation of Crystal Diodes as Mixers", Proc. of IRE, Vol. 45, Sept. 1957, pp. 1269-1283

72. George N. Kaposhilin, "Hot-Carrier Diode Opens New Vistas", Electronic Design, Vol. 14, 15 March 1966, pp. 178-185

73. David F. Allison, "Dielectric Isolation for Integrated Circuits", Solid State Design, Vol. 6, No. 1, Jan. 1965, pp. 29-34

74. Radio Corporation of America, RCA Linear Integrated Circuit Fundamentals, Technical Series IC-40, 1966

75. H. C. Kiehn, "Application of the RCA-CA3028 Integrated Circuit RF Amplifier in the HF and VHF Ranges", RCA Integrated Circuits Application Note, ICAN-5337

76. David Leenov, "PIN Diode Microwave Switches and Modulators", Solid-State Design, Vol. 6, No. 5, May 1965, pp. 33-37

77. C. Forge, "Driving the PIN Diode Switch", Microwaves, Vol. 6, No. 4, April 1967, pp. 30-36

78. S. Hamilton and R. Hall, "Shunt Mode Harmonic Generation Using Step Recovery Diodes", The Microwave Journal, Vol. 8, No. 4, April 1967, pp. 69-78

79. D. Chakroborty and R. Coackley, "Characterization of Varactor Diodes at Low Temperatures", The Radio and Electronic Engineer, Vol. 33, No. 2, Feb. 1967, pp. 97-104

80. Robert P. Rafuse and Joze Vugrinec, Very Low Noise PN Junction Microwave Mixers, Massachusetts Institute of Technology Report for Electronic Research Center, NASA, Cambridge, Mass., Grant NSG-419 and Grant NGR 22-009-163

81. J. Dangl and K. Steele, "Using Strip Transmission Line to Design Microwave Circuits, Part I", Electronics, Vol. 39, No. 3, 7 Feb. 1966, pp. 72-83

82. J. Dangl and K. Steele, "Using Strip Transmission Line to Design Microwave Circuits, Part II", Electronics, Vol. 39, No. 4, 21 Feb. 1966, pp. 90-100

83. J. Helszajn, "A Ferrite Ring Stripline Junction Circulator", The Radio and Electronic Engineer, Vol. 32, No. 1, July 1966

84. Leonce J. Sevin, Jr., Field-Effect Transistors, Texas Instruments Electronic Series, McGraw-Hill, 1965

85. T. K. Ishii, "Ferrite Cylinder Modulator Microwave Signals", Electronics, Vol. 39, No. 17, 22 Aug. 1966, pp. 96-97

86. L. R. Hodges Jr., G. P. Rodrique, G. R. Harrison, and A. D. Sanders, "Magnetic and Microwave Properties of Calcium Vandadium-Substituted Garnets", Journal of Applied Physics, Vol. 37, No. 3, 1 March 1966, pp. 1085-1086

87. D. H. Roth, "Investigation of Ferrimagnetic Materials at Low Temperatures and some Applications in Low-Noise Receivers", IEEE Transactions, Vol. MAG-2, No. 3, Sept. 1966, pp. 256-259

88. D. Greig and H. Englemann, "Microstrip - A New Transmission Technique for the Kilomegacycle Range", Proc. of the IRE, Vol. 40, Dec. 1952, pp. 1644-1650

89. D. Boswell and D. Giles, "Thin Film Circuits, A Review", Electrical Communication, Vol. 41, No. 4, 1966 Edition, pp. 378-390

90. M. Gilden and M. Hines, "Electronic Tuning Effects in the Read Microwave Avalanche Diode", IEEE Trans. on Electron Devices, Vol. ED-13, Jan. 1966, pp. 169-175.